



University of Kentucky
UKnowledge

Theses and Dissertations--Biosystems and
Agricultural Engineering

Biosystems and Agricultural Engineering


2022

EXPLORATION OF LIGNIN-BASED SUPERABSORBENT POLYMERS (HYDROGELS) FOR SOIL WATER MANAGEMENT AND AS A CARRIER FOR DELIVERING RHIZOBIUM SPP.

Toby Adjuik

University of Kentucky, adjuiktoby@gmail.com

Author ORCID Identifier:

 <https://orcid.org/0000-0003-4747-3019>

Digital Object Identifier: <https://doi.org/10.13023/etd.2022.306>

[Right click to open a feedback form in a new tab to let us know how this document benefits you.](#)

Recommended Citation

Adjuik, Toby, "EXPLORATION OF LIGNIN-BASED SUPERABSORBENT POLYMERS (HYDROGELS) FOR SOIL WATER MANAGEMENT AND AS A CARRIER FOR DELIVERING RHIZOBIUM SPP." (2022). *Theses and Dissertations--Biosystems and Agricultural Engineering*. 91.
https://uknowledge.uky.edu/bae_etds/91

This Doctoral Dissertation is brought to you for free and open access by the Biosystems and Agricultural Engineering at UKnowledge. It has been accepted for inclusion in Theses and Dissertations--Biosystems and Agricultural Engineering by an authorized administrator of UKnowledge. For more information, please contact UKnowledge@lsv.uky.edu.

STUDENT AGREEMENT:

I represent that my thesis or dissertation and abstract are my original work. Proper attribution has been given to all outside sources. I understand that I am solely responsible for obtaining any needed copyright permissions. I have obtained needed written permission statement(s) from the owner(s) of each third-party copyrighted matter to be included in my work, allowing electronic distribution (if such use is not permitted by the fair use doctrine) which will be submitted to UKnowledge as Additional File.

I hereby grant to The University of Kentucky and its agents the irrevocable, non-exclusive, and royalty-free license to archive and make accessible my work in whole or in part in all forms of media, now or hereafter known. I agree that the document mentioned above may be made available immediately for worldwide access unless an embargo applies.

I retain all other ownership rights to the copyright of my work. I also retain the right to use in future works (such as articles or books) all or part of my work. I understand that I am free to register the copyright to my work.

REVIEW, APPROVAL AND ACCEPTANCE

The document mentioned above has been reviewed and accepted by the student's advisor, on behalf of the advisory committee, and by the Director of Graduate Studies (DGS), on behalf of the program; we verify that this is the final, approved version of the student's thesis including all changes required by the advisory committee. The undersigned agree to abide by the statements above.

Toby Adjuik, Student

Dr. Sue E. Nokes, Major Professor

Dr. Michael Sama, Director of Graduate Studies

EXPLORATION OF LIGNIN-BASED SUPERABSORBENT POLYMERS
(HYDROGELS) FOR SOIL WATER MANAGEMENT AND AS A CARRIER FOR
DELIVERING *RHIZOBIUM SPP.*

DISSERTATION

A dissertation submitted in partial fulfillment of the
requirements for the degree of Doctor of Philosophy in the
College of Agriculture, Food, and Environment and the College of Engineering
at the University of Kentucky

By
Toby Awenlebo Adjuik
Lexington, Kentucky

Co- Directors: Dr. Sue E. Nokes, Professor of Biosystems & Agricultural Engineering
and Dr. Michael D. Montross, Professor of Biosystems & Agricultural Engineering
Lexington, Kentucky

2022

Copyright © Toby Awenlebo Adjuik 2022
[<https://orcid.org/my-orcid?orcid=0000-0003-4747-3019>]

ABSTRACT OF DISSERTATION

EXPLORATION OF LIGNIN-BASED SUPERABSORBENT POLYMERS (HYDROGELS) FOR SOIL WATER MANAGEMENT AND AS A CARRIER FOR DELIVERING *RHIZOBIUM SPP.*

Superabsorbent polymers (hydrogels) as soil amendments may improve soil hydraulic properties and act as carrier materials beneficial to soil microorganisms. Researchers have mostly explored synthetic hydrogels which may not be environmentally sustainable. This dissertation focused on the development and application of lignin-based hydrogels as sustainable soil amendments. This dissertation also explores the development of pedotransfer functions (PTFs) for predicting saturated hydraulic conductivity using statistical and machine learning methods with a publicly available large data set.

A lignin-based hydrogel was synthesized, and its impact on soil water retention was determined in silt loam and loamy fine sand soils. Hydrogel treatment significantly increased water retention at saturation/near saturation by $0.12 \text{ cm}^3 \text{ cm}^{-3}$ and at field capacity by $0.08 \text{ cm}^3 \text{ cm}^{-3}$ for silt loam soil compared to a control treatment with no added lignin hydrogel. Hydrogel application significantly increased water retention at -3 cm to -15,000 cm soil water pressure head by $0.01 - 0.03 \text{ cm}^3 \text{ cm}^{-3}$ for the loamy fine sand soil. Calculations demonstrated that at a 1% (w/w) concentration or lower, lignin-based hydrogels in silt loam and loamy fine sand soils would not increase plant available soil water storage. The incorporation of lignin-hydrogels significantly decreased saturated hydraulic conductivity. In unsaturated conditions, application of the lignin-based hydrogel at 0.1 and 0.3% (w/w) increased hydraulic conductivity.

New pedotransfer functions (PTFs) for predicting saturated hydraulic conductivity were developed using machine learning (ML) and a large public database. Random forest regression and gradient boosted regression both gave the best performances with $R^2 = 0.71$ and $\text{RMSE} = 0.47 \text{ cm h}^{-1}$ on the validation data set.

The concentration of lignin-alginate hydrogel added to *Rhizobial* cell culture did not affect cell survival. All treatments of wet bioencapsulated beads achieved a similar yield of 97% , however, the presence of starch in the lignin-alginate beads increased the survival of *Rhizobium* cells.

KEYWORDS: Lignin, Soil water retention curve, Super absorbent polymers, Pedotransfer functions, Soil amendments, and Bioencapsulation.

Toby Awenlebo Adjuik

[07/05/2022]

Date

EXPLORATION OF LIGNIN-BASED SUPERABSORBENT POLYMERS
(HYDROGELS) FOR SOIL WATER MANAGEMENT AND AS A CARRIER FOR
DELIVERING *RHIZOBIUM SPP.*

By

Toby Awenlebo Adjuik

Dr. Sue E. Nokes

Co-Director of Dissertation

Dr. Michael D. Montross

Co-Director of Dissertation

Dr. Michael Sama

Director of Graduate Studies

[07/05/2022]

Date

DEDICATION

This dissertation is dedicated to the memory of my beloved late mom Vida Adjuik. To my dad Martin Adjuik, my siblings (Sandra, Sinbad, Marian, Bene) and to my friends.

ACKNOWLEDGMENTS

I would like to first express my deepest appreciation to my advisors (Drs. Sue Nokes and Michael Montross) for believing in me and giving me the opportunity to work under their tutelage. They have supported me intellectually, mentored me, inspired me to pursue greater heights even when I doubted myself. My advisors did not only constructively critique my work in our weekly meetings, but importantly offered me suggestions as to how to address problems I encountered. Our informal discussions during our weekly meetings made me feel relaxed which made my PhD journey much less stressful. My advisors were also concerned about my personal well-being as they would always encourage me to take breaks, for that, I say thank you.

I am extremely grateful to my dissertation committee for providing me with timely and constructive comments during my qualifying exams, progress presentations and the writing of my dissertation. I am deeply indebted to Dr. Ole Wendroth. Through Dr. Wendroth's guidance and teaching, I went from someone who had limited background in soil physics to writing a dissertation that applies principles in soil physics. Dr. Wendroth warmly welcomed me every time I stepped into his office and gave me technical advice on my projects in addition to career and life advice, which I deeply appreciate. Dr. Wendroth's soil physics lab in the Plant and Soil Science Department was very crucial to the start and completion of this dissertation. I would also like to express my deepest gratitude to Dr. Michael Sama for his insightful feedback and comments that helped strengthen my dissertation, especially in the aspects of machine learning modeling.

I would like to extend my sincere thanks to Riley Jason Walton for his technical assistance in the soil physics lab. Jason always helped me with equipment troubleshooting, experimental design, and general instrumental operation. Jason helped me tremendously in data collection when I was out sick one time thus without his help, my data collection would not have been possible. Special thanks to Dr. William Ford and Dr. Saeid Nazari for their assistance when I needed a particle size distribution analyzer to run samples of my hydrogels. I very much appreciate Dr. Tyler Barzee for his tutorial on using his microscope in the microbiology lab. Thank you to Anthony Vascotto and Ryan Sarhan for helping me with data collection during my bioencapsulation project. I am grateful to Stephanie Kesnar for her timely procurement of lab supplies and helping with general lab equipment and to Alex Fogle for always attending to me when I had issues with lab equipment. I am also grateful to Dr. Akinbode Adedeji for teaching me how to use the gas pycnometer in his food engineering lab with which I collected important data. A big thank you to Dr. Bert Lynn for his technical input via discussions on lignin chemistry during my literature review. I also thank Diane Hunter for her assistance with soil analysis. Many thanks to Dr. Doo Young Kim and his graduate student, Udari Shyamika for helping me with FTIR data collection. I also thank Tim Smith for his assistance with the construction of soil collars. Many thanks to Dr. Jian Shi for allowing me to take BAE 775 while writing my qualifying exams which helped improve my writing skills. Thanks to Can Liu for the technical discussions we had in the chemistry lab.

My gratitude goes to Dr. Alicia Modenbach for always providing me with information needed to meet requirements for the completion of my degree. Thank you to

Karin Pekarchik for her support with BAEGLS and for her encouragement. I also thank Julie Tolliver for her assistance whenever I had issues with my student account. To all my friends in BAEGLS, who made our game nights fun and engaging, I say thank you.

Finally, my immense appreciation goes to my family for their love, support and prayers that enabled me to reach where I am today. To my uncles Joseph Akanyako and David Adjuik, thank you for your constant encouragement. And to all my friends, especially Prince Kwarase for the zoom writing sessions and support, thank you. To God be the glory.

TABLE OF CONTENTS

ACKNOWLEDGMENTS	iii
LIST OF TABLES.....	xi
LIST OF FIGURES	xiii
LIST OF EQUATIONS	xviii
CHAPTER 1. INTRODUCTION	1
1.1 Organization of Thesis.....	1
1.2 Introduction.....	2
1.3 Project Objectives and Hypotheses.....	6
CHAPTER 2. LITERATURE REVIEW	8
2.1 Summary.....	8
2.2 Introduction.....	10
2.3 Literature Search.....	17
2.4 Biodegradability of Synthetic and Biobased Hydrogels in Soil	19
2.5 Impact of Hydrogels on Soil Hydraulic Properties.....	40
2.5.1 Impact of hydrogels on soil water retention.....	40
2.5.2 Impact of hydrogels on soil hydraulic conductivity	46
2.5.3 Impact of hydrogels on soil water infiltration.....	53

2.5.4	Impact of hydrogels on soil water evaporation	54
2.5.5	Summary of how hydrogels influence soil hydraulic properties.....	67
2.6	The “Ideal” Hydrogel for Improving Soil Hydraulic Properties.....	69
2.7	Future Research Needs	72
2.8	Summary and Conclusion.....	76
CHAPTER 3. ALKALI LIGNIN-BASED HYDROGEL: SYNTHESIS,		
CHARACTERIZATION, AND IMPACT ON SOIL WATER RETENTION FROM		
NEAR SATURATION TO DRYNESS.....		
		80
3.1	Abstract.....	80
3.2	Introduction.....	81
3.3	Materials and Methods.....	85
3.3.1	Hydrogel Synthesis	85
3.3.2	Characterization of the lignin-based hydrogel	86
3.3.3	Swelling kinetics of lignin-based hydrogel in aqueous solutions	86
3.3.4	Water absorption capacity of lignin-based hydrogel in soil.....	87
3.3.5	Soil properties	88
3.3.6	Determination of soil water retention curve.....	89
3.3.7	Statistical analysis	93
3.4	Results and Discussions.....	94
3.4.1	Hydrogel synthesis.....	94
3.4.2	Characterization of hydrogel.....	95
3.4.3	Swelling kinetics of lignin-based hydrogel in aqueous solutions	98
3.4.4	Water absorption capacity of hydrogels in soil.....	100

3.4.5	Observation of swelling in hydrogel-soil mixture.....	102
3.4.6	Water retention curve.....	104
3.4.7	Effect of lignin-based hydrogel on saturated water content, field capacity, permanent wilting point, and plant available water capacity	110
3.4.8	Potential field applications	112
3.5	Conclusions.....	116
CHAPTER 4. LABORATORY DETERMINATION OF THE IMPACT OF		
INCORPORATED ALKALI LIGNIN-BASED HYDROGEL ON THE HYDRAULIC		
CONDUCTIVITY OF SOIL		
		119
4.1	Abstract.....	119
4.2	Introduction.....	120
4.3	Materials and Methods.....	123
4.3.1	Lignin-based hydrogel	123
4.3.2	Soil properties	124
4.3.3	Laboratory experiments	125
4.3.4	Theory for determination of soil hydraulic functions	130
4.3.5	Statistical analysis	132
4.4	Results and Discussion	132
4.4.1	Effect of lignin-based hydrogel on saturated hydraulic conductivity	133
4.4.2	Effect of lignin-based hydrogel on near-saturated hydraulic conductivity	135
4.4.3	Effect of lignin-based hydrogel on unsaturated hydraulic conductivity relationships using the evaporation method	137
4.4.4	Effect of lignin-based hydrogel on change in total water storage in the soil	140

4.5	Conclusions.....	142
CHAPTER 5. FEATURE SELECTION AND MACHINE LEARNING		
REGRESSION METHODS TO PREDICT SATURATED HYDRAULIC		
CONDUCTIVITY FROM A LARGE PUBLIC SOIL DATABASE 144		
5.1	Abstract.....	144
5.2	Introduction.....	146
5.3	Machine Learning Techniques.....	150
5.3.1	Multiple linear regression	150
5.3.2	Support vector regression.....	150
5.3.3	K-nearest neighbor regression.....	151
5.3.4	Deep neural network regression.....	151
5.3.5	Random forest regression.....	152
5.3.6	Gradient boosted regression.....	153
5.4	Materials and Methods.....	153
5.4.1	Process for the development of PTFs.....	153
5.4.2	Machine Learning Programming Method	156
5.5	Results and Discussion	159
5.5.1	Descriptive statistics of soil properties.....	159
5.5.2	Predictor selection.....	163
5.5.3	Model performance assessment	167
5.5.4	Performance improvement	174
5.5.5	Predictor importance	175
5.6	Conclusion	177

CHAPTER 6. EVALUATING THE FEASIBILITY OF USING A	
LIGNIN/ALGINATE HYDROGEL AS A CARRIER FOR ENCAPSULATING AND	
RELEASING <i>RHIZOBIUM SPP.</i>	179
6.1 Abstract.....	179
6.2 Introduction.....	180
6.3 Materials and Methods.....	183
6.3.1 Synthesis of lignin-alginate hydrogel.....	184
6.3.2 <i>Rhizobium</i> compatibility at different hydrogel concentrations	185
6.3.3 Bioencapsulation of <i>Rhizobia</i>	186
6.3.4 Efficiency of <i>Rhizobium</i> encapsulation.....	188
6.3.5 Release kinetics of <i>Rhizobium</i>	189
6.3.6 Microscopic observation and scanning electron microscopy of encapsulated beads	
189	
6.4 Statistical Analysis.....	190
6.5 Results and Discussion	190
6.5.1 Lignin-alginate hydrogel synthesis	190
6.5.2 <i>Rhizobium</i> compatibility at different lignin-alginate hydrogel concentrations	191
6.5.3 Efficiency of <i>Rhizobium</i> encapsulation.....	194
6.5.4 Microscopic Observation and Scanning Electron Microscopy	198
6.5.5 Release kinetics.....	204
6.6 Conclusions.....	206
CHAPTER 7. GENERAL CONCLUSIONS AND FUTURE WORK	209
7.1 General Conclusions	209

7.2 Future Work.....	211
APPENDICES	213
APPENDIX A. 1. Lignin-based Hydrogel Synthesis	213
APPENDIX A. 2. Observation of swelling in hydrogel-soil mixture.	214
APPENDIX B. 1. Determination of the impact of lignin-based hydrogel on soil hydraulic conductivity.	215
APPENDIX C. 1 Machine Learning Implementation	217
APPENDIX C. 2. Machine learning algorithm hyperparameters.....	218
APPENDIX C. 3. Early Stopping for DNNR.....	219
APPENDIX C. 4. Predictor Importance	220
APPENDIX C. 6. Python code for developing machine learning models to predict saturated hydraulic conductivity.....	223
GENERAL REFERENCES.....	246
VITA.....	267

LIST OF TABLES

Table 2.1. Synthetic and biobased hydrogels used as agricultural amendments, their main components and biodegradation in soil.....	36
Table 2.2 Summary of the impacts of synthetic and bio-based hydrogels on soil hydraulic properties.....	58
Table 3.1. The physical and chemical properties of the soils used in this study.	89
Table 3.2 Van Genuchten parameters fitted to measured water retention curves for different soil-hydrogel mixtures and the control.	109
Table 3.3. Soil water contents at field capacity (θ FC), permanent wilting point (θ PWP), plant-available soil water capacity (PAWC), and calculated plant available water storage (PAWS) result from the application of the lignin-based hydrogel at 1% (w/w) concentration for soil layers of different thickness.	114
Table 4.1. Physical and chemical properties of silt loam soil.....	132
Table 5.1. Descriptive statistics of the saturated hydraulic conductivity and the various input variables (n = 4686).....	161
Table 5.2. Component loadings for 9 soil physical properties and the explained variance of the principal components (PCs). PCs that explained small variances (PC6 – PC9) i.e., < 6 % of the total variance are not included.	165
Table 5.3. Evaluation metrics of machine learning models for predicting saturated hydraulic conductivity.	167

Table 6.1. The yield of <i>Rhizobium</i> cells in alginate, lignin-alginate, lignin-alginate-starch beads	197
--	-----

LIST OF FIGURES

Figure 2.1. A schematic showing hydrolysis-induced swelling of a polyacrylamide-based hydrogel in the presence of an aqueous solution of NaOH and water molecules; redrawn from Zhou & Jin (2020).....	13
Figure 2.2 Scope of the areas covered in this review.	17
Figure 2.3. Characteristics of synthetic, biobased and hybrid hydrogels for soil amendment.	34
Figure 2.4. Soil water retention curve showing the relationship between soil volumetric water content and soil water pressure head in sand, silt loam and clay soil (redrawn from Goss, (2003)).....	42
Figure 2.5. Conceptual diagram describing the impact of hydrogel on different soil hydraulic parameters, (redrawn and modified from Saha et al. (2020b)).....	69
Figure 3.1. Schematic for determining soil water retention curve.....	93
Figure 3.2. FTIR spectra for freeze-dried hydrogel and the alkali lignin backbone used to synthesize the hydrogel.....	96
Figure 3.3. SEM images of a cross-section of freeze-dried lignin-based hydrogel at various magnifications A) x50, B) x100, (C) x250, and (D) x1000.....	97
Figure 3.4. Swelling ratio of the freeze-dried lignin-based hydrogel after immersing in deionized water, tap water, and 0.9% NaCl at room temperature. Error bars indicate standard error of the means (n=3).....	99

Figure 3.5. Water absorption capacity of lignin-based hydrogel in soil at 0, 1, and 3% (w/w) concentration. Error bars indicate standard error of the means (n=3). 101

Figure 3.6 (a) Water retention curve of silt loam soil amended with lignin-base hydrogel to dryness using the combined methods (hanging water column, pressure plate apparatus, and dew point meter) (b) Water retention curve of the loamy fine sand soil amended with lignin-based hydrogel up to dryness using the combined methods (hanging water column, pressure plate apparatus, and dew point meter). 105

Figure 3.7. (a) Fitted curves and measured data of the silt loam soil amended with lignin-base hydrogel from near saturation to the permanent wilting point (b) fitted and measured curves of the loamy fine sand soil amended with lignin-base hydrogel from near saturation to the permanent wilting point. 108

Figure 3.8. Volumetric water content (VWC) at saturation, field capacity (FC), permanent wilting point (PWP), and plant available water content (PAWC) of silt loam soil amended with 0, 0.1, 0.3, and 1% (w/w) lignin-hydrogel for the silt loam soil (a) and 0 and 1% (w/w) amendment for the loamy fine sand soil. Error bars indicate standard error of the means (n=3). 111

Figure 4.1. Schematic of the double membrane tension infiltrometer method, redrawn from 127

Figure 4.2. Experimental set-up for determining the hydraulic conductivity of the hydrogel amended soils using the evaporation method. Redrawn from Wendroth et al. (1993), where q_1 and q_2 represent the upward volume flux density of water across the 4.5 cm and 1.5 cm boundaries respectively in the soil cores. The average upward volume flux density of water between the 1.5 and 4.5 cm boundaries is represented by q 129

Figure 4.3. Saturated hydraulic conductivity (K_s) of the lignin-based hydrogel-soil mixtures at 0%, 0.1%, and 0.3% (w/w) treatment application rates. Error bars indicate standard error of the means (n=3). 134

Figure 4.4. Near-saturated hydraulic conductivity (K) of the lignin-based hydrogel-soil mixtures at 0%, 0.1%, and 0.3% (w/w) treatment application rates. Error bars indicate standard error of the means (n=3). 136

Figure 4.5. Hydraulic conductivity functions for the silt loam soil when amended with 0, 0.1, and 0.3% (w/w) lignin-based hydrogel determined with the evaporation method (a) volumetric water content against hydraulic conductivity $K(\theta)$, and (b) soil water pressure head against hydraulic conductivity $K(h)$ 139

Figure 4.6. Change in total soil water storage in the 0, 0.1, and 0.3% (w/w) lignin-based hydrogel treatment after 73 hours of evaporation. 142

Figure 5.1. Histogram showing frequency distribution of the measured untransformed K_s data (n =4686). 160

Figure 5.2. USDA soil texture classification triangle showing the distribution of the soils used for this study. 163

Figure 5.3. Pearson Heat Map showing the correlation matrix between the predictor variables and saturated hydraulic conductivity. *K_s*, saturated hydraulic conductivity; VCS, very coarse sand; CS, coarse sand; MS, medium sand; FS, fine sand; VFS, very fine sand; T_sand, total sand; Silt, silt content; Clay, clay content; BD, bulk density. 166

Figure 5.4. Scatter plots of observed and predicted saturated hydraulic conductivities (n = 937) on the test datasets. Each of the algorithms randomly samples 20% of the original 8216 observations to use as testing datasets for the scatter plots. Linear regression (a), SVR (b), KNN regression (c), DNN regression (d), RF regression (e), and GB regression (f). The dotted diagonal line represents the 1:1 mapping of the observed vs predicted values..... 174

Figure 6.1. Survival of *Rhizobium* in 0, 3, and 5% hydrogel concentration. Error bars represent the standard error of the mean (n=3)..... 192

Figure 6.2. Survival of *Rhizobium* at various stages of microencapsulation process of the 195

Figure 6.3. Macroscopic images of the wet (a) lignin-alginate beads additive and (b) alginate beads. Images were not taken at the same camera zoom level and so not shown at scale. 199

Figure 6.4. Microscopic images of the surface structure of the different bead formulations (a) alginate; (b) lignin-alginate; (c) lignin-alginate with starch additive..... 201

Figure 6.5. Scanning electron micrographs of the surface of the dried beads (a) freeze-dried alginate bead, (b) oven-dried alginate bead, (c) freeze-dried lignin-alginate bead, (d) oven-dried lignin-alginate bead, (e) freeze-dried lignin-alginate beads with starch additive, and (d) oven-dried lignin-alginate bead with starch additive.... 203

Figure 6.6. Scanning electron micrographs of (a) immobilized *Rhizobium* cells adhering to surface of starch granules in the lignin-alginate beads with starch additive; (b) lignin-alginate bead with no visible *Rhizobium* cells. 204

Figure 6.7. Release of *Rhizobial* cells from encapsulated beads after 24 hours. (per 20 beads) (n=3). 206

LIST OF EQUATIONS

Equation 2.1	12
Equation 3.1	87
Equation 3.2	93
Equation 3.3	110
Equation 4.1	126
Equation 4.2	130
Equation 4.3	131
Equation 4.4	131
Equation 4.5	131
Equation 5.1	150
Equation 5.2	159
Equation 5.3	159
Equation 5.4	159
Equation 5.5	168
Equation 6.1	188

CHAPTER 1. INTRODUCTION

1.1 Organization of Thesis

There are seven chapters in this dissertation. In the first chapter, we give a general introduction to the dissertation and establish the importance for research gaps that this dissertation addresses. The general introduction also outlines the specific objectives and hypotheses of the dissertation. The second chapter serves as an extensive literature review for this dissertation.

Chapter three describes the experiments conducted to investigate the effects of amending lignin-based hydrogels on soil water retention in two soils (silt loam and loamy fine sand). A lignin-based hydrogel was synthesized, and its swelling kinetics were determined to ascertain the swelling ratio of the hydrogel. The hydrogel was characterized by studying its internal morphology and functional groups present which allows it to function as a water retention material. The soil water retention curve of the amended soils was then determined.

In the fourth chapter, we describe the impacts of amending the lignin-hydrogel on saturated and unsaturated soil hydraulic conductivity using various laboratory methods coupled with numerical simulations.

In the fifth chapter, we describe a process for developing new pedotransfer functions (PTFs) for predicting saturated hydraulic conductivity using machine learning (ML) algorithms and a large database of over 8000 soil samples.

Chapter six describes experiments investigating the feasibility of using lignin-alginate beads with a starch additive to bioencapsulate and release *Rhizobial* cells.

The seventh chapter summarizes the dissertation and identifies research areas for future exploration.

1.2 Introduction

Superabsorbent polymers (hydrogels) have been proposed as soil amendments that could be used to increase water use efficiency as the hydrogels trap water that would have otherwise drained beyond the plant roots (Andry et al., 2009). Hydrogels are materials with hydrophilic structures and networks of polymer chains that are known to absorb and retain copious amounts of water within their three-dimensional networks (Ahmed, 2015) while maintaining their stability and network structure (Ranganathan et al., 2019). Hydrogels have attracted attention from researchers from various backgrounds i.e., medicine, food, pharmaceutical and agricultural industries with the goal to capitalize on hydrogels' swelling capacities to solve diverse problems. Agriculture is known to be one of the highest consumers of water (Ghobashy, 2020) and thus, may benefit from soil amendments that are added to soil to prevent plant water stress or for improving soil physical properties.

Synthetic hydrogels have been the most widely utilized and researched form of hydrogels in agriculture, and these hydrogels are synthesized from polyacrylamide and polyacrylate (Mikkelsen, 1994). The wide usage of synthetic hydrogels has drawn the attention of researchers to investigate producing hydrogels from green alternatives i.e., biopolymers which are claimed to have the advantages of being easily degradable and biocompatible compared to synthetic hydrogels (Kalinowski & Shi, 2019; Ma et al., 2015; Meng et al., 2019b).

Lignin-based hydrogels have been successfully developed, characterized (Kalinowski & Shi, 2019; Passauer, 2012) and shown to be a viable option for agricultural soils since they are non-toxic to the environment and biodegradable (Meng et al., 2019b; Rico-García et al., 2020). Lignin is a naturally occurring phenolic polymer and the second most abundant polymer after cellulose. Lignin is a waste product of pulp and paper industries (Ciolacu et al., 2012). Despite lignin's natural abundance, lignin-based technologies are not fully developed to process lignin-derived materials into high value products (Kai et al., 2016). One reason for the lack of progress in development of lignin-based bioproducts is due to lignin's heterogeneity, thus lignin is mostly directly combusted for heat and power (Chen et al., 2020). However, lignin possesses properties that make it suitable for the development of hydrogels and subsequent application to soil. For example, lignins are high in antimicrobial properties, biodegradable and may help sequester carbon (Thakur & Thakur, 2015) potentially making lignin suitable for the synthesis of bio-based hydrogels.

The first two foci of this dissertation capitalize on the use of lignin as a basis for synthesizing bio-based hydrogels and their subsequent application as soil amendments that could impact soil hydraulic properties (soil water retention and soil hydraulic conductivity) positively. Soil water retention refers to the quantity of water soils can hold for crop use. Soil water retention is often quantified using the soil water retention curve (SWRC). Since hydrogels can hold and release water due to their swelling properties, researchers are interested in how the application of hydrogels affects the SWRC. However, most studies used synthetic-based hydrogels (Abdallah, 2019b; Abrisham et al., 2018; Akhter et al., 2004; Al-Humaid & Mofteh, 2007; Alkhasha & Al-Omran, 2020; Alkhasha et al., 2018;

Bai et al., 2010; Bhardwaj et al., 2007; Lentz, 2020; Liao et al., 2016; Saha et al., 2020a; Shahid et al., 2012). There is currently a dearth of research that explains how lignin hydrogels will affect soil moisture retention. Similarly, most studies in literature have focused on the effect of synthetic-based hydrogels on soil hydraulic conductivity (Abdallah, 2019b; Alkhasha et al., 2018; Andry et al., 2009; Bhardwaj et al., 2007; Han et al., 2013; Hussien et al., 2012; Mohawesh & Durner, 2019; Shahid et al., 2012; Smagin et al., 2019; Zhuang et al., 2013). Since soil hydraulic conductivity describes the movement of water in soil, hydrogels which can store water in saturated conditions and release water under unsaturated conditions are candidates for controlling how water moves in soil. However, no study of which we are aware has tested the effect of lignin-based hydrogels on soil hydraulic conductivity. It is therefore important to evaluate the effects of lignin-based hydrogels on soil hydraulic conductivity because data from such a study has practical agronomic implications.

Another aspect of this dissertation is the application of various machine learning algorithms to predict saturated hydraulic conductivity from publicly-available large data sets. Saturated hydraulic conductivity (K_s) is one of the most important hydraulic properties of soil measured in the laboratory (Reynolds, 2008) or in the field. Saturated hydraulic conductivity of a soil refers to its ability to conduct water when all pores are filled with water (Lal & Shukla, 2004). Direct in-situ and accurate measuring techniques for saturated hydraulic conductivity are costly, labor intensive, and time consuming which can be impractical for field scale applications (Zhang & Schaap, 2019). To address this problem, pedotransfer functions (PTFs) have been used to model and predict soil hydraulic properties (Cornelis et al., 2001; Pachepsky & Van Genuchten, 2011; Padarian et al., 2018).

Pedotransfer functions are models for predicting soil hydraulic properties i.e., water retention and hydraulic conductivity from more-easily measured soil properties i.e., particle-size distribution, organic matter (OM) content and bulk density (BD) (Cornelis et al., 2001; Padarian et al., 2018).

Pedotransfer functions have been widely developed using regression functions (Gupta & Larson, 1979; Rawls et al., 1982; Wösten et al., 1999). However, developing PTFs using regression functions is often limited by the assumptions implicit in traditional statistical methods (Elith et al., 2008). A popular and efficient modeling approach for deriving PTFs for soil hydraulic properties is with the use of machine learning (ML) algorithms (Padarian et al., 2018). Several researchers have developed PTFs for predicting saturated hydraulic conductivity (Agyare et al., 2007; Arshad et al., 2013; Elbisy, 2015; Jorda et al., 2015; Kashani et al., 2020; Kotlar et al., 2019; Nivetha et al., 2019; Rasoulzadeh, 2011). However, previous work in this field rarely justifies the selection of the input variables used to develop PTFs. Furthermore, when PTFs are developed using ML, they are often not easily interpreted. Based on the limitations associated with the development of PTFs mentioned above, we aim to develop new PTFs derived from a large public database of over 8000 soil samples. We hypothesize that by applying feature selection (principal component analysis coupled with correlation analysis) to the input data derived from the measured soil properties in the database, we can select the most relevant input variables that give a higher prediction accuracy for our PTFs using machine learning algorithms.

In the final part of this dissertation, we aimed to capitalize on the ability of hydrogels to slowly release active ingredients into their surrounding environment. Apart

from the ability of hydrogels to retain water in soil for plant use, hydrogels have also been increasingly utilized for controlled nutrient release (Guilherme et al., 2015; Mikkelsen, 1994; Ramli, 2019). Controlled nutrient release is possible since small nutrient molecules can diffuse through the hydrated polymer (Mikkelsen, 1994), hence prolonging the rate at which nutrients are released back into the soil. Similarly, several studies have succeeded in encapsulating beneficial microorganisms using different carriers e.g. peat (Malusá et al., 2012), however, lignin-based hydrogels have yet to be extensively tested as engineered carriers of *Rhizobium* which could be applied to soil. Hence this research is expected to add to the evidence base of using lignin-based hydrogels as engineered carriers of beneficial soil microorganisms (*Rhizobium*) by testing the biocompatibility of lignin-alginate hydrogel with *Rhizobium*, the encapsulation efficiency, and the release kinetics of the lignin-alginate hydrogel with *Rhizobium*.

1.3 Project Objectives and Hypotheses

The main goal of this project was to quantify the ability of lignin-based hydrogels to manage soil hydraulic properties, used as engineered carriers of *Rhizobium spp.* and to develop pedotransfer functions to simulate soil hydraulic conductivity. This study is divided into four main objectives as described below:

Objective 1: Quantify the ability of an alkali lignin-based hydrogel to increase soil water retention. The main hypothesis in this objective was that by amending soil with lignin-based hydrogels, the amended soils will retain more water with increasing soil matric suction which could be beneficial for crop water uptake.

Objective 2: Quantify the impact of incorporated lignin-based hydrogels on the soil hydraulic conductivity of a disturbed silt loam soil. It was hypothesized that amending soils with the lignin-based hydrogel would reduce hydraulic conductivity compared to unamended soil, which would reduce deep percolation of water in the soil while increasing soil water storage.

Objective 3: Develop a set of new PTFs for predicting saturated hydraulic conductivity (K_s) using machine learning algorithms and a large database of over 8000 soil samples while incorporating statistical methods to inform feature selection for the model inputs. The central hypothesis of this objective was that there is a relationship between easily measured soil properties (e.g., bulk density, % silt, % clay, % sand) and saturated hydraulic conductivity. Thus, by applying feature selection (principal component analysis coupled with correlation analysis) to the input data, the most relevant input variables that give a higher prediction accuracy can be selected and used to build the models to predict K_s .

Objective 4: Evaluate the feasibility of using lignin-alginate beads with a starch additive to bioencapsulate and slowly release *Rhizobial* cells. It was hypothesized that, the addition of the different concentrations of lignin-based hydrogel in a growth medium containing *Rhizobium* will provide a better condition for the growth of the *Rhizobial* cells when compared to a control incubation with no hydrogel. It was also hypothesized that the encapsulation efficiency and release kinetics of the bioencapsulated cells will differ based on the different combinations of lignin, alginate, and starch.

CHAPTER 2. LITERATURE REVIEW

2.1 Summary

Superabsorbent polymers (hydrogels) have been proposed as soil amendments to enhance soil water management. However, a lack of systematic reviews on the impacts of hydrogels on soil hydraulic properties makes it difficult to recommend specific types of hydrogels that positively impact soil water management. In addition, findings from previous research suggest contrasting effects of hydrogels when used as soil amendments. This systematic review surveys the published literature over the past two decades (i) reviews the biodegradability of biobased and synthetic hydrogels used as soil amendments; (ii) synthesizes the impacts of biobased and synthetic hydrogels on soil hydraulic properties (i.e. water retention, soil hydraulic conductivity, soil water infiltration, and evaporation); (iii) critically discusses the link between the source of the biobased and synthetic hydrogels and their impacts as soil amendments; and (iv) identifies potential research directions. This study found that synthetic hydrogels are the most common types of hydrogels and on average degrade at a lesser rate in soil compared to biobased hydrogels. The lower degradation rate of synthetic hydrogels is due to their higher molecular weights and the lack of reactive terminal groups in their molecular chains which makes it difficult for most microorganisms (without specialized enzymes) to break down these synthetic hydrogels. However, some specific fungi can break down the carbon in synthetic hydrogels. On the other hand, biobased hydrogels are more-easily degradable due to the availability of functional moieties that can participate in enzyme-mediated biodegradation in soil. In addition, the abundance of hydroxyl groups in most biobased hydrogels increases bonding with water which we hypothesize increases microbial activity (higher water activity)

leading to faster biodegradation. Both synthetic and biobased hydrogels increased water retention in soil compared to unamended soil with decreasing soil water pressure head, decreased saturated hydraulic conductivity, reduced infiltration, and decreased soil evaporation. Even though the faster degradation of bio-based hydrogel may be environmentally beneficial, hybrid hydrogels (i.e., blend of biobased and synthetic backbone materials) which exhibit moderate biodegradation may be needed to prolong the benefit of repeated water absorption in soil for the duration of the crop growing season.

2.2 Introduction

One of the major challenges in agriculture in arid and semi-arid regions is low crop water availability due to lower rainfall and water supply issues for irrigation. In addition, sandy soils are characterized by low water retention and low water storage due to high levels of sub-surface drainage of rain and irrigation water (Abdallah, 2019b). Superabsorbent polymers (hydrogels) have been proposed as soil amendments that could be used to increase water use efficiency as the hydrogels trap water that would have otherwise drained beyond the plant roots (Andry et al., 2009). The application of both synthetic polymers (Miller & Naeth, 2019) and natural products (i.e. crop residues) (Zhou et al., 2020) to increase soil productivity and water retention has become more prevalent as these materials improve the sustainability of agriculture particularly in arid and semi-arid regions (Alkhasha et al., 2018).

Hydrogels have attracted attention from researchers from various backgrounds i.e., medicine, food, pharmaceutical and agricultural industries with the goal to capitalize on hydrogels' swelling capacities to solve diverse problems. For example, in medicine, hydrogels have been used as scaffolds to provide mechanical protection to tissues where cells are adhered to or suspended within the gel (Slaughter et al., 2009). In the food industry, hydrogels are used to encapsulate active ingredients like probiotics which will be eventually released slowly in the body of the host (Amine et al., 2014). Hydrogels have also been widely used in agriculture as soil amendments to increase soil water retention (Abedi-Koupai et al., 2008). Agriculture, being one of the highest consumers of water, benefits substantially when soil amendments are added to soil to prevent water stress or for improving soil physical properties.

There are several ways of classifying hydrogels. Hydrogels have been classified based on their source, synthesis, or crosslinking (Prakash et al., 2021). In terms of their source, hydrogels have been described as either natural (biobased) or synthetic. Biobased hydrogels are hydrogels that are prepared using natural polymers while synthetic hydrogels are hydrogels are synthesized through chemical polymerization of synthetic monomers (Thakur & Thakur, 2018). Biobased hydrogels are prepared using polysaccharides like alginate, chitosan, and dextran (Thakur & Thakur, 2018) while synthetic hydrogels include poly (ethylene glycol) diacrylate, poly (acrylic amide), poly (vinyl alcohol) (Chirani et al., 2015). In this review, we use the term “biobased hydrogels” to represent the class of hydrogels that contain materials of biological origin.

An important feature of hydrogels is their ability to absorb and trap water into their three-dimensional structure. This property is usually referred to as its swelling capacity. The swelling capacity is one of the most important metrics used to ascertain how well a hydrogel will perform in retaining water in the soil matrix. High swelling capacities allow hydrogels to be applied in situations where liquids are absorbed from an environment or expelled into that environment (Blanco et al., 2013). According to Isik & Kıs (2004), the swelling characteristics of a hydrogel depend on the nature (i.e., ionic content, charge and crosslinking agent) of the polymer used to synthesize the hydrogel and the prevailing environmental conditions (i.e., pH and temperature of the solution surrounding the hydrogel). Ghobashy (2018) argued that the swelling process of a hydrogel is a transition from solid state to a fluid without dissolution and the two interfaces interact to become a “gel”. The change in volume of a hydrogel is driven by water diffusion and the equation

that has been used to describe the mechanism of diffusion of water into the polymeric network of hydrogel is Fick's first law (Masaro & Zhu, 1999).

Fick's First Law for Diffusion in One Direction

Equation 2.1

$$j = -D \frac{\partial C}{\partial Z} \quad (2.1)$$

where j is the flux per unit area, D is the diffusion coefficient, C is the concentration, Z is the distance and $\frac{\partial C}{\partial Z}$ is the concentration gradient along the Z axis.

Hydrogels need an aqueous environment to swell. According to Zhou & Jin (2020), when a polyacrylamide hydrogel is inserted into NaOH with a solvent i.e., water, a hydrolysis reaction takes place whereby the bonds in the polyacrylamide are broken by the hydroxyl ions allowing amide groups from the polyacrylamide chain to be converted into partially ionized carboxyl groups (Figure 2.1). The hydrogel then becomes a polyelectrolyte which allows the hydrogel to absorb considerable amounts of water (Zhou & Jin, 2020).

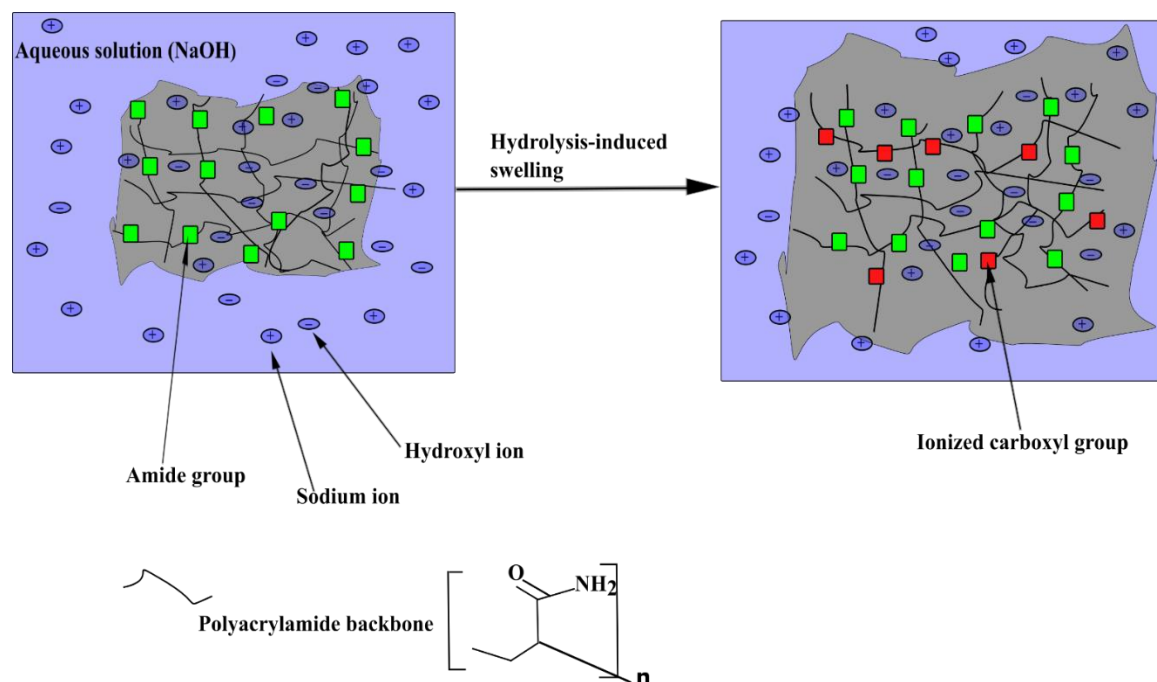


Figure 2.1. A schematic showing hydrolysis-induced swelling of a polyacrylamide-based hydrogel in the presence of an aqueous solution of NaOH and water molecules; redrawn from Zhou & Jin (2020).

Several agrophysical applications require the knowledge of the hydraulic properties of soil as these properties indicate the ability of soils to retain or transmit water (Van Genuchten & Pachepsky, 2011). The application of different types of hydrogels to change certain soil hydraulic properties has been done over the past few decades to improve sustainability of agriculture in arid and semi-arid areas (Alkhasha et al., 2018). As a result of the increased attention given to hydrogels and their application to agriculture, several researchers have reported results that show the ability of hydrogels to repeatedly absorb, retain, and release substantial amounts of water relative to the hydrogel's own weights (Alkhasha et al., 2018).

While synthetic hydrogels have been widely researched and claimed to possess superior properties like longer durability, high gel strength, and high absorption capacities (Behera & Mahanwar, 2020), bio-based hydrogels have also been shown to have high swelling capacities (Cannazza et al., 2014; Song et al., 2020; Tomadoni et al., 2020). In addition, increasing concerns arising from the use of synthetic hydrogels have propelled the increase in research in biobased hydrogels since they also have the advantage of being biocompatible, biodegradable (Kalinowski & Shi, 2019) and renewable (Li & Pan, 2010). Despite the considerable number of studies involved in elucidating the impacts both synthetic and biobased hydrogels have on soil hydraulic parameters, there are limited critical reviews of their impacts on soil as a function of the hydrogel's source. In addition, there is a general assumption that since biobased hydrogels have higher biodegradation rates and extents, then they are inherently better suited as soil amendments than synthetic hydrogels; neglecting the fact that certain biobased hydrogels (lignin-based) hydrogels have lower swelling capacities (Li & Pan, 2010) which may need to be improved to have a significant impact as a soil amendment.

There have been several recent reviews focusing on hydrogels and their various applications. Hüttermann et al. (2009) summarized the potential of using hydrogels to improve degraded and polluted lands by increasing water availability and thereby improving crop establishment. Zohuriaan-Mehr et al. (2010) highlighted the applications of hydrogels in non-hygienic industries (agriculture, textile/fiber, pharmaceutical, separation technologies, electrical and construction). Ahmed (2015) reviewed the classification, preparation processes, and process design considerations for large-scale production of hydrogels. Ullah et al. (2015) described the classification of hydrogels based

on their chemical and physical characteristics and how those characteristics influence hydrogel responses to stimuli in different applications (biomedical, environmental, and industrial). Guilherme et al. (2015) specifically reviewed polysaccharide-based hydrogels, their characteristics, synthesis and use as soil conditioners. Akhtar et al. (2016) detailed various cross-linking methods (physical and chemical) used to synthesize hydrogels. Cheng et al. (2017) reviewed studies on chitosan-based hydrogels specifically evaluating their preparation, cross-linking methods, and applications in various fields (biomedical, agriculture and water treatment). A few other review studies focused on the use of hydrogels for the controlled release of fertilizers (Majeed et al., 2015; Ramli, 2019). While the above-mentioned reviews focused on the properties, synthesis and broad application of hydrogels, no extensive discussion was given as to their impacts on agricultural soils.

Some studies reviewed the effects of hydrogels on water stress management (Saha et al., 2020b) and soil properties (physical, chemical, and biological) (Ostrand et al., 2020). Saha *et al.* (2020b) focused on the influence of superabsorbent hydrogels on soil physical properties such as water retention capacity, plant available water, saturated hydraulic conductivity, and soil infiltration. However, Saha et al. (2020b) did not extensively discuss the biodegradability of synthetic and biobased hydrogels. There was also limited discussion of the effects of hydrogel on soil-based evaporation. Ostrand et al. (2020) summarized the impact of hydrogels on the physical, chemical, and biological properties of soil but mostly with regards to the depth of application and rate of application of the hydrogel. This current review focuses specifically on summarizing available literature on applications of biobased and synthetic hydrogels to agricultural soil and addressing the questions: “Are biobased hydrogels more biodegradable than synthetic hydrogels in soil?;” and “Does the rate of

biodegradation of biobased and synthetic hydrogels affect their use as soil amendments for impacting soil hydraulic properties?”

A discussion of the impacts of both synthetic and biobased hydrogels on important soil hydraulic properties is needed to better understand the merits and limitations of using synthetic or biobased hydrogels as soil amendments. First, a summary of the numerous studies that investigated the biodegradability of synthetic and biobased hydrogels is given and the differences in their biodegradation assessments are discussed. Secondly, a thorough review of studies that investigated the impact of synthetic and biobased hydrogels on important soil hydraulic properties is given. Thirdly, a conceptual framework summarizing how hydrogels could impact soil hydraulic parameters is discussed. The final part of this review summarizes research gaps and outstanding questions that need to be answered to move forward.

The scope of this review is shown in Figure 2.2 This review does not discuss the impact of hydrogel application to plant growth parameters. The scope of this review also does not include the use of hydrogels as materials for slow release of nutrients in soil.

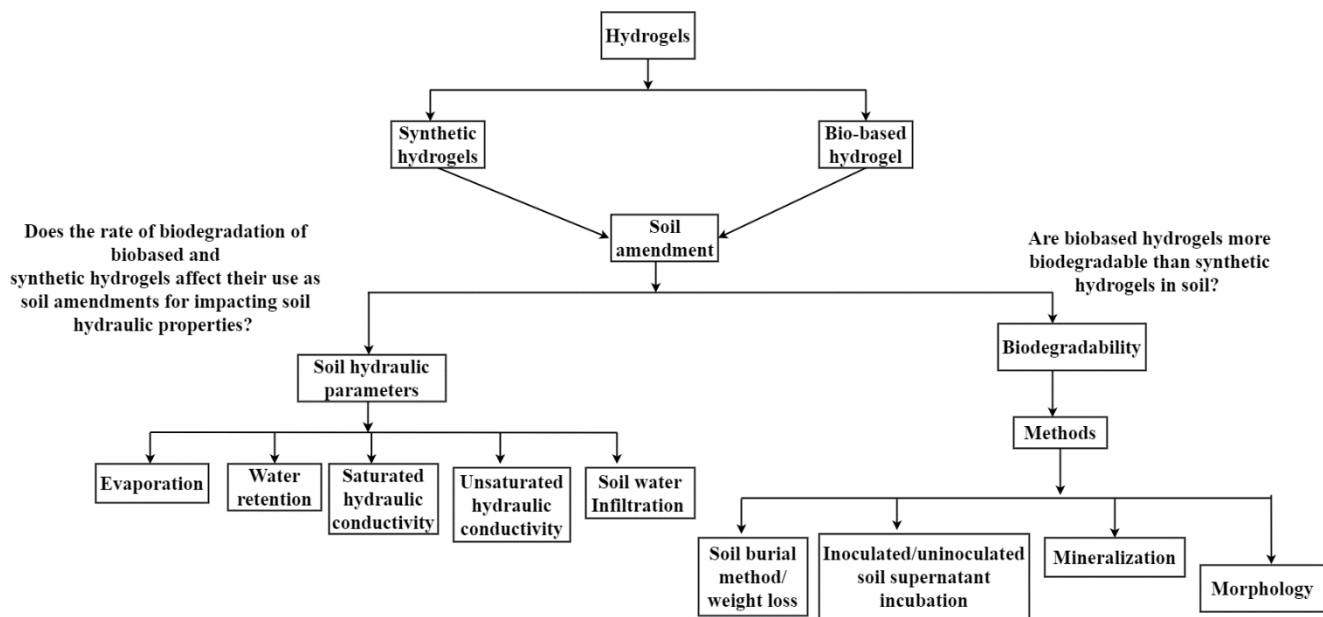


Figure 2.2 Scope of the areas covered in this review.

2.3 Literature Search

This systematic review follows a variation of the method described in Pickering & Byrne (2014) focusing on making the review systematic, quantitative, and critical. This study is systematic since the methods used to survey the literature and select the relevant literature for inclusion are defined and reproducible (Pickering & Byrne, 2014). This study is also quantitative in the sense that it assessed where research has been conducted and identifies research gaps for the future. Finally, papers included were critically evaluated to give an understanding of the current state of this research area. The databases used for the literature search included: Google Scholar, Web of Science, ProQuest and Science Direct. Key words used for the search were a combination of “hydrogel”, “superabsorbent polymers”, “hydraulic conductivity”, “water retention”, “soil water retention curve”, “natural”, “synthetic”, “applications”, “soil”, “hydraulic”, “biodegradability”,

“biodegradation”, “polymers”, “infiltration”, “evaporation”. The reference list of all literature was cross-checked to add relevant papers to the literature database.

This review was limited to papers published from the year 2000 – 2020. A total of 66 papers were included in this review. Relevant papers were included based on the following criteria: the paper was published in English, the paper was peer reviewed, some key words were found in paper, key explanatory and response variables were measured, and finally the paper was original research. Thus, reviews and meta-analysis were not included in the relevant data, even though review papers were a great resource for locating relevant papers and for understanding previous work in this field of study.

The selected articles were entered into a personal database and categorized based on the purpose of the paper, the location of the study, whether it was a laboratory study, greenhouse study or a field study, the soil textures used or compared in the study, the application rate of the hydrogel, the type of hydrogel used, the methodology used, the independent and dependent variables analyzed, the main findings of the paper, limitations, and recommendations of the paper. For the first section of the study, only studies that included the investigation of biodegradation rate and/or extent on hydrogels were included. If a paper merely referred to a synthesized hydrogel as “biodegradable” without any formal experiment to test its biodegradability, that study was not included in this review as it can be misleading and sometimes creates confusion for readers (Hamid, 2000). For the second part of the review, only papers that investigated the impacts of hydrogel on the soil hydraulic properties (soil water retention, soil hydraulic conductivity, soil water infiltration, and soil evaporation) were included.

Another criterion for inclusion was that the water retention of any of the soil textures should be measured using standard methods e.g., pressure plate apparatus, tensiometer, centrifugation, and evaporation method. It was important that the amount of water held by a soil was measured in relation to the change in soil water pressure head of the soil. Studies that merely quantified the water absorption capacity of a hydrogel in water without measuring the change in soil water pressure head were not included in this review.

2.4 Biodegradability of Synthetic and Biobased Hydrogels in Soil

Biodegradation refers to a type of degradation catalyzed by microorganisms leading to the reduction of organic material into carbon, CO₂, water, and new microbial biomass (Grima et al., 2000). Biodegradability is thus the property of a material which allows the materials to undergo biodegradation. Biodegradable materials are organic (i.e., plant and animal matter), derived from living organisms or are synthetic materials similar in nature to plants and animals such that microorganisms can act on them (Tahri et al., 2013). According to Lucas et al. (2008), biodegradation can be divided into four main stages: biodeterioration, biofragmentation, assimilation, and mineralization. Biodeterioration occurs when microbial communities, other decomposers and/or abiotic factors fragment biodegradable materials into smaller pieces (Lucas et al., 2008). Biofragmentation involves the cleavage of polymeric molecules reducing their molecular weights and generating oligomers, dimers, and monomers (Lucas et al., 2008). Assimilation is when energy, new biomass, and other primary and secondary metabolites are produced in the cytoplasm of microorganisms. Finally, mineralization involves the oxidation of simple and complex metabolites into CO₂, N₂, CH₄, and H₂O into the environment (Lucas et al., 2008). Scientists are interested in how polymers biodegrade in soil as the bioproducts of degradation have implications for the environment.

In recent times, there has been a worldwide interest in developing biodegradable polymers especially for agricultural applications (Van Der Zee, 2011). Complete biodegradation of polymers results in the break-down of all the organic components of the

polymers (Zumstein et al., 2018). Zumstein et al. (2018) argue that biodegradation of polymers in soil involves: the colonization of the polymer surface by microorganisms, depolymerization of the polymer into low molecular weight compounds, and the microbial uptake and utilization of these compounds and either incorporating the carbon released as microbial biomass or released as CO₂. The rate of biodegradation of a polymer determines how suitable the polymer can be applied for a specific role i.e., soil water management.

Despite the arguments supporting a shift to biobased hydrogels, few studies have compared the biodegradability of synthetic and biobased hydrogels in agricultural soils. The structure of carbon bonds in materials entering the soil determines the rate at which those materials will be decomposed into soil organic matter. In the same way, the type of carbon bonds in the backbone material used to synthesize a hydrogel will determine the rate at which it degrades in soil if it degrades at all. For example, carbohydrates have linear branched chains which make them easy to break down by soil microbes (Horwath, 2007) compared to lignin. Some biodegradable hydrogels currently investigated by researchers blend or graft hydrophilic monomers/polymers with natural or synthetic polymers such as starch, polylactic acid, chitosan, cellulose, clay (Vudjung & Saengsuwan, 2017) to form hybrid hydrogels which may have an advantage over purely synthetic hydrogels in terms of biodegradability. Others have also synthesized biodegradable hydrogels by cross-linking cellulose derivatives using difunctional molecules as cross-linkers which are capable of binding different polymers into three dimensional hydrophilic networks (Wang et al., 2008). By modifying hydrogels with natural polymers, new materials which are more biodegradable may be produced (Estrada-Villegas et al., 2019).

There are several ways to measure the biodegradability of hydrogels in soil. Biodegradability of hydrogels can be investigated by quantifying the CO₂ efflux from an incubation of soil and the hydrogel, measuring the biochemical oxygen demand (BOD) of the amended soil compared to the natural soil, measuring weight loss through soil burial method (van der Zee, 2005), monitoring the accumulation of microbial biomass, monitoring changes in the physical properties of the hydrogel with time (Hamid, 2000) or by labeling the hydrogel with radioactive ¹⁴C and tracking the ¹⁴C in the CO₂ or CH₄ released from metabolism of the polymer (Van Der Zee, 2011). However, the most common method of investigating the biodegradability of hydrogels in soil is through the soil burial method (Sarmah & Karak, 2019; Sharma et al., 2014; Song et al., 2020; Tanan et al., 2019). The soil burial method involves measuring a known amount of hydrogel and placing it at a depth in soil. Moisture is regularly added to the soil to simulate conditions in the field. After a specific period, the weight loss in the hydrogel is measured and assumed to represent the percentage of biodegradation in soil. While the soil burial and weight loss method are commonly used in literature, there are some limitations to this method. For example, the temperature, pH, and specific microorganisms present in the soil are rarely reported. Since biodegradability in soil is mostly due to the action of soil microorganisms, the temperature, pH, and water content of the soil should be measured and reported as these can help explain the rate of the degradation at the end of a certain period of incubation.

Some researchers have studied the mechanisms by which synthetic polymers may be degraded in soil. Synthetic polymers like polyacrylamides tend to degrade slowly in soil through chemical, photo, biological and mechanical processes i.e., tillage (Sojka et al., 2007) due to their high molecular weights. In terms of biological breakdown of synthetic

hydrogels, Wen et al. (2010) held the view that biodegradation of polyacrylamide/polyacrylate based hydrogels occurred as microorganisms utilized the amide group of the polymer as a nitrogen source and/or the carbon backbone as a carbon source (Xiong et al., 2018). Despite the ability of some microorganisms that utilize the amide groups, the carbon backbone of polyacrylate, which remains after deamination, still poses a challenge to most microorganisms to degrade as it is very recalcitrant (Nyysölä & Ahlgren, 2019). The rate of biodegradation of the carbon backbone depends primarily on physical properties, such as molecular weight and copolymers (Caulfield et al., 2002).

Photodegradation can occur when the C–C, C–H, and C–N bonds in polyacrylamide with bond strengths of 340, 420, and 414 kJ mol⁻¹ are exposed to light with wavelengths of 325, 288, and 250 nm, respectively (Sojka et al., 2007). UV radiation in sunlight at wavelengths below 300 nm usually gets absorbed by ozone, reducing the intensity of the wavelength reaching the earth surface (Sojka et al., 2007). According to Caulfield et al. (2002), the degradation of polyacrylamide by UV radiation results in the formation of other functional groups and a reduction in the molecular weight of the polyacrylamide.

From the studies surveyed, synthetic hydrogels undergo degradation in soil albeit certain conditions accelerate degradation. Smagin et al. (2014) asserts that the main controlling factors determining the biodegradation rate and extent of synthetic based (polyacrylamide and acrylate polymer hydrogels) are composition, soil temperature, and depth of placement of the hydrogel in soil. For practical purposes, prior to the application of synthetic hydrogels, the water absorption capacity should not be the only factor considered. The molecular weight of the hydrogel should be considered and if possible

controlled during polymerization to produce synthetic hydrogels with lower molecular weights. In addition, the abiotic stresses that are likely to exist on the farm in which the synthetic hydrogel is applied should also be considered such as tillage practices, freeze-thaw cycles, hydrodynamic shearing during mixing and application of the hydrogel into the soil (Nyyssölä & Ahlgren, 2019). A farm with frequent tillage, and experiences frequent freeze-thaw will experience higher degradation of hydrogels made from synthetic polymers than fallow fields that are not exposed to frequent freeze-thaw cycles.

Table 2.1 reports a survey of different studies that synthesized hydrogels and measured their biodegradability with the intention of utilizing those hydrogels in soil. Out of 19 studies surveyed, 6 of those studies used synthetic hydrogels made of materials such as polyacrylamide, polyacrylate, potassium acrylate, and polyacrylic acid. Of the 6 studies, 2 studies measured soil biodegradation using the soil burial method (Oksińska et al., 2018; Oksińska et al., 2016). Oksińska *et al.*, (2016) wrapped a dry technical copolymer of acrylamide and potassium acrylate containing 5.28% of unpolymerized monomer of a geotextile and incubated it in soil and reported a 31.7% decrease in mass of the hydrogel after 9 months caused by the colonization and action of *Rhizobium radiobacter* 28SG and *Bacillus aryabhatai* 31SG. A follow-up study by the authors (Oksińska et al., 2018) discovered that the microbes (*Bacillus megaterium* isolate 37SBG and the *Acremonium sclerotigenum* – *Acremonium egyptiacum* complex isolate 25SFG) that colonized the technical cross-linked potassium polyacrylate hydrogel used in their study degraded the hydrogel by 77.9% of the original weight of the hydrogel after 9 months. Wen et al. (2010) showed that biodegradation of polyacrylamide reached 70% of the original amount of polyacrylamide studied after 72 hours in the presence of *Bacillus cereus* and *Bacillus flexu.*

Their study argued that the microorganisms utilized the amide group of the polymer as a nitrogen source while the carbon backbone was used as a carbon source. Results from these studies indicate that with the right microorganism available in soil, some synthetic hydrogels could be as biodegradable as their biobased counterparts.

On the contrary, the three other studies (Bai et al., 2015b; Stahl et al., 2000; Wilske et al., 2014) that measured biodegradability of synthetic hydrogels in soil observed lower biodegradation rates ranging from 0.12 to 7.3%. For example, Stahl et al. (2000) demonstrated a mineralization rate of the synthetic hydrogels (polyacrylamide copolymer and polyacrylate) of 7.3% in 76 days (about 2 and a half months) when the hydrogels were incubated with inoculated sawdust containing white rot fungi (*Phanerochaeta chrysosporium*) in non-sterilized garden soil. Their findings suggest that contrary to the general belief that synthetic hydrogels are non-biodegradable, certain conditions (nutrient sources), when made available enable the fungi and native soil microbes to work synergistically to degrade synthetic hydrogels. There are two pathways that white rot fungi (*Phanerochaeta chrysosporium*) uses to degrade synthetic polymers, i) through the secretion of lignin degrading peroxidases (Sutherland et al., 1997) and ii) through the secretion of cellobiose dehydrogenase (Cameron et al., 2000). While the lignin degrading peroxidases require nutrient limiting conditions to effectively depolymerize synthetic polymers (Sutherland et al., 1997), cellobiose dehydrogenase does not require a nutrient limited condition provided the main carbon source provided externally for the enzyme is cellulose (Cameron et al., 2000).

Using a novel method whereby $^{13}\text{CO}_2$ efflux from ^{13}C -labeled compounds was measured, Bai et al. (2015b) observed that 1.85% of a lower molecular weight polyacrylic

acid hydrogel (molecular weight = 219,500 g mol⁻¹) biodegraded compared to 0.91% of the higher molecular weight polyacrylic acid hydrogel (molecular weight = 530,400 g mol⁻¹) after 149 days (about 5 months). Their results indicate that the biodegradation rate of the polyacrylic acid hydrogel depend on its molecular weight. Thus, for a 50% reduction in initial molecular weight of the polyacrylic acid hydrogel, degradation in soil doubled in extent, although at a low level. They concluded that their results indicate biodegradation mainly occurs at the terminal sites of the bonds in the hydrogel. Their findings are relevant because the molecular weight of the polymer is a parameter that can be controlled to some extent during polymerization. According to Hamid (2000), polymers with long chain-like molecular geometry decrease biodegradation as a larger concentration of the reactive terminal groups decrease with increasing chain length. However, certain enzyme systems, when present in soil, can react with these terminal groups to cause biodegradation even in higher molecular weight polymers (Hamid, 2000).

Similarly, Wilske et al. (2014) employed a system which analyzed the ¹²CO₂ and ¹³CO₂ effluxes from hydrogel samples. Their study investigated the biodegradability of a synthetic polyacrylate hydrogel made from polyacrylic acid. In the study by Stahl et al. (2000), the synthetic hydrogels were degraded up to 7.3% in 76 days when supplemented with certain species of white rot fungi. However, Wilske et al. (2014) added no external inoculum and so the degradation was assumed to come from soil microbes native to the different soil textures (sand, loamy, sand, sandy loam, and loam). Results from Wilske et al. (2014) concluded that the degradation rates did not vary for temperatures between 20-30°C and soil type did not significantly affect degradation rate of the hydrogel. Additionally, the polyacrylate main chain degraded only about 0.12-0.24% every six

months. Results from Wilske et al. (2014) are consistent with Stahl et al. (2000) who showed that mineralization, which is the last stage of degradation, was minimal i.e., 0.35% in 76 days in a co-polymer without any fungi inoculation and source of carbon. This implies that for effective biodegradation of synthetic polymers, white rot fungi along with a source of carbon e.g., sawdust which also serves as a source of metabolic water for the white rot fungi to survive and biodegrade synthetic polymers (Stahl et al., 2000).

The remaining 13 studies shown in Table 2.1 describe studies that either synthesized hydrogels using biobased materials or combined biobased materials with synthetic materials resulting in hybrid hydrogels. In this review, we refer to all hydrogels containing natural polymers as biobased. The most common backbone materials that were used for synthesizing these biobased hydrogels were cassava starch, different variations of cellulose, alginate, and lignin. Cellulose is one of the most common organic materials used for the synthesis of hydrogels because of the presence of several hydroxyl groups which easily form hydrogen bonds creating 3D networks (Hasan & Abdel-Raouf, 2019). Cellulose is highly favored for hydrogel synthesis due to its abundance and the fact that it is a naturally occurring polymer of glucose found as the main constituent of plants and natural fibers (Sannino et al., 2009). Other characteristics that make cellulose suitable for use as hydrogels include the ability of its molecular weight to be easily reduced, lower mechanical strength, and easy chemical alterability (Chen et al., 2019) which makes it easier to break down in soil compared to synthetic materials like polyacrylamide.

Nie et al. (2004) used sodium carboxymethylcellulose (Na-CMC) as the backbone material to synthesize a hydrogel. They varied the amount of cross-linker, antiseptic (antiscorbutic acid) and nutrient (urea) used to synthesize the hydrogel and studied how

those changes affected biodegradation of the hydrogel in soil. They observed that increasing antiseptic amount was detrimental to biodegradation of the hydrogel. Secondly, increasing the nutrient amount increased biodegradation of the hydrogel as the microbes responsible for biodegradation utilized nitrogen for growth and activities. Finally, the biobased hydrogel produced achieved a 50% degradation rate in 60 days, but the degradation rate was dependent on the type of soil i.e., there was higher degradation in sandy soils compared to finer soils. The authors asserted that the larger pores in sandy soils compared to finer soils increased aeration thus enhancing microbial activities. While Nie et al. (2004) attribute a difference in biodegradation of the hydrogel to the soil type, an earlier study (Goheen & Wool, 1991) found no significant difference in biodegradation of a polyethylene-starch blend polymer when applied to silt clay loam, silt loam, and fine sand soils. Since data for the carbon and nitrogen ratio of the soils used by Goheen & Wool (1991) was not reported, it could be argued that the carbon to nitrogen ratio (C:N) of the three soils could be similar which explained why the soil type had no effect on biodegradation. Generally, C:N of soil affects the rate of biodegradation of organic material in soil (Turioni et al., 2021). The lower C:N is, the higher biodegradation rates of hydrogels have been shown by Turioni et al. (2021).

Wang et al. (2008) developed a novel amphoteric hydrogel from carboxymethyl cellulose, acrylic acid, acrylamide and [2-(methylacryloyloxy) ethyl] trimethylammonium chloride using inverse suspension copolymerization. Results from their soil biodegradability test indicated a 43.6% degradation after 100 days using the soil burial method. It appears from these studies that cellulose hydrogels can degrade as fast as 50% in just two months. By inference, it can be assumed that approximately 100% of a cellulose

hydrogel can degrade in less than 7 months especially when used in conjunction with nitrogen fertilizers, since microorganism activity increase with the presence of nitrogen for growth and metabolism (Mašková & Kunc, 1988; Nie et al., 2004). Biodegradation of cellulose in soil is a fairly well understood process and requires the participation of several enzymes (Bisaria & Ghose, 1981). According to Horwath (2007), the enzyme systems known as cellulase composed of endoglucanase, exoglucanase, and β -glucosidase collectively degrade cellulose even though they play distinct roles. Endoglucanases randomly cleave the β (1-4) linkages yielding glucose, then exoglucanases cleave the nonreducing ends of the cellulose chains yielding glucose, cellobiose, and cellotriose. Finally, β -glucosidase hydrolyses the glucose chain into individual glucose subunits.

As seen in Table 2.1, five studies synthesized hydrogels using starch as a backbone material (Riyajan et al., 2015; Sahoo & Rana, 2006; Sarmah & Karak, 2019; Tanan et al., 2019; Vudjung & Saengsuwan, 2017). The highest degradation rate was observed by Riyajan et al. (2015) who reported 80% biodegradation of their hydrogel in 30 days using the soil burial method. Sahoo & Rana (2006) observed that adding starch alone or poly (ethyl methacrylate) in alluvial soil led to lower biodegradation of about 38% and 20% respectively after 12 months of incubation using the soil burial method. The composite of starch and poly (ethyl methacrylate), however, achieved about 50% degradation in 12 months. Riyajan et al. (2015) prepared a biobased hydrogel made up of maleated poly (vinyl alcohol) and cassava starch through a grafting reaction. Their results demonstrated an increase in biodegradation up to 80% in 30 days when the two polymers were used to synthesize hydrogel in the ratio of 6:4. Their result implies that with an increase in starch content of a hydrogel, biodegradation rate and extent increases. While the rapid

degradation of the hydrogels in Riyajan et al. (2015) were assumed to result from the action of bacteria and fungi, there was no formal identification of the causative mechanisms.

Vudjung & Saengsuwan (2017) synthesized three biodegradable hydrogels based on cross-linked natural rubber latex and modified cassava starch and a hybrid using the interpenetrating polymer network method. Their rationale for testing these three versions was because starch has a high biodegradation rate while natural rubber has slow biodegradation rates hence by combining the two polymers, a hydrogel with a moderate degradation rate would be obtained. Their findings reported a degradation extent of 2.6, 96, and 49% in the natural rubber-based hydrogel, cassava starch-based hydrogel and the hybrid (natural rubber/ cassava starch) based hydrogels, respectively after 90 days. Apart from the fact that increasing cassava starch content increased biodegradation, Vudjung & Saengsuwan (2017) observed that biodegradation in the hydrogel decreased as the amount of cross-linker in the hydrogel increased. This observation was earlier confirmed (Roy et al., 2006) who reported that uncrosslinked rubber degraded faster than crosslinked rubber. Roy et al., (2006) hypothesized that excessive crosslinking reduced the volume of the polymer networks which limited microbial access leading to lower biodegradation rates (Vudjung & Saengsuwan, (2017). The practical implication of their results is that optimized crosslinking should be a key variable during hydrogel synthesis as excessive crosslinking slows down biodegradation (Roy et al., 2006; Vudjung & Saengsuwan, 2017) and limits the swelling capacity of hydrogels (Xie et al., 2009).

Tanan et al. (2019) synthesized a biodegradable semi-interpenetrating polymer network (semi-IPN) hydrogel based on cassava starch. Their study reported a degradation extent of 7.89, 17.6, 31.9, 54.7 and 72.7% after 15, 30, 60, 90, and 120 days respectively

indicating a linear degradation rate of the starch-based hydrogel. The authors ascribe the high degradability of the hydrogel to the gradual decrease in network linkages over time in the internal structure of the hydrogel. The hydrogel is hygroscopic and so encourages the growth of microorganisms that metabolize the carbon in the hydrogel. Sarmah & Karak (2019) synthesized a biodegradable hydrogel by reacting starch with acrylic acid with, N – methylene bisacrylamide being the cross-linking agent. Their study tested biodegradation using two methods. They exposed the hydrogel to culture media containing *Bacillus subtilis* and *Pseudomonas aeruginosa* in a 6-week incubation study. The presence of starch in the hydrogel resulted in weight loss of approximately 57% of the original weight of the hydrogel when incubated with both *Bacillus subtilis* and *Pseudomonas aeruginosa* compared to approximately 8% weight loss in a synthetic poly (acrylic) acid hydrogel. Secondly, a soil burial test resulted in 40% degradation of the starch- modified poly acrylic acid hydrogel compared to a <5% weight loss in the poly (acrylic) acid hydrogel alone after 3 months of exposure to soil. Although some studies (Tanan et al., 2019; Vudjung & Saengsuwan, 2017) have shown a higher degradation rate when only starch was used to synthesize hydrogels, Sahoo & Rana et al. (2006) claimed that their composite hydrogel of starch and a synthetic polymer (poly ethyl methacrylate) had a higher degradation rate because it had super porous networks that held more water to aid in the growth of the microorganisms that degraded the hydrogel.

In summary, starch-based hydrogels are easily degradable, and the biodegradation rate of a starch-based hydrogel will depend on the starch ratio present. The higher the starch ratio, the faster the biodegradation. According to Hamid (2000), the availability of functional moieties that can participate in enzyme-mediated biodegradation is an important

requirement for a biodegradable polymer. Thus, the presence of abundant hydroxyl groups in starch is an advantageous property for enhancing biodegradation in soil. In addition to the abundant hydroxyl groups present, starch also possesses some advantageous properties i.e., it is an abundant natural biopolymer, it is renewable, it is economically feasible to obtain, relatively easy and inexpensive to prepare and has a high swelling capacity in water (Ismail et al., 2013). Using starch alone for synthesizing hydrogels could potentially compete with its use as a food source, thus efforts to use other non-food forms of carbohydrate biopolymers such as cellulose should be considered (Galanakis, 2020).

Few studies have investigated the use of lignin for the synthesis of hydrogels for soil amendment. From our review, among all the biobased materials used to synthesize biodegradable hydrogels, lignin hydrogels had the slowest biodegradation rate. Lignin, which forms one of the main components of lignocellulosic plants and is the second most abundant plant polymer after cellulose (Meng et al., 2019b) has been successfully used to synthesize biodegradable hydrogels. Mazloom et al. (2019) synthesized a lignin hydrogel and tested its biodegradation rate. In their study, the microbial inoculum for biodegradation was extracted from dry soil through centrifugation. The inoculum was then added to the hydrogel samples and incubated. The authors' results demonstrated a 6.5% degradation of the hydrogel after 40 days of incubation. Likewise, Passauer et al. (2015) synthesized cross-linked hydrogels made from oxyethylated lignins with the aim of investigating the biodegradation behavior of these hydrogels in soil. By measuring the CO₂ evolved as a final product of biomineralization, the biodegradation of the lignin and oxyethylated lignin in the hydrogels was quantified. After 14 days of incubation, biodegradation ranged from 0.9% - 3.2%. They also found that as the molecular weight of the hydrogel increased due

to the Poly (ethylene glycol) diglycidyl ether (PEGDGE) cross-linking, phenolic OH groups of lignin were less susceptible to microbial oxidation (Kirk & Farrell, 1987). The low degradation of lignin is due to low assimilation of carbon in the hydrogel as soil microorganisms do not utilize the recalcitrant carbon in lignin (Martin et al., 1980). According to Horwath (2007), the dense nature, hydrophobicity, and nonspecific structure of lignin makes it difficult for enzymes to cleave thus lignin must be broken into smaller fragments before extensive decomposition can occur.

This review also noted that alginate-based hydrogels tend to have higher biodegradation rates than lignin-based hydrogels. For instance, Phang et al. (2011) synthesized an alginate-based hydrogel by grafting acrylamide, itaconic acid and acrylic acid onto an alginate backbone. Their results suggested 82.6% degradation of the hydrogel in soil supernatant with nutrient (200 mL of sterile minimum mineral culture medium) added, 82.8% without nutrient added and 63.5% degradation in soil burial test after 40 days. However, the extent of biodegradation in the hydrogels was dependent on the type of soil used to incubate the hydrogel. Song et al. (2020) synthesized a biodegradable hydrogel by cross-linking lignosulfonate with sodium alginate, and kanjaku flour. Biodegradation in the resulting hydrogel was tested using soil burial test. The synthesized biobased hydrogel degraded by 6% of its weight in 60 days and 14% of its weight in 120 days.

Figure 2.3 summarizes some properties of synthetic and bio-based hydrogels that may be considered when deciding to use them as soil amendments. Synthetic hydrogels have a slower degradation rate compared to biobased hydrogels without the addition of any external microorganism or nutrient. The lower degradation rate in synthetic hydrogels is partly due to their long chain-like molecular geometry which reduces the concentration of

reactive terminal groups available for certain microbial enzyme systems to act on (Hamid, 2000). To circumvent this limitation, some specific bacteria (*Pseudomonas putida*, *Enterobacter aerogenes*, *Rhodococcus sp.*, *Helicobacter pylori*, *Bacillus sp.*, *Acinetobacter sp.*, *Azomonas sp.*, *Pseudomonas sp.*, *Chlostridium sp*) and fungi (*Phanerochaeta chrysosporium*) could be inoculated into soil to break down the carbon in some synthetic hydrogels. However, it is still much harder for microorganisms to mineralize the carbon backbone of polyacrylamide-based hydrogels as a sole carbon source due to the lack of appropriate enzymes. On the other hand, the higher degradation rates even without microbial inoculation for biobased hydrogels is due to the type of carbon chains in the backbone materials. Cellulose and starch for example have linear branched chains which make them easy to break down (Horwath, 2007). Juxtaposing the carbon chain structure of cellulose and starch with lignin, which is another form of organic material used for biobased hydrogels, lignin's more complex structure poses a challenge for most microbial organisms to access its carbon. The soil microbial consortium is less effective at degrading lignin hence a lower biodegradation compared to polysaccharide-based hydrogels. This means for any carbon-based material in the form of hydrogel coming into the soil, hydrogel material with more cellulose or starch will have a higher mineralizable rate compared to hydrogels with more lignin.

The difference in rate of biodegradation in the synthetic and biobased hydrogels means that prior to choosing and applying any kind of hydrogel, the specific utility of the hydrogel should be considered. If a hydrogel is meant to be used solely as a water retention material, one option is to synthesize hydrogels that possess properties of both synthetic and biobased hydrogels. Ghobashy (2020) suggests that combining biobased polymers with

synthetic polymers to make hydrogels with increased swelling properties, increased mechanical strength, enhanced biodegradability, and enhanced thermostability of the polymeric network formed.

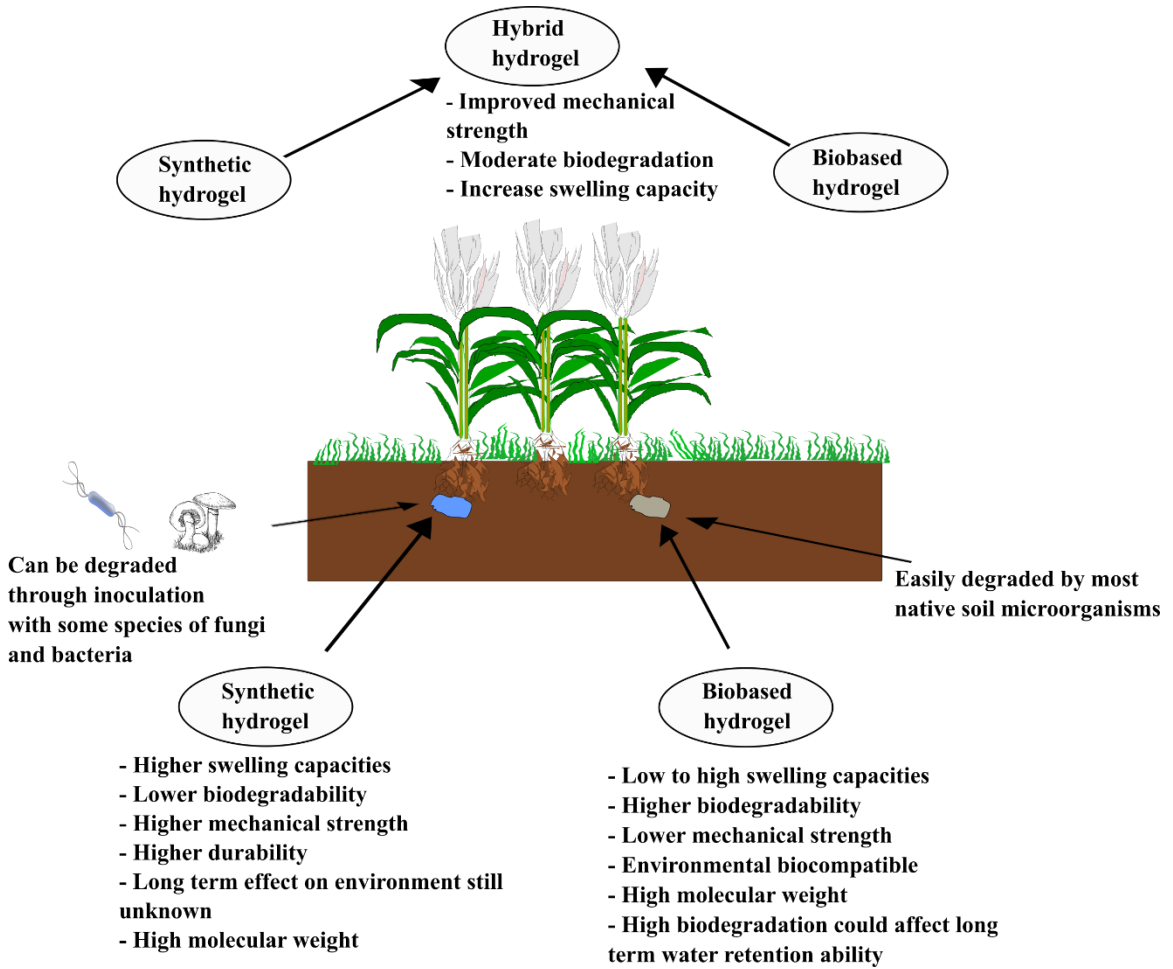


Figure 2.3. Characteristics of synthetic, biobased and hybrid hydrogels for soil amendment.

Table 2.1 shows the various studies reviewed that performed biodegradation tests on hydrogels. Specific information reported includes the types of hydrogels used in the study, the backbone material used to synthesize the hydrogel, the method of testing for biodegradation in the hydrogel, and the extent of biodegradation. Certain abiotic conditions

like temperature, pH, relative humidity, and soil water content are not included in the table because these conditions are mostly not reported despite their being crucial for replication of experiments investigating biodegradability of synthetic and biobased hydrogel

Table 2.1. Synthetic and biobased hydrogels used as agricultural amendments, their main components and biodegradation in soil.

Reference	Type of Hydrogel	Backbone components of hydrogel	Method for testing biodegradation	Extent of biodegradation
1. Stahl et al. (2000)	Synthetic	Polyacrylamide copolymer and polyacrylate	Inoculation with white rot fungi and measuring mineralization	7.3% degradation in 76 days
2. Wen et al. (2010)	Synthetic	Polyacrylamide	Incubation in liquid media inoculated with microorganisms	70% degradation after 72 hours
3. Wilske et al. (2014)	Synthetic	Polyacrylate hydrogel made from poly (acrylic acid).	Measuring efflux from ¹³ C-labelled hydrogel in soil incubations	0.12-0.24% every 6 months
4. Bai et al. (2015b)	Synthetic	Cross-linked polyacrylic acid	Measuring efflux from ¹³ C-labelled hydrogel in soil incubations	0.91% for high MW hydrogel and 1.85% for low MW hydrogel after 5 months

5. Oksińska <i>et al.</i> , (2016)	Synthetic	Technical crosslinked polymer of potassium acrylate and ultra-pure polymer	Soil burial method and measuring weight loss	31.7% degradation after 9 months
6. Oksińska <i>et al.</i> , (2018)	Synthetic	Technical crosslinked polymer of potassium acrylate and ultra-pure polymer	Soil burial method and measuring weight loss	77.9% degradation after 9 months
7. Nie <i>et al.</i> (2004)	Bio-based	Sodium carboxymethylcellulose as the backbone and crosslinking with $AlCl_3$	Enzymatic degradation and soil burial method	50% degradation in 2 months
8. Tanan <i>et al.</i> (2019)	Bio-based	Cassava starch and acrylic acid	Soil burial method and measuring weight loss	7.89, 17.6, 31.9, 54.7 and 72.7% degradation after 15,30,60,90, and 120 days.
10. Vudjung & Saengsuwan (2017)	Bio-based	Cross-linked natural rubber latex and cassava starch	Soil burial method and measuring weight loss	2.6, 96, and 49% for rubber based, starch based and hybrid respectively after 9 days

11. Riyajan et al. (2015)	Bio-based	Maleated poly(vinyl alcohol) and cassava starch	Soil burial method and measuring weight loss	80% degradation in 30 days
12. Wang et al. (2008)	Bio-based	Carboxymethyl cellulose, acrylic acid, acrylamide and [2-(methylacryloyloxy) ethyl] trimethylammonium chloride	Soil burial method and measuring weight loss	43.6% degradation after 100 days
13. Mazloom et al. (2019)	Bio-based	Alkali lignin, NaOH and poly (ethylene glycol) diglycidyl ether	Soil supernatant incubation and measuring weight loss	6.5% degradation after 40 days
14. Passauer et al. (2015)	Bio-based	Lignin, NaOH and poly (ethylene glycol) diglycidyl ether	Incubation in soil and measuring CO ₂ evolution	0.9% - 3.2% after 14 days
15. Sarmah & Karak (2019)	Bio-based	Starch and acrylic acid with N, N – methylene bisacrylamide as cross-linker	Bacteria media incubation and soil burial method and measuring weight loss	40% degradation after 3 months
16. Sharma et al. (2014)	Bio-based	Gum ghatti and methacrylic acid (monomer) using N, N' - methylene-bis-acrylamide as a cross-linker	Soil burial method with physical appearance observation, morphology, weight loss and FTIR spectroscopy	66% and 86% after 2 months

17. Song et al. (2020)	Bio-based	Lignosulfonate, sodium alginate, and kanjaku flour	Soil burial test and measuring weight loss	14% degradation in 4 months
18. Phang et al. (2011)	Bio-based	Acrylamide, itaconic acid and acrylic acid and alginate backbone	Incubation in soil supernatant with and without nutrient addition, direct soil burial, and morphological observation under illuminated stereo microscope.	63.5% degradation in soil after 40 days
19. Sahoo & Rana et al. (2006)	Bio-based	Starch, ethyl methacrylate, benzoyl peroxide as initiator and sodium acrylate as cross-linker	Degradation in activated sludge, degradation in cultured medium and soil burial method.	50% degradation in 12 months.

2.5 Impact of Hydrogels on Soil Hydraulic Properties

In agriculture, hydrogels are used to retain soil water in mostly dry soils. They may also be used to reduce irrigation frequency by serving as temporary storage materials in soils (Saha et al., 2020b). According to Durner & Flühler (2006), soil hydraulic properties refer to the macroscopic interactions between the chemical potential, phase concentration, and transmission behavior of fluids in soil. Soil hydraulic properties are used to quantify the capacity of a soil to store and transmit water (Van Genuchten & Pachepsky, 2011). These hydraulic properties include soil water retention, saturated hydraulic conductivity (K_s), unsaturated hydraulic conductivity (K), soil water infiltration rate, and soil evaporation rate.

2.5.1 Impact of hydrogels on soil water retention

There have been numerous studies that investigated the impacts of hydrogels on the above-mentioned soil hydraulic properties, however soil water retention is the most reported in literature (summarized in Table 2.2). Soil water retention refers to the quantity of water a particular soil can hold for crop use. Soil water retention is often quantified using the soil water retention curve (SWRC). Researchers are interested in how the application of hydrogel affects the SWRC (Figure 2.4) as the results have important agronomic implications for farmers. The SWRC describes the relationship between volumetric water content and the soil water pressure head at a given location in soil (Van Genuchten & Pachepsky, 2011; Wendroth et al., 2018). This curve will be different for every soil type. Due to capillary forces in soil pores and adsorption of water on solid surfaces, soil water

pressure head in soil is typically negative (Van Genuchten & Pachepsky, 2011). As soil water pressure head moves closer to zero, soil water is mostly held by capillary forces and as pressure decreases (becomes increasingly negative) the remaining water is tightly bound in the smallest pores in soil making it difficult for plants to access.

The part of the SWRC that is most relevant for agricultural decision-making is between the field capacity (FC) and the permanent wilting point (PWP) and is known as the plant available water capacity (PAWC). The field capacity of a soil is often described as the amount of water retained by a soil after a rain or irrigation event once drainage has become negligible. The permanent wilting point is the soil water content below which plants wilt permanently (Abedi-Koupai et al., 2008). The field capacity of soil will differ according to soil texture. Coarse soil, like sand, will have a lower field capacity than finer soils like clay. The soil water content available to plant roots is thus defined as PAWC as the difference in field capacity (FC) minus the permanent wilting point (PWP). From Figure 2.4, the soil water pressure head can be represented with an effective pore diameter. Thus, as soil water pressure head decreases, soil water is held by smaller pores. When soil is nearly saturated, water in the soil would be held by pores with average diameters corresponding to 3000 μm (Goss & Ehlers, 2003). As the soil dries and the pressure in the soil approaches the permanent wilting point, water in soil will be held by pores with average diameters corresponding to 0.2 μm (Goss & Ehlers, 2003).

There have been several studies that examined the impact applying hydrogels had on the shape of the SWRC in diverse soil textures. Studies have predominantly reported a statistically significant increased water retention when the hydrogel application was in sandy soils with hydrogel concentrations ranging from 0.1 to 2% (w/w) (Abdallah, 2019b;

Andry et al., 2009; Banedjschafie & Durner, 2015; Bhardwaj et al., 2007; Dehkordi, 2018; El-Tohamy et al., 2014; Montesano et al., 2015).

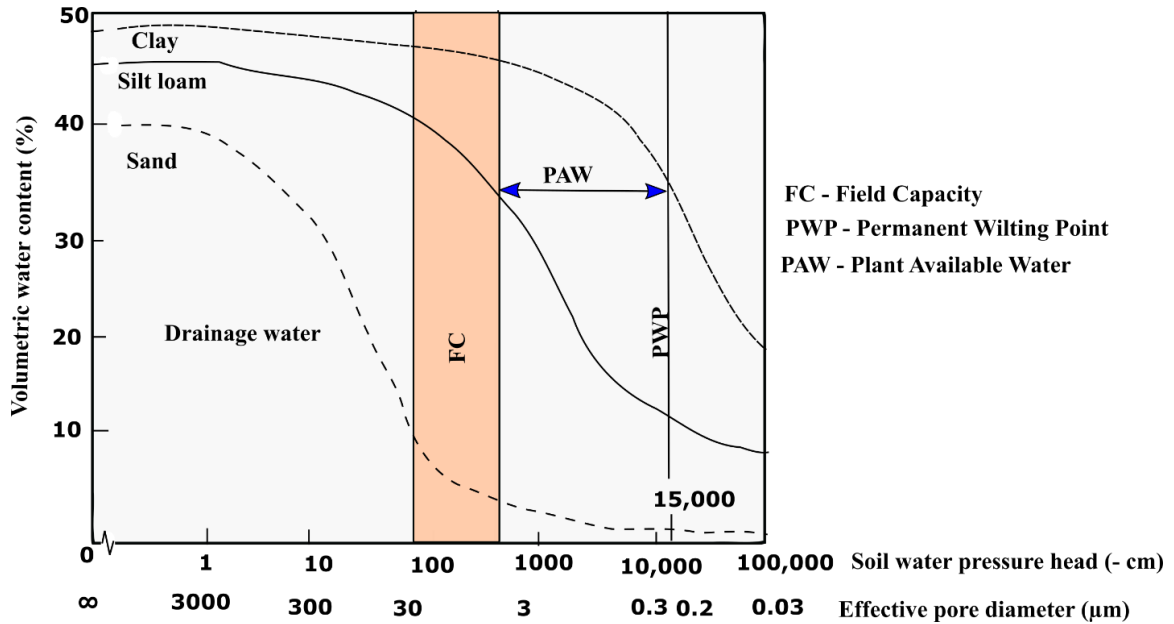


Figure 2.4. Soil water retention curve showing the relationship between soil volumetric water content and soil water pressure head in sand, silt loam and clay soil (redrawn from Goss, (2003)).

Over the last two decades, many studies have investigated the application of hydrogels to soils for the purpose of improving soil water retention, summarized in Table 2.2. The effects of hydrogels on soil water retention were consistent in all the studies reviewed i.e., soil water retention increased in all reviewed studies. Ten studies applied biobased hydrogels to different soils. Six of these studies (Andry et al., 2009; Cannazza et al., 2014; Demitri et al., 2013; Montesano et al., 2015; Narjary & Aggarwal, 2014; Narjary et al., 2012) applied cellulose-based hydrogels to mostly sandy soils and soil water retention increased by a range of 6-500% in the range of soil water pressure head from

saturation to permanent wilting point with a concentration of hydrogels between 0.1 and 1.5% w/w.

For all the biobased hydrogels, soil water retention at a given pressure head increased. However, the increased water retention in (Hu et al., 2019) was attributed to the added polyacrylamide in the hydrogel which indicated that biobased hydrogels can be enhanced by blending them with synthetic hydrogels. The application rate for the biobased hydrogels ranged from 0.1 to 1.5% (w/w). While most of the studies in this review were conducted in lab conditions, among the biobased hydrogel studies, Narjary et al. (2014) conducted a field study and reported an increase of 6-8% in relative available water capacity of a sandy loam soil with a cellulose-based hydrogel concentration of 5 kg ha⁻¹ which was among the lowest increase in soil water retention. With an estimated soil density of 1430 kg m⁻³, this would result in an application rate of 0.0005 % (w/w) in the top 7 cm of soil. An earlier study by the same author (Narjary et al., 2012) reported the highest increase of 400% in moisture content in sandy soil in a lab study with a hydrogel concentration of 0.7%(w/w). These results reflect a disparity between lab tests and field tests of hydrogels where conditions are not controlled, and real-world settings may reduce the efficacies of hydrogels.

Another trend regarding experiments using biobased hydrogels was that 70% of the studies tested the hydrogels on sandy soils. There is a dearth of studies examining the impact of biobased hydrogels on water retention in other soil textures. In addition, most biobased studies use cellulose-based hydrogels which have been shown to work effectively at increasing water retention in soil but biodegrade within a few days to a month. The limited studies using other biobased materials calls for a shift in attention to the less

explored biobased materials like lignin. For instance, only two studies were found from this review that applied a lignin-based hydrogel (Passauer et al., 2011; Song et al., 2020). Passauer et al. (2011) reported a significant increase in soil water content specifically for soil water pressure range between -3 cm and -15,000 cm. At a hydrogel concentration of 0.5% (w/w) which was the highest concentration used, soil water content increased by 14.2% at -300 cm. Song et al. (2020) applied a lignin-based sodium alginate hydrogel and reported an increase of soil water content by 2.98-8.96% at soil water pressure heads of -1000 cm to -15,000 cm. This was similar to the range of soil water pressure head Passauer et al. (2011) observed a 14.2% increase in soil water retention. One reason for fewer studies using lignin hydrogels could be due to lignin's hydrophobic nature, and its complex and heterogeneous structure which makes utilization difficult (Passauer, 2012). However, the presence of numerous hydrophilic functional groups (hydroxyl and carboxyl) on lignin's backbone (Li & Pan, 2010) makes it a suitable candidate for synthesizing hydrogels that could assist in retaining water in soil. The advantage of using lignin is that it can be crosslinked with other materials like sodium alginate to obtain a hydrogel which is biodegradable, non-toxic with high water retention (Song et al., 2020) and is a biological waste with minimal alternative uses unlike starch.

Synthetic hydrogels which are mostly made of polyacrylamide and polyacrylate remain the most widely researched form of hydrogels, (Mikkelsen, 1994). A total of 31 studies applied synthetic hydrogels to mostly two soil textures to test their ability to increase soil water retention (Table 2.2). Thirteen studies applied hydrogels originating from acrylamide/polyacrylamide (Abdallah, 2019b; Abrisham et al., 2018; Akhter et al., 2004; Al-Humaid & Mofteh, 2007; Alkhasha & Al-Omran, 2020; Alkhasha et al., 2018;

Bai et al., 2010; Bhardwaj et al., 2007; Lentz, 2020; Liao et al., 2016; Saha et al., 2020a; Shahid et al., 2012; Zhao et al., 2019b) to mostly sandy soils and sandy loam soils to quantify their soil water retention ability at an application range of 0-1.5% (w/w). The soil water retention increase in the soils amended with acrylamide/polyacrylamide-based hydrogel studies ranged from 0.76-330%. Another six studies (Agaba et al., 2010; Agaba et al., 2011; Bai et al., 2010; Geesing & Schmidhalter, 2006; Leciejewski, 2009; Zhuang et al., 2013) applied polyacrylate based hydrogels mostly to sandy soils at application rates ranging from 0-1% (w/w) which led to a soil water retention increase of 6.2-319%.

The effects of hydrogel on soil water retention seem to be more consistent than for other soil hydraulic properties. However, the impacts have often been significant only for coarse soils i.e., sandy soils. Studies by (Abdallah, 2019; Banedjschafie & Durner, 2015; Montesano *et al.*, 2015, Bhardwaj *et al.*, 2007; Andry *et al.*, 2009; El-Tohamy et al., 2014; Dehkordi, 2018) applied hydrogels at varying concentrations ranging from 0 -2.5% (w/w) to sandy soils. Montesano *et al.* (2015) reported a 400% increase in soil moisture at FC with 2% (w/w) application rate while in Banedjschafie & Durner (2015), the highest water content was observed at an application rate of 1% (w/w). Similarly, Dehkordi (2018) reported a significant increase of 45.5% in saturated water content with a hydrogel application of 0.6% (w/w) and concluded that irrigation needs may decrease by 10-30% with hydrogel treated sandy soil. Studies by Bhardwaj et al. (2007) and Andry et al. (2009) also showed a significant soil water retention after hydrogel treatment to sandy soils.

Studies on the impact of hydrogels on PAWC have been consistent i.e., PAWC increases with increasing application rate of hydrogels but to a larger extent in coarse-textured soils (Narjary et al., 2012). In general, sandy soils hold the lowest PAWC

(Wendroth et al., 2018), hence applying hydrogels to sandy soils may result in higher benefits. With hydrogel application rates of 0, 0.1, 0.2 and 0.4% (w/w), Saha et al. (2020b) observed an increase in PAWC in sandy soil by a factor of up to 3.3% compared to a control treatment. Their study also found that PWP of the sandy soil was delayed by 32 days at the 0.4% hydrogel treatment compared to the control treatment. Their study recommended a 0.1% (w/w) application rate for coarse textured soils and a 0.2% for fine-textured soils, however they only tested a range from 0-0.4% w/w hydrogel.

When soils are saturated, hydrogels in the soil absorb a substantial portion of the water while acting as additional pores for storage of the water. As the soil dries, the stored water is released back into the soil for plant roots (Saha et al., 2020b). Several reasons can be attributed to the ability of hydrogels to retain and release water in the soil matrix. According to Yang *et al.* (2014), the increase in soil water retention with hydrogel application could be due to the strong adsorption and complexing capacities from hydrophilic functional groups, such as hydroxyl, carboxyl, amide, and sulfonic groups from the cross-linking in synthetic hydrogels. Higher soil water retention could also be due to a decrease in median pore diameter with the application of hydrogel (Narjary et al., 2012). Narjary et al. (2012) explains that as pore diameters decrease, smaller retention pores are likely to be found in soil and these pores can hold more water tightly due to the increase in porosity.

2.5.2 Impact of hydrogels on soil hydraulic conductivity

Hydraulic conductivity describes the ability of soil to transmit water (Klute & Dirksen, 1986). Besides increasing water availability in soils, hydrogels have been shown to affect hydraulic conductivity in soil. The effect of hydrogels on saturated hydraulic

conductivity (K_s) has been inconsistent though most studies on soil hydraulic conductivity have focused on K_s . Out of the 14 studies surveyed that investigated the effects of hydrogels on K_s , 9 of the 14 studies indicated a decrease in K_s (Abdallah, 2019b; Alkhasha et al., 2018; Mohawesh & Durner, 2019; Narjary & Aggarwal, 2014; Narjary et al., 2012; Shahid et al., 2012; Smagin et al., 2019; Song et al., 2020; Zhuang et al., 2013), however, three studies (Andry et al., 2009; Hu et al., 2019; Hussien et al., 2012) reported an increase and three studies reported an initial decrease in K_s then a subsequent increase in K_s with time (Bhardwaj et al., 2007; Han et al., 2013; Hussien et al., 2012).

Of the nine studies that report a decrease in saturated hydraulic conductivity, three of them used biobased hydrogels (Narjary & Aggarwal, 2014; Narjary et al., 2012; Song et al., 2020). Narjary et al. (2012) applied a cellulose-based polyacrylate hydrogel at 0, 0.5, and 0.7% (w/w) to different soils in a laboratory PVC column experiment. They reported a 55% decrease of K_s in the sandy soil with the 0.7% (w/w) hydrogel treatment. In a follow-up field study (Narjary & Aggarwal, 2014), the authors observed a decrease of 45% and 60% in hydraulic conductivity in a sandy loam with 2.5 and 5 kg ha⁻¹ application of a cellulose-based hydrogel respectively. Song et al. (2020) applied a lignin-based sodium alginate hydrogel to a sandy-loam soil and observed a decrease of 63.2-89.5% in K_s of a sandy loam soil with an increase in concentration of the hydrogel from 0 to 0.975% (w/w). The three studies that used biobased hydrogels also observed a decrease in K_s in coarse soils. The hypothesis is that due to the high swelling rates of the biobased hydrogels, the hydrogel's expansion in the presence of water reduced the size of drainage pores while causing aggregation of the soil particles which reduced the number of pores available for downward movement of water in soil, thus reducing K_s .

It is worth noting that, despite the evidence for a decrease in K_s when biobased hydrogels are amended to soil, two different studies (Andry et al., 2009; Hu et al., 2019) offer contradictory results. Andry et al. (2009) examined the effects of two hydrophilic polymers (carboxymethylcellulose and isopropyl acrylamide) on the K_s of a sandy soil as affected by temperature and water quality in a temperature-controlled environment. Their results suggested that K_s decreased with an increase in concentration of the two hydrogels. However, they also reported an increase in K_s only when soil temperature was increased to 35°C. The authors also observed that water retention at field capacity reduced due to an increase in temperature from 25°C to 35°C which they hypothesized will be taken by plant roots or lost by percolation. Based on their water retention and K_s measurements, it was thus recommended that to maximize water storage in soil through a decrease in K_s , irrigation should be done early in the morning when temperatures are lower than 25°C specifically for arid regions. The increase in K_s as soil temperature increases is due to a decrease in soil water viscosity (Levy et al., 1988). Similarly, Hu et al. (2019) reported a significant increase in K_s with the application of biobased hydrogels to sandy loam soil. They explain their results by hypothesizing that the hydrogel improved soil structure, decreased bulk density and increased porosity which increased K_s .

While there is convincing evidence that biobased hydrogels reduce K_s , the reduction could be hydrogel dependent. Hence, the specific properties of the hydrogel like the swelling capacity in aqueous solutions and in soil could be the major factors that impact K_s . A biobased hydrogel with a high swelling capacity is likely to decrease K_s as more water is stored in the hydrogels thus reducing water percolating deep into the soil. Comparisons of different types of biobased hydrogels with different properties (swelling

capacities) used under similar conditions (e.g., temperature) will help determine the specific factors influencing K_s .

Much of the evidence for decreases in K_s was found in studies that used synthetic hydrogels. A total of six studies (Abdallah, 2019b; Alkhasha et al., 2018; Mohawesh & Durner, 2019; Shahid et al., 2012; Smagin et al., 2019; Zhuang et al., 2013) using various synthetic hydrogels definitively argue that hydrogels decrease K_s . Four of the six studies applied hydrogels to high sand content soils underscoring the need for more studies using other soil textures. Mohawesh & Durner (2019) observed a significant decrease in K_s by a factor of 3 when a synthetic hydrogel was applied to sandy soil. In a study by Shahid et al. (2012), K_s was reduced by 16%, 36%, 48%, and 53% for hydrogel application rates of 0.1, 0.2, 0.3 and 0.4%, respectively using a poly (Acrylamide-co-acrylic acid) based hydrogel. Zhuang et al. (2013) reported a decrease in K_s by 42.53, 55.45, 87.55, and 96.5% when sodium polyacrylate hydrogel was applied at 0.08, 0.2, 0.5 and 1% (w/w), respectively. The author's explained that, as hydrogel concentration increased, the swelling of the hydrogel decreased the paths available for downward movement of water. Smagin et al. (2019) noticed that partially swollen hydrogels decreased K_s by up to 3.2 times compared to when dried hydrogel was applied which gave 1.4 reduction in K_s . They therefore advised that hydrogels be applied in swollen form to gain full benefits of reduction in K_s . Their recommendation is similar to Wei & Durian (2014) who emphasized that applying hydrogels in a wet state allowed hydrogels to quickly clump together forming reservoirs in sandy soil pores decreasing the downward percolation of soil water.

Abdallah (2019b) applied a polyacrylamide-based hydrogel to a sandy soil at 0 and 0.3% (w/w). Their study showed that K_s was significantly reduced, and the reduction was

dependent on the particle size of the hydrogel. There was a greater (68.8%) reduction when the hydrogel particle sizes were between 0.8 – 1.0 mm compared to hydrogels with particle sizes between 2 – 4 mm (38.9%). Their result implied that hydrogels with smaller particle sizes may be more useful at reducing K_s in sandy soils. It is worth investigating the impact of particle size of biobased hydrogels to understand how particle size impacts K_s , since to the best of our knowledge no study investigates this topic. For the studies surveyed in this review, the particle size distribution of the hydrogels was rarely reported and so there is a question as to the link that particle size distribution of biobased hydrogel has on the impact on soil hydraulic properties.

Other studies using synthetic hydrogels have also reported a decrease in K_s , but the decrease was not consistent with all application rates neither was it true for the entire duration of the study. Han et al. (2013) investigated the effect of different synthetic hydrogel types (Acrylate Sodium Co-polymers (ASC) and Polyacrylamides (PAM)) on K_s . Their results suggest that K_s decreased sharply on initial hydrogel application, but K_s then gradually increased with time. Initially, the swelling of hydrogels led to the blockage of soil pores, but repeated absorption and desorption resulted in a loss of swelling capacity in the hydrogel thus soil pores were unblocked, and K_s increased.

The pressure exerted above the location of a hydrogel can also influence its role in limiting K_s . Bhardwaj et al. (2007) reports an initial decrease of K_s with a subsequent increase due to pressure from the soil above the hydrogel causing it to drain water. Hussein et al. (2012) showed a decrease in K_s (53.68-87.19%) at low concentration of the hydrogel (0.5 and 1%) and an increase (107.6-516.3%) at higher concentration (2%). The authors attribute the decrease in K_s to a reduction in the pore spaces between the soil particles and

aggregates caused by swelling in the hydrogel which blocks movement of water. The authors argue that the higher concentration led to weaker hydrogel soil matrix which was unable to withstand the hydraulic head exerted by the soil above. It could be argued that the influence of synthetic hydrogels on K_s is directly dependent on the residence time of the hydrogel in soil as well as the concentration. The longer the hydrogel stays in the soil the lower its efficacy at reducing K_s . Secondly, as you increase the concentration of the hydrogel, K_s reduces up to a certain threshold concentration at which point K_s starts to increase drastically.

A possible explanation for the contradictory results regarding the effect of both biobased and synthetic hydrogel on K_s could be due to restricted swelling caused by the pressure exerted from the soil layers above the hydrogel in the soil (Saha et al., 2020b). For instance, when hydrogel is placed at a depth below the surface of the soil, it begins to swell by absorbing water into its 3D network. To keep the water absorbed in the hydrogel and at that specific height, the weight of the hydrogel must withstand the weight of soil exerting the downward pressure on the hydrogel. However, with time, the weight of the hydrogel decreases as water gradually moves out of the hydrogel into the surrounding soil due to an increase in matric suction in the soil. At this stage, the ability of the hydrogel to hold onto water now depends on the load applied by the upper layer (Lejcuś et al., 2018; Misiewicz et al., 2019) coupled with the matric suction in the soil. These two forces eventually overwhelm the strength of the hydrogel causing the water to drain out creating additional pores through which percolating water drains thereby increasing the hydraulic conductivity as a result (Saha et al., 2020b).

Like K_s , unsaturated hydraulic conductivity (K) is important for the movement of water in soil, although fewer studies have investigated the impacts of hydrogels on K . A survey of literature found two studies since the year 2000 that measured K after applying hydrogel (Liao et al., 2016; Smagin et al., 2019). Both studies reported a decrease in K with the application of hydrogel. Liao et al. (2016) measured the K of a sandy loam soil when a synthetic polyacrylamide and acrylic acid-based hydrogel were applied at rates of 0, 0.01, 0.03, and 0.06% (w/w). Their results reveal a decrease in K of 85.5 to 94.1% on day 0, 75.1 to 82.9% on day 30 and 65 to 76.2% on day 50. Smagin et al. (2019) noticed that at high matric potentials i.e., > -10 to -15 kPa, K was reduced up to 2-3 times at hydrogel concentrations ranging from 0.01-0.05% (w/w) and a reduction of 10-50 times at 0.1-0.2% hydrogel concentration. However, at low matric potentials i.e., -20 to -700 kPa, K increased with an increase in hydrogel application rate.

In general, when soil is saturated or near saturation, there are plenty of conducting pores for water to move through soil thus an increase in K is observed. Eventually as conditions around the soil become unsaturated and tortuous, a decrease in K is observed. A hydrogel which can retain bound water for a period of time could gradually release the bound water during extremely dry conditions which creates a wider path/increase cross sectional area for the movement of water thus potentially increasing K . Field soils where hydrogels may be applied will mostly be limited by water and constantly be in an unsaturated state hence the importance of more studies investigating effect of hydrogel application to unsaturated hydraulic conductivity.

2.5.3 Impact of hydrogels on soil water infiltration

A hydrogel meant to be used for soil water management could alter soil water infiltration rate. Infiltration refers to the entry of water into soil and subsequent downward movement (Blanco-Canqui, 2017; Kirkham, 2014). Water content, field density, suction head, temperature, rainfall intensity and soil texture all influence soil infiltration rate (Sihag et al., 2018). For example, coarse textured soils have larger pores which allow water to quickly move below the reach of crop roots. A review of literature corroborates a decrease in infiltration rate with an increase in hydrogel application rate (Abrisham et al., 2018; Guo et al., 2019; Lentz, 2007; Reddy et al., 2015; Zhuang et al., 2013). Unlike hydraulic conductivity, studies have mostly agreed that the swelling process of hydrogels fills up the larger pores in soil serving as a barrier to the downward movement of water.

From the eight studies surveyed for this paper shown in Table 2.2, only one study investigated the impact of a biobased hydrogel (Poly- γ -glutamic acid-based hydrogel) on infiltration rate of sandy loam soil (Guo et al., 2019). The remaining seven studies all used either polyacrylamide, polyacrylate or acrylic acid derived hydrogels to apply to soil to study their impacts on infiltration rate of mostly sandy soils. With application rates of 0, 0.08, 0.2, 0.5 and 1% (w/w), Zhuang et al. (2013) observed a decrease in the migration velocity of water into the deep soil layers while also decreasing infiltration rate in sandy soil. Three studies (Guo et al., 2019; Lentz, 2007; Reddy et al., 2015) applied hydrogels at rates ranging from 0-1.17% (w/w) to mostly loam soils. Guo et al. (2019) concluded that hydrogels decreased infiltration volume of water thereby increasing soil water at field capacity. Lentz (2007) emphasized that initially, the added hydrogel may decrease the seepage rate of water by absorbing water and preventing downward percolation, however,

in the long term, it is the change in pore-size distribution of soil by hydrogel amendment that will reduce infiltration. Reddy et al. (2015) compared the infiltration rate of sandy loam soil amended with four different hydrogels. Their study reports a decrease in infiltration rate of 90% in the best performing hydrogel. Hydrogel reduces infiltration rate by altering pore structure (Lentz, 2007; Saha et al., 2020b) of soils especially in sandy soils where bigger drainage pores are reduced to smaller retention pores.

2.5.4 Impact of hydrogels on soil water evaporation

Evaporation refers to a process that occurs when liquid water changes into water vapor and diffuses into the atmosphere (Shuttleworth, 1979). Evaporation is an important process to the earth in terms of the hydrological cycle, for temperature control in warm-blooded mammals and for cooling in industries (Carrier et al., 2016). There are three stages of soil evaporation. Stage 1 is where soil is sufficiently wet, so water is readily available at the surface for evaporation (Rose, 1968). There is a higher evaporation rate in stage one. One reason for this sharp increase is that the soil is saturated, and evaporation begins at the surface of the soil caused by environmental factors like atmospheric temperature, wind speed, and humidity (Idso et al., 1974). During stage 2, evaporation shifts from the surface water to the sub-surface water resulting in the formation of a dry surface layer (Rose, 1968). The soil starts to heat up and the water in the soil profile is unable to move to the surface of the soil fast enough to meet the demands of the evaporation at the surface (Idso et al., 1974). Finally, during stage 3, constant evaporation is seen controlled by absorptive forces acting over molecular distances at the solid-liquid interfaces within the soil (Idso et al., 1974). The rate of water moved is very low at this stage.

There are differences in the drying rates of different textured soils. For example, when stage 2 of the drying process begins, evaporation rates will depend on the energy level of the soil which is also a function of the water retention capacity of soil. Coarse textured soils have large pores, thus through capillary action, the soil beneath the surface dries faster creating a higher tension between soil particles and thin layers of water. This high tension reduces the amount of water that moves up to the surface of the soil, hence decreasing evaporation. While in the case of fine soils, they have a higher water holding capacity and a lower energy level. Thus, during the second stage of drying, there are higher amounts of water available to move to the surface of the soil resulting in increased evaporation compared to sandy soils. Hydrogels can both retain water and reduce evaporation (Table 2.2). One study showed an increase in evaporation with hydrogel application (Guo et al., 2019). However, few studies in literature investigated how the application of hydrogels to soil impacted soil evaporation.

From our review, there was only one study (Guo et al., 2019), that studied the effects of a biobased hydrogel (Poly- γ -glutamic acid-based hydrogel) on evaporation and the only study that argued that hydrogels increased evaporation rate. Guo et al. (2019) tested a poly- γ -glutamic acid-based hydrogel on soil evaporation by filling small round PVC columns with hydrogel-soil mixtures at rates of 0, 0.05, 0.10, 0.15, and 0.20%. The experiment occurred in a constant temperature incubator at 50°C. Evaporation was then measured by the change in mass of the samples every 12 hours. Their results indicate that the poly- γ -glutamic acid-based hydrogel increased cumulative evaporation in soil compared to a control treatment. The authors attributed the increase in evaporation to the

increase in water storage in the soil because of the hydrogel which provides water for the first stage of evaporation to easily occur.

On the other hand, the remaining six studies that investigated evaporation (Alkhasha et al., 2018; Dehkordi, 2018; Taban & Movahedi Naeini, 2006; Yang et al., 2015; Yu et al., 2012; Zhao et al., 2019a) indicated a decrease in soil evaporation with application of different synthetic hydrogels. In a laboratory experiment, Yang et al. (2015) filled a rectangular sand box with a height of 117 cm. A 10 cm soil-hydrogel layer was placed 20 cm below the soil surface and irrigated. After 4 and 9 days of evaporation, water content was highest in the soil-hydrogel layer followed by the bottom layer and the surface layer had the lowest water content. In a similar study by Zhao et al. (2019a), a soil-hydrogel layer of 10 cm was placed at a depth of 10 cm with 10 cm sand above and 40 cm of Sandy loam soil below. Application rates of 0.2, 0.5 and 1% (w/w) significantly decreased evaporative loss with an increased water storage at the 2 and 18 cm depths after 10, 20 and 30 days of evaporation. Two other studies (Yu et al., 2012; Yu et al., 2017) also confirmed the ability of hydrogel-soil mixture to retain more water after drying in an oven at 60°C for 5 hours. Yu et al. (2012) suggested that after applying acrylamide-based hydrogel at a rate of 5 g hydrogel /kg soil, the amount of retained water in the soil increased thus extending the first stage of evaporation.

With these background studies, it can be deduced that hydrogels may alter the drying stages by increasing water storage. By placing hydrogels at a specific depth near the surface of the soil, hydrogels can reduce saturated hydraulic conductivity (Yang et al., 2015) thus, keeping more water in the topsoil for a longer time. This prolongs stage 1 drying since there would still be enough water at the surface of the soil. Secondly, as the

soil profile gradually dries under natural conditions and enters stage 2, hydrogels can intercept the movement of water upwards as some water will be absorbed and kept at the level just beneath the soil surface. The extent of the changes in soil evaporation will however depend on the type and amount of the hydrogel applied.

Table 2.2 Summary of the impacts of synthetic and bio-based hydrogels on soil hydraulic properties.

Reference	Type of study	Soil textures	Hydrogel application rate	Hydrogel used	Water retention	Ks	Soil water infiltration	Evaporation
1. Abdallah (2019b)	Lab and greenhouse	Sandy soil	0.3 and 0% (w/w)	WaterSorb (WS) (Synthetic)	Gravimetric water content increased by 260%	Decreased 38.9-68.8%	N/A	N/A
2. Abedi-Koupai et al. (2008)	Lab	Sandy loam, Loamy, and Clay	2, 4, 6, and 8 g hydrogel/kg soil	PR3005A and Tarawat A100 (Synthetic)	Available water content increased 180% in clay and 220-320% in loamy and sandy loam	N/A	N/A	N/A
3. Agaba et al. (2010)	Greenhouse	Sand, Sandy loam, Loam, Silt loam and Clay	0, 0.2, and 0.4% (w/w)	Luquasorb hydrogel, a powder type of potassium polyacrylate (Synthetic)	Plant available water increased 300% in sand, 200% in silt loam	N/A	N/A	N/A
4. Agaba et al. (2011)	Greenhouse	Sandy soil	0, 0.2, and 0.4% (w/w)	Luquasorb hydrogel, a powder type of potassium	100% increase in retained water in top 25 cm of soil	N/A	N/A	N/A

				polyacrylate (Synthetic)				
5. Akhter et al. (2004)	Potted study in lab	Sandy loam, and Loam	0.1, 0.2 and 0.3% (w/w)	Acrylamide-based hydrogel (Synthetic)	Increased soil water content at field capacity by 17- 46% in sandy loam and 23-50% in loam.	N/A	N/A	N/A
6. Bai et al. (2010)	Lab and potted study	Sandy clay loam	0, 0.05, 0.1, 0.2 and 0.3% (w/w)	Polyacrylate/polyacrylamide-based hydrogels (Synthetic)	Relative soil moisture increased 6.2-32.8%.	N/A	N/A	N/A
7. Cannazza et al. (2014)	Green house potted study	Red soil (Clay soil) and white soil	0, 0.2, 0.5, 1.0 and 1.5% (w/w)	Cellulose-based hydrogel (Biobased)	Increased water retention by 50%.	N/A	N/A	N/A
8. Koupai et al. (2008)	Lab and field study	Sandy loam and Clay	4 and 6 g/ kg soil	Superab A200 (Synthetic)	Available water content increased by 230%.	N/A	N/A	N/A
9. Leciejew	Lab study	Loamy sand	0.02, 0.08, 0.17, and	Potassium polyacrylate-based	Soil water increased by 200-250%.	N/A	N/A	N/A

ski (2009)			0.25% (w/w)	hydrogel (Synthetic)				
10. Liao et al. (2016)	Potted in lab	Sandy loam	0, 0.01, 0.03, 0.06%	Polyacrylamide and acrylic acid- based hydrogel (Synthetic)	Soil water content increased by 2.7- 26.5%.	N/A	N/A	N/A
11. Montesano et al. (2015)	Lab study	Sandy soil	0, 0.5, 1 and 2% (w/w)	Cellulose- based hydrogel (Biobased)	Increased soil water content at FC by 400%.	N/A	N/A	N/A
12. Sarmah & Karak (2020)	Lab study	Silty and Sandy	0.1 and 0.25%	Starch based hydrogel (Biobased)	Water holding capacity increased by 120%	N/A	N/A	N/A
13. Saha et al. (2020a)	Lab study	Fine sand, Silt loam and Clay	0, 0.1, 0.2, and 0.4% (w/w)	Stockosorb, acrylic-based polymer with acrylamide cross-linking. (Synthetic)	Plant available water capacity increased by 120- 330% in fine sand.	N/A	N/A	N/A
14. Abrisham et al. (2018)	Field study	Sandy loam	0 ,1, and 3 g hydrogel/ dm ⁻³ of soil	Stockosorb, an acrylamide/a crylic acid copolymer potassium	Available water content increased by 21.5%.	N/A	Soil water infiltration decreased by 21.5%.	N/A

				Salt. (Synthetic)				
15. Bhardwaj et al. (2007)	Lab study	Sandy soil	0, 0.5, 2.5, and 5.0 g hydrogel /kg of soil.	Cross-linked acrylamide or acrylic acid copolymers (Synthetic)	Increased	Decreased then an increase with time	N/A	N/A
16. Andry et al. (2009)	Lab study	Sandy soil	0 , 0.1, and 0.2% (w/w)	Carboxymeth ylcellulose (biobased) and isopropyl acrylamide (Synthetic)	Available water content increased by 400-500%	Increased	N/A	N/A
17. Lentz (2020)	Potted study and lab study	Degrad ed calcare ous Silt loam	0.25 or 0.5% dry weight (5.6 or 11.2 Mg ha ⁻¹)	Polyacrylami de copolymer and polyacrylic acid- potassium salt hydrogels. (Synthetic)	Plant available water increased by 42%.	N/A	N/A	N/A
18. Shahid et al. (2012)	Lab study	Sandy loam soil	0.1, 0.2, 0.3 and 0.4% (w/w)	Poly (Acrylamide- co-acrylic acid)/AlZnFe 2O4	Water retention at field capacity increased by 60- 100%.	Decreased by 16- 63%.	N/A	N/A

				nanocomposite hydrogels (Synthetic)				
19. Hayat & Ali (2004)	Lab and potted greenhouse study	Sandy loam	0,0.25,0.5,0.75,1.00, 1.25, and 1.50% (w/w)	Aquasorb (Synthetic)	Soil moisture content increased by 30-850%	N/A	N/A	N/A
20. Yu et al. (2012)	Lab	Loamy sand, Sandy Loam, Sandy clay loam and Clay loam	0.5% (w/w)	WOTE, GNKH, PR3005S, and BJ-210 IXM (Synthetic)	Water absorption capacity increased by two orders of magnitude.	N/A	N/A	Decreased evaporation up to 338% after 7 hours of drying.
21. Banedjshafie & Durner (2015)	Lab	Sand	0, 0.3, 0.6, and 1% w/w	Superab A200 (Synthetic)	Plant available water increased by %5500	N/A	N/A	N/A
22. Baran et al. (2015)	Lab	Loamy sand and Sand	0, 0.2, 0.6, 1%, and 2% (w/w)	AgroaquaGel (Synthetic)	Increased maximum water capacity by 32-69%.	N/A	N/A	N/A

23. Demitri et al. (2013)	Lab and greenh ouse	Red soil	0.2, 0.5, and 1% (w/w)	Cellulose- based hydrogel (Biobased)	Increased	N/A	N/A	N/A
24. Geesing (2006)	Lab	Loam, Silty clay loam and Sandy loam	0, 1, 3, or 5 g/L of soil	Sodium polyacrylate (Synthetic)	Increased only at rate > 3g/L	N/A	N/A	N/A
25. Hu et al. (2019)	Lab	Sandy loam	0, 2 and 4 (t /ha)	Biomaterials and polyacrylami de (Synthetic and biobased)	Soil water content increased by 12.1- 23.4%.	Increased 91-122%.	N/A	N/A
26. Dehkordi (2018)	Green house study	Sandy soil	0,0.20, 0.40 and 0.6% (w/w)	Superab A20 0 (Synthetic)	Soil water retention increased 175-375%.	N/A	N/A	Evaporatio n rate decreased by 80% on the third day.
27. Narjary et al. (2012)	Lab	Sand, alluvial Sandy loam, red	0, 0.7, and 0.5% (w/w)	Pusa, a polyacrylate cellulose-	Soil water content increased by 400% in sandy soil at soil	Decreased by 118, 708, and 95% in sand, red	N/A	N/A

		Sandy loam and black Clay		based hydrogel. (Biobased)	pressures of 10-100kPa.	sandy loam and alluvial sandy soil respectively.		
28. Narjary & Aggarwal (2014)	Field*	Sandy loam	0, 2.5, and 5 (kg /ha)	Pusa, a polyacrylate cellulose-based hydrogel. (Biobased)	Plant available water capacity increased by 6-8%.	Decreased 45-60%	N/A	N/A
29. Salim (2015)	Lab and field	Sandy loam	0, 4, 8, and 12% (w/w)	Sky Gel, copolymer of acrylic acid and sodium acrylic acid (Synthetic)	Water holding capacity increased by 63.2-302.8%.	N/A	N/A	N/A
30. Špitalnik et al. (2019)	Lab	Coarse sand, Loamy sand, and Sandy loam		Water absorbent geocomposite (Synthetic)	Soil water retention increased by 54.8-191.6%.	N/A	N/A	N/A
31. Zhao et al. (2019b)	Lab	Sandy loam	0,0.1, 0.2, 0.5, and 1% (w/w)	Acrylamide - based hydrogel (Synthetic)	Soil water content increased by 0.76-3.74%.	N/A	Mean infiltration rate decreased	N/A

							by 9-51.5%.	
32. Alkhasha et al. (2018)	Lab	Loamy sand	0, 0.2, 0.4, 0.6, and 0.8% (w/w)	PagriSap (polyacrylamide-based hydrogel) (Synthetic)	Soil moisture increased by 2.49-5.53%.	Decreased 31.4-71.4%.	Cumulative infiltration increased from 9.32-21.87%	The 0.2% treatment decreased cumulative evaporation by 10.77% while 0.4-0.8% decreased cumulative evaporation by 6.87-14.86%.
33. Alkhasha & Al-Omran (2020)	Lab	Sandy loam	0, 0.2, 0.4, 0.6, and 0.8% (w/w)	PagriSap (polyacrylamide-based hydrogel) (Synthetic)	Soil water content increased by 3.3%.	N/A	N/A	N/A
34. Al-Humaid & Moftah (2007)	Field	Sandy soil	0.1%, 0.2%, 0.4% or 0.6% (w/w)	Stockosorb K400, a cross-linked polyacrylamide (Synthetic)	Soil water content increased by 13.3-300%.	N/A	N/A	N/A
35. Zhuang	Lab	Sandy soil	0, 0.08, 0.2, 0.5 and 1%	Sodium polyacrylate (Synthetic)	Maximum water supply quantity	Decreased by 42.53 – 96.5%.	Decreased	N/A

et al. (2013)					increased by 45.61-318.89%.			
36. Song et al. (2020)	Lab	Sandy loam soil	0, 0.375, 0.650, 0.975% (w/w)	Lignin-based sodium alginate hydrogel (Biobased)	Maximum water holding capacity in soil increased by 2.98-8.96%	Decreased 63.2-89.5 %	N/A	N/A
37. Passauer et al. (2011)	Lab	Coarse silica	0, 0.1, 0.25, and 0.5% (w/w)	Lignin-based hydrogel (Biobased)	Soil water content increased by 300- 400%.	N/A	N/A	N/A
38. Kashkuli & Zohrabi (2013)	Lab	Sandy soil	0, 0.03, 0.06, 0.08, 0.2, and 0.4% (w/w)	Super AB A200 and Herbasorb (Synthetic)	Soil available water increased 350 and 320%.	N/A	N/A	N/A
39. Sivapalan (2001)	Lab	Sandy	0, 0.03 and 0.07 % (w/w)	ALCOSORB ® 400 (anionic acrylic copolymer) (Synthetic)	Soil water retention increased 23 and 95%.	N/A	N/A	N/A
40. Han et al. (2013)	Lab study	Sandy loam	ASC or PAM in soil at a mass ratio of	Acrylate Sodium Co- polymers (ASC) and Polyacrylami	N/A	Decrease then an increase with time	N/A	N/A

			1:2,000 (SAP:soil).	des (PAM) (Synthetic)				
41. Hussein et al. (2012)	Lab	Sandy and Sandy clay loam	0.5, 1.0 and 2.0% (wt/wt)	Poly (acrylic acid)-co- acrylamide hydrogel (Synthetic)	N/A	Decreased by 53.68- 87.18% with lower rates (0.5 and 1%) and an increase by 107.6- 516.3% at 2%	N/A	N/A
42. Smagin et al. (2019)	Lab	Silty sand	0.01 to 0.3 % (w/w)	Technical polyacrylamide (PAA) hydrogel and a co- polymer of acrylamide and (sodium acrylate (Synthetic)	N/A	Decreased by 200- 800%.	N/A	N/A
43. Mohawes h & Durner (2019)	Lab	Sandy soil	0.1, 0.25, and 0.5% (w/w)	Luquasorb (Synthetic)	Soil water content increased up to 86.9%	Decreased by 300%	N/A	N/A
44. Guo et al. (2019)	Lab	Sandy loam	0, 0.05, 0.10, 0.15, and 0.20% (w/w)	Poly- γ - glutamic acid-based	Soil water content at FC increased by 8.7-58.3%.	N/A	Cumulativ e infiltration decreased	Cumulative evaporation increased

				hydrogel (Biobased)			32.4- 52.0%.	17.1- 25.3%.
45. Lentz (2007)	Lab	Silt loam, Loam, Loamy sand, and Clay loam	0, 0.25, and 0.5% (w/w)	Polyacrylami de hydrogel (Synthetic)	N/A	N/A	Decreased infiltration by 84- 97%.	N/A
46. Reddy et al. (2015)	Lab	Sandy loam	0, 0.25, 0.75, 1.25 and 1.75%	RDW-W, RDW-I, RDW-W and RDW-F (Synthetic)	N/A	N/A	Maximum reduction of 90% in steady state infiltration .	N/A
47. Yang et al. (2015)	Lab	Sand, loam, Silt	0.6% (w/w)	Acrylic sodium copolymer (Synthetic)	N/A	N/A	Decrease and increase	Decreased
48. Zhao et al. (2019a)	Lab	Sandy loam	0, 0.2, 0.5 and 1% (w/w)	Polyacrylami de and acrylic acid- based hydrogel (Synthetic)	N/A	N/A	N/A	Decreased by 0.3-14% at 20 cm on day 30.

49. Taban et al. (2006)	Lab	Loam and Loamy sand	0.14 and 0.7% (w/w)	Aquasorb PR3005A, a salt copolymer polyacrylamide (Synthetic)	N/A	N/A	N/A	Decreased about 31.25% after 2500 hours.
----------------------------	-----	---------------------	---------------------	---	-----	-----	-----	--

2.5.5 Summary of how hydrogels influence soil hydraulic properties

Figure 2.5 conceptually illustrates how hydrogels may impact the reviewed soil hydraulic properties. When rain falls or soil is irrigated, infiltration is initially high and water percolates into the soil profile making it available to plant roots until the soil becomes saturated, and infiltration stops. Near the roots of the plant, hydrogels swell by absorbing water. As the soil becomes dry and soil water pressure head decreases, the water absorbed by the soil is slowly released into the soil matrix making it available for plant roots to use. Some water also leaves the soil into the atmosphere through evaporation.

Within large pores of soil, the swollen hydrogel could prevent the downward flux of water thus decreasing K_s . However, the soil water pressure head eventually increases, and soil pores gradually become air filled, the flow path of water becomes tortuous as drag forces between the water and soil phase increases (Van Genuchten & Pachepsky, 2011). Assuming hydrogels can retain water in saturated conditions and release that water when soil water pressure head decreases, then it is expected that the gradual release of water from the hydrogel creates a less tortuous path for water flow hence potentially increasing unsaturated hydraulic conductivity.

A noteworthy trend from this review is that, as soil water retention increased because of the application of both biobased and synthetic hydrogels, K_s decreased. This trend was noticed in 83% of the studies that measured the effects of hydrogel on both soil water retention and K_s . The increase in soil water retention ranged from 0.76 – 318.89% while the decrease in K_s ranged from 9-708%. This trend implies that as the hydrogel swells and holds water at the position of the soil profile where it is placed, movement of water is limited as the swollen hydrogels occupy the drainage pores thus decreasing K_s . Another

trend worth mentioning is that as soil water retention increased with application of hydrogel, cumulative evaporation decreased in 3 out of 4 studies that quantified both soil water retention and cumulative evaporation. However, this trend may only be valid if the hydrogel is positioned strategically at a location below the surface of the soil. When placed near the soil surface, soil water retention increased accompanied by increased cumulative evaporation (Guo et al., 2019) since the swollen hydrogel provides a larger concentration of water which increases the concentration gradient between the soil surface and the atmosphere for evaporation of water.

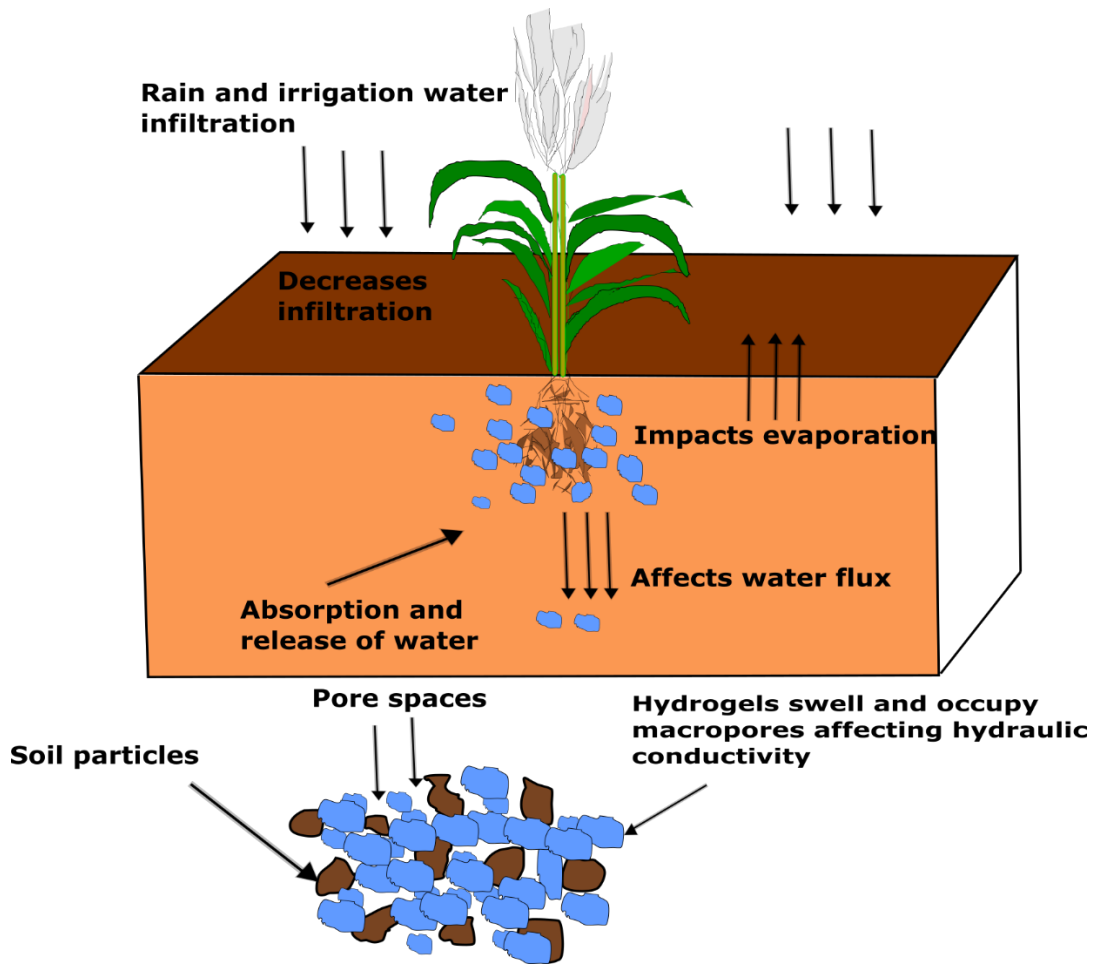


Figure 2.5. Conceptual diagram describing the impact of hydrogel on different soil hydraulic parameters, (redrawn and modified from Saha et al. (2020b))

2.6 The “Ideal” Hydrogel for Improving Soil Hydraulic Properties

While it is impossible to synthesize an “ideal” hydrogel, the following are some properties of hydrogels that may enable them to efficiently improve soil hydraulic properties when applied to soil:

1. Stability of hydrogel in soil should be at least 5 months and at most a year. The stability of the hydrogel depends on its biodegradability. The more biodegradable it is, the less stable it is in soil. For example, a hydrogel that is made entirely of

starch will be less stable than one made with synthetic materials or lignin. Starch, being a hydrophilic polymer, swells with water repeatedly with time. The presence of water and readily available carbon increases microbial activity which increases biodegradation leading to the breakdown of the network linkages in the hydrogel (Tanan et al., 2019). One way of circumventing the high degradation is to keep the starch content below 30% when blending the hydrogel with synthetic materials. A study by (Goheen & Wool, 1991) indicated that a starch content of 67% in a polymer blend with low-density polyethylene led to higher degradation in soil (56% degradation in 240 days) compared to a starch content of 29% which led to a slower degradation (13% degradation in 240 days). Previous studies by (Majeed et al., 2017; Majeed et al., 2016) show the biodegradation of starch could be impeded by reinforcing starch films with 10% lignin. They explain that lignin impedes the action of starch degrading enzymes like α and β - amylase through non-productive binding on lignin. This non-productive binding obstructs the starch-degrading enzymes from attacking the α 1-4 glycosidic linkages which are usually broken during degradation hence increasing the resistance of starch to degradation. The practical implication of the results from (Majeed et al., 2017; Majeed et al., 2016) is that polysaccharide-based hydrogels could be blended with lignin to produce hydrogels that are moderately biodegradable increasing their time to positively impact soil hydraulic properties. The practical use of a specific hydrogel should however be considered in making a judgement as to the need for stability. That judgement could be made based on the specific crop and the growing season of the geographical area in which the crop is grown. For longer growing seasons e.g., > 5

months, a hydrogel with less starch and higher synthetic material may be preferred while in a growing season < 5 months, a higher blend of starch could be preferred. The lack of a standard biodegradation rate and quantification method for bio-based and synthetic hydrogel makes it challenging to prescribe an ideal hydrogel. Hamid (2000) suggests that pending the standardization of a “reasonable” rate of biodegradation for polymers, biobased polymers have been suggested due to the argument that they are more environmentally acceptable.

2. Swelling capacity of a hydrogel in aqueous solutions and in soil is an important indicator of performance. The swelling capacity of a hydrogel enables the hydrogel to absorb and expel water from its environment (Blanco et al., 2013). From this review, the swelling capacity of a hydrogel directly affects all the soil hydraulic properties discussed. Since hydrogels will have to be in the presence of soil to influence soil hydraulic properties, it is worth quantifying the swelling capacity of the hydrogel when confined in soil. As shown in section 5 above, a hydrogel with a higher swelling capacity will absorb more water in soil which increased water retained in the soil. The increase in surface area of the hydrogel with swelling also impeded the downward movement of water thus decreasing hydraulic conductivity and soil water infiltration. Higher swelling in hydrogels also leads to higher water storage which reduces evaporation when placed at an appropriate depth in soil.
3. Swelling characteristics when confined under soil pressure impacts hydraulic properties. An ideal hydrogel should be able to withstand the pressure exerted by the surrounding soil. Hydrogels should be designed to be able to absorb water causing it to swell, changing the shape, mass, and volume of the hydrogel in the

process, even at depth within the soil. According to Misiewicz et al. (2020), during swelling of hydrogels, the hydrogel-soil mixture exerts pressure on the top layer of the soil. Due to this pressure exerted by the hydrogel during swelling, the hydrogel can repeatedly absorb and release water in soil against the pressure exerted by the soil. Misiewicz et al. (2020) further explains that the cause of the pressure exerted by the hydrogel during swelling depends on the available pore capacity and the grain size distribution of the hydrogel. Similarly, Louf et al. (2021) recently demonstrated that in a three-dimensional granular medium e.g. soil, the extent of swelling in a hydrogel depends on the antagonistic competition between the force exerted by the hydrogel osmotic pressure and the force exerted by the surrounding soil. While these studies (Louf et al., 2021; Misiewicz et al., 2020; Misiewicz et al., 2019) tested the swelling behavior of synthetic hydrogels (polyacrylamide and acrylate-based) hydrogels, there are currently no studies that examine these questions using biobased hydrogels. It is possible that differences in the mechanical strength between biobased and synthetic hydrogels could influence the pressure the hydrogel can withstand in soil. According to Ahmed (2015), synthetic hydrogels possess a higher mechanical strength than biobased hydrogels, which could be advantageous in withstanding pressure. The challenge thus lies in synthesizing hydrogels with optimized mechanical strength with improved elasticity that allows the hydrogel to swell.

2.7 Future Research Needs

Here are the outstanding questions that need to be addressed in relation to the application of biobased hydrogels to soil as an amendment.

1. More studies are needed to understand how the particle size distribution of biobased hydrogels affects soil hydraulic properties. From this review, only one study Abdallah (2019b) tested the impact of particle size of a synthetic polyacrylamide hydrogel on soil water retention properties. However, to better understand how new biobased hydrogels could be tuned to improve certain soil properties, it is important to quantify the specific particle size ranges. Investigators can then start to determine the relationship between particle size and the hydrogel's ability to swell in soil which has been shown to affect several hydraulic properties like soil water retention and hydraulic conductivity.
2. The particle density of hydrogels can affect soil physical properties like porosity and bulk density which in turn affects how water moves through soil. Studies that investigate how the particle density of various hydrogels affect soil physical properties will help in the development of hydrogels with specific properties that improve soil hydraulic properties.
3. Most studies tend to test the effects of hydrogel on sandy soils. Though the impacts of hydrogel application to finer soils like clay and silt are currently not definitive, there is value in investigating the impact of hydrogels over a large application range.
4. There are currently limited studies that compare the impacts of both synthetic and biobased hydrogel applications on the distribution and metabolism of microorganisms in soil. The degradation of hydrogels may lead to the formation of byproducts which may influence the type of microorganisms in a particular soil as some microorganisms rely on carbon for metabolic activities.

5. Most studies in literature currently apply hydrogel in powdered or granular form by mixing with soil. More research into different application methods to ascertain the effectiveness of those methods, e. g. spraying in liquid form, applying hydrogels in swollen form, or applying hydrogels in dry solid form is needed. Some investigators suggest that the hydrogels should be applied after they have been swelled. Studies are needed to quantify the benefit of applying swollen hydrogels and, if useful, to determine how to effectively apply swollen hydrogels.
6. There are limited studies on the impacts of hydrogels on soil unsaturated hydraulic conductivity (K). Most studies concentrate on the effects of hydrogels on saturated hydraulic conductivity and in laboratory experiments, likely due to the ease of measuring K_s compared to K . However, under field conditions, soils will mostly be unsaturated thus more research is needed to understand how hydrogels affect K .
7. An almost unexplored area is the use of hydrogels to manage drainage, i.e., to remove excess water from the plant root zone. While artificial subsurface drainage may be installed to remove excess water from poorly drained soils (Franzmeier et al., 2001), could hydrogels be placed beneath the surface of soil at a specific depth to absorb water from heavy rains and subsequently release the water back during dry periods? To fill this gap in our knowledge and test the potential capabilities of hydrogels as drainage materials, more field applications of hydrogels are needed in addition to real simulations of rainfall in the field.

8. When hydrogels are applied to soil, the surrounding soil tends to exert a force against the hydrogel, hence reducing the hydrogel's swelling capacity. Research is needed to design hydrogels that can withstand the various biotic, abiotic, and mechanical stresses that soil exerts on hydrogels over at least one growing season.
9. The degradation of both synthetic and biobased hydrogels can eventually lead to carbon sequestration. However, there is limited data to quantify how much of the carbon from biodegradation of a hydrogel is eventually converted into soil organic matter. Hence, quantification of the long-term impacts of hydrogels on soil carbon sequestration is needed to confirm the suitability of hydrogels as long-term soil amendments for carbon sequestration.
10. Research is needed to quantify the effects of hydrogels on soil greenhouse gas emissions. Depending on the constituents of a particular hydrogel, increased carbon dioxide (CO₂), nitrous oxide (N₂O) or methane gas (CH₄) emissions may be unintended consequences of hydrogel soil augmentation.
11. This review raises important questions. To understand the underlying physical chemistry at work in the soil/hydrogel system, investigators should be collecting data on all the parameters that impact soil physical properties and biodegradation. For example, a standard should be developed by the hydrogel research community that lays out protocols for quantifying biodegradation rate and extent, and listing what other properties would constitute a complete data set along with standard protocols to collect those meta-data. Only by having data that is comparable across laboratories will progress be made in understanding the underlying mechanisms at

work. With complete data sets we can begin to unravel the contradictory or inconclusive studies.

12. Once a complete data set is established, a predictive mathematical model can be developed to summarize our understanding of the effects of the various properties on soil hydraulic properties and biodegradation. For example, can we predict the concentration of hydrogels that when applied to a specific soil decreases/increases K_s ? This information will increase the usefulness of this knowledge so, for example, farmers know the amount of hydrogel to be applied when a particular soil is used to grow a crop. Secondly, if that range of suitable hydrogel application is obtained, is it system dependent e.g., hydrogel type, soil type, climate, soil temperature or can that recommended range be generalized to all hydrogels and soil types?

2.8 Summary and Conclusion

This systematic review of available literature within the past two decades elucidates the impacts of various synthetic and biobased hydrogels on soil hydraulic properties. The biodegradability of synthetic hydrogels compared to biobased hydrogel was also critically examined. Knowledge of the biodegradability of a hydrogel is important when it is to be applied to soil as an amendment. Due to the increased interest in environmental sustainability, the research community is moving away from synthetic hydrogels and experimenting with biobased hydrogels as they are claimed to be more biodegradable and biocompatible.

1. This study indicates that there are several ways of measuring biodegradability of hydrogels in soil, but the most common method is the soil burial method because it is the easiest and least expensive method to conduct. However, a disadvantage of the soil burial method is that biodegradation is determined only based on the weight loss of the hydrogel and there is usually no further information about the specific group of microorganisms that may be causing the biodegradation in soil except when the soil used is sterilized and specific microorganisms are inoculated to degrade the hydrogels. Another major challenge is the lack of standardized methods to measure biodegradation in soil. Standardization can be achieved when the abiotic and biotic conditions considered for determination of biodegradation of a hydrogel for example, the temperature, pH, moisture content, relative humidity, and enzyme availability of a soil used for biodegradation experiments are specified where possible. These parameters will help future researchers easily replicate experiments and contribute to existing theories regarding the biodegradability of synthetic and biobased hydrogels in soil.
2. In comparing the biodegradability of synthetic hydrogels to biobased hydrogels, this review reveals that contrary to the widely held notion that synthetic hydrogels are not biodegradable, some polyacrylate and polyacrylamide-based hydrogels do undergo degradation in soil (varied from 0.12% to 77.9%) within the first year. Nevertheless, certain conditions must be present to make the degradation faster in soil such as inoculation with specific bacteria (e.g., *Bacillus cereus* and *Bacillus flexu*) and fungi (*Phanerochaeta chrsosporium*). Since most synthetic hydrogels have a high molecular weight, the rate of biodegradation will depend on the ability

of microorganisms to gradually breakdown the recalcitrant carbon backbone which makes up most synthetic hydrogels.

3. The review also finds that most biobased hydrogels (cellulose, starch, alginate, lignin) can degrade in soil rapidly compared to synthetic hydrogels (0.9% to 86%) within the first 90 days without inoculation which is an advantage over synthetic hydrogels which require inoculation to reach those levels of biodegradation.
4. Both synthetic and biobased hydrogels were effective at increasing soil water retention when applied within a range of 0.1 to 1% hydrogel (w/w). Though the increase in water retention was definitive in sandy soils, few studies tested other soil textures.
5. The impact of hydrogels on saturated hydraulic conductivity (K_s) was found to be the most inconsistent. Results on the effect of biobased hydrogels on K_s were fewer than for synthetic hydrogels. Biobased hydrogels were found to decrease K_s by up to 60% in sandy soils. However, biobased hydrogels also tended to increase K_s when soil temperature was high i.e., 35 °C. The overwhelming evidence for a decrease in K_s was with synthetic hydrogels. The high swelling capacity of synthetic hydrogels stores more water and closes drainage pores thus reducing K_s . Unsaturated hydraulic conductivity (K) was found to decrease at lower matric suctions and increased at higher matric suctions. However, few studies exist that investigate the impact of hydrogels on K .
6. The application of synthetic hydrogels mostly reduced soil water infiltration by up to 90%. Only one study was found to measure the impacts of biobased hydrogel on

soil water infiltration which also confirmed a decrease in infiltration. Hydrogels alter soil structure decreasing the number of drainage pores and retaining water.

7. Like soil water infiltration, hydrogel application mostly decreased soil evaporation as soil water is bound to the hydrogel reducing how much water is lost to the atmosphere. Hydrogels near the soil surface can also increase evaporation by storing water making it easy for stage one of evaporation to occur.

In conclusion, the fast degradation of biobased hydrogels may not be suitable for their long-term use as water absorbing amendments. Thus, attention should be given to hydrogels that are derived from a combination of both biobased and synthetic sources as the benefits of higher swelling capacity will be gained from the synthetic materials while the ability to degrade moderately will be gained from the biobased materials. The performance of both synthetic and biobased hydrogels on soil hydraulic properties will depend on the type of hydrogel, soil texture, application rate, particle size distribution of the hydrogel, swelling capacity of the hydrogel, location of placement, and how these properties vary over time.

CHAPTER 3. ALKALI LIGNIN-BASED HYDROGEL: SYNTHESIS, CHARACTERIZATION, AND IMPACT ON SOIL WATER RETENTION FROM NEAR SATURATION TO DRYNESS

3.1 Abstract

Superabsorbent polymers (hydrogels) have been proposed as soil amendments to increase plant available water in soil. Synthetic hydrogels have been widely investigated for use in agriculture. Due to increasing environmental concerns related to synthetic hydrogels, hydrogels from natural sources which should be more degradable and biocompatible compared to synthetic hydrogels are being developed. Here, a lignin-based hydrogel was synthesized. Using the hanging water column, pressure plate method, and water potential using a dew point potentiometer, the soil water retention curve was measured from saturation to oven-dryness for silt loam and loamy fine sand soils. For this purpose, the soil was amended with the lignin-based hydrogel at concentrations of 0, 0.1, 0.3, and 1% (w/w) for the silt loam soil and 0 and 1% for the loamy fine sand soil. The treatments were replicated three times and analysis of variance was employed to determine differences between treatments. Results showed a maximum swelling ratio of 2030% of the hydrogel's original mass in deionized water, 1092% in tap water, and 825% in a 0.9% NaCl solution. FTIR spectra of the hydrogel showed the presence of O-H bonds from the lignin structure which we hypothesize renders the hydrogel reactive to a crosslinker i.e., Poly (ethylene glycol) diglycidyl ether (PEGDGE) forming insoluble bonds allowing the hydrogel to swell with water as a result. SEM images of the lignin-hydrogels showed the presence of large macropores which allowed for water absorption. Application of hydrogels significantly increased ($p < 0.01$) water holding capacity of the soil. Hydrogel treatment significantly increased ($p < 0.05$) water retention at saturation/near saturation (-

3 cm to -10 cm), field capacity (FC), and in the dry range (-20,000 to -500,000 cm) for silt loam soil compared to a control treatment with no added lignin hydrogel. Hydrogel application increased water retention over the range of soil water retention curve from -3 to -15,000 cm for the loamy fine sand soil. In the dry range, lignin-based hydrogel treatment increased water retention from -20,000 cm to -50,000 cm in the loamy fine sand but not between -100,000 to -1,000,000 cm. In the capillary regions of the soil water retention curve (SWRC) where soil water is easily accessible to plant roots, volumetric water content (VWC) was increased. To demonstrate the feasibility of using hydrogels in the field, calculations were carried out based on results from the laboratory study. Our calculations demonstrated that at a 1% (w/w) concentration, the application of the lignin-based hydrogels to a 15 cm layer of silt loam and loamy fine sand soils in the field would not increase plant available soil water storage (PAWS). Hydrogels applied at 1% concentration to a 15 cm layer of loamy fine sand soil is equivalent to applying 2300 kg/ha or 1.0 ton/acre.

These results are useful because it gives us preliminary data upon which further lignin-based hydrogel amendment studies could build upon by testing higher ranges of hydrogel concentrations to ascertain the impact on soil water retention especially in the capillary region of the SWRC.

3.2 Introduction

The growing impacts of climate change, water scarcity, and desertification have negatively impacted agriculture (Durpekova et al., 2020). Increasing the amount of plant available water in the soil in arid and semiarid regions has become imperative as these areas frequently experience droughts which negatively affect plant yield (Saha et al.,

2020a). Superabsorbent polymers (hydrogels) have been proposed as soil amendments that could be used to increase water use efficiency (Suresh et al., 2018), reduce nitrate leaching (Islam et al., 2011), reduce seepage losses in irrigation reservoirs (Lentz & Kincaid, 2008), and trap water that would have otherwise drained out of the root zone (Andry et al., 2009). The addition of hydrogels to soils may improve not only the water retention capacity of a soil but also increase the amount of plant available water which is especially important during critical growth stages (Agaba et al., 2010). Hydrogels have hydrophilic groups in their 3-dimensional polymeric networks which become hydrated upon contact with water causing them to swell (Akhtar et al., 2016).

Synthetic hydrogels have been the most widely utilized and researched form of hydrogels, which are mainly polyacrylamide and polyacrylate polymers (Mikkelsen, 1994). The wide usage of synthetic hydrogels has drawn the attention of researchers to look into producing hydrogels from green alternatives i.e. biopolymers which have the advantages of being easily degradable and biocompatible compared to synthetic hydrogels (Kalinowski & Shi, 2019; Ma et al., 2015; Meng et al., 2019b). Biobased hydrogels from polysaccharides like cellulose (Cannazza et al., 2014; Demitri et al., 2013; Montesano et al., 2015) and starch (Sarmah & Karak, 2020) have been successfully used to increase water retention in soil. However, due to the rapid degradation of polysaccharide-based hydrogels, their beneficial effects on soil water retention are not long-lasting (Passauer et al., 2015). An alternative that has received limited attention is the use of lignin for the synthesis of hydrogels. Lignin-based hydrogels have been successfully developed and characterized (Kalinowski & Shi, 2019; Passauer, 2012) and have been shown to be a viable option for agricultural soils since they are non-toxic and biodegradable (Passauer et al.,

2015). However, there is limited data quantifying how lignin hydrogels affect soil moisture retention.

Lignin is the second most abundant plant polymer after cellulose and forms one of the three main components of lignocellulosic plants (Meng et al., 2019b). Recently, biorefineries mainly process cellulose into ethanol and value-added chemicals while lignin (a by-product of biorefineries) can currently not be converted into value-added chemicals with the available technologies (Li & Pan, 2010). One reason for the slow progress in development of lignin-based products is due to lignin's heterogeneity, thus most lignin is directly combusted for heat and power which does not take full advantage of the lignin structure (Chen et al., 2020). Li & Pan (2010) emphasize that lignin, with numerous hydrophilic functional groups (hydroxyl and carboxyl) on its backbone, is a good feedstock for hydrogels. Lignin possesses properties that makes it suitable for use as agricultural hydrogels. For example, they are high in antimicrobial properties, biodegradable and may help sequester carbon (Thakur & Thakur, 2015) making it suitable for the synthesis of bio-based hydrogels. Several studies have investigated different methods for the synthesis of lignin-based hydrogels (Feng et al., 2014; Mazloom et al., 2019; Meng et al., 2019a; Morales et al., 2020; Nishida et al., 2003; Zerpa et al., 2018), but studies are needed to test the applicability of these hydrogels in the soil to understand the benefits they bring in terms of managing soil water efficiently.

Numerous studies over the past two decades have applied different types of hydrogels to increase soil water retention (Abdallah, 2019b; Abedi-Koupai et al., 2008; Abrisham et al., 2018; Agaba et al., 2010; Alkhasha & Al-Omran, 2020; Andry et al., 2009; Bhardwaj et al., 2007; Leciejewski, 2009; Liao et al., 2016; Montesano et al., 2015; Narjary

et al., 2012; Passauer et al., 2011; Saha et al., 2020a; Shahid et al., 2012; Song et al., 2020). A few of these studies utilized hydrogels derived from lignin (Passauer et al., 2011; Song et al., 2020). Passauer et al. (2011) synthesized an oligo(oxyethylene) lignin hydrogel and tested its ability to retain water in sandy soil. They reported a significant increase in soil water content specifically in the pressure range of -3.0 to -1,500 cm. Their study also revealed that at a hydrogel concentration of 0.5% (w/w) which was the highest concentration used, soil water content increased by 14.2% at -316 cm soil water pressure head. Song et al. (2020) synthesized a lignin-based hydrogel by cross-linking lignosulfonate, sodium alginate, and konjaku flour. They then applied the lignin-based sodium alginate hydrogel to a sandy loam soil and reported an increase of soil water content by 2.98 to 8.96% at soil water pressure heads of -1,000 to -15,000 cm.

The objectives of this study were to (a) synthesize a lignin-based hydrogel using alkali lignin as the backbone of the hydrogel, (b) determine the swelling properties of the hydrogel formed in three aqueous solutions (deionized water, tap water, 0.9% NaCl), (c) determine the water absorption capacity of silt loam soil amended with the lignin-based hydrogel, (e) characterize the lignin-based hydrogel using SEM, FTIR, Gas Pycnometry and (f) determine the soil water retention curve of a silt loam soil amended with the lignin-based hydrogel at rates of 0, 0.1, 0.3, and 1% from near saturation to dryness (w/w) concentration and loamy fine sand at concentrations of 0 and 1% (w/w). We hypothesized that the lignin-based hydrogel will contain macropores and reactive functional groups that make it possible to react with a cross-linker hence allowing the hydrogel to swell with water. Secondly, we hypothesized that amending soil with the lignin-based hydrogel can increase the water absorption capacity of the soil compared to an unamended soil. The

final hypothesis was that by amending soil with lignin-based hydrogels, the amended soils will retain more water as soil water pressure head decreased potentially making water available to plants.

3.3 Materials and Methods

3.3.1 Hydrogel Synthesis

Analytical grade alkali lignin (low sulfonate content) with an approximate molecular weight of 10,000 g/mol and pH 10.5, Poly (ethylene glycol) diglycidyl ether (PEGDGE) with average molecular weight ~500 g/mol, and NaOH were purchased from Sigma Aldrich (St. Louis, Missouri). The method of hydrogel synthesis followed a similar method as described in Passauer et al. (2011) and in Mazloom et al. (2019) with some modifications. A 1.5 M NaOH solution was prepared, and 16 ml was added to 10 g of the alkali lignin and the mixture was stirred using a glass rod for 5 mins. For thorough mixing and to allow the alkali lignin to dissolve completely, the mixture was further stirred on a magnetic stirrer (Heidolph™ MR Hei-Tec Magnetic Stirrer with Heating) set at 450 rpm for 24 hrs. Stirring the lignin alkali solution increased its viscosity. Then 0.5 mmol (1 ml) of a cross-linker (PEGDGE) was added to the alkali lignin solution using a micro-pipette. This solution was immediately stirred using a glass rod for 1min. The solution was then placed on a heat source (Heidolph™ MR Hei-Tec Magnetic Stirrer with Heating) set at 50°C while stirring continuously for 10-15 mins until the viscosity increased. The stirring was discontinued, and the solution was cast into 35 mm petri plates and placed in ambient temperature for 24 hours to allow for complete solidification. The formed hydrogels were then removed and soaked in deionized (DI) water for 7 days to wash out unreacted

monomers. The DI water was changed daily during the 7-day period. Lastly, the soaked hydrogels were freeze dried at -48°C in a freeze-drier (Labonco, Cat. No 7753024) to obtain a dried lignin-based hydrogel.

3.3.2 Characterization of the lignin-based hydrogel

The lignin-based hydrogel and alkali lignin were characterized by FTIR spectroscopy (Nicolet is50 FT-IR spectrometer, Thermo Fisher) in the frequency range of 4000 cm^{-1} to 500 cm^{-1} (Mazloom et al., 2019) at a resolution of 4 cm^{-1} . The morphology of the freeze-dried hydrogel was observed by scanning electron microscopy (SEM) using a Hitachi S4300 FE-SEM using an incident electron energy of 2 keV. Prior to SEM analysis, the hydrogels were freeze-dried at -48°C for 48 hours. The fractured surfaces of the freeze-dried hydrogel were directly attached to the holder using carbon tape (Ted Pell Inc.) and no conductive coating was deposited prior to imaging. The particle density (ρ) of the hydrogel was determined using a fully automated, high-precision helium pycnometer (Micromeritics AccuPyc II 1345), an average of 3 consecutive measurements. The instrument measured the apparent volume of the hydrogel sample placed in it (total volume of the hydrogel, excluding the open pores but including the closed pores). The particle density of the hydrogel was then determined by dividing the mass of the hydrogel sample by the volume obtained from the pycnometer. The method for determining the apparent volume was done following a method described by Adedeji and Ngadi (2011).

3.3.3 Swelling kinetics of lignin-based hydrogel in aqueous solutions

The swelling ratio of a hydrogel is important as it expresses the change in swelling capacity per unit of time in the hydrogel (Kipak et al., 2014). To measure the swelling rate

of a hydrogel, the swelling capacity is plotted against time. The swelling ratio of the hydrogel was determined using a modification of previously described procedures (Kalinowski & Shi, 2019; Liang et al., 2015). An initial amount of the freeze-dried hydrogel (1 g) was measured into a beaker using a weighing scale (Fisher Science Education™ Analytical Balances). Excess (1000 ml) deionized water, tap water, or 0.9% NaCl were then added to 1g of the hydrogel and stirred with a glass rod to ensure the hydrogel particles made full contact with the solutions. After 20 mins of swelling, the solutions were passed through a cloth filter to remove excess water and retain the hydrogel. The mass of the swollen hydrogel was then recorded. The swollen hydrogel was re-immersed into the same beaker of water, filtered and the mass recorded after 40, 60, 80, 100, and 120 min. The formula for calculating the swelling ratio of the hydrogel is given as:

Equation 3.1

$$S_t = \frac{M_f - M_i}{M_i} \times 100\% \quad (3.1)$$

where S_t is the swelling at time (t), M_f is the mass of the swollen hydrogel at time (t) and M_i is the mass of the initial dry hydrogel.

3.3.4 Water absorption capacity of lignin-based hydrogel in soil

The water absorption capacity of the hydrogel in soil was determined using a modification of methods described by (Singh et al., 2011). Air-dried soil (silt loam) was ground and sieved through a 2 mm sieve. The lignin hydrogel was hand mixed into soil at

rates of 0% (10 g of soil with no hydrogel added), 1% w/w (0.1 g of hydrogel mixed with 10 g of soil), and 3%. The mixed samples were transferred into pre-weighed ceramic cups with perforated bases fitted with filter papers. Each cup was immersed in a beaker of DI water overnight to saturate the soil samples through capillary water rise. The samples were then dried in an oven at 104°C overnight. The water absorption capacity of the hydrogel in soil was calculated based on the difference between the saturated sample mass minus the oven-dried mass divided by the oven-dried mass.

3.3.5 Soil properties

The silt loam soil was obtained from the University of Kentucky North Farm located north of Lexington, Fayette County, Kentucky (38° 6' 18.07 "N 84° 29' 36.11" W). The silt loam soil was obtained from the University of Kentucky Spindletop Farm located north of Lexington, Fayette County, Kentucky (38° 6' 18.07 "N 84° 29' 36.11" W). The loamy fine sand was obtained from Maceo, a town 8 miles northeast of Owensboro in Daviess County, Kentucky (37° 55' 21" N). The soils were air-dried, ground, and sieved through a 2 mm sieve. Total nitrogen and carbon, cation exchange capacity, base saturation, exchangeable K, Ca, Mg, Na, pH and soil texture were determined on the prepared soil. The texture of the soil was determined using the micropipette method (Miller & Miller, 1987). Cation exchange capacity (CEC) was analyzed using ammonium acetate extraction, bases (Mg, Ca, Na, K) were analyzed using inductively coupled plasma spectrophotometry (Jones Jr, 1999), and base saturation was determined as $\text{total bases/CEC} \times 100\%$. Total nitrogen was determined using the LECO combustion method (Yeomans et al., 1991). The pH of the soil was determined in water by using a glass electrode (Reed & Cummings,

1945). The physical and chemical properties of the soils used in this study are shown in Table 3.1.

Table 3.1. The physical and chemical properties of the soils used in this study.

Soil texture	Clay (%)	Silt (%)	Sand (%)	Total N (%)	Total C (%)	CEC	Ex. Mg	Ex. Ca	Ex. Na	Ex. K	Base saturation (%)	pH
Silt loam	18.18	72.25	9.57	0.178	1.769	18.68	1.37	11.2	0.03	0.67	71	5.73
Loamy fine sand	4.87	9.66	85.47	0.081	1.198	5	2.09	6.42	0.04	0.26	176.31	7.76

CEC - cation exchange capacity, exchangeable (Ex.) Mg, Ca, Na, and K were all measured in meq/100g of soil. The pH was measured in water.

3.3.6 Determination of soil water retention curve

3.3.6.1 Soil water retention

Freeze-dried hydrogel was ground with a blender to obtain micron sized particles of the hydrogel. Three treatments were prepared by mixing soil and hydrogel at concentrations of 0, 0.1, 0.3 and 1% (w/w) for the silt loam soil and at concentrations of 0 and 1% for the loamy fine sand soil. The samples were then packed into three metal rings with a volume of 136.4 cm³ (radius of 2.69 cm and height of 6 cm). There were three replications for each treatment. Packing was done by compacting the soil into the rings to a target bulk density of 1.33 g cm⁻³ for both soil textures using a metallic plunger. The samples were then placed in a glass container and saturated through capillary rise for 48 h. After the first wetting cycle, saturated water content of the samples was measured, and the samples were then allowed to dry through evaporation. Three subsequent wetting and

drying cycles were conducted for particle reorientation and to observe a stable swelling/shrinking behavior of the samples.

After the 4th wetting and drying cycles, the samples were placed in a hanging water column apparatus and saturated for 48 h. After sample saturation, the hanging water column method (Berliner et al., 1980) was used to measure the soil water pressure head and volumetric water content in the samples at -3, -10, -20, and -50 cm soil water pressure heads. In our setup, the hanging water column method is limited to water pressure heads down to -50 cm. The pressure plate apparatus (Soil Moisture Equipment Company, Santa Barbara, California) was then used to determine the soil water retention curve from -100 cm to -15,000 cm. Briefly, the low-pressure plate was first pre-saturated. The sample cores taken from the hanging water column were placed on the wet ceramic plate of the pressure plate apparatus. The plate was connected to outlet tubes for later draining the excessive water from the samples at a given pressure head. The pressure chamber was then closed, and air pressure of 100 cm was applied from an air compressor. Pressure within the pressure plates were frequently checked using a manometer. Once the pressure was established, water flowed out of the samples. After outflow of water stopped, the core samples were retrieved 24 hours later, and their weights recorded. The procedure was repeated for pressure head steps of -330, -500, -1000, -3000, -5000, and -15,000 cm. Volumetric water content (VWC) at -1000, -3000, -5000, and -15,000 cm soil water pressure head was calculated by multiplying the gravimetric water content (GWC) by the bulk density of the three treatments samples. To determine the VWC at -3000, -5000, and -15,000 cm, sub samples were taken from each sample after pressure head step -1000 cm. These sub samples were placed in plastic rings, rewetted, and placed in their respective pressure

chambers (3, 5, and 15 bar pressure chambers). The sub samples were placed in plastic rings to shorten the equilibration time of the samples. Once the respective pressure heads were established and outflow of water ceased, the samples were retrieved, and their gravimetric water content determined.

To determine the soil water retention curve beyond the permanent wilting point, the WP4 Dewpoint PotentialMeter (Decagon Devices, Inc. Pullman, WA, USA) for water potentials from -6,000 cm to -100,000 cm was used. An AQUALAB water activity meter (Decagon Devices, Inc. Pullman, WA, USA) was used to measure water potentials from -100,000 cm to -1,000,000 cm. Both devices are based on a chilled mirror to measure the soil water pressure head after the tests with the pressure plate apparatus were completed (Schelle et al., 2013). At equilibrium, the water potential of the air in the headspace of the chamber containing the sample equals the water potential of the sample when using the WP4. While at equilibrium, the relative humidity of the air in the chamber is the same as the water activity of the sample when using the AQUALAB (Decagon Devices, 1998-2007). Prior to measurement, the WP4 Dewpoint PotentialMeter and AQUALAB were calibrated using a standard 0.5 M KCl solution with known water potential. About 8 g of each sample was measured into sample cups and placed into the meter chamber. After a reading was taken, the lid of the sample cups was removed to allow water to evaporate from the samples for 15-20 min until the humidity of the atmosphere was in equilibrium with the soil moisture status at the next soil water pressure head. The soil water pressure head and the weight of the samples were recorded. At the end, the samples were oven-dried to calculate the final GWC and the VWC. The GWC and VWC at each soil water pressure head were calculated from the final GWC and the weights of the samples at each soil water

pressure head. Figure 3.1 presents a summary schematic of the set-up used to obtain data for the soil water retention curve of the amended soil to dryness.

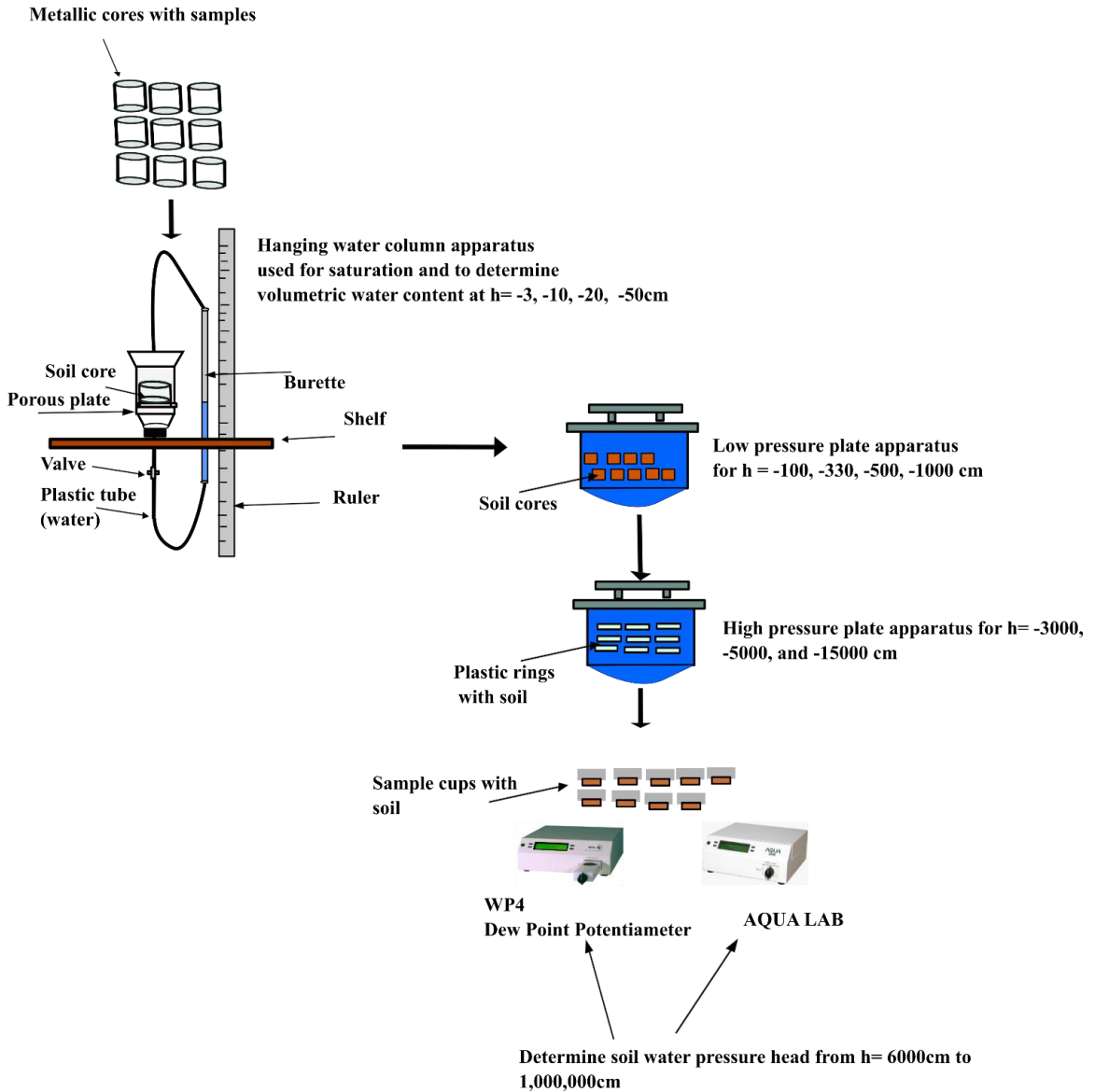


Figure 3.1. Schematic for determining soil water retention curve.

The experimental data for soil water pressure head, h (-cm) was plotted on a log scale against the volumetric water content data (θ) on a linear scale. The soil water pressure head and volumetric water content data were also fitted to a non-linear relationship using a least-squares optimization technique, i.e., the RETC program for describing the hydraulic properties of unsaturated soils (Van Genuchten et al., 1991). The program was used to obtain optimal model parameters (θ_r , θ_s , α , m , and n) where $m = 1-1/n$ for nonlinear equations with multiple parameters (Van Genuchten et al., 1991) for measured data from -3 cm soil water pressure head to the permanent wilting point. The Van Genuchten function is given as:

Equation 3.2

$$\theta = \theta_r + \frac{(\theta_s - \theta_r)}{[1 + (\alpha h)^n]^m} \quad (3.2)$$

where α (cm^{-1}) and n (dimensionless) are fitting parameters which can be estimated from observed soil-water retention data. θ_r ($\text{cm}^3 \text{ cm}^{-3}$) and θ_s ($\text{cm}^3 \text{ cm}^{-3}$) are and represent the saturated and residual volumetric water contents, respectively.

3.3.7 Statistical analysis

Analysis of variance (ANOVA) was used to test for the difference among the three treatments for the silt loam samples and if a difference was detected, Tukey's test (Tukey, 1949) was used to determine which treatment(s) differed significantly from the others. For the loamy fine sand samples, a two-tailed Student's t-test was used to test for significant differences between the two treatments. Before the statistical tests were conducted the data were checked for normality and equal variance assumptions and appropriate tests were

applied. All statistical tests and graphing were done in (SigmaPlot version 14.0, Systat Software, Inc., San Jose, CA, USA, www.systatsoftware.com). An alpha of 0.05 was used for all statistical comparisons.

3.4 Results and Discussions

3.4.1 Hydrogel synthesis

The alkali lignin served as the primary biopolymer while NaOH dissolved the alkali lignin allowing the crosslinker (PEGDGE) to form insoluble bonds producing a gel. Three concentrations of the PEGDGE were tested for synthesizing the hydrogel (0.1, 0.5, and 1 mmol). The concentration of the crosslinker that produced an insoluble hydrogel was 0.5 mmol which is consistent with Mazloom et al. (2019). At PEGDGE concentration of 0.1 mmol, it took 30-45 min of stirring at 50°C for the lignin alkali solution to increase in viscosity compared to 5-10 min for 0.5 mmol concentration of PEGDE. When 0.1 mmol of the PEGDGE was used, the formed hydrogel was completely solubilized after only 24 h of washing in deionized water indicating there was not enough cross-linker to form a strong permanent network in the hydrogel. According to Passauer et al. (2011), smaller amounts of the PEGDGE result in the formation of water-soluble hydrogels indicating that to form an insoluble hydrogel, a critical network density should be reached. However, a high amount of cross-linker produces additional network structures that do not allow water to enter the network structure hence decreasing the swelling capacity (Xie et al., 2009). At PEGDGE concentration of 0.5 mmol, a hydrogel was formed after only 5 min of stirring at 50°C. The hydrogel formed was insoluble in water after soaking in deionized water for

a week with daily changing of the water. APPENDIX A. 1 (Figure A. 1) shows the process for the synthesis of the lignin-based hydrogel.

3.4.2 Characterization of hydrogel

Figure 3.2 illustrates the FTIR spectra of the alkali lignin powder, and the synthesized lignin-based hydrogel. The FTIR spectra show the presence of active functional groups in the hydrogel and alkali lignin. The broad peak in both the alkali lignin powder and the lignin hydrogel which occur at a wavenumber between 3300 - 3500 cm^{-1} was identified to be the O-H stretching absorption band. This is formed due to the intermolecular and intramolecular hydroxy stretching vibration which makes the hydrogel hydrophilic (Saha et al., 2020a). The O-H group allows the hydrogel to absorb water and other aqueous solutions that result in hydrogel expanding and occupying a larger volume referred to as swelling (Peppas, 2000). The presence of C-O stretching found in lignin was observed at 1267 cm^{-1} (Shi et al., 2012). The appearance of the C-O bonds in the lignin hydrogel indicates a successful introduction of crosslinking from the PEGDGE (Mazloom et al., 2019). According to Rico-García et al. (2020) crosslinking occurs by an etherification reaction between the PEGDGE and the phenolic O-H groups of lignin due to the phenoxide nucleophile attack on the epoxide groups of PEGDGE. As a result of the crosslinking, during swelling, the cross-linked structure of hydrogels prevents the dissolution and destruction of the linkages (Peppas, 2000). In addition, a C-H stretching bond was observed at frequency range of 2929 cm^{-1} while a C-H deformation appeared at 1460 cm^{-1} which both came from the alkali lignin (Rashid et al., 2016).

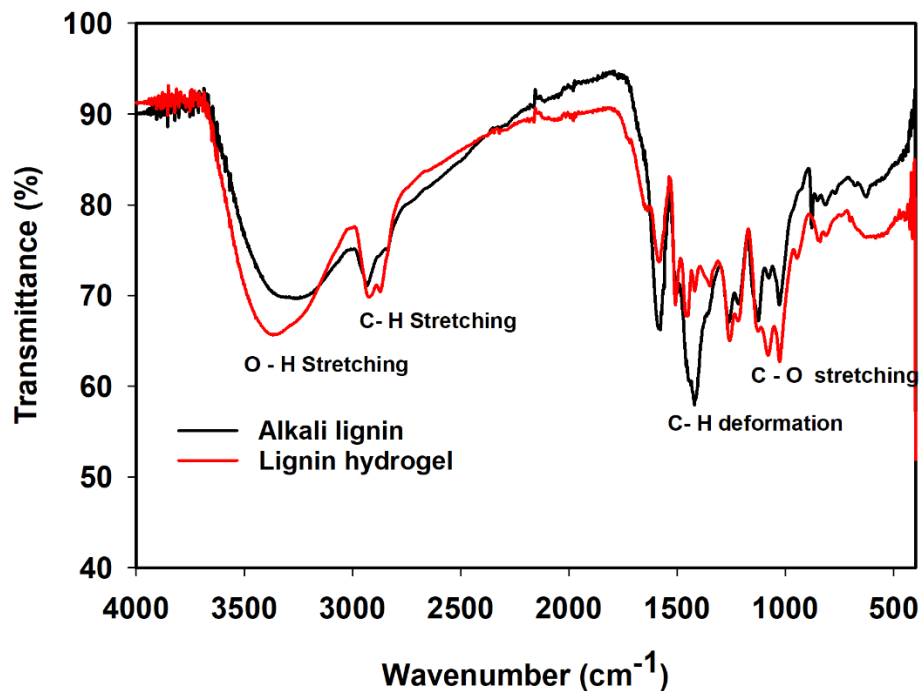


Figure 3.2. FTIR spectra for freeze-dried hydrogel and the alkali lignin backbone used to synthesize the hydrogel.

Figure 3.3 presents the SEM analysis showing the morphology of the alkali-lignin based hydrogel. The magnification of the images moves from lowest (x50) shown in (a) to highest (x1000) shown in (d). Figure 3.3 (b) and (c) shows the surface of the hydrogel with several large pore structures. According to Dinu & Dragan (2018), hydrogels with macropores have large and/or interconnected pores which allows them to absorb water at a faster rate. These large pores serve as entry points for permeation of water into the polymeric network of the hydrogel causing swelling (Baki & Abedi-Koupai, 2018). Cross-linking of the hydrogel with PEGDGE helped to produce the large pores seen in Figure 3.3. This property is especially important for hydrogels that would be amended to soil for

their water retention property. As shown in Figure 3.3, the hydrogel produced varied pore sizes ranging from 5 μm (d) to 140 μm (a).

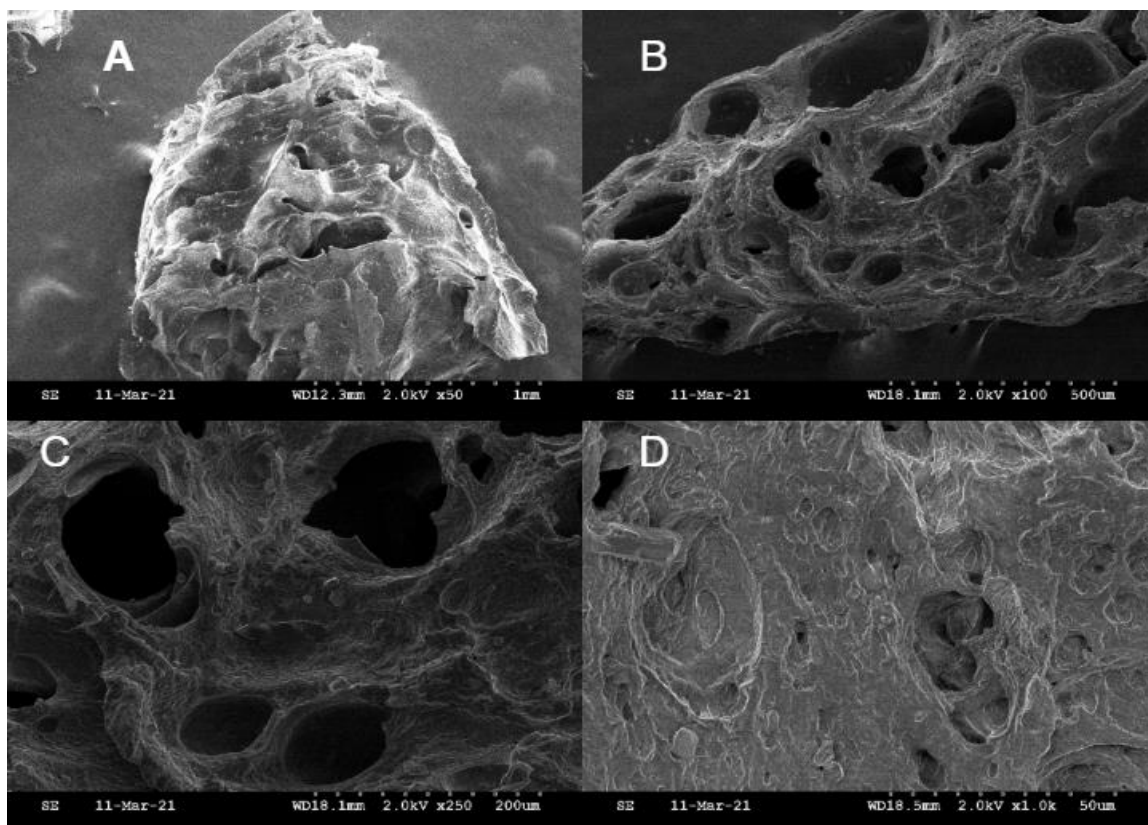


Figure 3.3. SEM images of a cross-section of freeze-dried lignin-based hydrogel at various magnifications A) x50, B) x100, (C) x250, and (D) x1000

The apparent volume of the lignin-based hydrogel was measured using a gas pycnometer after which particle density (ρ) was calculated. Two replicates of the particle density were obtained. Each replicate consisted of three cycles. A cycle refers to a series of commands implemented to obtain a single volume measurement. After the three cycles, the density of the hydrogel was determined to be 1.52 g cm^{-3} with a standard deviation of 0.01. The density for the second replicate was determined to be 1.49 g cm^{-3} with a standard deviation

of 0.01. Thus, the average of the two replicates gave a value of 1.5 g cm^{-3} as the particle density of the lignin-based hydrogel. The particle density of hydrogels can affect soil physical properties like porosity and bulk density which in turn affects how water moves through soil. The impact of the hydrogel concentration on soil particle density, bulk density, and porosity were out of the scope of this study. However, considering the low particle density of the hydrogel in this study compared to the particle density of soil (assumed to be constant at 2.65 g cm^{-3}) indicates a potential to reduce bulk density and particle density of soil while increasing porosity with high application rates of hydrogels.

3.4.3 Swelling kinetics of lignin-based hydrogel in aqueous solutions

The swelling of a hydrogel is influenced by the properties of the surrounding solution such as the charge number and ionic strength (Zhang et al., 2006). Figure 3.4 reports the swelling ratio of the lignin-based hydrogel with time. The swelling ratio was measured in deionized water (DI), tap water, and 0.9% NaCl solution. The equilibrium swelling ratio in the DI water was 2030% at 60 min. The equilibrium swelling ratio of the hydrogel in the tap water and 0.9% NaCl solution was 1092% and 825%, each occurring after 20 min of immersion. Statistical analysis conducted suggest the equilibrium swelling ratio in DI was significantly higher ($p < 0.001$) than tap water and 0.9% NaCl solution. Equilibrium swelling ratio in tap water was significantly higher than the equilibrium swelling ratio in 0.9% NaCl ($p < 0.05$). The lower swelling ratio in the tap water and the 0.9% NaCl solution is due to the presence of salt ions (Saha et al., 2020a). Since the tap water and the 0.9% NaCl solution had more free ions i.e., Na^+ ions, the osmotic pressure in the solutions increased thus leading to a reduction in swelling ratio (Feng et al., 2014; Saha et al., 2020a).

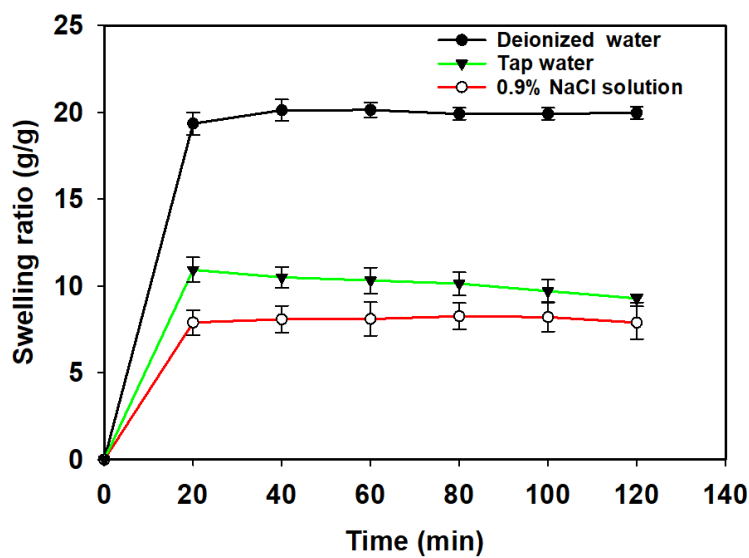


Figure 3.4. Swelling ratio of the freeze-dried lignin-based hydrogel after immersing in deionized water, tap water, and 0.9% NaCl at room temperature. Error bars indicate standard error of the means (n=3).

In addition, the free Na^+ ions tended to bond with hydrophilic groups i.e. OH groups present in the lignin hydrogel thus decreasing the attraction between the hydrogel and water molecules (Feng et al., 2014). It can thus be deduced that, as the soil salinity increases, the swelling ratio of lignin-hydrogels tends to decrease (Mazloom et al., 2019). When the swelling ratio of a commercial hydrogel i.e., Stockosorb was measured in DI water, 0.9% NaCl solution and tap water by Saha et al. (2020a), the 0.9% NaCl solution reduced the swelling ratio of the hydrogel by 74% compared to the DI water while a decrease in swelling ratio of 37% was recorded in tap water. Mazloom et al. (2019) reported a reduction of 64% in the swelling of a lignin-based hydrogel in a salt solution (with $\text{EC} = 8 \text{ dSm}^{-1}$) compared to swelling in DI water when a lignin-based hydrogel was studied. This study

found a decrease in swelling of the lignin-based hydrogel by 46% in tap water and 59% in 0.9% NaCl that was similar to previous studies.

The swelling ratio of a hydrogel is an important metric used to ascertain how well a hydrogel will perform in retaining water in the soil matrix. This swelling phenomenon results from the diffusion of solvent molecules into the 3D structure of the hydrogel due to its high hydrophilicity caused by the expansion of the polymeric chains (Tomadoni et al., 2019). Compared to synthetic hydrogels which can easily attain a swelling capacity of 100 g water/ g hydrogel, the swelling capacity of lignin-based hydrogels is generally less than 5 g water/ g hydrogel (Li & Pan, 2010). The maximum swelling in terms of amount of water the lignin-based hydrogel in our study could hold was 20.3 g of water/ g hydrogel in deionized water which is higher than is expected for most lignin-based hydrogels according to Li & Pan (2010). Li & Pan (2010) note that while lignin-based hydrogels have environmentally friendly benefits, there are still challenges with regards to developing simple procedures to enhance the water absorbency and mechanical strength of lignin-based hydrogels.

3.4.4 Water absorption capacity of hydrogels in soil

While there are numerous studies published in the literature that measure the swelling ratio of hydrogels in water and other aqueous solutions (Bao et al., 2011; Demitri et al., 2013; Isik & Kıs, 2004; Li et al., 2004; Xie et al., 2009), the quantification of the water absorption capacity (WAC) of a hydrogel in soil is needed to give us information about how that hydrogel will perform when amended to soil. In soil, conditions are often different with varying temperatures, pH, electrical conductivities, and salinity which influence the WAC of the hydrogel. The WAC of the soil was first measured at hydrogel

concentrations of 0.1% and 0.3% but there was no difference between the two treatments and the control treatment (no hydrogel added). Thus, higher concentrations (1% and 3%) were tested. Figure 3.5 presents the WAC of the lignin-based hydrogel in soil. The WAC of the hydrogel in the control treatment was 59% followed by the 1% (w/w) treatment at 64% and 3% (w/w) treatment was 77%. The 3% treatment was significantly higher ($p < 0.01$) than the control and the 1%. There was however no significant difference between the control and the 1% treatment. The WAC of the 3% treatment was 16.9% and 23.4% more than the 1% and 0% treatments, respectively. These results indicate that WAC of the lignin-based hydrogel in soil increased with higher application rate.

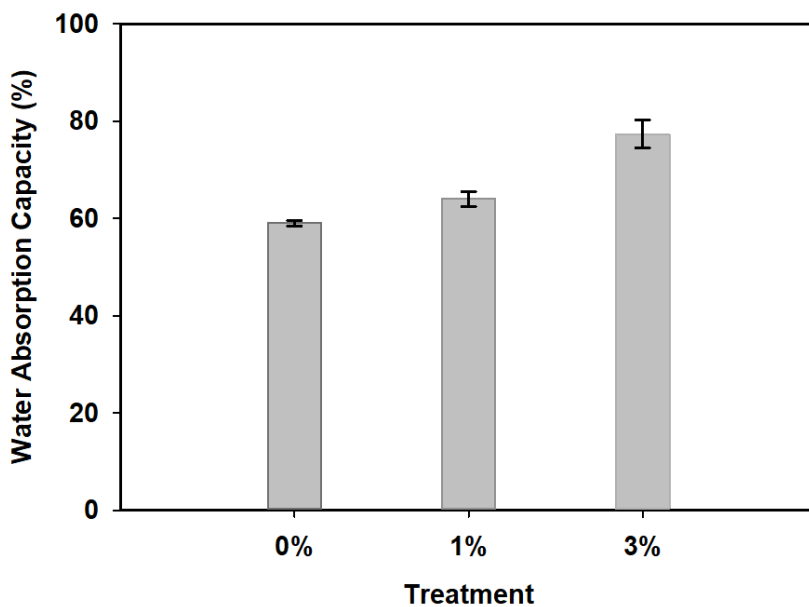


Figure 3.5. Water absorption capacity of lignin-based hydrogel in soil at 0, 1, and 3% (w/w) concentration. Error bars indicate standard error of the means ($n=3$).

Bai et al. (2015a) determined the water holding capacity of a starch-based hydrogel by mixing (2.6, 7.8, and 13.0 mg) of the hydrogel with 10 g of soil in a tube and saturated

the tube with water. They reported a 52.2% water holding capacity of soil with application rate of 0.13% (w/w) compared to 44% for the control treatment. Singh et al. (2011) determined the water absorption capacity of a sandy loam soil by mixing 50 g of soil with a hydrogel at rates of 0.5% and 0.75%. The mixtures were placed in a cup with a perforated base fitted with filter paper. Samples with 0.5% and 0.75% treatment had water absorption capacities of ~ 90% and 115% compared to ~ 45% in the control treatment at 25°C. In a study by Baki & Abedi-Koupai (2018), 5 g of a sodium alginate-based hydrogel was mixed with 200 g of dry soil i.e., 2.5% (w/w) and 200 g of tap water in a beaker at room temperature and left for 5 days. They concluded that with hydrogel amendment, water retention was above 70% compared to 53.4% in a control treatment after 20 days on a dry basis (Baki & Abedi-Koupai, 2018). Our results closely mirror their results as 3% treatment resulted in a 77% water holding capacity in our study while with the 2.5% treatment in Baki & Abedi-Koupai (2018), 70% swelling capacity was obtained.

3.4.5 Observation of swelling in hydrogel-soil mixture

Prior to beginning the water retention experiment, the swelling behavior of the soil-hydrogel treatments were observed. Observation of the hydrogel swelling behavior was done to evaluate the potential of the soil to expand over the metallic rings used to hold the samples in the hanging water column. Additionally, allowing the samples to undergo multiple wetting and drying cycles allowed the samples to attain a structure similar to undisturbed field soil. After the swelling tests, samples were placed in the pressure plate apparatus.

After the first wetting and drying cycle of the samples, there were visual structural changes in the samples. All treatment samples swelled vertically which was more apparent

in the 1% treatment. The samples swelled about 1 mm above the top edge of the metallic ring. After the samples dried at room temperature, cracks due to lateral shrinkage developed in all treatment samples. Prior to the 2nd wetting cycle, 1 g of soil was used to fill the visible cracks in the samples and a load (2.5 kg) was placed on the samples to prevent further swelling. Upon saturation for 48 hours, the load was removed, and the extent of swelling was reduced in all treatments. Though the extent of swelling was not quantified, a visual observation showed minimal swelling after the load was removed.

The 3rd drying cycle resulted in less shrinkage but there were a few cracks and shrinkage which mostly occurred laterally away from the walls of the metallic rings. According to Taboada (2004), when a soil sample is dried, the soil decreases its volume by shrinkage, and desiccation cracks appear because of internal stresses in the shrunken and dried soil mass. As a result of shrinkage, soil decreases its height by caving inwards. Upon wetting, the soil increases its volume by swelling, the cracks are closed, and soil level rises (Taboada, 2004). The increase in water content of the soil when it is rewetted causes an increase in volume of the voids in the sample (swelling) (Estabragh et al., 2015).

To minimize the shrinkage, approximately 1 g of soil was used to fill the visible cracks in the samples using a spatula APPENDIX A. 2 (Figure A.2). The additional soil was considered when determining the bulk densities of the samples. After the 4th cycle, minimal cracking and shrinkage were observed. According to Haines (1923), at the shrinkage limit of a soil sample, the decrease in the volume of soil is less than the volume of water lost as the particles come in contact. When all the particles are close together, no further shrinkage occurs even while water is still being lost (Estabragh et al., 2015; Tripathy et al., 2002). After the swelling and shrinkage experiments, the soil samples were

ready for further experiments. Swelling and shrinkage in the samples affects the accuracy of results obtained when using the pressure plate apparatus (Gee et al., 2002).

3.4.6 Water retention curve

The rationale for applying hydrogels to soil is that their structures allow them to store large quantities of water which can be used by plants in soil. The water potential of soil is useful for determining the amount of water available to crops and how easy plant roots can gain access to that water. This study determined the water retention curve of a silt loam soil amended with hydrogels at 0, 0.1, 0.3 and 1% (w/w) and a loamy fine sand amended at 0 and 1%.

Figure 3.6 (a) and (b) show measured and fitted data for the water retention curve from near saturation to dryness for the silt loam and loamy fine sand soils respectively when treated with the lignin-based hydrogel.

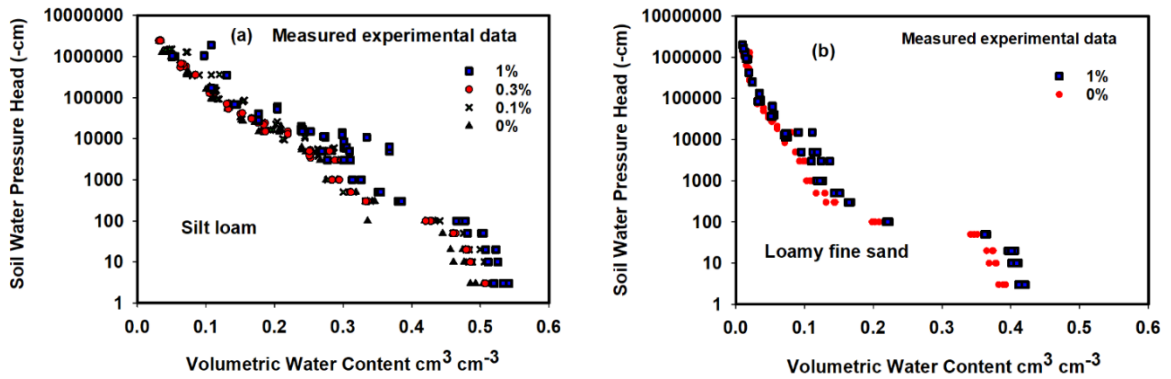


Figure 3.6 (a) Water retention curve of silt loam soil amended with lignin-base hydrogel to dryness using the combined methods (hanging water column, pressure plate apparatus, and dew point meter) (b) Water retention curve of the loamy fine sand soil amended with lignin-based hydrogel up to dryness using the combined methods (hanging water column, pressure plate apparatus, and dew point meter).

The results of the soil moisture retention curves (SWRC) suggest that the control treatment retained less water at any soil water pressure head compared to the 1% (w/w) treatment. For the silt loam soil, the SWRC demonstrates an increase in water retention in the 1% (w/w) treatment compared to the control sample at near saturation (-3 to -10 cm) ($p = 0.006$) and field capacity (-100 cm) ($p = 0.04$). At field capacity, the 1% (w/w) treatment was 16% ($0.08 \text{ cm}^3 \text{ cm}^{-3}$) higher than the control treatment. It could be inferred that the lignin hydrogel is effective in the capillary regime of the soil water retention curve i.e. 0 to 100 cm where soil water is controlled mainly by capillary water and less by absorbed water (Lu, 2016). This region of the SWRC also corresponds to the range dominated by large pores with effective pore diameters of 30 to 3000 μm (Goss & Ehlers, 2003). For the loamy

fine sand soil, the 1% (w/w) treatment significantly increased water retention at -3, -10, -20, -50, -100, -500, -1000, -3000, and -15000 cm ($p < 0.05$).

For the silt loam soil in the dry range i.e., below PWP of the SWRC, the highest application rate of hydrogel (1%) significantly increased water retention at -20,000, -30,000, -50,000, -100,000, and -500,000 cm ($p < 0.05$). Similarly, hydrogel application significantly increased soil water retention at -20,000, -30,000 and -50,000 cm ($p < 0.05$) in the loamy fine sand soil. However, there was no significant increase in water retained in the loamy fine sand soil between -100,000 cm to -1,000,000 cm ($p > 0.05$). The increase in water retention due to hydrogel application in the dry range of the SWRC curve is consistent with (Mohawesh & Durner, 2019) who found that a synthetic hydrogel (Luquasorb) increases water retention of sandy soil at low matric potentials i.e. -10,000 to -10,000,000 cm.

Measurements using the dew point meters enabled us to extend the SWRC into the dry region where the SWRC is rarely reported in literature examining the impacts of hydrogels on soil water retention. At such high soil water pressure heads, soil water retention is modulated by the absorptive forces existing between the solid surfaces and the soil solution (Mohawesh & Durner, 2019). At those high soil pressures, the bound water in the micron sized lignin hydrogel is likely released due to water potential differences between the soil particles and the lignin hydrogel which increases the soil water. According to Yang *et al.* (2014), the increase in soil water retention with hydrogel application may also be due to the strong adsorption and complexing capacities from the hydrophilic functional groups e.g., hydroxy group in the hydrogel.

Figure 3.7 (a) and (b) show measured and fitted data for the water retention curve from near saturation to dryness for the silt loam and loamy fine sand soils respectively when treated with the lignin-based hydrogel. To obtain the fitted values, the three replicates of the experimentally measured data from -3 cm soil water pressure head to the permanent wilting point for each treatment were averaged before using the Retention Curve (RETC) program to obtain the fitted values. We used the Van Genuchten model because it is an acceptable model in literature for describing the water content (θ) as a function of the soil water pressure head (h) for the range from saturation to the permanent wilting point (Van Genuchten, 1980). Fitting the data to the Van Genuchten model allowed us to compare model parameters between treatments as has been done by similar studies (Abedi-Koupai et al., 2008; Al-Darby, 1996; Alkhasha & Al-Omran, 2020; Kashkuli & Zohrabi, 2013) when hydrogels were amended to soil. In both Figure 3.7 (a) and (b), we observed slight hump-like deviations in the measured data especially for the 1% (w/w) treatment when the SWRC transitioned from the capillary water regime into the absorbed water regime (i.e., below -1000 cm).

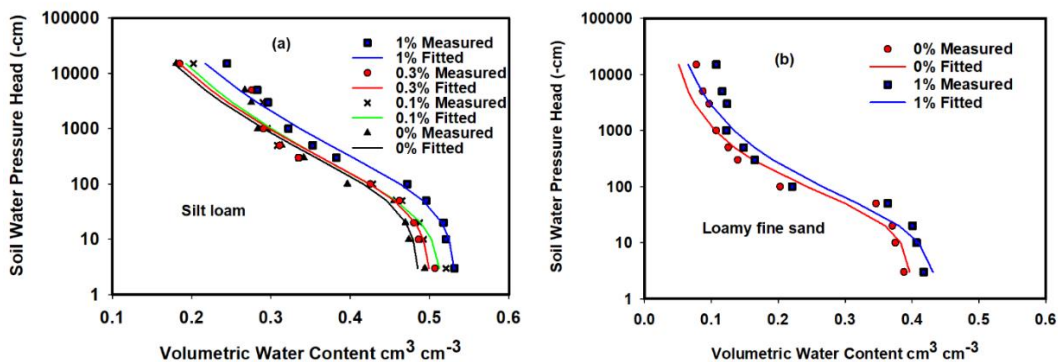


Figure 3.7. (a) Fitted curves and measured data of the silt loam soil amended with lignin-base hydrogel from near saturation to the permanent wilting point (b) fitted and measured curves of the loamy fine sand soil amended with lignin-base hydrogel from near saturation to the permanent wilting point.

Table 3.2 shows the optimized values for the fitted Van Genuchten parameters of the silt loam and loamy fine sand soils amended with lignin-based hydrogel. Comparatively, the parameter θ_s was higher in the 1% treatment than in the 0% treatment for both the silt loam and loamy fine sand soils. While α is an empirical parameter in the Van Genuchten model, its inverse is often considered as the air-entry pressure or bubbling pressure (Van Genuchten et al., 1991). At the air-entry pressure i.e. the pressure in the SWRC where air first starts to enter the largest pores in the soil and desaturation begins (Lu & Likos, 2004), there is a significant difference ($p = 0.01$) between the 1% (w/w) treatment and the control treatment in the silt loam soil, suggesting the control treatment transitions into an unsaturated state faster than for the 1% (w/w) treatment. The air-entry pressure for the control treatment was -29 cm while the air-entry pressure for the 1% (w/w) was -83 cm. The air-entry pressure was calculated by taking the average of the α values of three replicates before finding the inverse of the average α values for each treatment. Again, there is a significant difference ($p < 0.01$) in air-entry pressure between the 1% (w/w) treatment and the control treatment. Air-entry pressure in the control treatment was -9.8cm while air-entry pressure in the 1% (w/w) treatment was -59 cm.

Table 3.2 Van Genuchten parameters fitted to measured water retention curves for different soil-hydrogel mixtures and the control.

Treatment	θ_r ($\text{cm}^3 \text{ cm}^{-3}$)	θ_s ($\text{cm}^3 \text{ cm}^{-3}$)	α (cm^{-1})	n (-)
Silt loam				
Control	0.040	0.498	0.034	1.170
0.1% (w/w)	0.199	0.514	0.022	1.410
0.3% (w/w)	0.132	0.507	0.026	1.250
1% (w/w)	0.219	0.529	0.012	1.446
Loamy fine sand				
Control	0.095	0.385	0.102	2.464
1% (w/w)	0.121	0.41	0.016	2.000

There are limited studies in literature that investigate the effects of hydrogels, especially lignin-based hydrogels, on soil beyond the PWP of soil (-15,000 cm). The few studies that applied lignin-based hydrogels (Passauer et al., 2011; Song et al., 2020) to soil and measured water retention up to PWP found similar results to this study. Passauer et al. (2011) reports a significant increase in soil water content specifically for the soil water pressure range of -1,000 to -15,000 cm while Song et al. (2020) reported an increase of soil water content by 2.98-8.96% at soil water pressure heads of -1000 to -15,000 cm. While water retained beyond the PWP of soil may not be readily available for plant use, this study offers preliminary evidence of the potential of increasing soil water which could be useful for dry soil conditions present in arid regions.

3.4.7 Effect of lignin-based hydrogel on saturated water content, field capacity, permanent wilting point, and plant available water capacity

Plant available water capacity (PAWC) is considered an important parameter used to quantify the amount of water held in soil that is accessible to plant roots (Saha et al., 2020a). PAWC describes the water content between field capacity (FC) and permanent wilting point (PWP) which has practical implications for irrigation (Silva et al., 2014). First described by Veihmeyer & Hendrikson (1927), FC can be considered the upper limit of PAWC and occurs at a range of (-100 cm to -330 cm) depending on the location and the method used for determining it (Wendroth et al., 2018). FC in Kentucky soils is considered to occur at -100 cm soil water pressure head (Wendroth et al., 2018; Zhang et al., 2019), thus, for this study, FC was chosen to be -100 cm. PWP is also considered the lower limit of PAWC since at this soil water pressure head, plants irreversibly wilt and die due to inadequate water available (Wendroth et al., 2018)

Equation 3.3

$$PAWC = \theta_{FC} - \theta_{PWP} \quad (3.3)$$

Figure 3.8. illustrates the VWC at saturation, FC, and PWP of the silt loam and loamy fine sand soils. For the silt loam soil, saturated volumetric water content was 0.45 cm³ cm⁻³ in the control treatment, and 0.51, 0.48, and 0.57 cm³ cm⁻³ in the 0.1%, 0.3%, and 1% (w/w) treatment, respectively. The 1% (w/w) treatment significantly increased ($p < 0.001$) saturated water content compared to all other treatments in the silt loam soil. In addition, the 0.1 and 0.3% (w/w) treatments also significantly increased saturated water content compared to the control treatment ($p < 0.01$). For the loamy fine sand soil, saturated

water content was $0.44 \text{ cm}^3 \text{ cm}^{-3}$ in both the control and 1% (w/w) treatment. Thus, hydrogel treatment did not increase saturated water content in the loamy fine sand soil. Our finding of increased saturated water content in the silt loam soil agrees with findings in (Abedi-Koupai et al., 2008; Dehkordi, 2018; Han et al., 2013; Kashkuli & Zohrabi, 2013; Saha et al., 2020a) as they reported increases in saturated water content with hydrogel application.

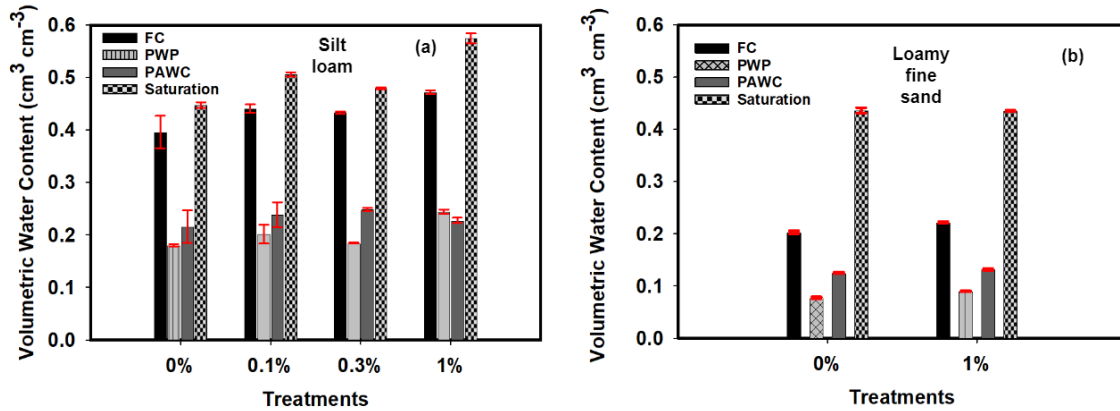


Figure 3.8. Volumetric water content (VWC) at saturation, field capacity (FC), permanent wilting point (PWP), and plant available water content (PAWC) of silt loam soil amended with 0, 0.1, 0.3, and 1% (w/w) lignin-hydrogel for the silt loam soil (a) and 0 and 1% (w/w) amendment for the loamy fine sand soil. Error bars indicate standard error of the means (n=3).

At FC, VWC was $0.40 \text{ cm}^3 \text{ cm}^{-3}$ in the control treatment and 0.44, 0.43, and 0.47 $\text{cm}^3 \text{ cm}^{-3}$ for the 0.1%, 0.3%, and 1.0% (w/w) treatment, respectively in the silt loam soil. VWC at FC in the 1% (w/w) treatment was $0.08 \text{ cm}^3 \text{ cm}^{-3}$ higher and significantly different than the control treatment ($p = 0.04$). Application of hydrogel to the loamy fine sand soil also increased VWC at FC ($p = 0.005$). The increase in VWC at FC in this study is consistent with previous studies (Guo et al., 2019; Montesano et al., 2015; Shahid et al.,

2012). At the maximum hydrogel concentration (1%), the increase in VWC at PWP was $0.06 \text{ cm}^3 \text{ cm}^{-3}$ compared to the control treatment, but that increase was not significantly different ($p = 0.05$) for silt loam soil. On the contrary, there was a significant ($p = 0.001$) increase by $0.019 \text{ cm}^3 \text{ cm}^{-3}$ in VWC at PWP for the 1% (w/w) treatment compared to the 0% (w/w) treatment in the loamy fine sand soil. These results indicate that a higher water retention does not always translate to available water for crop use as water retained at PWP is held in soil pores finer than $0.2 - 0.5 \mu\text{m}$ which cannot be extracted by plant roots (Saha et al., 2020a).

This study found no significant difference between the PAWC due to hydrogel treatment in the silt loam soil or the loamy fine sand soil ($p > 0.05$). While studies on the impact of hydrogel on PAWC have been mostly consistent i.e. PAWC increases with increasing application rate of hydrogels, this increase has been observed mostly in coarse-textured soils i.e. sandy soil (Abdallah, 2019a; Agaba et al., 2011; Andry et al., 2009; Banedjschafie & Durner, 2015; Bhardwaj et al., 2007; Narjary et al., 2012) and with synthetic hydrogels. PAWC is generally lowest in sandy soil and largest in silt loam (Goss & Ehlers, 2003). To increase water retention, Narjary et al. (2012) argue that hydrogel decreases the median pore diameter in soil. The decrease in pore diameter can increase smaller retention pores which can hold water due to an increase in porosity (Narjary et al., 2012). Silt loam soil which contains a large percentage of medium-sized pores ($3 \mu\text{m}$ to $30 \mu\text{m}$) (Goss & Ehlers, 2003) may be much less affected by hydrogel application at any rate compared to sand soil with large pores with effective diameter between 300 and $50 \mu\text{m}$.

3.4.8 Potential field applications

To demonstrate the potential field applications of this study, we performed calculations

based on results from the laboratory study following example calculations in Wendroth et al. (2018). We first calculated the plant available water content from the field capacity and the permanent wilting point. To determine the potential amount of water that would be available at a depth of 15 cm (5.9 inches), we calculated the total amount of that could be stored in the soil profile given the depth. We chose a depth of 15 cm because hydrogel will typically be applied to the topsoil in the field. Table 3.3 shows the measured volumetric water content at FC, PWP, and calculated plant available water storage (PAWS) for two soil textures based on a lignin-based hydrogel amendment at 1% (w/w) concentration compared to control treatments. The PAWS was calculated by multiplying the value of PAWC by the depth of the soil layer. As shown, PAWS was equal (3.45 cm) in the 0% and 1% (w/w) treatments in the silt loam soil. Thus, application of lignin-based hydrogel at 1% (w/w) to a silt loam soil at a 15 cm depth will not increase PAWS. Additionally, for the loamy fine sand, the increase in PAWS was not significant (0.15 cm). Therefore, based on results from the laboratory experiments, there is no evidence to indicate that application of lignin-based hydrogel at 1% (w/w) will increase PAWS in both silt loam and loamy fine soils. A higher concentration of the lignin-based hydrogel may lead to an increase in PAWS, but our data do not support an increase in PAWS

Table 3.3. Soil water contents at field capacity (θ FC), permanent wilting point (θ PWP), plant-available soil water capacity (PAWC), and calculated plant available water storage (PAWS) result from the application of the lignin-based hydrogel at 1% (w/w) concentration for soil layers of different thickness.

Soil type/ Application concentration	θ FC	θ PWP	PAWC	PAWS	PAWS
	(cm ³ /cm ³)	(cm ³ /cm ³)	(cm ³ /cm ³)	15 cm field soil depth	Inches soil depth (5.9)

Silt loam/ 1% (w/w)	0.47	0.24	0.23	3.45	1.36
Silt loam/ 0% (w/w)	0.40	0.18	0.23	3.45	1.36
Loamy fine sand /1% (w/w)	0.22	0.09	0.13	1.95	0.77
Loamy fine sand /0% (w/w)	0.20	0.08	0.12	1.8	0.71

To determine the amount of lignin-based hydrogel that will be needed to be applied to a 1 ha field of a 15 cm loamy fine sand layer at 1 % (w/w), we made the following assumptions given: Bulk density of silt loam soil = 1.5 g cm^{-3}

Depth of hydrogel application = 15 cm

Volume of soil layer in 1 ha of the silt loam at a depth of 15 cm is calculated as:

$$V_s = \text{Area of 1 ha of field} \times \text{depth of top soil}$$

$$V_s = 10,000 \text{ m}^2 \times 0.15 \text{ m}$$

$$V_s = 1500 \text{ m}^3 = 1.5 \times 10^9 \text{ cm}^3$$

Mass of soil in 1 ha of the field = *Volume of soil layer* × *bulk density*

$$= (1.5 \times 10^9 \text{ cm}^3) \times 1.5 \text{ g cm}^3$$

$$= 2.3 \times 10^9 \text{ g} = 2.3 \times 10^6 \text{ kg} = 2300 \text{ MT}$$

From Table 3.3, at 1% (w/w) treatment of the lignin-based hydrogel, change in PAWS = 0.15 cm (0.06 inches)

To store 0.15 cm in a 15 cm layer of 1 ha of a loamy fine sand soil

$$\text{Concentration (\%)} = \frac{\text{mass of hydrogel}}{\text{mass of soil}} \times 100\%$$

$$1 (\%) = \frac{\text{mass of hydrogel}}{2.3 \times 10^6 \text{ kg}} \times 100$$

$$\text{mass of hydrogel} = 2300 \text{ kg} = 2.3 \text{ MT}$$

Hence, to store 0.15 cm of rain or irrigation water in a loamy fine sand soil, 2.3 MT of dry lignin-hydrogel will be needed to amend the top 15 cm of the soil. A 0.15 cm increase in PAWS is not economically feasible from a farmer's perspective.

3.5 Conclusions

The shift from the use of synthetic hydrogels to biobased hydrogels especially hydrogels made from lignin creates an opportunity to limit the environmental impacts of synthetic hydrogels. In this study, a lignin-based hydrogel was synthesized. Our main hypothesis was that by amending soil with lignin-based hydrogel, the amended soils will retain more water with increasing soil water suction than soils not amended with hydrogel, which could be beneficial for crop water uptake. The swelling properties of the hydrogel

were tested in different aqueous solutions, and found to have a high swelling ratio compared to other lignin-based hydrogels (Kalinowski & Shi, 2019; Morales et al., 2020). Using FTIR spectroscopy, the hydrogel was confirmed to contain hydroxyl (O-H) functional groups that enable the hydrogel to react with a cross-linker forming hydrophilic 3D networks further allowing the hydrogel to swell with water. SEM analysis of the lignin-based hydrogel showed the presence of large interconnected macropores which allowed them to absorb water at a faster rate. The lignin-based hydrogel significantly increased the water holding capacity in soil. Analysis of the soil water retention curve (SWRC) indicated that application of the lignin-based hydrogel increased water retention at saturation, near saturation (-3 cm to -10 cm soil water pressure head), field capacity (FC), and in the dry range i.e., -20,000, -30,000, -50,000, -100,000, and -500,000 cm soil water pressure head for silt loam soil. For the loamy fine sand soil, the lignin-based hydrogel increased water retention over the range of SWRC from -3 cm to -15000 cm soil water pressure head except at -5000 cm. In the dry range, lignin-based hydrogel treatment increased water retention between -20,000 cm to -50,000 cm soil water pressure head in the loamy fine sand but not between -50,000 cm to -1,00,000 cm soil water pressure head. While plant available water capacity was not different in amended and unamended samples in either soil types, in the capillary regions of the SWRC where soil water is easily accessible to plant roots, volumetric water content (VWC) was increased. To demonstrate the feasibility of using hydrogels similar to those used this study in an agricultural field, calculations were carried out based on results from the laboratory study. Our calculations indicate that at a 1% (w/w) concentration, the application of the lignin-based hydrogels to a 15 cm layer will not increase PAWS in both silt loam and loamy fine sand soils. It is possible a higher

concentration than 1% (w/w) may be needed to observe an increase in PAWS in the two soils.

CHAPTER 4. LABORATORY DETERMINATION OF THE IMPACT OF INCORPORATED ALKALI LIGNIN-BASED HYDROGEL ON THE HYDRAULIC CONDUCTIVITY OF SOIL

4.1 Abstract

Superabsorbent polymers (hydrogels) have been studied for their ability to improve soil hydraulic conductivity as hydrogels are able to store and release water due to their swelling properties. However, concerns related to the increased use of synthetic hydrogels has led researchers to switch their focus to biobased hydrogels which have the advantages of being more biocompatible, renewable, and biodegradable when compared to synthetic hydrogels. Here, we synthesized a lignin-based hydrogel, and amended a silt loam soil with it at concentrations of 0, 0.1, and 0.3% (w/w). The treatments were replicated three times and analysis of variance was employed to determine differences between treatments. A laboratory permeameter and double membrane tension infiltrometer were used to measure saturated and near-saturated hydraulic conductivity, respectively. The laboratory evaporation method coupled with Wind's iterative procedure were used in this study to obtain data for two main hydraulic conductivity functions i.e. hydraulic conductivity as a function of soil water pressure head $K(h)$ and hydraulic conductivity as a function of volumetric water content $K(\theta)$. Saturated hydraulic conductivity was statistically significantly decreased with the application of hydrogel at 0.1 and 0.3% (w/w) compared to the control treatment. In the near-saturation zone ($-10 \text{ cm} < h < 0 \text{ cm}$ soil water pressure head), application of 0.3% (w/w) lignin-based hydrogel significantly decreased hydraulic conductivity only at -1 cm soil water pressure head. Hydraulic conductivity in the 0.1 and 0.3% (w/w) treatments was increased along the $K(\theta)$ curve in the unsaturated zone ($-750 \text{ cm} < h < -10 \text{ cm}$) compared to the control treatment which we hypothesized was due to

bound water in the hydrogel being released creating a wider path for movement of water. The 0.1 and 0.3% hydrogel treatments also tended to store more water than the control treatment especially after 24 hours of evaporation. The implication of this study is that lignin-based hydrogel could be used to retain water in saturated soils and the bound water could be useful for improving the flow of soil water when in unsaturated state thereby reducing the water stress of plants as plants require less energy to move and absorb water. However, the lignin-based hydrogel should be tested on other textures of soil to ascertain its ability to influence hydraulic conductivity in those soil textures.

4.2 Introduction

Hydraulic conductivity describes the ability of soil to transmit water (Klute & Dirksen, 1986). Water flow in the vadose zone is regulated by unsaturated hydraulic conductivity (K) which is a function of the water retention curve $\theta(h)$ (Van Genuchten, 1980), where h is the soil matric potential. According to Gallage *et al.* (2013), when matric potential decreases as soil becomes unsaturated, some large pores become filled with air thus forcing water to flow through the smaller pores. A further decrease in matric potential decreases water filled pores thus increasing resistance to water flow and thus decreasing hydraulic conductivity. Perkins (2011) notes that to describe most models of water flow and solute transport, you need to know the relationship between K and volumetric water content (θ) which is a nonlinear relationship.

Hydrogels have been studied for their ability to influence soil hydraulic conductivity. Hydrogels are three dimensional hydrophilic materials that form a network in the presence of an aqueous solution (Peppas, 2000). Hydrogels are known to possess a

high swellability hence their use in various industries i.e., medicine, food, and agriculture. The formation of hydrogels occurs through the crosslinking of polymer chains dispersed in any aqueous medium by mechanisms including physical entanglements, ionic interactions, and chemical crosslinking (Zhang & Khademhosseini, 2017). In recent times, the increased usage of synthetic hydrogels has led researchers to switch their focus to biobased hydrogels which have the advantages of being easily degradable and biocompatible relative to synthetic hydrogels (Meng et al., 2019b). The application of hydrogels can affect hydraulic conductivity of soil as the high swelling capacity of some hydrogels stores substantial amounts of water in soil which blocks drainage pores thus reducing saturated hydraulic conductivity (K_s) (Al-Darby, 1996).

Numerous studies within the past few decades have investigated the impacts of hydrogel application on saturated hydraulic conductivity (K_s). In terms of the types of hydrogels applied to soil to investigate K_s , some studies applied biobased hydrogels (Demitri et al., 2013; Narjary & Aggarwal, 2014; Narjary et al., 2012; Song et al., 2020) while most studies in literature applied synthetic hydrogels (Abdallah, 2019b; Alkhasha et al., 2018; Andry et al., 2009; Bhardwaj et al., 2007; Han et al., 2013; Hussien et al., 2012; Mohawesh & Durner, 2019; Shahid et al., 2012; Smagin et al., 2019; Zhuang et al., 2013). While the addition of hydrogel to soil mostly decreased saturated hydraulic conductivity (K_s) (Abdallah, 2019b; Alkhasha et al., 2018; Mohawesh & Durner, 2019; Narjary & Aggarwal, 2014; Narjary et al., 2012; Shahid et al., 2012; Smagin et al., 2019; Song et al., 2020; Zhuang et al., 2013), some studies have observed an increase (Andry et al., 2009; Hu et al., 2019; Hussien et al., 2012) and others report a decrease and then a subsequent increase with time (Bhardwaj et al., 2007; Han et al., 2013; Hussien et al., 2012). The

inconsistency of results regarding the effects of hydrogel application to K_s leaves room for further studies to probe into applying other types to hydrogels to ascertain their effects on soil K_s .

Similarly, a survey of literature found three studies that measured unsaturated hydraulic conductivity (K) after applying hydrogel (Al-Darby, 1996; Liao et al., 2018; Smagin et al., 2019). All three studies reported a decrease in K . Al-Darby (1996) estimated K using a numerical method i.e., using Van Genuchten hydraulic function. Al-Darby (1996) observed a 63, 92 and 9% decrease in K corresponding to application rates of 0.2, 0.4 and 0.8% (w/w) hydrogel. Liao et al. (2016) measured the K of a sandy loam soil when a synthetic polyacrylamide and acrylic acid-based hydrogel were applied at rates of 0, 0.01, 0.03 and 0.06% (w/w). Their results revealed a decrease in K of 85.5 to 94.1% on day 0, 75.1 to 82.9% on day 30 and 65 to 76.2% on day 50. Smagin et al. (2019) noticed that at high matric potentials i.e., < -10 to -15 kPa, K reduced up to 2-3 times at concentrations ranging from 0.01-0.05% (w/w) and a reduction of 10-50 times at 0.1-0.2% concentration. However, at low matric potentials i.e., -20 to -700 kPa, K increased with an increase in application rate. The lack of studies investigating the impacts of bio-based hydrogels on K necessitates a further probe into applying and studying the impact of alternative bio-based hydrogels on K .

To the best of the author's knowledge, there are currently no studies that investigate the impacts of alkali lignin-based hydrogels on soil hydraulic conductivity under saturated and unsaturated conditions. Thus, there is a critical need to explore the impact of alkali lignin-based hydrogels on these two soil hydraulic properties especially for silt loam soil which is rarely considered in soil amendment studies involving hydrogels. Information on

the impact of lignin-based hydrogels on soil hydraulic conductivity will add to the growing evidence for the application of lignin-based bioproducts to soils to reduce waste and enhance carbon sequestration into the soil. The objectives of this study were thus to (a) determine the impacts of amending the lignin-based hydrogel on the saturated hydraulic conductivity (K_s), (b) determine the impacts of the lignin-based hydrogel on near saturation hydraulic conductivity, (c) determine the impacts of the lignin-based hydrogel on the change in total water storage in the soil and, (d) estimate the unsaturated soil hydraulic conductivity (K) of a disturbed silt loam soil amended with a lignin-based hydrogel from evaporation experiments using the Wind method. It was hypothesized that amending soils with the lignin-based hydrogel could reduce hydraulic conductivity compared to unamended soil. The lower hydraulic conductivity would reduce deep percolation of water in the soil while increasing soil water storage.

4.3 Materials and Methods

4.3.1 Lignin-based hydrogel

A lignin-based hydrogel was first synthesized following a synthesis method similar to that described in Passauer et al. (2012) and in Mazloom et al. (2019) with some modifications. A 1.5 M NaOH solution was added to the lignin alkali and the mixture was stirred using a glass rod for 5 min. For thorough mixing and to allow the lignin alkali to be dissolved completely, the mixture was further stirred on a magnetic stirrer (Heidolph™ MR Hei-Tec Magnetic Stirrer with Heating) set at 450 rpm for 24 hours. Then 0.5mmol of the cross-linker (PEGDGE) was added to the lignin alkali solution. This solution was placed on a heat source (Heidolph™ MR Hei-Tec Magnetic Stirrer with Heating) at 50°C

while stirring continuously for 10-15 minutes until the hydrogel was formed. The formed hydrogel was then removed and soaked in deionized (DI) water for 7 days to wash out unreacted monomers. Lastly the soaked hydrogels were freeze dried at -48°C in a freeze-drier (Labonco, Cat. No 7753024) to obtain a dried lignin-based hydrogel. The freeze-dried hydrogel was ground with a blender to obtain micron sized particles.

4.3.2 Soil properties

Bulk silt loam soil was obtained from the University of Kentucky Spindletop Farm located north of Lexington, Fayette County, Kentucky ($38^{\circ} 6' 18.07''\text{N } 84^{\circ} 29' 36.11''\text{W}$). Silt loam soil was selected because most of the studies on the effects of hydrogel on soil hydraulic properties have mainly investigated sandy soils with few based on silt loam soil. Secondly, silt loam soil was selected because it is the most common soil type in Kentucky and the southeastern United States, and it does not excessively expand in volume with changing moisture content (Arias et al., 2019). The soil was air-dried, ground, and sieved through a 2 mm sieve to obtain a homogeneous soil sample. Total nitrogen and carbon, cation exchange capacity, base saturation, exchangeable K, Ca, Mg, Na, pH, and soil texture were determined on the prepared soil. The texture of the soil was determined using the micropipette method (Miller & Miller, 1987). Cation exchange capacity (CEC) was analyzed using ammonium acetate extraction, bases (Mg, Ca, Na, K) were analyzed using inductively coupled plasma spectrophotometry (Jones Jr, 1999), and base saturation was determined as $\text{total bases/CEC} \times 100\%$. Total nitrogen was determined using the LECO combustion method (Yeomans et al., 1991). The pH of the soil was determined in water by using a glass electrode (Reed & Cummings, 1945).

4.3.3 Laboratory experiments

All hydraulic conductivity experiments were conducted in the soil physics laboratory of the Kentucky Agricultural Experiment Station, University of Kentucky, Lexington. Nine cylindrical metal rings of volume 245.12 cm^3 (height of 6 cm and diameter of 8.58 cm) were obtained. Three treatments were prepared by mixing soil and hydrogel at concentrations of 0, 0.1, and 0.3 (w/w). There were three replications for each treatment. The prepared soil samples were then packed into the metal rings to an approximate bulk density of 1.3 g cm^{-3} by gradually adding the samples and compacting with a wooden rummer with a flat bottom that fits into the metal rings. The samples were then placed into ring holders and double-sieve rings mounted to the bottom of the samples. The ring holders were placed in the permeameter in which there is a reservoir of water and gradually saturated by regulating the water table. The saturated hydraulic conductivity (K_s) of the hydrogel-amended soils was measured using the permeameter (Eijkelkamp, 2017). The experimental set-up for measuring K_s is shown in APPENDIX B. 1 (Figure B. 1). The K_s was measured using the constant water head method based on the percolation rate of the samples (Klute & Dirksen, 1986). The water table within the ring holder rose quickly (within minutes to hours) to the level of the reservoir, thus a constant water head method was used for determining the K_s .

For the constant head, the volumetric water flow rate through the soil samples was recorded at time intervals. The hydraulic head applied to a sample was determined by taking the difference between the water level in the container and the water in the ring holder.

K_s was then calculated by rearranging the Darcy equation:

Equation 4.1

Where Q is the water flowing per unit time (cm^3/day)

A is the cross-sectional area of the sample (cm^2)

Δh is the hydraulic head causing the flow as measured by the level of water in the manometer (cm)

L is the length of the sample (cm)

K_s is the proportionality constant/ saturated hydraulic conductivity

To determine hydraulic conductivity near saturation, a tension infiltrometer apparatus consisting of a double pressure plate-membrane at the top and the bottom of the soil core was used (Wendroth et al., 1999). After K_s measurements were completed, the soil samples were transferred to the tension infiltrometer apparatus. Similar pressure heads were applied to both the upper and the lower boundaries of the soil cores to achieve steady-state flow conditions (Wendroth et al., 1999). The main parts of the double plate tension infiltrometer (Figure 4.1) include the water reservoir, the upper and the lower membrane plates, and the bubbling tower. The bubbling tower is connected to the water reservoir and water flows through the permeable membrane into the soil when air enters the air entry tube and into the water reservoir. The same pressure heads are then applied to the upper and lower permeable membrane by controlling the height of water in the bubbling tower

using a suction control tube. Hydraulic conductivity was determined by applying pressure heads of -10, -5 and -1 cm.

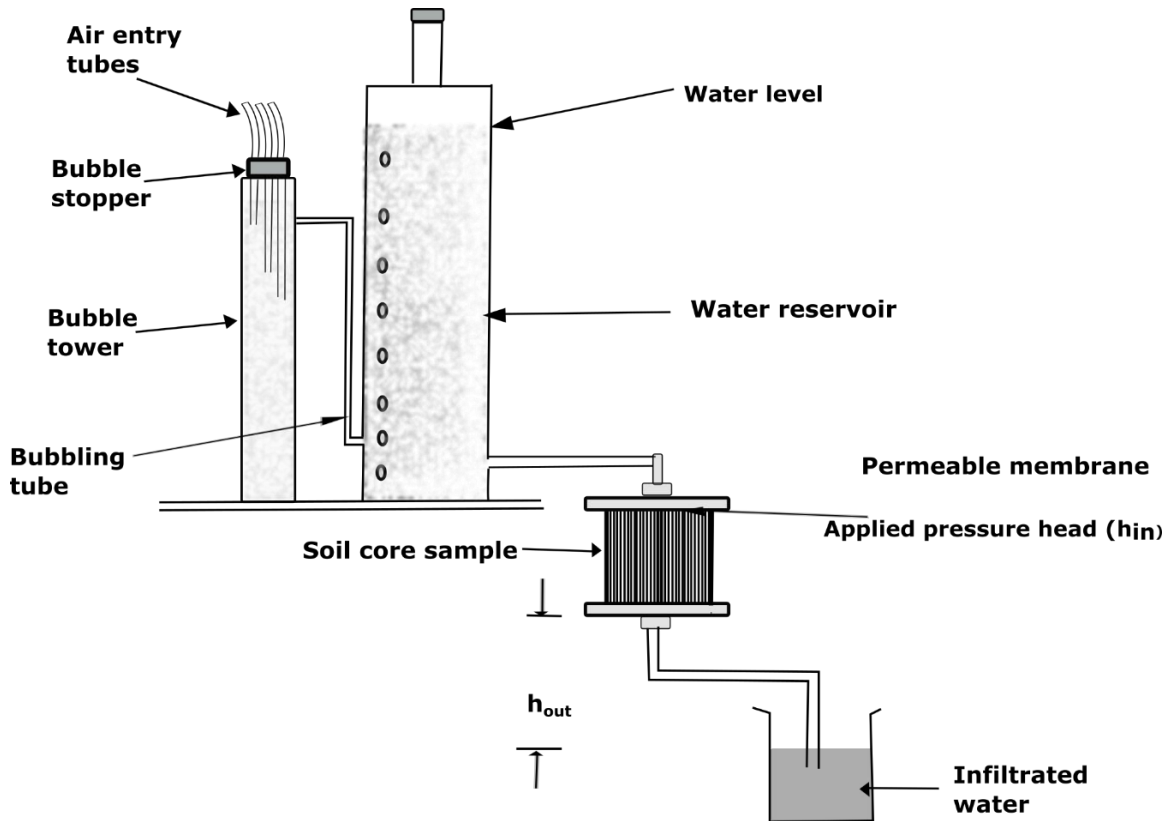


Figure 4.1. Schematic of the double membrane tension infiltrometer method, redrawn from (Wendroth et al., 1999) for measuring hydraulic conductivity near saturation.

To calculate the hydraulic conductivity in the different hydrogel-soil samples, the infiltration of water into the sample was first determined. The application of the same pressure head at both ends of the soil cores allowed for the establishment of steady-state infiltration conditions which was obtained when flowrate of the percolating water through the samples became constant. This constant infiltration rate was then multiplied by the area

of the reservoir and divided by the area of the metallic core to obtain the hydraulic conductivity in the sample.

The laboratory-based evaporation method was used to determine the unsaturated hydraulic conductivity relationship [$K(h)$ or $K(\theta)$] on the cores of treatments (Wendroth et al., 2008) from the range of -10 to -750 cm soil water pressure head at two soil depths. The evaporation method was conducted following methods described in (Schindler & Müller, 2006; Tamari et al., 1993; Wendroth et al., 2008; Wind, 1966). Two electronic pressure transducer tensiometers with cups of length 6 cm and 0.6 cm outer diameter (o.d) were inserted horizontally into pre-drilled holes in cylindrical metal rings of volume 245.12 cm³ (height of 6 cm and diameter of 8.56 cm) containing the soil treatments. The holes were located at 1.5 cm and 4.5 cm respectively from the surface of the soil core.

The cylindrical metal rings with samples were then placed on an in-house designed box containing the data logging system (CR3000 datalogger, Campbell Scientific Inc.) which was used to record the change in pressure in the tensiometers. The contact points between the bottom of the metal rings and the box were fitted with O-rings to prevent evaporation of water. The set-up for the evaporation is shown in APPENDIX B. 1(Figure B. 2). The samples were covered with plastic wraps and left standing for 24 hours to avoid evaporation while hydrostatic equilibrium was being established. Hydrostatic equilibrium was indicated by steady tensiometer readings equal to the height difference between the two tensiometers (3 cm) (Wendroth et al., 2008). After establishing the initial pressures in the upper and lower tensiometers, the evaporation process was initiated by removing the plastic wraps from the top of the soil cores. Initial sample weights were recorded using the data logger. The evaporation process was started and terminated when the top tensiometer

(1.5 cm from the soil core surface) reached a soil water pressure head of $h \approx -750$ cm. Pressure head and water content in the samples were logged every 5 minutes. At the end of evaporation, the mass of the tensiometers, the box, the ring, and wet soil were recorded. Residual water content was determined by drying the wet soil with the ring at 105°C for 24 hours. A schematic of the experimental set-up is shown in Figure 4.2.

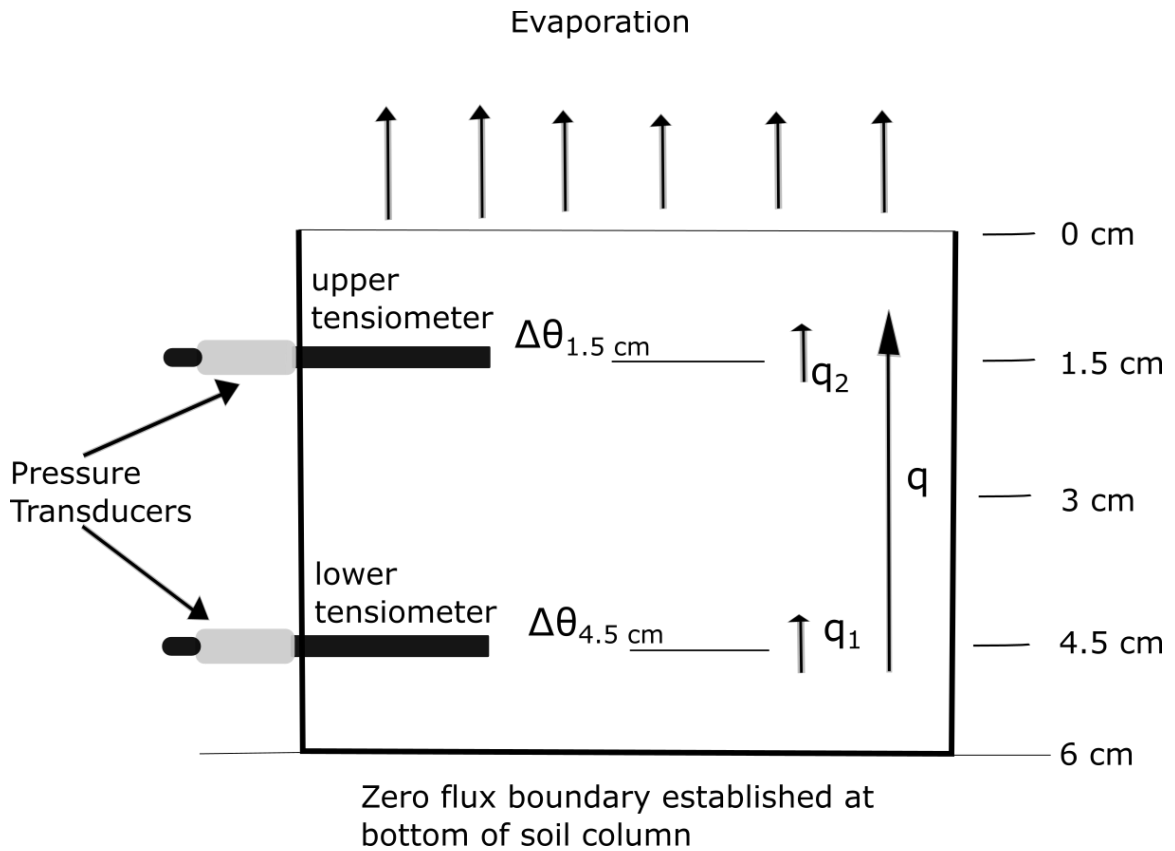


Figure 4.2. Experimental set-up for determining the hydraulic conductivity of the hydrogel amended soils using the evaporation method. Redrawn from Wendroth et al. (1993), where q_1 and q_2 represent the upward volume flux density of water across the 4.5 cm and 1.5 cm boundaries respectively in the soil cores. The average upward volume flux density of water between the 1.5 and 4.5 cm boundaries is represented by q .

4.3.4 Theory for determination of soil hydraulic functions

To derive the functions for unsaturated hydraulic conductivity, we assumed that the soil water retention and the unsaturated hydraulic conductivity curves which are both non-linear functions can be described using the analytical form closed-form equation proposed by van Genuchten (Van Genuchten, 1980):

Equation 4.2

$$\theta = \theta_r + \frac{(\theta_s - \theta_r)}{[1 + (ah)^n]^m} \quad (4.2)$$

Where h is the measured soil water pressure head from the tensiometer readings, θ_s , θ_r , α , and n are fitting parameters. The hydraulic conductivity (K) was then estimated for each time interval following the reevaluated procedure via numerical simulations described by Wendroth et al. (Wendroth et al., 1993; Wendroth et al., 2008).

Briefly, the schematic of the soil sample shown in Figure 4.2 is composed of two compartments and the water content in the soil is assumed to change with time according to the measured soil water pressure head values at the two tensiometer locations (1.5 cm and 4.5 cm). An initial guess for the water retention parameters was used to calculate the water storage in the upper 3 cm and lower 3 cm of the soil core. The total water storage in the two compartments was then estimated based on the volumetric water content calculated using the van Genuchten function. That estimated total water storage was then compared with the total amount of water in the soil core determined using mass loss of the soil core. The curve fitting van Genuchten equation was then used to update the water contents to get new set of fitting parameters (θ_s , θ_r , α , and n). This process is repeated until the difference between the estimated water content and the measured water contents were <

0.0001 cm³ cm⁻³. After convergence of the solution i.e., when the measured soil water storage equals the estimated soil water storage for the two depths, the final water content values were then used for calculating the water fluxes between the two depths (Arias et al., 2019). The hydraulic conductivity (K) for a given time was calculated using:

Equation 4.3

$$K = -\frac{q}{Ave. grad} \quad (4.3)$$

Where q (cm s⁻¹) is the average water flux between the two tensiometers and *Ave. grad* is the average hydraulic head gradient causing flux between two successive time intervals of measurements.

The corresponding h and θ values were calculated using:

Equation 4.4

$$\bar{h} = \frac{h_{i,-1.5cm} + h_{i+1,-1.5cm} + h_{i,-4.5cm} + h_{i+1,-4.5cm}}{4} \quad (4.4)$$

Equation 4.5

$$\bar{\theta} = \frac{\theta_{i,-1.5cm} + \theta_{i+1,-1.5cm} + \theta_{i,-4.5cm} + \theta_{i+1,-4.5cm}}{4} \quad (4.5)$$

Where $h_{i,z}$ and $\theta_{i,z}$ represent the measured soil water pressure head and the volumetric water content from the water retention curve estimated, respectively, while i and z represent the time step and depth of insertion of the tensiometers.

4.3.5 Statistical analysis

Analysis of variance (ANOVA) was used to test for the difference in means among the three treatments for the samples and if a difference was detected, Tukey's test (Tukey, 1949) was used to determine which treatment(s) differed significantly from the others. Before the statistical tests were conducted the data were checked for normality and equal variance assumptions and appropriate tests were applied. All statistical tests and graphing were done in (SigmaPlot version 14.0, Systat Software, Inc., San Jose, CA, USA, www.systatsoftware.com). A significant level of 5% ($\alpha = 0.05$) was used for all statistical comparisons.

4.4 Results and Discussion

The physical and chemical properties of the soils used in this study are shown in Table 4.1.

Table 4.1. Physical and chemical properties of silt loam soil.

Soil texture	Clay (%)	Silt (%)	Sand (%)	Total N (%)	Total C (%)	CEC	Ex. Mg	Ex. Ca	Ex. Na	Ex. K	Base saturation (%)	pH
Silt loam	18.18	72.25	9.57	0.178	1.769	18.68	1.37	11.2	0.03	0.67	71	5.73

CEC is the cation exchange capacity, exchangeable (Ex.) Mg, Ca, Na, and K were all measured in meq/100g of soil. The pH was measured in water.

A detailed description of characteristics of the synthesized lignin-based hydrogel is reported in Chapter 3.4.2 of this dissertation. The synthesized hydrogel was freeze-dried and ground with a blender to obtain micron sized particles before proceeding to amend the soil with it.

4.4.1 Effect of lignin-based hydrogel on saturated hydraulic conductivity

The first objective of this study was to amend the silt loam soil with lignin-based hydrogels and quantify the variation of K_s in the soil by laboratory measurements and calculations using Darcy's law. Figure 4.3 presents the measured values of K_s for the lignin-based hydrogel-soil mixtures at different hydrogel concentrations. The K_s in the 0% (w/w) treatment was $339.19 \pm 104.5 \text{ cm d}^{-1}$, $38.81 \pm 15.80 \text{ cm d}^{-1}$ in the 0.1% (w/w) treatment, and $45.04 \pm 19.60 \text{ cm d}^{-1}$ in the 0.3% (w/w) treatment.

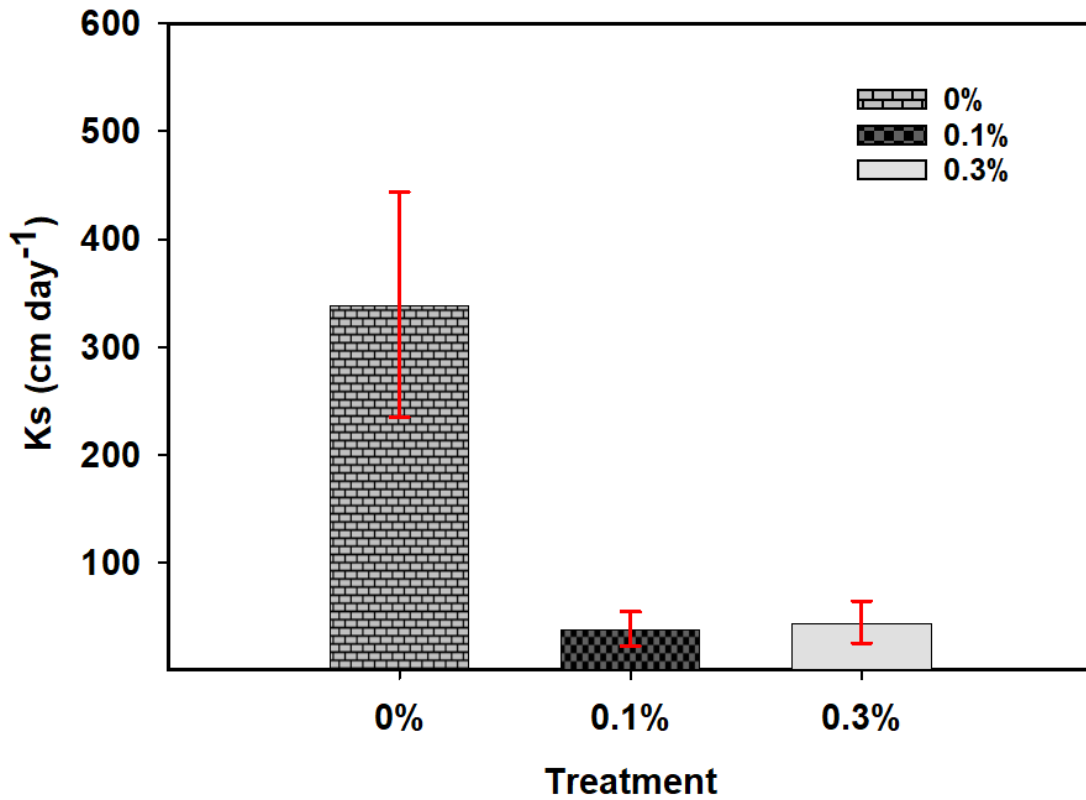


Figure 4.3. Saturated hydraulic conductivity (K_s) of the lignin-based hydrogel-soil mixtures at 0%, 0.1%, and 0.3% (w/w) treatment application rates. Error bars indicate standard error of the means ($n=3$).

Saturated hydraulic conductivity was statistically significantly decreased with the application of hydrogel at 0.1 and 0.3% (w/w) compared to the control treatment ($p < 0.05$). The 0.1% (w/w) treatment decreased K_s by 88.5% while the 0.3% (w/w) treatment decreased K_s by 87%. However, there was no statistically significant difference in K_s between the 0.1 and 0.3% (w/w) treatments. Our results agree with previous studies (Abdallah, 2019b; Alkhasha et al., 2018; Mohawesh & Durner, 2019; Narjary & Aggarwal, 2014; Narjary et al., 2012; Shahid et al., 2012; Smagin et al., 2019; Song et al., 2020; Zhuang et al., 2013) that reported a decrease in K_s with application of hydrogels to various soils. Half the studies reported similar decreases in K_s and half reported decreases in K_s one order of magnitude smaller than what we found.

Among the studies listed above, only one study (Song et al., 2020) applied a similar bio-based hydrogel. Song et al. (2020) applied a lignin-sodium alginate hydrogel to a sandy-loam soil and observed a decrease of 63.2-89.5% in K_s of a sandy loam soil with an increase in concentration of the hydrogel from 0 to 0.975% (w/w). The magnitude of decrease in K_s in Song et al. (2020) is similar to the decrease observed in our study. Our results indicate that alkali lignin could be used with other polymers to synthesize hydrogels that could be useful in reducing K_s in soils. A possible explanation for the decrease in K_s could be attributed to the swelling characteristic of the lignin-based hydrogel. Swelling experiments conducted on the lignin-based hydrogel in Chapter 3 determined the swelling rate to be 20.3 g of water/ g hydrogel in deionized water. Due to the swelling characteristic

of the lignin-based hydrogel, its expansion in the presence of water reduced the size of drainage pores in the soil while causing aggregation of the soil particles (Al-Darby, 1996; Narjary et al., 2012) which reduced the number of pores available for downward movement of water in soil.

4.4.2 Effect of lignin-based hydrogel on near-saturated hydraulic conductivity

Near saturation K was determined using the double membrane tension infiltrometer apparatus. Figure 4.4 presents results of the effect of the different treatments of the lignin-based hydrogel at soil water pressure of -1, -5, and -10 cm on hydraulic conductivity. Near saturated K values were two orders of magnitude lower than K_s values. The sharp decrease in hydraulic conductivity across small soil water head pressure range changes near saturation ($-10 \text{ cm} < h < 0 \text{ cm}$) is attributed to the effects of structural macropores (Jarvis & Messing, 1995; Jarvis et al., 2002). At $h = -1 \text{ cm}$, the K value in the 0% (w/w) treatment was $2.16 \pm 0.14 \text{ cm d}^{-1}$, $2.08 \pm 0.25 \text{ cm d}^{-1}$ in the 0.1% (w/w) treatment, and $0.45 \pm 0.03 \text{ cm d}^{-1}$ in the 0.3% (w/w) treatment. Hydraulic conductivity was statistically significantly decreased with the application of hydrogel at 0.3% (w/w) compared to the 0 and 0.1% (w/w) treatments ($p < 0.01$). However, there was no statistically significant difference in K between the 0 and 0.1% (w/w) treatments. Our results imply that the effect of lignin-based hydrogels in decreasing hydraulic conductivity is intensified as soil water pressure increases towards saturation. In saturated and near saturated states, a higher dose of lignin-based hydrogel decreases hydraulic conductivity, but that decreasing effect diminishes as soil water pressure head decreases.

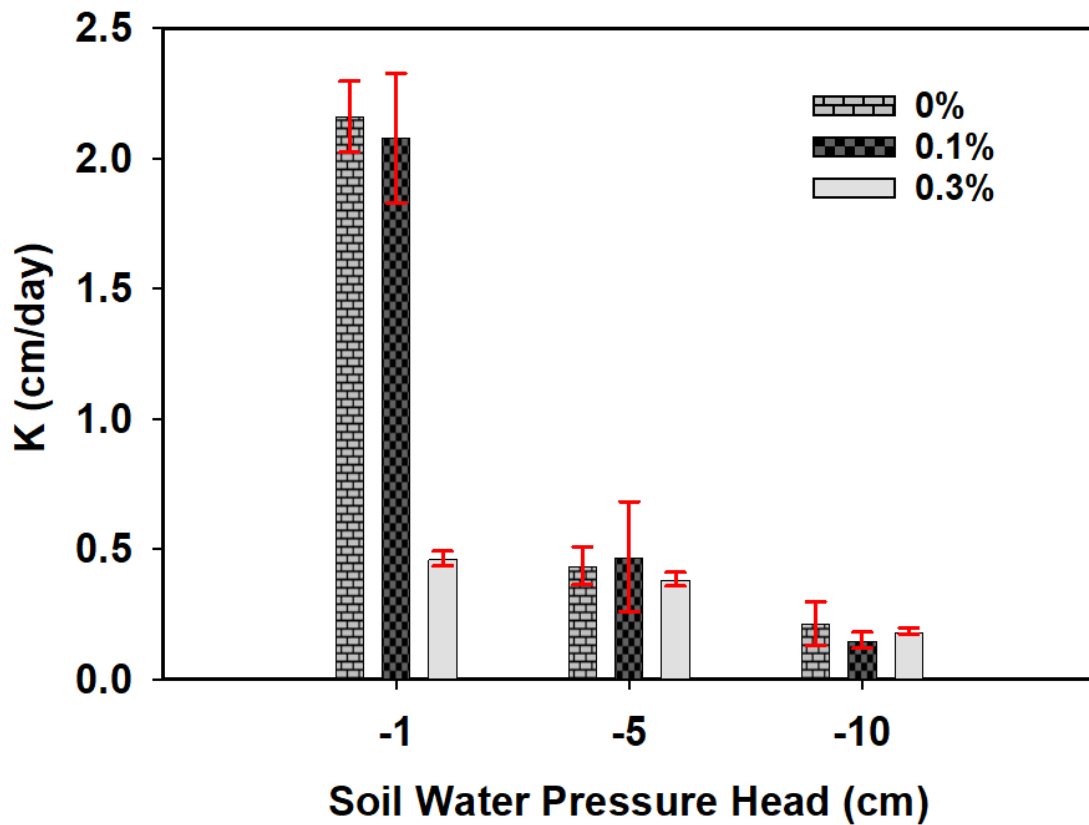


Figure 4.4. Near-saturated hydraulic conductivity (K) of the lignin-based hydrogel-soil mixtures at 0%, 0.1%, and 0.3% (w/w) treatment application rates. Error bars indicate standard error of the means ($n=3$).

While several studies have mostly focused on exploring the effects of hydrogel applications on saturated hydraulic conductivity, few studies (Smagin et al., 2019) attempted to extend the measurement to near saturated condition i.e. ($-10 \text{ cm} < h < 0 \text{ cm}$) through modeling techniques. Smagin et al. (2019) tested a radiated-cross-linked technical polyacrylamide hydrogel on a silty sand soil at 0.01 to 0.3 % (w/w) application rates. They reported 2-3 times decrease in hydraulic conductivity between soil water pressure heads of

less than -100 cm at hydrogel application rates of 0.01 to 0.05% (w/w) and a decrease of 10-50 times in hydraulic conductivity with application rates of 0.1 to 0.2% (w/w).

4.4.3 Effect of lignin-based hydrogel on unsaturated hydraulic conductivity relationships using the evaporation method

The evaporation method coupled with Wind's iterative procedure (Wind, 1966) was used to determine the unsaturated hydraulic conductivity relationship [$K(h)$ or $K(\theta)$] when the silt loam soil was amended with lignin-based hydrogel. Figure 4.5a depicts the estimated volumetric water content plotted against the hydraulic conductivity while Figure 4.5b depicts the estimated soil water pressure head plotted against the hydraulic conductivity for the three soil-hydrogel treatments. While running simulations using the Wind's method, some values for K were rejected. Due to high uncertainty of tensiometer readings at low gradients i.e., close to 0, all K values obtained from gradients < 0.2 cm were rejected in this study (Peters & Durner, 2008; Wendroth et al., 1993). Three replicates of each treatment were obtained and averaged for volumetric water content, soil water pressure head, and hydraulic conductivity. From Figure 4.5a, hydraulic conductivity decreased with a decrease in volumetric water content in all treatments. This decrease is due to soil becoming increasingly unsaturated since less pore spaces are filled with water, thus flow paths become tortuous, and drag forces between the soil particles and the water increases (Van Genuchten & Pachepsky, 2011). The textural properties of the silt loam soil used in this experiment will also affect the K as soil texture is less variable and will dominantly affect K in the unsaturated range (Lal & Shukla, 2004). Noticeably, K in the 0.1 and 0.3% (w/w) treatments was increased along the entire curve compared to the control treatment. Similarly, from Figure 4.5b, K decreased drastically by three orders of

magnitude from -80 cm to -750 cm which is typical as soil becomes unsaturated regardless of hydrogel treatment. While we see a clear increase in K as soil water content decreased, the difference between the three treatments is not apparent when soil water pressure is plotted against K .

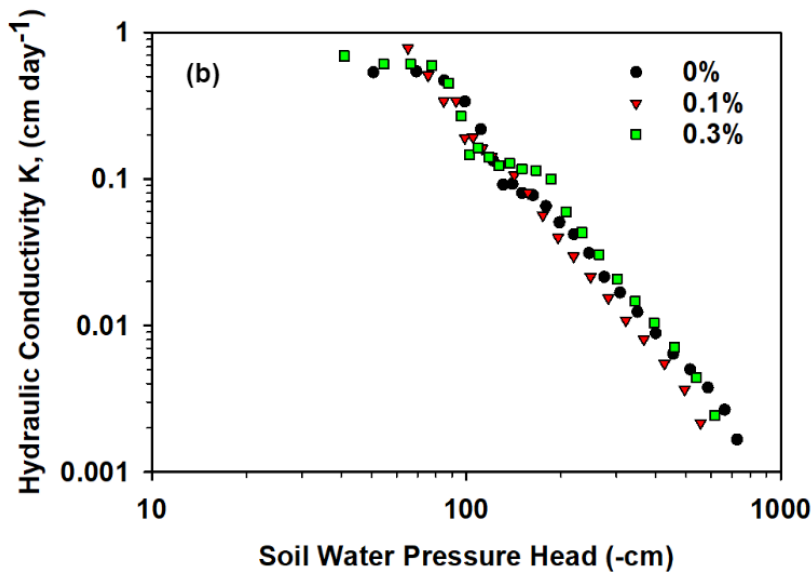
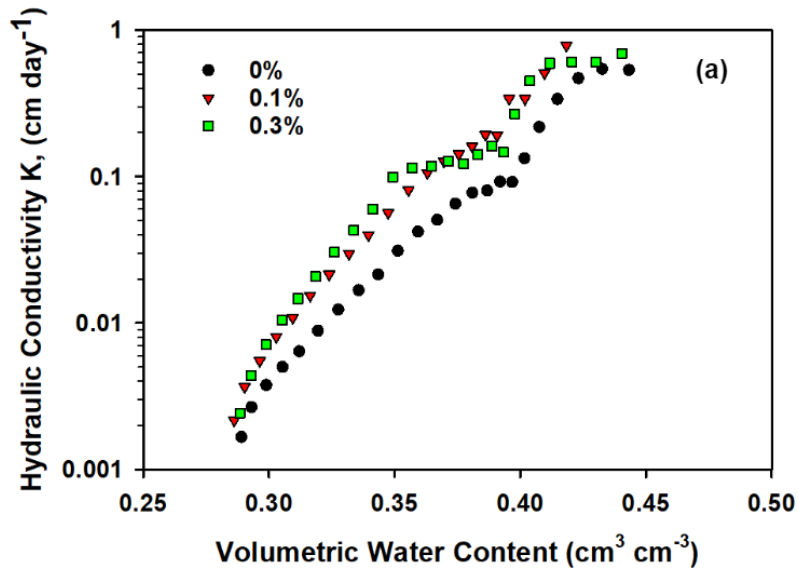


Figure 4.5. Hydraulic conductivity functions for the silt loam soil when amended with 0, 0.1, and 0.3% (w/w) lignin-based hydrogel determined with the evaporation method (a) volumetric water content against hydraulic conductivity $K(\theta)$, and (b) soil water pressure head against hydraulic conductivity $K(h)$.

A hypothesized reason the application of the lignin-hydrogel at 0.1 and 0.3% (w/w) increased K is that as soil moves from the saturated phase into the unsaturated phase, the swollen hydrogels particles create smaller drainage pores. The hydrogel which retains bound water for a period gradually releases the bound water as soil dries which creates a wider path/increases cross sectional area for the movement of water thus increasing K .

There are limited studies in literature that investigate the effects of hydrogels, especially lignin-based hydrogels on unsaturated hydraulic conductivity compared to saturated hydraulic conductivity. The few studies that determined the unsaturated hydraulic conductivity of soils after hydrogel amendment used various synthetic-based hydrogels (Al-Darby, 1996; Liao et al., 2018; Mohawesh & Durner, 2019; Smagin et al., 2019). Al-Darby (1996) estimated K using a numerical method i.e., using Van Genuchten hydraulic function. Al-Darby (1996) observed a 63, 92 and 99% decrease in K corresponding to application rates of 0.2, 0.4 and 0.8% (w/w) of the hydrogel. Liao et al. (2016) observed a decrease in K of 85.5 to 94.1% on day 0, 75.1 to 82.9% on day 30 and 65 to 76.2% on day 50 when synthetic polyacrylamide and acrylic acid-based hydrogels were applied to sandy loam soil. Mohawesh & Durner (2019) measured the unsaturated hydraulic conductivity of a sandy soil after applying bentonite, biochar, and hydrogel to the soil. The hydrogel was amended at rates of 0, 0.1, 0.25, and 0.5% (w/w). The authors reported that all soil amendments decreased unsaturated hydraulic conductivity in the wet range i.e., saturated

and near saturated conditions. They attributed the decrease to an increase in tortuosity and particle packing. Smagin et al. (2019) observed that at high matric potentials i.e., < 10 to 15kPa, K reduced up to 2-3 times at concentrations ranging from 0.01-0.05% (w/w) and a reduction of 10-50 times at 0.1-0.2% concentration. However, at low matric potential i.e., 200 to 3030 kPa, K increased with an increase in application rate.

Our results contrast with the findings of Al-Darby (1996) and Liao et al. (2016) as they report decreases in K . It is possible the different soil types used in Al-Darby (1996) and Liao et al. (2016) was the reason K decreased as opposed to increased. The two studies used mostly sandy soils which have large pores which drain faster compared to fine-textured soils like silt loam soil (Lal & Shukla, 2004) used in our study. Thus, the presence of the hydrogels in their sandy soils tended to increase tortuosity which reduced K (Mohawesh & Durner, 2019). Our results, however, agree with Smagin et al. (2019) who reported 10-20 times increase in K in the unsaturated regions. The authors attributed the increase in K to a change (increase) in the pore space of the sandy soil used in their study because of the hydrogels applied.

4.4.4 Effect of lignin-based hydrogel on change in total water storage in the soil

The total soil water storage was estimated for each treatment by first calculating the volumetric water contents at the two tensiometer elevations ($\theta_{1.5}$ and $\theta_{4.5}$) at each time step. The two volumetric water contents were then added, and the result multiplied by the depth between them i.e., 3 cm to obtain the total soil water storage. Change in total soil water storage over time is shown in Figure 4.6. From Figure 4.6, at the start of evaporation, the amount of water stored in all treatments was approximately 2.6 cm. As evaporation continued, the 0.1 and 0.3% treatments tended to store more water than the control

treatment especially after 24 hours ($p < 0.005$) and to lesser extent after 48 hours ($p = 0.059$). At the end of the evaporation experiment, total soil water storage was similar in all treatments ($p = 0.23$) at 1.51 cm for the control treatment, 1.58 cm for the 0.1% (w/w) treatment, and 1.55 cm for the 0.3% (w/w) treatment. Overall, the effect of the concentration of the hydrogel on total soil water storage was not significant at the beginning of the evaporation experiment, however, we hypothesize there was an influence of the lignin-based hydrogel on the total soil water storage during stage 2 of evaporation. During stage one, evaporation is influenced by environmental factors like atmospheric temperature, wind speed, and humidity (Idso et al., 1974). During stage 2, evaporation shifts from the surface water to the sub-surface water resulting in the formation of a dry surface layer (Rose, 1968). Hydrogels can intercept the movement of water upwards as some water will be absorbed and kept at the level just beneath the soil surface thus increasing total soil water storage.

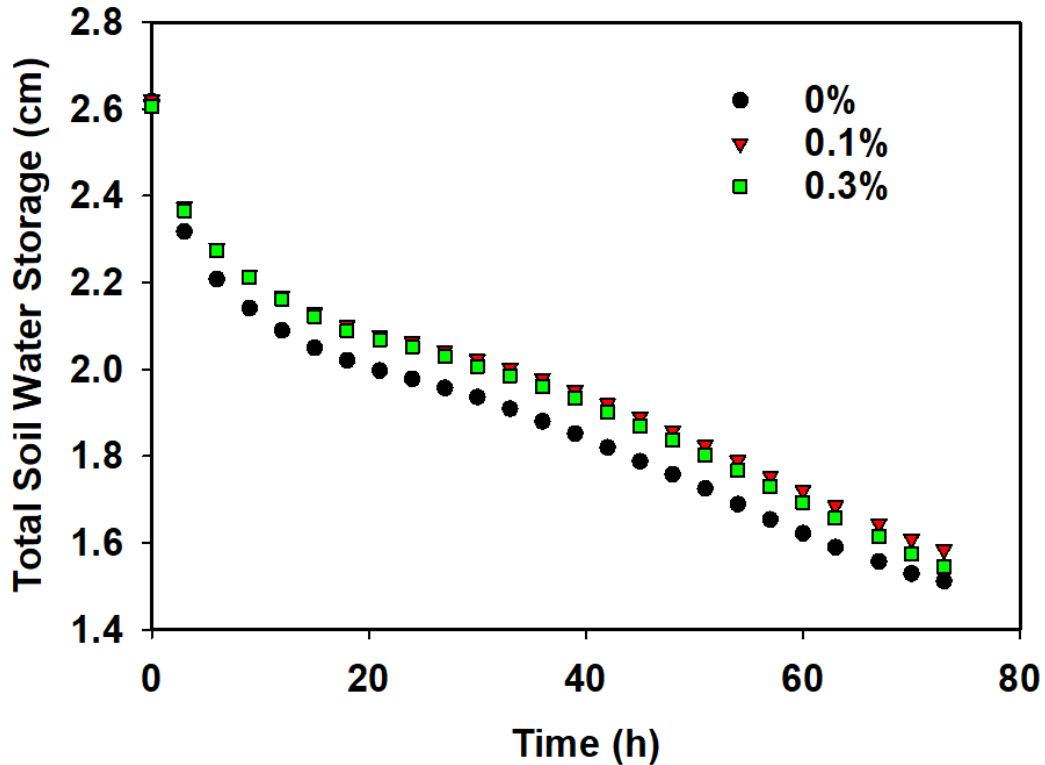


Figure 4.6. Change in total soil water storage in the 0, 0.1, and 0.3% (w/w) lignin-based hydrogel treatment after 73 hours of evaporation.

4.5 Conclusions

This study resolved the impacts of three application rates of lignin-based hydrogel on the saturated hydraulic conductivity, near saturated hydraulic conductivity, unsaturated hydraulic conductivity, and soil water storage in a silt loam soil. Our main hypothesis of a decrease in hydraulic conductivity was supported but only in the saturated and near-saturation zone ($-10 \text{ cm} < h < 0 \text{ cm}$) of soil water pressure head. Saturated hydraulic conductivity was statistically significantly decreased with the application of hydrogel at 0.1 and 0.3% (w/w) compared to the control treatment. In the near-saturation zone (-10

cm < h < 0 cm), application 0.3% (w/w) lignin-based hydrogel significantly decreased hydraulic conductivity. Noticeably, unsaturated hydraulic conductivity (K) in the 0.1 and 0.3% (w/w) treatments was increased along the $K(\theta)$ curve in the unsaturated zone (750 cm < h < 10 cm) compared to the control treatment. A clear trend was however not seen in the $K(h)$ curve as the three treatments were indistinguishable. Our results also suggest the 0.1 and 0.3% treatments tended to store more water than the control treatment especially after 24 hours of evaporation. Future studies should be conducted to test the lignin-based hydrogel on other textures of soil. Regardless, the implication of this study is that lignin-based hydrogel could be used to retain water in saturated silt loam soils and the bound water could be useful for improving the flow of soil water when in unsaturated state thereby reducing the water stress of plants as plants require less energy to absorb water.

CHAPTER 5. FEATURE SELECTION AND MACHINE LEARNING REGRESSION METHODS TO PREDICT SATURATED HYDRAULIC CONDUCTIVITY FROM A LARGE PUBLIC SOIL DATABASE

5.1 Abstract

One of the most important soil hydraulic properties for modeling water transport in the vadose zone is saturated hydraulic conductivity. However, it is challenging to measure it in the field. Pedotransfer Functions (PTFs) are mathematical models that can predict saturated hydraulic conductivity (K_s) from easily measured soil characteristics. Though the development of PTFs for predicting K_s is not new, the tools and methods used to predict K_s are continuously evolving. Most current PTFs do not justify the selection of features from the soil database while developing PTFs. However, ideal model performance depends on choosing soil features that explain the most amount of K_s variance with the fewest input variables. In addition, the lack of interpretability in most “black box” machine learning models makes it difficult to extract practical knowledge as the learning process obfuscates the relationship between inputs and outputs in the PTF models. The objective of this study was to develop a set of new PTFs for predicting K_s using machine learning algorithms and a large database of over 8000 soil samples while incorporating statistical methods to inform feature selection for the model inputs. Feature selection using principal component analysis coupled with correlation analysis was used to select five influential soil properties (% clay, % silt, % fine sand, % medium sand, and bulk density) for model development. Using six different machine learning (ML) algorithms i.e., multiple linear regression (MLR), k-nearest neighbor (KNN) regression, support vector regression (SVR), deep neural networks regression (DNNR), random forest regression (RF), and gradient boosted regression (GB), PTFs were developed to predict K_s using a training data set. The performance of the PTFs

in estimating K_s was evaluated using coefficient of determination (R^2), mean absolute error (MAE), and root mean square error (RMSE) on an independent test data set (data not used in the training of the model).

Of the ML models tested, random forest regression and GB both gave the best performances with $R^2 = 0.71$ and $RMSE = 0.47 \text{ cm h}^{-1}$ on the test data (validation data set). However, the RF regression model produced a slightly lower $MAE = 0.32 \text{ cm h}^{-1}$ than the GB regression model with $MAE = 0.33 \text{ cm h}^{-1}$ on the validation data. The permutation feature importance technique was applied to determine which variables described the most variability for predicting K_s in a validation (data not used in training the models). The GB and RF regression models showed comparable results where clay content described the most variation in the data, followed by bulk density. Both GB and RF algorithms use regression trees, and despite the complex nature of boosted regression trees, they do possess advantages that make them favorable for predictive modeling. Regression trees can reduce bias and mean square error compared to traditional machine learning algorithms and are also suited for predicting non-linear relationships between input and output variables. While the PTFs developed in this study are not generalizable for all soils and geographical locations, this study offers a process to compare alternative machine learning based PTFs when using large public soil databases. The implication of this study is that, when predicting K_s using the Florida Soil Characterization Database, priority should be given to obtaining quality data on clay content and bulk density as they are the most influential predictors for estimating K_s in the random forest and gradient boosted regressions, the ML algorithms that performed the best on both the training and the testing datasets.

5.2 Introduction

Saturated hydraulic conductivity (K_s) is the most important hydraulic property of soil measured in the laboratory (Reynolds, 2008) or in the field. The hydraulic conductivity as a function of soil water content or soil water pressure head and the water retention properties of soil determines the behavior of soil water flow systems. Hydraulic conductivity describes the ability of the soil to transmit water (Klute & Dirksen, 1986) and is important for describing the dynamic processes in fluid flow (Schwartz, 2002). Additionally, saturated hydraulic conductivity is often used in combination with soil water retention functions to predict unsaturated hydraulic conductivity due to the difficulty in measuring the complete unsaturated hydraulic conductivity function directly (Zhang et al., 2019).

One option for indirectly determining saturated hydraulic conductivity in soil is using pedotransfer functions (PTFs). PTFs are models that can predict soil hydraulic properties, i.e., water retention curve and the saturated hydraulic conductivity, from easily measured soil characteristics like particle-size distribution, organic matter content and bulk density (Cornelis et al., 2001; Padarian et al., 2018; Wösten et al., 1995). PTFs are essentially regression functions that are used to predict soil properties whose measurements may be impeded by cost, time, difficulty, or hazards involved in obtaining reliable measurements (Padarian et al., 2018). PTFs have been broadly categorized into *class* PTFs and *continuous* PTFs (Rasoulzadeh, 2011; Van Looy et al., 2017; Wösten et al., 1995). Class PTFs predict hydraulic properties from textural classes (the USDA defines twelve major soil texture classifications (sand, loamy sand, sandy loam, loam, silt loam, silt, sandy clay loam, clay loam, silty clay loam, sandy clay, silty clay, and clay) while

continuous PTFs utilize measured percentages of clay, silt, sand, bulk density, and organic matter to determine various hydraulic properties (Rasoulzadeh, 2011; Van Looy et al., 2017). In recent times, large international soil datasets e.g., UNSODA (Leij, 1996), HYPRES (Wösten et al., 1999) and NRCS National Soils Information System (Rawls et al., 2007) have been used by various researchers to develop PTFs. The past two decades have seen a drastic increase in PTF developments in literature. These recent studies also developed PTFs for soil water retention (Haghverdi et al., 2015; Lamorski et al., 2008; Nemes et al., 2006; Schaap & Leij, 1998b; Twarakavi et al., 2009; Wang et al., 2012; Wösten et al., 1999) and saturated hydraulic conductivity PTFs which we will introduce below.

Despite the success of using more traditional regression equations (e.g., linear logarithmic, or exponential) for estimating parameters for PTFs, their application may be limited in the sense that, the mathematical relationship between the predictors and soil property of interest may vary within the training dataset used, i.e., the underlying model may change over the geographical area of interest (Van Looy et al., 2017). In addition, regression is often limited by the assumptions implicit in traditional statistical methods (Elith et al., 2008). However, another approach for predicting soil hydraulic properties which does not require an assumed underlying model or the existence of a pre-assumed relationship within the predictor variables is machine learning (ML) modeling (Elith et al., 2008). For example, according to Nemes et al. (2006), in regression-based models, one first identifies the right equations while assuming that the probability distribution of the error is similar across the data space, an assumption that may be difficult to prove. However, ML techniques use similarities between samples to predict a new sample, which

is advantageous when the form of the relationship between the input and output variables are unknown before analysis (Nemes et al., 2006). Machine learning methods develop models based on patterns identified in the dataset used to train them. Along with big data technologies and high-performance computing, ML has emerged as a tool to create new opportunities to reveal, quantify and understand data-intensive processes in agriculture (Liakos et al., 2018), such as modeling soil physical properties.

Several researchers have developed PTFs for predicting saturated hydraulic conductivity (Agyare et al., 2007; Arshad et al., 2013; Elbisy, 2015; Jorda et al., 2015; Kashani et al., 2020; Kotlar et al., 2019; Nivetha et al., 2019; Rasoulzadeh, 2011) and near saturated hydraulic conductivity (Jarvis et al., 2002; Jorda et al., 2015; Kotlar et al., 2019) using various machine learning techniques. Machine learning (ML) algorithms use pattern recognition approaches, which help describe relationships between input parameters and output parameters by “learning” characteristics of the relationships using a training dataset (Twarakavi et al., 2009). Because ML is not restricted to the same assumptions as traditional regression modeling techniques, machine learning can achieve more accurate and more reliable predictions than traditional regression models (Achieng, 2019; Lamorski et al., 2008; Schaap & Leij, 1998a).

While considerable research has been devoted to developing machine learning based PTFs for predicting K_s , the current PTFs developed rarely justify the *a priori* selection of predictors used for developing PTFs. However, model performance depends on choosing appropriate predictors that result in explaining the optimal amount of data variance with the model when used to predict a response variable. Lastly, the lack of interpretability in most “black box” machine learning models used to develop PTFs makes

it difficult to understand the practical implications of PTFs. One of the key contributions of this study is that correlation analysis was used to complement principal component analysis (PCA) in selecting relevant predictors to develop the ML-based models. To the best of our knowledge, only few papers have applied tree-based ML methods to large soil databases to predict K_s (Jorda et al., 2015; Araya & Ghezzehei, 2019), thus this study describes a process which represents an alternative approach (using various turn-key machine learning tools available in Python) to predict K_s using large public databases while intentionally selecting the most influential predictors *a priori* to training the ML algorithms.

The main objectives of this paper were to (i) select influential predictors by applying principal component analysis coupled with correlation analysis and (ii) train commonly available ML algorithms to predict K_s using the influential predictors selected in step (i). Multiple machine learning algorithms should be used to develop the models including multiple linear regression (MLR), support vector regression (SVR), K-nearest neighbor regression (KNN), deep neural networks regression (DNNR), random forest regression (RF), and gradient boosted regression (GB). Additional objectives include (iii) comparing ML model predictions using an independent test data set and (iv) applying the permutation importance technique to determine which soil properties were most influential post-model development in the test model and interpreted this information into practical advice for improving data quality. The central hypothesis of this objective was that there is a relationship between easily measured soil properties (e.g., bulk density, % silt, % clay, % sand) and saturated hydraulic conductivity. Thus, by applying feature selection (principal component analysis coupled with correlation analysis) to the input data,

the minimum relevant input variables that explain a greater variation in Ks can be used to build the models.

5.3 Machine Learning Techniques

5.3.1 Multiple linear regression

Multiple linear regression models (Yan & Su, 2009) are generally represented by the following equation:

Equation 5.1

$$Y = a + b_1X_1 + b_2X_2 + \dots + b_iX_i, \quad (5.1)$$

Where Y is the output variable (Ks), a represents the intercept, b_1, \dots, b_i represent the regression coefficients, X_1 to X_i represent the input variables.

5.3.2 Support vector regression

Support vector regression (SVR) employs regression analysis by regressing a dependent variable on an independent variable according to a weight vector and a bias term (Achieng, 2019). SVR was adopted from the support vector machine (SVM) learning algorithm (Drucker et al., 1997). The underlying principle behind SVM is to determine the optimal separation of classes by selecting the class which has the least generalization error from an infinite number of linear classifiers (Sihag, 2017). An important property of SVR models is the ability to generalize on test datasets which increases model accuracy for prediction on future datasets (Lamorski et al., 2014). A detailed explanation of the theory behind the SVR algorithm can be found in (Awad & Khanna, 2015; Elbisy, 2015; Pasolli et al., 2011; Smola & Schölkopf, 2004; Twarakavi et al., 2009).

5.3.3 K-nearest neighbor regression

The k- nearest neighbor regression (KNN) algorithm is an adaptation of the KNN classification algorithm. In the KNN algorithm, predictions for new instances are made based on the average of the values of its “k” nearest (most similar) neighbors in the training dataset (Araya, 2019). KNN regression is used for estimating continuous variables. KNN algorithms are considered as simple algorithms with respect to their underlying principle (Araya & Ghezzehei, 2019) and their easy interpretability. In KNN classification, the algorithm predicts a target class of a new observation by comparing it to “k” similar cases in the training data set, where “k” is a parameter specified by the user. In applying KNN regression, the KNN algorithm computes the average outcome of the “k” training observations that are most similar to the new observations and returns the output as the predicted value of the new observation (Al-Dosary et al., 2019). A detailed explanation of the theory behind the KNN regression algorithm can be found in (Altman, 1992) while an easy implementation of the KNN algorithm in the Scikit-learn module in python can be found in (Müller & Guido, 2016).

5.3.4 Deep neural network regression

Artificial neural networks (ANN), also called neural networks, can be described as a collection of units/nodes organized into layers, that receive inputs and deliver outputs usually compared to how neurons in biological systems transmit information in the brain. The basic components of neural networks are input layers, hidden layers, and output layers. In between the input and the output layer lies at least a layer consisting of neurons with connections called weights that carry information from one layer to the next layer (Achieng, 2019). Outputs are generated through the neurons based on activation functions

e.g., sigmoid, rectified linear units (RELU), and linear functions (Achieng, 2019). During training, input data are fed into the neural network to compute the output of every neuron in each consecutive layer. The output error (difference between measured and predicted value) is then measured and the algorithm computes how much each neuron in the previous hidden layer contributed to each output neuron's error (Géron, 2017). Deep neural networks are neural networks of multiple non-linear layers (Min et al., 2016).

5.3.5 Random forest regression

The random forest (RF) algorithm is another ML technique that has gained popularity (Van Looy et al., 2017) for its use in predicting soil hydraulic properties. RF regression is based on the decision tree algorithm. It works by constructing several decision trees during training of the data and outputs the class that occurs most (classification) or the mean prediction (regression) of the individual trees (Ho, 1995). However, a weakness of decision trees is the limitation on how complex a tree can grow. Thus, decision trees risk overfitting the training data if it becomes too complex (Ho, 1995). The technique of using multiple trees to make the prediction is called bootstrap aggregation (Liaw & Wiener, 2002). The algorithm for RF regression involves creating a random bootstrap dataset from the original dataset with replacement, then a RF regression tree is created using the bootstrapped dataset by randomly selecting a subset of the predictors and choosing the best split from the subset of predictors. Finally, based on the resulting ensemble tree, a new prediction is made by averaging the predictions. A detailed explanation of the RF algorithm for regression is described in (Breiman, 2001).

5.3.6 Gradient boosted regression

Gradient boosted regression (GB) is based on the idea of “boosting” which is a method of improving the performance of a learning algorithm by reducing errors of “weak” learning algorithms (Freund & Schapire, 1996). Originally proposed by Freund & Schapire (1996) in which the AdaBoost algorithm was developed, GB connected the AdaBoost algorithm to statistical concepts of loss functions, additive modeling, and logistic regression (Kuhn & Johnson, 2013). According to Kuhn & Johnson (2013), the main principle of gradient boosting is that given a loss function (e.g., mean square error) and a weak learner (e.g., regression trees), the algorithm seeks to find an additive model that reduces the loss function. In other words, once a loss has been calculated, gradient descent is calculated, and trees are sequentially added to reduce the loss function. A detailed description of the algorithm for the GB algorithm is described in Friedman (2002).

5.4 Materials and Methods

5.4.1 Process for the development of PTFs

5.4.1.1 The database

The data used in this modeling study were obtained from the Florida Soil Characterization Database (FSCD) (<https://soils.ifas.ufl.edu/flsoils/index.asp>). The database consisted of 1292 soil profiles with 8235 horizons distributed in 58 of 68 counties in Florida collected from 1965-1996 (Florida Soil Characterization Database, 2009). The FSCD was chosen for this study for several reasons; the database contained a wide range of soil horizons, the number of observations was large (8235), and the database contains many predictors to choose from, making it a favorable alternative to other large soil

databases (e.g., USKSAT database) used by others (Pachepsky & Park, 2015). Data were retrieved from seven printed books spanning the period from 1974-1990 and are the most comprehensive database of soils in Florida from 1965-1996 (Florida Soil Characterization Database, 2009). The database tracks 144 parameters which include physical and chemical properties of various soil samples. According to the Florida Soil Characterization Database (2009), the field and laboratory standards of the Natural Resources Conservation Service and Soil and Water Science Department were followed in checking the quality of the data in the database. Data for the particle size distribution i.e., sand, clay, and silt were obtained using the pipette method (Florida Soil Characterization Database, 2009) and K_s was determined using the constant head method.

5.4.1.2 Preprocessing

Since the Florida Soil Characterization Database is a large database, there are missing data points. The first step of preprocessing was to identify and remove soil samples from the database with missing data points. The original dataset contains 8216 samples and after missing datapoints were removed, the total number of samples remaining was 4686, which constituted the subset database. Where replicates of measured parameters for each soil sample were present in the original database these were averaged to obtain a mean parameter in the subset database. However, because values of K_s vary by orders of magnitude across soil types and form a log-normal distribution (See Results and Discussion Section), it is the custom when working with K_s to log-transform the data to bring the data to a normal distribution. Therefore, the three replicates of K_s were log-transformed before averaging K_s . For this study, a subset of parameters (very coarse sand content, coarse sand content, medium sand content, fine sand content, very fine sand content, total sand content,

silt content, clay content, and bulk density) were chosen as the most probable predictors for saturated hydraulic conductivity based on knowledge of soil physics and previous modeling studies (Araya & Ghezzehei, 2019; Arshad et al., 2013; Twarakavi et al., 2009).

5.4.1.3 Predictor selection

Prior to implementing the machine learning algorithms, it was important to eliminate any input variables that did not significantly explain variation in the output variable (K_s). Using the scikit-learn library (Pedregosa et al., 2011) in Python, principal component analysis (PCA) and Pearson correlation analysis were used to identify the most influential predictive variables among the input predictors. PCA is a mathematical algorithm that can be used to reduce the dimensionality (number of model input variables) while retaining the amount of variation in the original data explained by the model input variables (Jolliffe, 2002). Dimensional reduction is achieved by identifying principal components along which the variation in the data is highest (Ringnér, 2008). PCA results in new variables i.e., the principal components that are linear combinations of the original input variables (Ringnér, 2008). The component loadings of each variable in a PC indicates the amount of influence each variable has on that PC. Variables with moderate to high component loadings were assumed to represent variables that explained a high portion of the variation in K_s and best represented the system attributes (Mandal et al., 2015; Yao et al., 2015; Zhang et al., 2019). The principal components (PCs) obtained were then analyzed and the PCs comprised of variables with moderate to high component loadings were retained (Mandal et al., 2015).

The Pearson correlation matrix was then used to determine the strength of the relationships between the variables chosen after PCA analysis with K_s and between

themselves. Data were normally transformed using a Box-Cox normal transformation (Box & Cox, 1964) prior to Pearson correlation analysis. Thus, variables chosen to represent the PCs will ideally be strongly correlated with *Ks* and have weak correlations between the other variables.

5.4.2 Machine Learning Programming Method

5.4.2.1 Computational software

The DNNR was programmed using Tensorflow software library (Version 2.3.0, Tensorflow developers) (Abadi et al., 2016) in Python. Specifically, the Tensorflow implementation of Keras (tf.keras) which is an integration of the Keras API (Gulli & Pal, 2017) into Tensorflow was used in this study. Tensorflow is an open-source software library which provides a platform for implementing deep neural networks in Python. For easy understanding of the workflow of this study, the code was written in Jupyter Notebook (Kluyver et al., 2016). Jupyter Notebook is an open-source web application that allows for easy creation and sharing of code, data cleaning, machine learning modeling and data visualization.

5.4.2.2 Machine learning implementation

The preprocessing and feature selection steps described above were done for all ML algorithms. The steps that were followed in implementing four of the machine learning algorithms (KNN, RF, GB, and SVR) using the scikit-learn module are similar and shown in APPENDIX C. 1 (Figure C. 1). In detail, after the preprocessing and feature selection steps, the input variables were normalized to ensure all input variables had a mean and standard deviation of 0 and 1, respectively. Normalization was necessary so that no variable

had an undue influence on the regression just by virtue of having larger values. The dataset was randomly split into two as follows: a training set (80%) with 3748 soil samples used to build the models and a test set (20%) containing 938 soil samples that was used as an independent data set to see how the trained model performed on data not used in the model training.

Hyperparameter tuning was done using the GridSearchCV function in scikit learn. Hyperparameters refer to the parameters used to configure an algorithm to minimize the loss function thus increasing performance of the final models obtained (Yang & Shami, 2020). The loss functions here describe the optimization functions to evaluate how well the algorithms modeled the subset data (i.e., the training dataset). The GridSearchCV function works by combining all given hyperparameter configurations to obtain the best set of hyperparameters that give the best performance. The training dataset is passed to GridSearchCV which then repeatedly combines the various hyperparameters, calculates the accuracy metrics and results in the best values for the hyperparameters. In selecting the optimum parameters, k-fold cross validation was implemented within the GridSearchCV algorithm. In the k-fold cross validation implementation, the entire data set was randomly split into k equal sizes ($k = 5$ for this study). In the first fold, a single subsample was reserved as the “validation data” for testing the trained model, and the remaining $k-1$ subsamples used to train the model and the accuracy calculated. The cross-validation was then repeated five times with each of the five subsamples used exactly once as the validation set. A single estimate was calculated by averaging the five evaluations. This method is known to increase out-of-sample accuracy while reducing overfitting in the model during training (Vabalas et al., 2019).

The optimum hyperparameters obtained were used to rerun the model. A validation prediction of K_s was found using the testing dataset. The separate test dataset was used to ensure that the models were not overfitted to the training dataset. Overfitting occurs when the performance of a model on a test dataset differs from the performance observed on the training dataset, thus its generalizable error is high (Yeom et al., 2020). Implementation of the MLR algorithm followed the same steps as for KNN, RF, GB, and SVR except in the MLR, there was no hyperparameter search since MLR has no hyperparameters. Thus, immediately after training the model, predictions on the validation dataset were made.

In addition to the traditional machine learning models, this study implemented a DNNR to predict K_s which differed from how the KNN, RF, GB, SVR, and MLR were implemented. For the DNNR, a sequential model with two densely connected hidden layers each with 64 nodes, and an output layer that returned a single, continuous value (K_s) were built. A batch size of 10 with 1000 iterations were used to train the model. One advantage of DNNR is that it can unravel feature combinations, combine them to reduce complexity which leads to better generalization capability of a model (Cai et al., 2019). The DNNR was trained using the five input parameters obtained after predictor selection (clay content, silt content, bulk density, medium sand content, and fine sand content). The optimization function used in Python was the ‘RMSprop’.

The criteria for evaluating the accuracy of the predictive models were statistical performance measurements of mean absolute error (MAE), root mean squared error (RMSE), and the coefficient of determination or R-Squared (R^2).

The equations for the evaluation criteria are given below:

Equation 5.2

$$MAE = \frac{1}{n} \sum_{i=1}^n [y - \hat{y}] \quad (5.1)$$

Equation 5.3

$$R^2 = 1 - \frac{\sum_{i=1}^n [y - \hat{y}]^2}{\sum_{i=1}^n [y - \bar{y}]^2} \quad (5.2)$$

Equation 5.4

$$RMSE = \sqrt{\frac{1}{n} \sum_{i=1}^n (y - \hat{y})^2} \quad (5.3)$$

Where y is the measured K_s , \hat{y} is the predicted K_s , \bar{y} is the mean of the measured K_s , and n is an observation in the data.

5.5 Results and Discussion

5.5.1 Descriptive statistics of soil properties

Descriptive statistics of the measured saturated hydraulic conductivity (K_s) and the selected input variables (from the database) were calculated and are shown in Table 5.1. The descriptive statistics shown are using the untransformed measured data from the original database. The measured untransformed K_s values of the studied soils ranged from 0.01–362 cm h^{-1} with standard deviation of 24.33 cm h^{-1} (Figure 1). The mean K_s in the selected

samples was 20.07 cm h^{-1} . The range of clay, silt, and total sand were 0-93.4%, 0-94.5%, and 0.2 – 100% respectively.

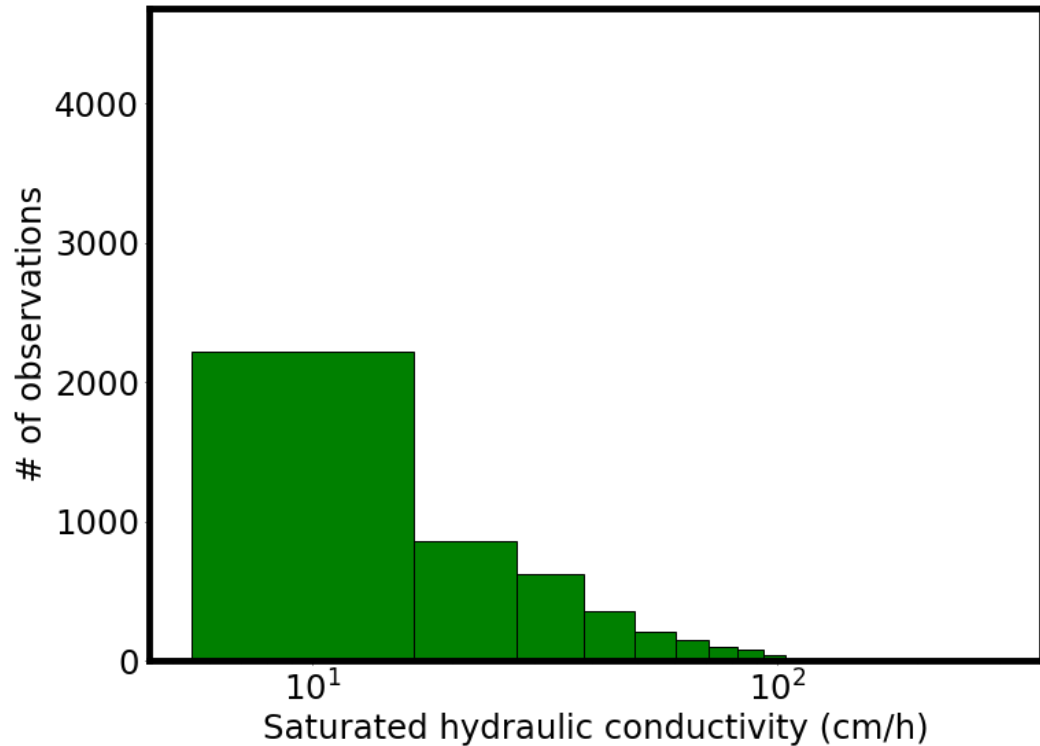


Figure 5.1. Histogram showing frequency distribution of the measured untransformed K_s data ($n=4686$).

All textural classes of the USDA soil texture classification triangle except silty clay soils were present in the subset database (Figure 5.2). From Figure 5.2, most of the soils were predominantly in five soil texture classes (sandy clay, sandy clay loam, sandy loam, loamy sand, and sand). A high percentage of the soils could be described as sandy as the mean of the total sand fraction was 85.6% with a standard deviation of 15.6%. Expectedly, bulk density was negatively correlated with K_s (Figure 5.3). The amount of silt was also negatively correlated with K_s .

Table 5.1. Descriptive statistics of the saturated hydraulic conductivity and the various input variables (n = 4686).

Input Variables	Max.	Min	Mean	SD
Very Coarse Sand (%)	19.6	0	0.291	0.906
Coarse Sand (%)	44.6	0	3.55	4.278
Medium Sand (%)	77.7	0	20	15.88
Fine Sand (%)	96.2	0.1	50.89	20.05
Very Fine Sand (%)	56.4	0	10.77	8.59
Total Sand (%)	100	0.2	85.6	15.6
Clay (%)	93.4	0	8.74	11.79
Silt (%)	94.5	0	5.63	7.16
Bulk density (g cm ⁻³)	2.09	0.49	1.53	0.163
K _s (cm h ⁻¹)	361.50	0.01	20.06	24.32

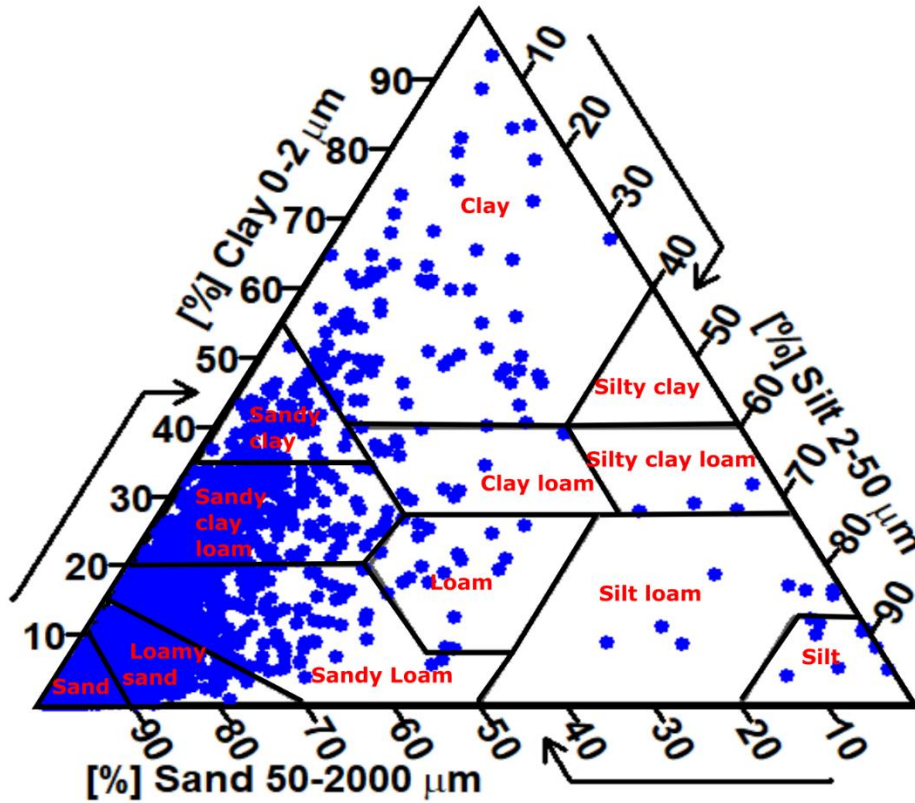


Figure 5.2. USDA soil texture classification triangle showing the distribution of the soils used for this study.

5.5.2 Predictor selection

The degree of linear association between the input and output variables were determined using Pearson correlation analysis (Figure 5.3). Three predictors (% very coarse sand, % coarse sand, % very fine sand) had a significant ($p < 0.001$) but low correlation with K_s ($r = 0.02, 0.16,$ and -0.23 respectively). While there was significant ($p < 0.001$) moderate correlation between K_s and medium sand, fine sand, bulk density, and clay content ($r = 0.33, 0.30, -0.34,$ and $-0.28,$ respectively). There was a significant negative correlation ($p < 0.001$) between silt content and K_s ($r = -0.68$) and a significant positive correlation ($p < 0.001$) between total sand and K_s ($r = 0.64$). The first five PCs accounted for 92% of the variation in the measured soil properties (Table 5.2). The first PC explained

31.3% of the total variation in the data when all the terms were included. The first PC had moderate negative component loadings from silt (-0.57), and moderate positive loadings from clay (0.49) and fine sand (0.45) which together constituted 75% of the variation in the first PC. From the Pearson correlation, the K_s was significantly negatively correlated with silt content and moderately correlated with clay and fine sand content. The silt, clay and fine sand content were thus retained as dominant variables in PC1. The second PC explained 27.7% of the total variation in the data. The second PC had positive component loading from coarse sand (0.57), medium sand (0.53), and very coarse sand (0.36). However, coarse sand and very coarse sand had very weak correlations with K_s . Thus, because K_s was strongly correlated with % medium sand than with % coarse and with % very coarse sand, medium sand was assumed to be a dominant variable in PC2. The third PC was clearly dominated by bulk density with a negative component loading of 0.77 which accounted for 59% of the variance explained by PC3. The fourth PC had positive component loading of 0.57 from very coarse sand and 0.42 from total sand. Here, total sand was chosen to represent PC4 because of its high correlation with K_s ($r = 0.64$) compared to very coarse sand ($r = 0.02$). The fifth PC was also dominated by total sand and very coarse sand with positive component loads of (0.52 and 0.5, respectively). Total sand was again chosen to represent PC5. From the PCA and correlation analysis, six variables (% clay, % silt, % fine sand, % medium sand, % total sand, and bulk density) were chosen as potential predictors for developing the ML models.

Table 5.2. Component loadings for 9 soil physical properties and the explained variance of the principal components (PCs). PCs that explained small variances (PC6 – PC9) i.e., < 6 % of the total variance are not included.

Soil property	PC1	PC2	PC3	PC4	PC5
VCS	0.16	0.36	-0.14	0.57	0.50
CS	0.11	0.57	-0.04	0.22	0.03
MS	-0.08	0.53	0.18	-0.30	-0.38
FS	-0.45	-0.32	0.05	0.09	0.40
VFS	0.43	-0.11	0.25	0.28	-0.23
T_sand	0.09	-0.29	-0.53	0.42	-0.52
Silt	-0.57	0.15	-0.06	0.14	-0.12
Clay	0.49	-0.13	-0.07	-0.35	0.30
BD	-0.00	0.17	-0.77	-0.36	0.11
Variance explained (%)	31.3	27.7	12.5	11.2	9.4

Silt content was highly correlated with total sand content ($r = -0.9$) which introduces the problem of multicollinearity. Multicollinearity exists whenever an independent variable has a high correlation with one or more other independent variables in a regression model

(Allen, 1997). Multicollinearity poses a challenge as it can negatively affect the precision of estimates of the coefficients and affect statistical significance of an independent variable (Allen, 1997). To reduce multicollinearity, % total sand was removed as a predictor while % silt content was retained. Silt content (%) was retained because it had a higher correlation (-0.68) with K_s than total sand (%) (0.64).

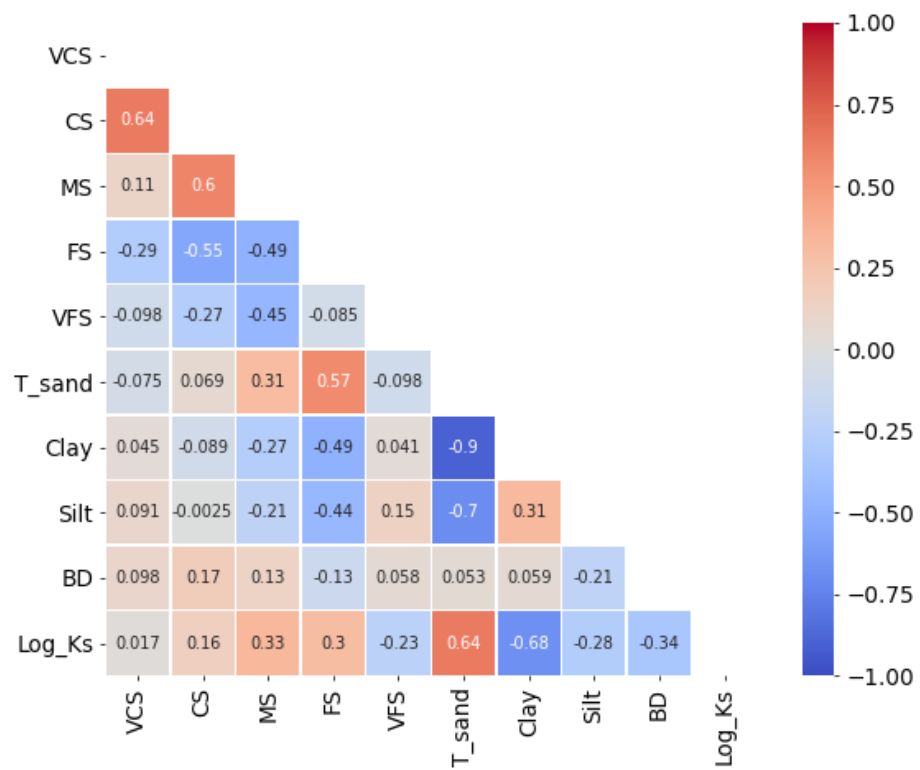


Figure 5.3. Pearson Heat Map showing the correlation matrix between the predictor variables and saturated hydraulic conductivity. K_s , saturated hydraulic conductivity; VCS, very coarse sand; CS, coarse sand; MS, medium sand; FS, fine sand; VFS, very fine sand; T_sand, total sand; Silt, silt content; Clay, clay content; BD, bulk density.

5.5.3 Model performance assessment

Table 5.3 presents the evaluation metrics for the different predictive models. Model hyperparameters obtained after implementing GridSearchCV are shown in APPENDIX C. 2 (Table C. 1).

Table 5.3. Evaluation metrics of machine learning models for predicting saturated hydraulic conductivity.

Model	Training dataset			Testing dataset		
	R ²	RMSE (cm h ⁻¹)	MAE (cm h ⁻¹)	R ²	RMSE (cm h ⁻¹)	MAE (cm h ⁻¹)
Multiple Linear Regression	0.61	0.55	0.39	0.60	0.56	0.39
KNN Regression	0.68	0.50	0.35	0.63	0.54	0.37
Support Vector Regression	0.70	0.49	0.32	0.67	0.49	0.33
Deep Neural Network Regression	0.80	0.39	0.26	0.57	0.50	0.34
Random Forest	0.82	0.37	0.22	0.71	0.47	0.32
Gradient Boosted Regression	0.86	0.33	0.23	0.71	0.47	0.33

5.5.3.1 Multiple linear regression

The multiple linear regression (MLR) model generally performed satisfactorily in terms of evaluation metrics for the training dataset with (R² = 0.61, MAE = 0.39 cm h⁻¹,

and RMSE = 0.55 cm h⁻¹). The MLR did not overfit the training data and was able to perform almost as well on the test dataset with ($R^2 = 0.60$, MAE = 0.39 cm h⁻¹, and RMSE = 0.56 cm h⁻¹). After training the MLR algorithm on the training dataset, the regression equation that was derived is shown in equation (5). Coefficients of the MLR model were tested for significance after model development. All coefficients were statistically significant ($p < 0.001$) in predicting K_s in the MLR model (equation (5)).

Equation 5.5

$$K_s = 3.279 + 0.017MS + 0.006FS - 0.037Clay - 1.791BD - 0.007Silt \quad (5.4)$$

Where K_s is saturated hydraulic conductivity, MS is % medium sand, FS is % fine sand, $Clay$ is % clay content, BD is bulk density in kg/m³, and $Silt$ is % silt content.

The correlation coefficients (r) of those input variables with K_s were low to moderate except for % silt content which had an $r = 0.68$ with K_s . These low correlations for the input variables could indicate a non-linear relationship between the input variables and K_s for this database. Garguilo & Morgan (2015) developed multiple regression models using the Florida Soil Characterization Database (same for this study) to simulate missing data soil parameters and found that models with very good performance could be obtained to predict silt, clay, organic carbon, CEC, bulk density, and sand content while K_s was not satisfactorily predicted. Garguilo & Morgan's (2015) findings support our results that multiple linear regression is not appropriate for predicting K_s using the Florida Soil Characterization Database. Kotlar et al. (2019) reported an $R^2 = 0.26$ on their test dataset when a stepwise linear model was used to predict K_s . Arshad et al. (2013) reported an R^2 value of 0.69 on their training data and 0.5 on their testing dataset when MLR model was

developed to predict K_s . The MLR model developed in this study performed relatively better and was more generalizable compared to the studies mentioned above based on the R^2 values on the test dataset.

5.5.3.2 KNN regression

A slightly better performing algorithm than the MLR model was the KNN regression model. Using the KNN, the training dataset resulted in: $R^2 = 0.68$, MAE = 0.35 cm h⁻¹, and RMSE = 0.50 cm h⁻¹ and the results for the test dataset were $R^2 = 0.63$, MAE = 0.37 cm h⁻¹, and RMSE = 0.54 cm h⁻¹. The hyperparameters tuned for the KNN was the K neighbors (in this case the number of soil samples) to use for estimating the output K_s for a particular soil sample. The optimal k obtained was 10. An initial guess for k was from 1 – 50, with increments of 1. It was observed that as k increased, the scores were constant until k reached 11 and the scores started decreasing. The range for k was then restricted to a range of 1-11 which resulted in 10 being the optimal number of k that gave the best score for predicting the test results. Among the three distance functions (Euclidean, Manhattan or Minkowski), the Manhattan distance function gave the best scores hence was chosen as the optimal distance function.

5.5.3.3 Support vector regression

The SVR algorithm performed better on the training dataset with $R^2 = 0.70$, MAE = 0.32 cm h⁻¹, RMSE = 0.49 cm h⁻¹ compared to the MLR and KNN algorithms. The results on the test dataset using SVR were: $R^2 = 0.67$, MAE = 0.33 cm h⁻¹, RMSE = 0.49 cm h⁻¹. The hyperparameters that were tuned in this study were C, ϵ , γ and the kernel function. (Elbisy, 2015). As the hyperparameter C increased, the algorithm tended to overfit the data as it tried to limit the error in prediction of the output which led to a high variance. On the

other hand, as γ increased, bias increased and the accuracy of the model on the training dataset decreased drastically. The training stage of the SVR algorithm aimed to find optimal estimates of the hyperparameters in order to get the best generalization of the model (Twarakavi et al., 2009) using the GridSearchCV module. Using GridSearchCV to select the optimum hyperparameters resulted in $C = 40$, $\epsilon = 0.1$, $\gamma = 0.001$. Overall, the radial basis function (RBF) kernel model performed better than the other kernels tested (linear and sigmoid).

5.5.3.4 Deep neural network regression

The DNNR algorithm performed well on the training dataset with $R^2 = 0.80$, MAE = 0.26 cm h^{-1} , and RMSE = 0.39 cm h^{-1} but tended to overfit the data thus resulting in a lower performance on the test dataset with $R^2 = 0.57$, MAE = 0.34 cm h^{-1} , RMSE = 0.50 cm h^{-1} . A possible reason for this low generalization performance on the test set is the lack of a bigger test set and the small nature of the DNNR architecture. It is useful to observe how the accuracy of the DNNR model increases on the training and validation set as the number of epochs increase. Comparison of the training and test error before and after early stopping is illustrated in Figure. C.3 (a) and (b) respectively (APPENDIX C. 3). There was only a little improvement, or even an increase in the test error after about 10 epochs, therefore there was no need to train further. As the size of the dataset used to train and test a DNNR increases, the performance of the algorithm also increases (Ng, 2019). For this study, obtaining more training and test data may improve the performance of the DNNR model. Alternative machine learning algorithms, e.g., tree-based algorithms, SVR or KNN may be more suitable when training small datasets as deep neural networks perform better particularly when training large datasets (Sarker, 2021; Sarker et al., 2019).

5.5.3.5 Tree-based algorithms

Tree-based algorithms like random forest regression (RF) and gradient boosted regression (GB) are two of the best performing algorithms for supervised learning as they average many individual tree-based models by searching for a predictor that ensures the best node split that results in the lowest error (Araya & Ghezzehei, 2019) . The random forest regression and the gradient boosted regression algorithms produced higher model performance compared to the other algorithms used to predict K_s in this study, especially the multiple linear regression model. Linear regression assumes a linear relationship between input and output variables, however in this study, it was shown that there was low correlation between the input variables and the output variables, thus the absence of a linear relationship. Thus, alternative algorithms (tree-based algorithms) performed better especially on the test dataset since a linear relationship does not need to exist between the input and output variables to develop high performing models. The evaluation metrics for the test dataset for the RF regression models were: $R^2 = 0.71$, $MAE = 0.32 \text{ cm h}^{-1}$, and $RMSE = 0.47 \text{ cm h}^{-1}$ (Figure 5.4).

The GB model had similar performance as the RF model with ($R^2 = 0.71$, $MAE = 0.33 \text{ cm h}^{-1}$, and $RMSE = 0.47 \text{ cm h}^{-1}$) on the test dataset. However, the GB model attained a slightly higher R^2 value of 0.85 compared to $R^2 = 0.83$ on the training dataset for the RF model. Araya & Ghezzehei (2019) compared the performance of four different machine learning algorithms for predicting K_s using the USKSAT database. Their results suggest that the GB algorithm outperformed all other algorithms with RF regression algorithm following closely behind. They reported a prediction accuracy for root-mean-squared log-transform error $RMSLE = 0.295 \text{ cm/day}$ using a test dataset of 4461 soil samples. While

the performance of the model obtained in Araya & Ghezzehei (2019) is higher than this model, the results in this study agreed with Araya & Ghezzehei (2019) that GB and RF were the two superior performing models for predicting K_s . Jorda et al. (2015) used an assembled database of 487 data entries from 85 different peer-reviewed articles to develop Boosted regression tree (BRT) models to predict K_s and near saturated hydraulic conductivity. The highest $R^2 = 0.15$ was achieved when they used a four-parameter model. The R^2 obtained in this study for predicting K_s using the GB regression model was thus 78% higher than the reported R^2 in Jorda et al. (2015).

Although GB has many hyperparameters that can be tuned to increase the accuracy of a model, for this study, we focused our attention on optimizing the number of estimators (`n_estimators`), the learning rate, maximum depth (`max_depth`), the loss function, `alpha`, and `min_sample_split`. Like the RF algorithm, the number of estimators represents the number of trees in the forest. As the number of estimators increase, so does the learning ability of the algorithm on the training dataset. However, increasing `n_estimators` comes with a computational cost and thus requires more time to train the model. Secondly, the learning rate of the algorithm controls the size of the steps the algorithm takes to minimize the loss function. If a higher learning rate is chosen, the algorithm may miss the target of the minimum and keep oscillating. However, a smaller learning rate means the algorithm may take many iterations to reach the minimum which can prolong training time. Thus, the essence of implementing the `GridSearchCV` module was to find a combination of the parameters (`n_estimators`, learning rate, maximum depth, `alpha` and minimum sample split) that achieves a minimum predictive error (Elith et al., 2008). The advantage of the GB model is that decision trees are iteratively fitted to the training data to increase emphasis

on observations that were poorly predicted by the existing collection of trees (Elith et al., 2008).

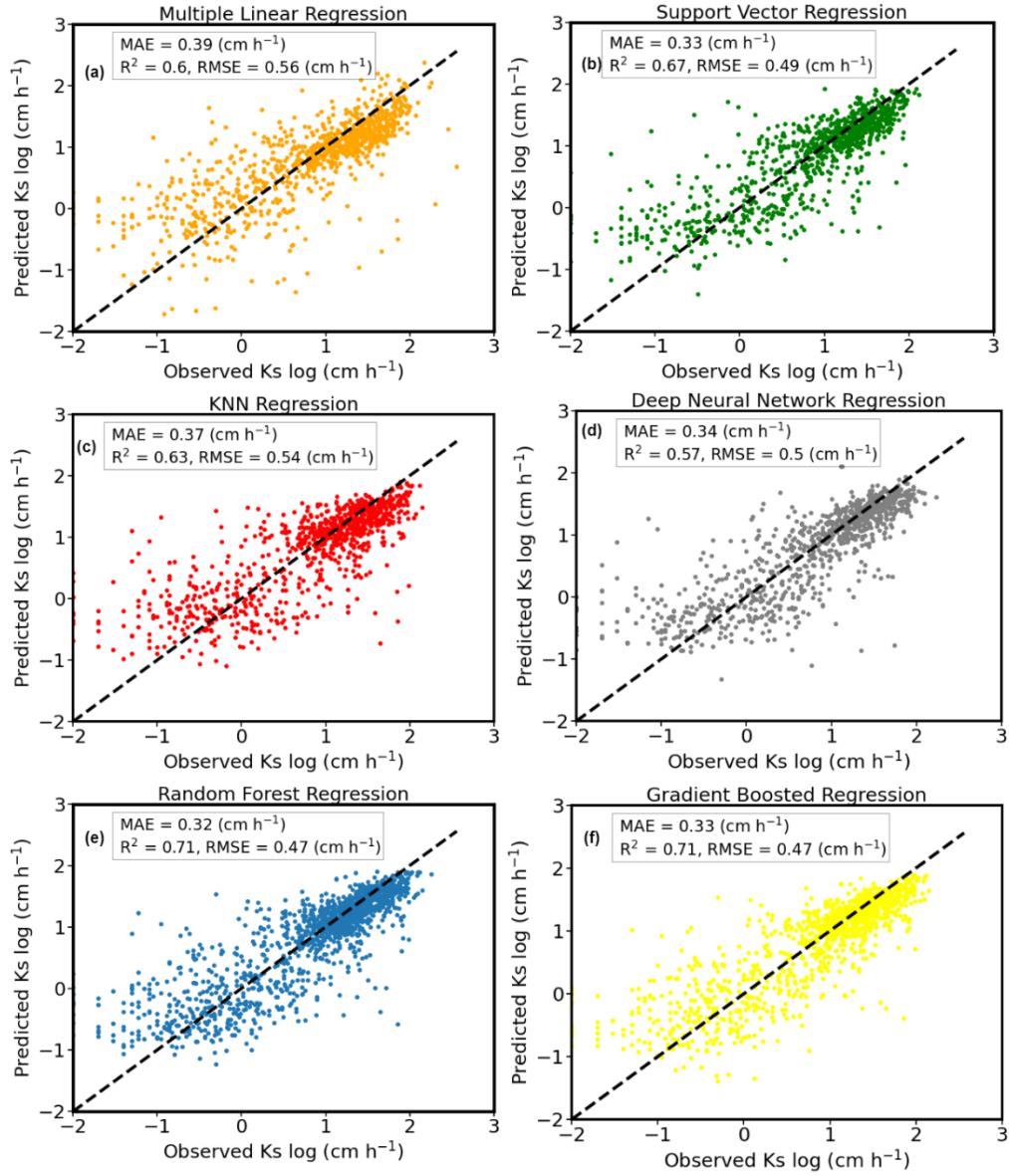


Figure 5.4. Scatter plots of observed and predicted saturated hydraulic conductivities ($n = 937$) on the test datasets. Each of the algorithms randomly samples 20% of the original 8216 observations to use as testing datasets for the scatter plots. Linear regression (a), SVR (b), KNN regression (c), DNN regression (d), RF regression (e), and GB regression (f). The dotted diagonal line represents the 1:1 mapping of the observed vs predicted values.

5.5.4 Performance improvement

While $\log_{10} K_s$ was well predicted at low K_s range for all models, at the high K_s range i.e., $\log_{10} K_s$ between 1.0-2.0, K_s was underpredicted which is reflected in the mean bias error of -0.022 for all the models in this study. The mean bias error refers to the average of the errors of a sample space and captures the average bias in the prediction (Pal, 2016; Ruiz & Bandera, 2017). Thus, a negative value indicates that the model underpredicted K_s whereas a positive value indicates an overprediction. This could be due to a few reasons. The first is an inherent weakness of the Florida Soil Characterization Database (FSCD). The FSCD contains numerous missing data and efforts have been made to fill in missing data using statistical estimation methods (Gargiulo & Morgan, 2015). The performance of machine learning models often depends on obtaining a complete and accurate database of measured soil properties for agricultural and environmental research studies especially at larger regional scales (Gargiulo & Morgan, 2015).

Secondly, errors could have been introduced during measurement of K_s in the field and laboratory due to the use of different measuring methods which can lead to heterogeneity in the entire database. This situation could lead to the loss of many data

elements critical for modeling K_s . Zhang et al. (2019) recommend that to improve data quality in large databases for the development of PTFs, methods and protocols for measuring K_s be consistent across all studies. Lastly, it is possible certain input parameters in the FSCD could have been more relevant for predicting K_s were not included in the 9 variables chosen for this study e.g., pH, organic carbon, and CEC.

5.5.5 Predictor importance

The purpose of intentionally implementing feature selection prior to ML model development is to select a minimal-size subset of predictors that leads to a parsimonious model which is easily interpretable and less computationally expensive for predicting output variables (Borboudakis & Tsamardinos, 2019; Tsamardinos & Aliferis, 2003). Following model development, model interpretation is also introduced in interpreting the influence of the predictors in the model using a novel method, Permutation Feature Importance (Breiman, 2001).

In machine learning, it is often useful to interpret a developed model in terms of the relative importance of the various predictors in a model. Typically, when parametric models e.g., linear models are developed to predict an output variable, the practical interpretation of the model is easily done. However, with non-parametric and non-linear models such as random forests, boosted regression and neural networks with superior predictive abilities have led to development of predictor importance methods which are able to provide insights into how influential predictors are to the overall models developed (Molnar et al., 2020).

One such method is the permutation feature importance technique (Breiman, 2001). Elith et al. (2008) notes that the numerous trees that are created in gradient boosting pose

a challenge for interpretability, however there are ways of interpreting these models similar to regression models. Variable importance in gradient boosting aims to quantify the improvement in squared error due to each predictor which is then summed within each tree (Kuhn & Johnson, 2013). The “permutation feature importance” function in scikit-learn was used to calculate the feature importance of the estimators in this study. Permutation importance refers to the decrease in a model’s score when a single predictor is randomly shuffled (Breiman, 2001). Thus, a predictor will be considered important if shuffling its value leads to an increase in the error of the prediction. It is worth noting that permutation importance on the test dataset is of more importance or interpretability than that on the training dataset. When fitting a model to a training dataset, the algorithm learns minute details of the data thus typically resulting in a much lower error rate than on the test dataset. Since the permutation importance technique depends on the estimation of the error to choose which predictor is important, it may be useful to place more emphasis on the permutation importance obtained on the test set i.e., independent data not used to train the model since the test set is a proxy for real world data and reflect the actual variables which are important for predicting K_s .

The GB and the RF models both indicate clay content to be the most important predictor and bulk density to be the second most important variable of the five selected for predicting K_s (APPENDIX C. 4, Figure C. 4). These results are corroborated by the MLR model developed in this study which also found clay content and bulk density to be the most dominant variables in predicting K_s . Our results are also in agreement with (Araya & Ghezzehei, 2019) who found clay followed by bulk density to be the most important predictors of K_s . A study by (Zhang et al., 2019) also found that about 60% of variance in

K_s could be explained by soil texture and macroporosity. They concluded that clay content and macroporosity for pores with diameters $> 75 \mu\text{m}$ better represented each component in their PCA analysis than all the other soil properties investigated in their study.

5.6 Conclusion

In this study, we demonstrate the application of popular machine learning algorithms to develop models that can be used to predict K_s using a readily available database (Florida Soil Characterization Database) of 4686 soil samples distributed across 58 counties in Florida. Our central that feature selection (principal component analysis and correlation analysis) could be applied to input soil data to develop machine learning models to predict saturated hydraulic conductivity was confirmed. This hypothesis was made based on there being a relationship between easily measured soil properties and saturated hydraulic conductivity. We tested PTF models developed using MLR, KNN, SVR, DNNR, RF regression, and GBR with a total of five predictors (total clay, total silt, bulk density, medium sand, and fine sand) chosen from an original set of nine predictors. Based on our analysis, GBR outperformed all the algorithms on the training dataset with $R^2 = 0.86$, MAE = 0.23 cm h^{-1} , and RMSE = 0.33 cm h^{-1} but was equal in performance to the RF regression with ($R^2 = 0.71$, MAE = 0.32 cm h^{-1} , and RMSE = 0.37 cm h^{-1}) on the test dataset.

Since the GB and the RF models were determined to be the best performing models, permutation feature importance technique was also applied to determine which predictors were most important for predicting K_s when using a test dataset. The GB and RF models both showed a similar ranking on the most important predictor which is the clay content followed by bulk density. The substantial impact and relevance of clay content may be

because the FSCD mainly consisted of sandy soils. Thus, priority should be given to obtaining quality data on clay content as it is the most influential predictor for K_s in the FSCD. Due to the ensemble nature of boosted regression tree algorithms, they can reduce overfitting and underfitting when used for prediction thus are known to be superior predictive machine learning tools.

It should be noted that this study was primarily concerned with comparing the capabilities of different machine learning algorithms to predict K_s and so there was limited comparison of the performance of the models developed with the numerous PTFs already existing. Regardless, this study offers an alternative process to developing PTFs using parametric models and notwithstanding its limitations, the prediction of K_s is approaching the accuracy where the GB PTF would be useable for design and deployment.

CHAPTER 6. EVALUATING THE FEASIBILITY OF USING A LIGNIN/ALGINATE
HYDROGEL AS A CARRIER FOR ENCAPSULATING AND RELEASING
RHIZOBIUM SPP.

6.1 Abstract

Immobilizations in polymers have proven successful in protecting the nitrogen-fixing bacteria *Rhizobium* for over four decades. Cell immobilization provides a physical protection for viable *Rhizobial* cells in a confined carrier material allowing for the cells' slow release into the environment. One material that has been underutilized as a *Rhizobial* cell carrier is lignin. The present study was conducted to evaluate the feasibility of using lignin-alginate beads with a starch additive to bioencapsulate and release *Rhizobial* cells slowly. First, a compatibility study was conducted. A lignin-alginate hydrogel was synthesized and cultured at different concentrations (0%, 3%, and 5% hydrogel) with inoculum of *Rhizobium meliloti* and *Rhizobium leguminosarum* and growth quantified. The *Rhizobium* cells were then bioencapsulated into the lignin-alginate beads (ratio of 2 g lignin to 1 g alginate) and their efficiency [(log of number of cells in wet beads/log of number of cells in solution matrix) x 100%] and release kinetics determined. Finally, light microscopy and scanning electron microscopy were used to investigate the surface morphology of the beads. Increasing the concentration of lignin-alginate hydrogel does not affect the survival of *Rhizobial* cells with time ($p = 0.71$). After 7 days of incubation, *Rhizobial* populations in the control treatment was 7.53 ± 0.28 log CFU/mL, 7.90 ± 0.67 log CFU/mL in the 3% treatment, and 8.03 ± 0.12 log CFU/mL in the 5% treatment. Our results show that all variations (alginate, lignin-alginate, and lignin-alginate with starch additive) of the wet bioencapsulated beads achieved a similar efficiency of approximately 97%. However, the presence of starch in the lignin-alginate beads increased the survival of *Rhizobium* cells

after oven-drying from 61 to 84% compared to only alginate encapsulation. These results imply that lignin, a readily available plant biopolymer is a potential component for the manufacture of carrier materials for encapsulating *Rhizobium* cells.

6.2 Introduction

The introduction of beneficial microbes into the soil environment is not new, as it has been done for centuries by farmers when they mixed soil taken from previous leguminous crops and applied it to new plots on which non-leguminous crops were grown for higher yields (Bashan, 1998). However, the carrier material used to protect/encapsulate these beneficial microbes is still an evolving research area. Some concerns are that carrier-based inoculants typically have are lower shelf-life of the microorganisms, poor survival of the microorganisms under unfavorable weather conditions, as well as conflicting field results on the performance of hydrogel-based bioinoculants (Suman et al., 2016). Cell immobilization in biopolymers has been shown to increase survival during production and storage of *Azospirillum brasilense* Cd (ATCC 29710) and *Pseudomonas sp.* strain 84313, important nitrogen-fixing bacteria (Bashan, 1986). Cell immobilization in this context refers to the physical confinement of viable microbial cells within a specific area of a carrier material in order to limit free movement while retaining their catalytic activities (Martins et al., 2013; Žur et al., 2016).

The use of peat has been the standard commercial carrier material for *Rhizobial* immobilization and inoculation (Bashan, 1998) due to its favorable characteristics like high water holding capacity and high surface area enabling the survival and growth of *Rhizobia* (Tittabutr et al., 2007). However, Tittabutr *et al.* (2007) argue that peat-based

inoculants requires considerable processing such as harvesting, drying, and milling which makes production in commercial quantities expensive. To improve on the use of peat-based inoculants, others have investigated the use of different polymeric materials as carriers for *Rhizobia* (Deaker et al., 2007; Denardin & Freire, 2000; Dommergues et al., 1979; Jung et al., 1982; Rivera et al., 2014; Suman et al., 2016; Tittabutr et al., 2007). For example, Rivera *et al.* (2014) assessed the effectiveness of eight different polymers on the cellular viability of *Rhizobium* sp. G58 during a 2-month period. Among eight different polymers investigated, sodium alginate (0.5-1%) and hydroxypropyl methyl cellulose- HPMC (0.125-0.5%) were most effective in improving the viability of *Rhizobium* sp. G58. Suman *et al.* (2016) found that beneficial microbes (*Azotobacter chroococcum*, *Pseudomonas fluorescence* and *Trichoderma viride*) encapsulated with a cellulose-based hydrogel enhanced the growth of wheat seeds. Other existing carriers for *Rhizobia* include; mineral soil (silt loam) (Chao & Alexander, 1984), alginate (Bashan, 1986), saw dust (Arora et al., 2008), and polyacrylamide (Dommergues et al., 1979; Jung et al., 1982).

Encapsulating microorganisms in synthetic and/or natural-based polymeric inoculants is currently an experimental field of research for introducing microorganisms into the soil environment (Bashan et al., 2014) unlike the organic-based inoculants such as peat which have been used on a large-scale. According to John *et al.* (2011), encapsulation involves the creation of a protective covering around an active ingredient or cells (e.g., microbe) for better functionality of the cells in the soil. Typically, the encapsulation process involves the immobilization of live microorganisms in a polymeric matrix to keep the cells viable (Bashan et al., 2014). Ideally, the polymeric matrix will then protect and keep the immobilized microbial cells viable until their subsequent release to colonize plant roots

when the polymeric matrices are biodegraded by native soil microorganisms (Bashan et al., 2014).

While several petroleum-based polymers e.g., from acrylic monomers have been tested for encapsulating microbes, petroleum-based polymers are often less biodegradable in the environment and are toxic to cells which may adversely affect the viability of the cells (Rathore et al., 2013; Rosevear, 1984). Numerous studies have also utilized different biopolymers (e.g. starch, chitosan, pectin, gelatin, and alginate) for encapsulating microorganisms (Saber-Riseh et al., 2021) for agricultural applications, but no studies have attempted to encapsulate microorganisms (*Rhizobium*) using lignin-alginate hydrogel beads. Lignin is a readily abundant plant polymer which forms one of the three main components of lignocellulosic plants (Meng et al., 2019b).

Lignin is classified into native and technical lignin (Chio et al., 2019). Native lignin is lignin that is isolated from lignocellulosic material without any modification (e.g. the solvent used for isolation does not react or alter its original structure) (Brauns, 1939). On the other hand, technical lignin refers to lignin that has been modified during the extraction process of lignin from biomass or industrial by-products (Chio et al., 2019). Thus, there are different forms and structures of technical lignins depending on the source and method of extraction of the lignin (Ekielski & Mishra, 2020). Alkali lignin is one form of a technical lignin which has been used to synthesize lignin-based hydrogels (Jiang et al., 2018) but have been underutilized as biopolymers for encapsulating *Rhizobium sp.*

The most common application of technical lignin in the encapsulation industry has been for the controlled release of fertilizers (Vejan et al., 2019). Other studies have also investigated the use of nano and micro-scaled lignin materials but mainly to study their

anti-bacterial and cytotoxicity characteristics on living cells (Sipponen et al., 2019). It would seem, therefore, that further investigations are needed to ascertain the suitability of alkali-lignin as a potential biopolymer for encapsulation of microorganisms.

Thus, the objectives of this study were to (a) investigate the biocompatibility of a alkali lignin-alginate hydrogel with a mixture of *Rhizobium meliloti* and *Rhizobium leguminosarum* (b) investigate the surface morphology of alginate beads, lignin-alginate beads, and lignin-alginate starch beads to confirm the presence of cells and (c) to compare the encapsulation efficiency and release kinetics of the *Rhizobial* species when encapsulated in only alginate beads, lignin-alginate beads, and lignin-alginate starch beads. The central hypothesis of this objective was that the addition of the different concentrations of the lignin-based hydrogel in a growth medium containing *Rhizobium spp.* will provide a better condition for the growth of the *Rhizobium meliloti* and *Rhizobium leguminosarum* cells. It was also hypothesized that the encapsulation efficiency and release kinetics of the bioencapsulated cells will differ based on the different combinations of lignin, alginate, and starch.

6.3 Materials and Methods

Rhizobium inoculum containing *Rhizobium meliloti* and *Rhizobium leguminosarum* biovar trifolli was obtained from Carolina Biological Supply Company (Charlotte, NC). Analytical grade alkali lignin (low sulfonate content) with molecular weight ~ 10,000, pH 10.5, and 3 wt. % in water was obtained from Sigma Aldrich (St. Louis, MO). Alginic acid sodium salt from brown algae (sodium alginate with medium viscosity) was obtained from Sigma Aldrich (St. Louis, MO). Low viscosity sodium alginate and corn starch were

obtained from Fisher Scientific (Waltham, MA, USA). Sodium citrate, sodium chloride, and calcium chloride were obtained from VWR International (Radnor, PA). Premixed yeast mannitol broth (YMB) and yeast mannitol agar (YMA) were obtained from Sigma Aldrich. The YMA consisted of yeast extract (1g/l), Mannitol (10 g/l), Dipotassium Phosphate (0.5 g/l), Magnesium Sulfate (0.2 g/l), Sodium Chloride (0.1 g/l), Calcium Carbonate (1 g/l) and Agar (15 g/l) with a pH of 6.8 +/- 0.2. The YMB had the same ingredients as the YMA but without the agar component.

6.3.1 Synthesis of lignin-alginate hydrogel

Optimum amounts of the reagents used for synthesizing the lignin-alginate hydrogel were 2 g of alkali lignin, 5 ml of DI water, 2% (w/v) of low-density sodium alginate, and 150 ml of CaCl₂. Briefly, two grams of alkali lignin were dissolved in 5 ml of deionized water. The mixture was stirred for 1 hour on a magnetic stirrer (Heidolph™ MR Hei-Tec Magnetic Stirrer with Heating) at 450 rpm and 25°C to allow for complete dissolution of the alkali lignin. Sodium alginate powder (1 g) was then dissolved in 50 ml deionized water to a concentration of 2% (w/v) and stirred continuously for 30 minutes for complete dissolution. The sodium alginate solution was added to the alkali lignin solution and stirred for 1 hour. The lignin-alginate mixture was then added to 0.1M calcium chloride solution (150 ml) and stirred. Upon contacting the calcium chloride, crosslinking between the Ca ions and the polymers occurred and the hydrogel was formed. The mixture was then cast into 35 mm petri dishes before freeze drying at -48°C for 48 hours to obtain the lignin-alginate hydrogel.

6.3.2 *Rhizobium* compatibility at different hydrogel concentrations

To determine the compatibility of the *Rhizobium* cells in the different concentrations of the lignin-alginate hydrogel, 10 g of the *Rhizobium* inoculum was suspended in 100 ml of deionized water to obtain a stock solution. Different concentrations of hydrogel (0%, 3%, and 5%) were prepared by mixing 0, 0.3, and 0.5 g of the lignin-alginate hydrogel in 10 ml of deionized water and shaken on a rotary shaker at 150 rpm for 12 hours to dissolve. The dissolved hydrogel solutions were transferred into test tubes and sterilized in an autoclave at 121°C for 15 minutes. After sterilization, each hydrogel sample was cooled to room temperature, and transferred into the 250 ml incubation flasks containing 10 ml of yeast mannitol broth growth media. One milliliter of the *Rhizobium* inoculum was added into each flask containing the hydrogel and growth media. The flasks were then incubated at 28°C with shaking at 150 rpm to enable aeration and to prevent the cells from settling down at the bottom of the flask. To quantify the effect of the different hydrogel concentrations on the growth of the *Rhizobium* cells, one ml samples from the different treatment flasks were taken on days 0, 3, and 7 after incubation and were transferred with a pipette into 10 ml test tubes containing 9 ml of a diluent (0.85% sodium chloride solution) to obtain a 1/10 dilution. The function of the salt solution was to adjust the tonicity of the suspending medium to that of the *Rhizobial* cells to avoid osmotic shock (Zuberer, 1994). Subsequent serial dilutions were done to obtain a final dilution of 1/10⁷. The surface spread method (Buck & Cleverdon, 1960) was used to enumerate the *Rhizobia*. Briefly, 0.1ml of four dilutions (1/10⁴, 1/10⁵, 1/10⁶, and 1/10⁷) were pipetted into YMA plates. With a sterile bent glass rod ("hockey" stick), the inoculum was evenly distributed over the surface of the plates. The inoculum was allowed to be absorbed into the YMA

plates which were then inverted and incubated at 28°C. After 48 hours of incubation, the *Rhizobia* colonies were counted using the standard plate count method and used to determine the number colony forming units (CFUs) in the treatments, with the assumption that each CFU was started by one cell. There were three replications for all the hydrogel concentrations. Aseptic techniques were implemented, thus all labware used for the experiment were sterilized prior to use. In addition, experiments were conducted under a lamina flow biosafety cabinet to prevent contamination. The population of *Rhizobia* was then determined for each treatment using the standard plate count method.

6.3.3 Bioencapsulation of *Rhizobia*

6.3.3.1 Preparation of *Rhizobial* cells

The bioencapsulation process was achieved using a modification of the ionic gelation technique (Bashan, 1986; Schoebitz et al., 2012; Young et al., 2006). All labware and solutions used in the bioencapsulation process were sterilized in an autoclave at 121°C for 15 minutes. *Rhizobium* cells were prepared by pipetting 1 ml of the *Rhizobium* inoculum into 100 ml of a sterilized YMB in a volumetric flask and allowed to grow for 48 hours at 28°C. The *Rhizobium* broth was then streaked onto YMA and incubated at 28°C for 48 hours. Cultures were prepared by transferring a single colony of the *Rhizobium* cells into a 100 ml aliquot of YMB in 250 ml Erlenmeyer flasks and incubated at 28°C on a shaker rotating at 150 rpm for 48 hours to obtain a fresh inoculum broth. Next, 40 ml of the bacterial culture was then pipetted and separated from the media by centrifugation (3150 × g, for 5 mins at 4°C) in a Marathon 2100 Fisher Scientific centrifuge. After

centrifugation, the cell pellets were resuspended in (0.85% NaCl, w/v) and mildly agitated with a vortex mixer.

6.3.3.2 Preparation of alginate, lignin-alginate, and lignin-alginate starch beads

Alkali lignin (2 g) was dissolved in 5 ml of deionized water. The mixture was stirred for 1 hour on a magnetic stirrer (Heidolph™ MR Hei-Tec Magnetic Stirrer with Heating) at 300 rpm and 25°C to allow for complete dissolution of the alkali lignin. One gram sodium alginate (medium viscosity) powder was dissolved in 50 ml deionized water to obtain a concentration of 2% (w/v). The mixture was manually stirred continuously with a spatula for 1 hour till dissolution. Air bubbles were formed during stirring; thus, the sodium alginate solution was placed in a Branson® Ultrasonic bath to degas the solution. The mixture was subsequently added to the alkali-lignin solution and stirred for 1 hour for complete dissolution. Two grams of corn starch were added to the mixture before stirring for another hour. At this stage, three different solutions/treatments were prepared separately: 2% alginate solution, 2% alginate solution added to the alkali lignin solution, and 2% alginate solution added to the alkali lignin solution with starch 2% starch added. The separated *Rhizobium* cells were resuspended in the three solutions and stirred for 30 minutes.

The three solutions were each added dropwise with syringes (BD 3 ml Syringe Luer-Lok™ Tip) into three beakers of 150 ml of 0.1M CaCl₂ solution and gently stirred at 150 rpm at room temperature on a magnetic stirrer. After adding the mixtures dropwise into the 0.1M CaCl₂ solution, beads started forming upon contact. The beads were maintained in the solution for another 1 hour for complete crosslinking before the solutions

were filtered through a filter paper to obtain the respective beads. The beads were immediately washed with sterilized DI water twice and incubated in YMB for another 48 hours on a rotary shaker at 30°C to allow the *Rhizobium* to multiply inside the beads. After incubation, the beads were washed again with sterilized DI water three times. The beads were then collected, placed on a filter paper in a petri dish and dried in an oven at 30°C for 24 hours, after which they were stored in hermitically sealed bottles at 4°C in 0.1M citrate buffer.

6.3.4 Efficiency of *Rhizobium* encapsulation

To determine the encapsulation efficiency, the encapsulated beads were dissolved following methods used in (Schoebitz et al., 2012). Briefly, 10 beads were immersed in 10 ml of sterilized sodium citrate solution (pH 8.5; 60 g l⁻¹) in a 50 ml Erlenmeyer flask for 30 mins at 20°C on a rotary shaker till complete dissolution. The released *Rhizobium* cells were counted by plate count method on a YMA. The *Rhizobium* cells were counted at the initial culture stage i.e., after growing the cells in YMB, after mixing with the three solutions, after the formation of the beads, and after drying. The efficiency of the *Rhizobium* cells was calculated following a method used in (Lotfipour et al., 2012).

Equation 6.1

$$Efficiency = \frac{Log_{10}N_{beads}}{Log_{10}N_{suspension}} \times 100 \quad (6.1)$$

Where N_{beads} is the total viable counts recovered from the encapsulated beads and $N_{suspension}$ refers to the total viable cell count in the three solutions (cells added to the biopolymer mixture).

6.3.5 Release kinetics of *Rhizobium*

Release kinetics of *Rhizobia* cells was determined according to a method by (Bashan, 1986). Twenty beads containing the immobilized *Rhizobia* cells were immersed into 75 ml of sterile saline solution (0.85% w/v NaCl) and shaken at 30 °C for 24 hours. Three samples of the 0.5 ml of the saline solution were plated on YMA media and the number of released *Rhizobia* cells determined using the plate count method. The beads were then rinsed twice with deionized water and immersed in fresh saline solution again. Counting of released *Rhizobia* cells was done after 24 hours.

6.3.6 Microscopic observation and scanning electron microscopy of encapsulated beads

Dry alginate beads, lignin-alginate beads, and lignin-alginate starch beads were investigated under a VWR Compound Microscope (76122-380, VWR International, LLC., Compound Microscope) equipped with a camera (Motic Moticam 1SP 1.3PM) and (software Motic Images Plus 3.0) at 4× magnification. For scanning electron microscopy, the three bead samples were first rinsed by immersion in ultrapure de-ionized (UP DI) water for 15 minutes. They were then fixed by immersion in 3% glutaraldehyde in Sorenson phosphate buffer (pH 7.2) for 24 hours. After rinsing for 5 minutes in UP DI water, the fixed samples were dehydrated in ethanol series: 50%, 75%, 95% (ethanol volume in UP DI water) for 15 minutes each, then immersed in 100% ethanol (200 proof) for 1 hour. The samples were then dried using an automated critical point dryer (EM CPD 300, Leica, Wetzlar, Germany) and sputter coated with 4 nm of platinum (EM ACE 600, Leica, Wetzlar, Germany) to provide surface electrical conductivity for electron microscopy. High-resolution imaging was conducted on a scanning electron microscope

(Quanta 250 FEG-SEM, FEI/Thermo Fisher Scientific, Hillsboro, OR USA) at 5 kV accelerating voltage for surface sensitivity and low beam current for mitigation of charging effects.

6.4 Statistical Analysis

Two types of statistical analyses were conducted. The first was to compare the *Rhizobial* populations between the three treatments on days 0, 3, and 5 using a one-way ANOVA and Tukey's pairwise test. Secondly, since multiple measures of the *Rhizobium* population were taken from the same treatments over a 1-week period, a one-way repeated measures ANOVA was used to analyze the difference between the *Rhizobium* population at the different time points (0, 3, and 7 days) within each treatment. Secondly, statistical analysis was also done to determine if there was a significant difference between the *Rhizobium* cell counts at various stages of the bioencapsulation. There were three treatments in this case: alginate beads, lignin-alginate beads, and lignin-alginate starch beads. There were three replicated trials for each experiment and the results are presented as averages with standard error. All statistical tests and graphing were done in (SigmaPlot version 14.0, Systat Software, Inc., San Jose, CA, USA, www.systatsoftware.com). An alpha of 0.05 was used for all statistical comparisons.

6.5 Results and Discussion

6.5.1 Lignin-alginate hydrogel synthesis

The formation of the hydrogel suggests that the alkali lignin did not impede the crosslinking reaction between the sodium alginate and the CaCl_2 . However, we speculate that the phenolic O-H groups of alkali lignin may form hydrogel bonding with H^+ of the

sodium alginate to form water which changes the pH of the solution thus affecting the crosslinking reaction. The production of additional water explains why when larger amounts of the alkali lignin were used, no crosslinking occurred. The main mechanism for the formation of the hydrogel is the crosslinking between calcium ions (Ca^{2+}) and the carboxyl groups in the alginate molecules which occurs instantaneously at the interface of the lignin-alginate matrix and the CaCl_2 solution (Hu et al., 2020). As stirring continued, the reaction continued until the Ca^{2+} cations diffused into the lignin-alginate matrix to react with all the alginate available.

6.5.2 *Rhizobium* compatibility at different lignin-alginate hydrogel concentrations

Figure 6.1 depicts the log of the *Rhizobial* populations in the three treatments of lignin-alginate hydrogel on days 0, 3, and 7. On day 0, the *Rhizobial* population was 6.66 ± 0.13 log CFU/mL in the 0% treatment, 6.49 ± 0.18 log CFU/mL in the 3% treatment, and 6.60 ± 0.20 log CFU/mL in the 5% treatment. A one-way ANOVA test conducted found no difference in populations between the three treatments on day 0 ($p = 0.809$). On day 3, the *Rhizobial* population was 8.83 ± 0.07 log CFU/mL in the 0% treatment, 9.06 ± 0.12 log CFU/mL in the 3% treatment, and 8.81 ± 0.06 log CFU/mL in the 5% treatment. There was no significant difference in populations between the three treatments on day 3 ($p = 0.153$). On day 7, the *Rhizobial* population was 7.53 ± 0.28 log CFU/mL in the 0% treatment, 7.90 ± 0.67 log CFU/mL in the 3% treatment, and 8.03 ± 0.12 log CFU/mL in the 5% treatment. There was no significant difference ($p = 0.711$) between the *Rhizobial* populations in the three treatments.

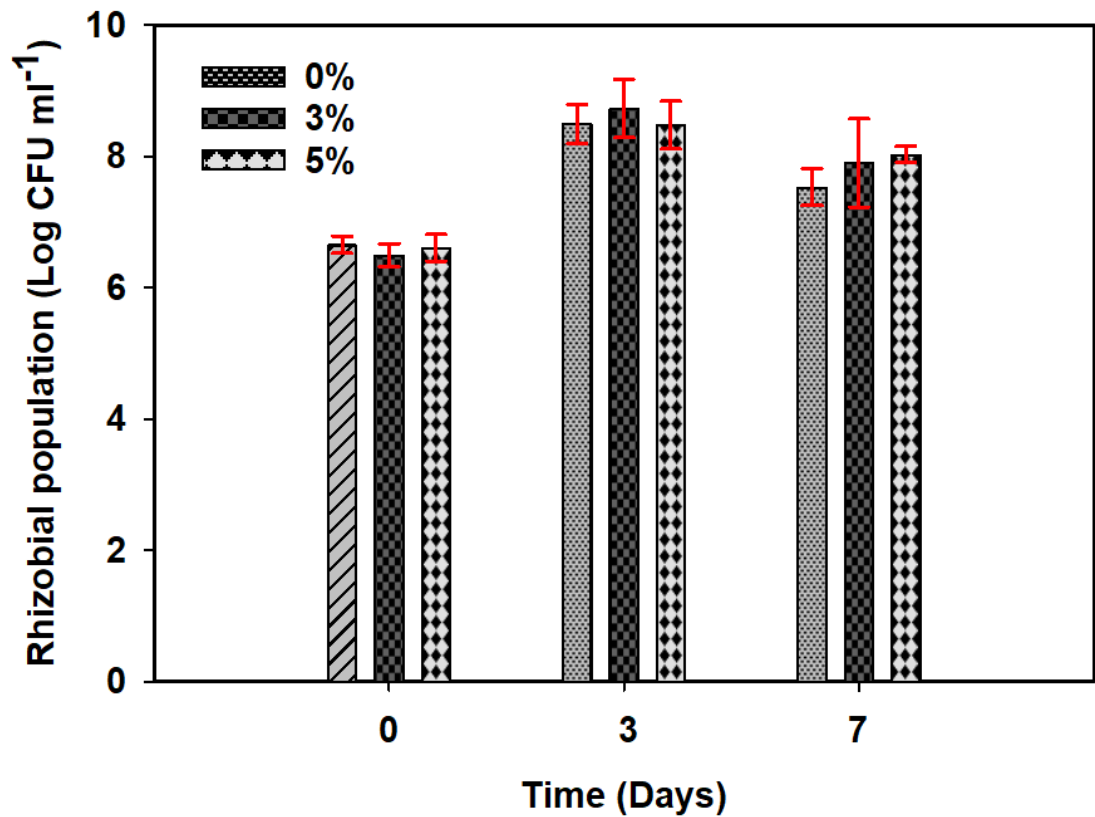


Figure 6.1. Survival of *Rhizobium* in 0, 3, and 5% hydrogel concentration. Error bars represent the standard error of the mean (n=3)

Overall, the results suggest that the growth and survival of the *Rhizobial* cells were not affected by increasing the concentration of the lignin-alginate hydrogel in the culture broth. While our results do not show that the presence of hydrogel enhanced the growth of the *Rhizobial* cells, we can however infer that lignin-alginate hydrogel does not adversely affect growth of *Rhizobium*. A similar study by Suman et al. (2016) incubated Pusa hydrogel at concentrations of 0, 0.5, 1, 2, and 3% with a microbial consortia (*Azotobacter chroococcum*, *Pseudomonas fluorescens*, and *Trichoderma viride*) and observed their compatibility. They concluded that the 2% concentration of hydrogel increased the population and provided better conditions for growth of the microbial species. It is possible

in their study the hydrogel used contained sufficient C and N sources which complemented the C and N supplied by tryptone yeast extract agar to the microbes. In our study, the C and N content of the hydrogel added was not quantified, hence, we were unable to deduce if the hydrogel provided any labile C and N to the microbes.

While the presence of hydrogel did not significantly enhance *Rhizobial* growth, statistical analysis showed that it did not impede growth of *Rhizobium*. A one-way repeated measures ANOVA was used to analyze the effect of the hydrogel concentrations within treatments in the 7-day period of incubation. Our results suggest there was a statistically significant difference ($p = 0.001$) in *Rhizobial* population in the 0% (control) treatment between days 0, 3, and 7. Day 3 population was higher than days 0 ($p = 0.001$) and 7 ($p = 0.005$). Day 7 population was also higher than day 0 ($p = 0.023$). Similarly, the *Rhizobial* population for the 3% treatment was significantly different ($p = 0.01$) for the three days. *Rhizobial* population on day 3 was higher than day 0 ($p = 0.012$). However, day 3 was similar to day 7 ($p = 0.164$) and day 7 was similar to day 0 ($p = 0.094$). For the 5% treatment, *Rhizobial* population on day 3 was higher than day 0 ($p = 0.002$). *Rhizobial* population was higher on day 7 than day 0 ($p = 0.004$).

From our results, the growth phases of the *Rhizobium* cells occurred in the treatment cultures shown in Figure 6.1. Upon inoculating the *Rhizobial* culture into the three treatments of hydrogel with YMB, the cells entered the lag phase on day 0 with no apparent increase in number. At this stage, the *Rhizobial* cells were getting accustomed to their new environment, synthesizing new proteins needed for the coming log phase. By day 3, the cells entered the exponential growth phase whereby growth was increased in all treatments. On day 7, the cell numbers decreased in all treatments and went into the stationary and

death phase. However, the extent of decrease in cell number was larger in control treatment since cells numbers on day 3 and 7 were significantly different. Though C and N were not quantified in the treatments pre and post incubation, we speculate that the presence of the lignin-alginate hydrogel provided a better condition for the survival of the *Rhizobium* cells.

6.5.3 Efficiency of *Rhizobium* encapsulation

The efficiency of the bioencapsulation process was quantified at various stages during formation of the beads. Cell numbers were counted at the initial culture stage i.e., after growing the cells in YMB, after mixing with lignin, sodium alginate and starch, after the formation of the beads, and after drying. The survival of *Rhizobium* at various stages of the bioencapsulation process using the different combinations is shown in Figure 6.2.

For the alginate beads, the initial cell count was 9.64 ± 0.29 log CFU/mL. After mixing the cells with the alginate solution, the cell count decreased to 8.29 ± 0.08 log CFU/mL. After encapsulation, cell count was 8.1 ± 0.05 log CFU/mL which further dropped to 5.07 ± 0.12 log CFU/mL after oven drying. A one-way ANOVA test conducted to test the difference in cell numbers between the four stages during encapsulation indicated a statistically significant difference ($p = 0.001$). Initial cell number was significantly higher than cell numbers in the matrix solution ($p = 0.002$), wet encapsulated beads ($p < 0.001$), and dry encapsulated beads ($p < 0.001$). Cell numbers in the solution matrix were not significantly different from cell numbers in the wet beads ($p = 0.859$). Expectedly the wet encapsulated beads had higher cell numbers than the dry encapsulated beads ($p < 0.001$).

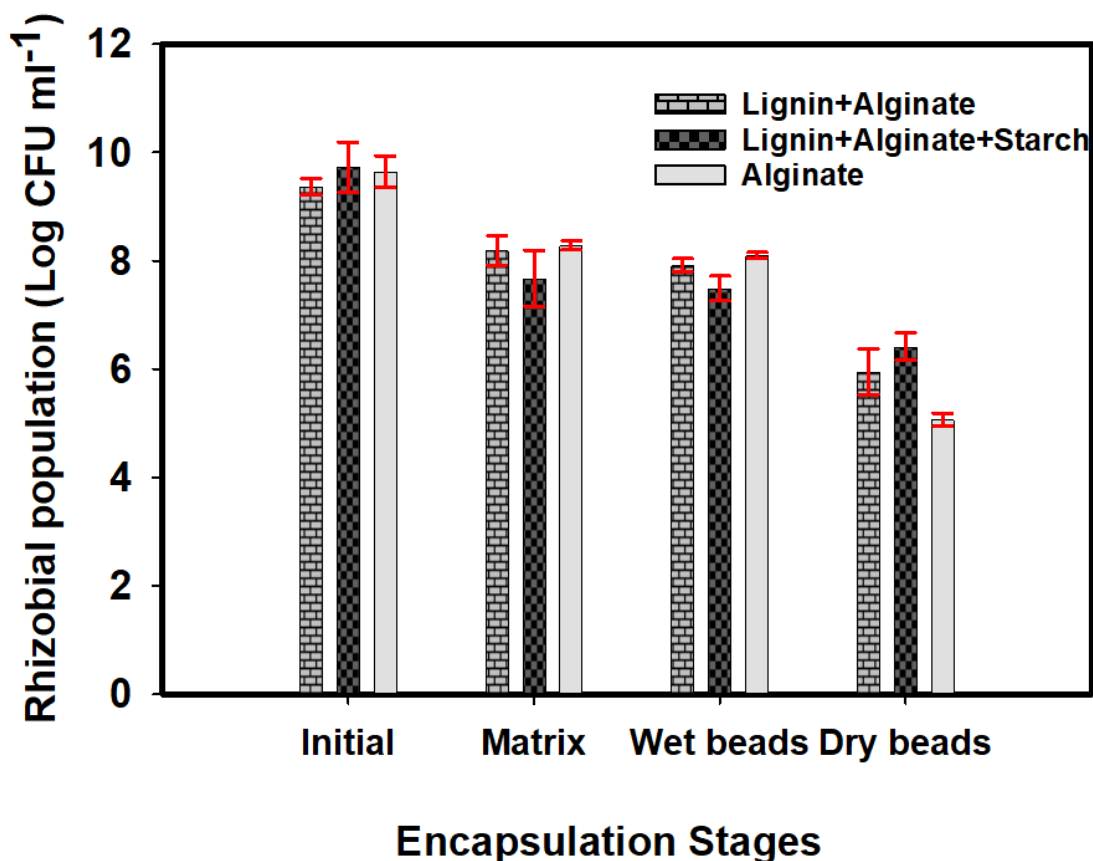


Figure 6.2. Survival of *Rhizobium* at various stages of microencapsulation process of the lignin-alginate beads (per 10 beads). Error bars represent the standard error of the mean (n=3).

For the lignin-alginate beads, the initial cell count of *Rhizobium* before bead preparation was 9.36 ± 0.16 log CFU/mL. After mixing *Rhizobium* cells in the lignin and alginate component and stirring for 1 hr, cell numbers reduced to 8.19 ± 0.27 log CFU/mL. After encapsulation, cell count was reduced to 7.92 ± 0.12 log CFU/mL which further reduced to 5.95 ± 0.42 log CFU/mL after drying. Initial cell number was significantly higher than cell numbers in the wet encapsulated beads ($p < 0.001$) and in the dry beads ($p < 0.001$). There was no difference between cell numbers in the solution matrix and the wet encapsulated beads ($p = 0.883$). Thus, the solution matrix did not adversely affect cell

numbers. Expectedly the dry beads had significantly lower cell numbers than the wet encapsulated beads ($p < 0.004$).

For the lignin-alginate-starch beads, initial cell numbers were 9.73 ± 0.46 log CFU/mL, 7.67 ± 0.51 log CFU/mL in the matrix solution, 7.48 ± 0.23 log CFU/mL in the wet encapsulated beads, and 6.42 ± 0.25 log CFU/mL in the dry encapsulated beads. Initial cell numbers were significantly higher than cells numbers in the wet encapsulated beads ($p < 0.016$), solution matrix ($p < 0.021$), and dry beads ($p < 0.002$). Cell numbers in the solution matrix, wet encapsulated beads, and dry beads were not significantly different ($p > 0.05$).

From the statistical analysis, encapsulated beads made with only sodium alginate protected the *Rhizobium* cells the least, followed by the lignin-alginate beads. The lignin-alginate beads with starch additive were most efficient at protecting cell viability. Table 6.1 shows the encapsulation efficiency of the *Rhizobial* cells in the three treatments. All encapsulation methods achieved a high yield (efficiency) in retaining viability of cells in the beads of at least 97% before drying. The difference, however, is seen during the drying stage of the beads after encapsulation. Drying the beads significantly reduced the cell viability in all treatment albeit less in the lignin-alginate -starch beads. Drying led to a 3-log reduction in cell numbers in the alginate beads, a 2-log reduction in the lignin-alginate beads, and only a 1-log reduction in the cell numbers in the lignin-alginate beads with starch additive. As seen in Table 6.1, the presence of starch in the lignin-alginate beads increased the survival of *Rhizobium* cells after drying from 61 to 84% compared to only alginate encapsulation. When compared to lignin-alginate beads only, there was an increase from 73 to 84% in encapsulation efficiency.

Table 6.1. The yield of *Rhizobium* cells in alginate, lignin-alginate, lignin-alginate-starch beads

Encapsulated bead type	Yield (%) (Wet beads)	Yield (%) (Dry beads)
Alginate	97.8	61.2
Lignin + Alginate	96.6	72.7
Lignin +Alginate+ Starch	97.6	83.6

Results in this study agree with results observed by Schoebitz et al. (2012) who found a significant improvement in yield of *Azospirillum brasilense* from 0.63 to 10.4% after oven-drying when alginate beads were supplemented with starch. Jankowski et al. (1997) developed alginate-starch capsules for encapsulating *Lactobacillus acidophilus* cells. Cell viability in their study was measured by the fermentation activity through acidification of the encapsulated *Lactobacillus acidophilus* cells compared to the fermentation activity of the free cell culture. Their study observed that cell viability in encapsulated capsules made with alginate-starch were comparable to cell viability in free culture solution. Sultana et al. (2000) encapsulated probiotic bacteria (*Lactobacillus acidophilus* and *Bifidobacterium* spp.) in alginate starch beads and observed that as the concentration of starch increased from 0 to 2%, the recovery of the probiotic bacteria increased from 4×10^8 CFU/g to 3×10^{11} CFU/g. During drying, an increase in osmotic stress coupled with a decrease in water activity leading to plasmolysis reduces the survival of viable bacterial cells (Morgan et al., 2006; Schoebitz et al., 2012). Schoebitz et al. (2012) hypothesized that the presence of starch in the beads slows down the drying rate as a result of a reduced water content of the alginate beads. Paul et al. (1993) showed that a high

drying (5 g/g dry weight per hour) was more detrimental to the survival of *Azospirillum lipoferum* than a low drying rate (1.18 g/g dry weight per hour) when bioencapsulated in alginate. While the water activity was not a parameter measured in our study, Przyklenk et al. (2017) also found that an increase in starch content in bioencapsulate *Metarhizium brunneum* conidia reduced the water activity of the bioencapsulated beads which increased the survival of the *Metarhizium brunneum* conidia by 85% after drying. Starch also serves as a platform for the bacterial cells to adhere to thus protecting them during adverse conditions such as drying (Vassilev et al., 2020).

6.5.4 Microscopic Observation and Scanning Electron Microscopy

The size of the lignin-alginate and lignin-alginate starch beads were similar while the alginate beads were slightly bigger (Figure 6.3). The wet lignin-alginate beads had similar sizes to the wet lignin-alginate starch beads. All beads exhibited spherical and smooth surfaces. The average diameter of the wet lignin-alginate and lignin-alginate starch beads was 2.5 mm while the average diameter of the wet alginate beads was 3.5 mm. The wet alginate beads were creamy-transparent in color. The color of the lignin-alginate beads and lignin alginate starch beads were deep brown caused by the dark-brown color of the alkali-lignin used to synthesize them.

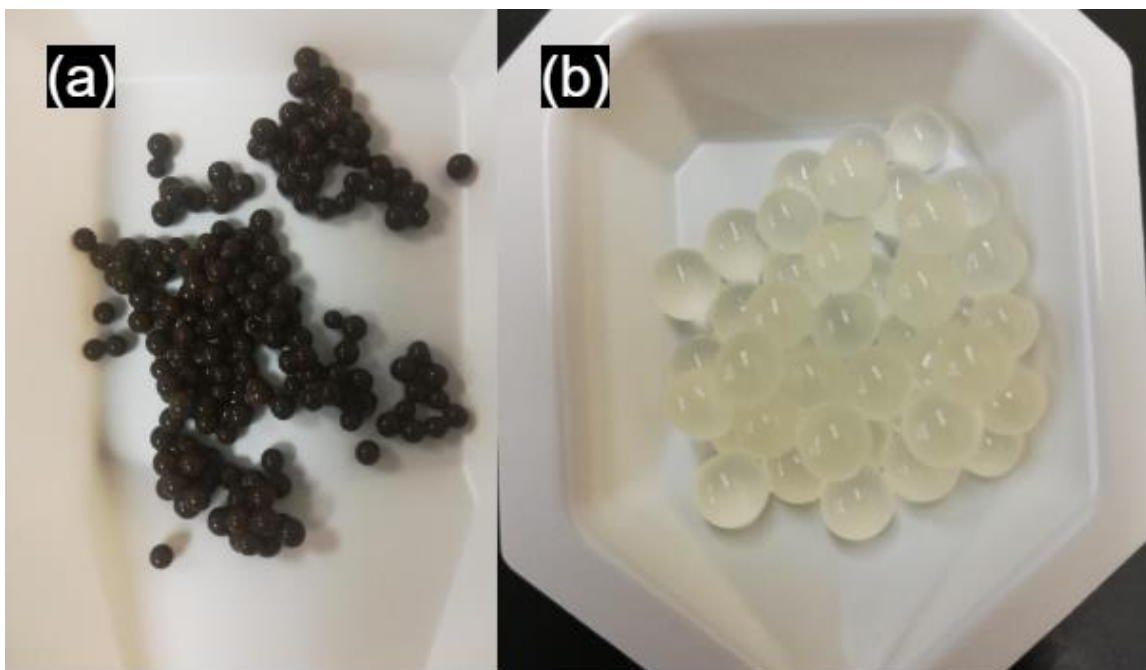


Figure 6.3. Macroscopic images of the wet (a) lignin-alginate beads additive and (b) alginate beads. Images were not taken at the same camera zoom level and so not shown at scale.

After drying the beads in an oven, microscopic structure of the beads was observed at a magnification of 4X (Figure 6.4). The size of the dry beads was determined using Image J (version 1.53k) (Schneider et al., 2012). All beads shrunk significantly due to the loss of water. While the dried lignin-alginate and lignin-alginate starch beads maintained a spherical shape after oven drying, the alginate beads assumed a distorted shape with rough surfaces. Chan et al. (2011) showed that when alginate beads were lyophilized, the drying process caused the beads to collapse as water sublimated from the beads. However, when starch (100g/L) was added to the alginate beads, the beads maintained their sphericity after drying. Thus, the starch acts as a structural support for the bead to control the level of shrinking (Chan et al., 2011). The dried alginate beads (Figure 6.4a) had an average diameter of 0.89 ± 0.02 mm which indicated a decrease in diameter of 74% compared to

the wet alginate beads. This result is similar to Arriola et al. (2016) who reported a decrease in diameter of 65% after drying alginate beads used to encapsulate aqueous leaf extract of *Stevia rebaudiana* Bertoni. The dried lignin-alginate beads (Figure 6.4b) had an average diameter of 0.52 ± 0.03 mm while the dried lignin-alginate beads with starch (Figure 6.4c) had an average diameter of 0.69 ± 0.01 mm.

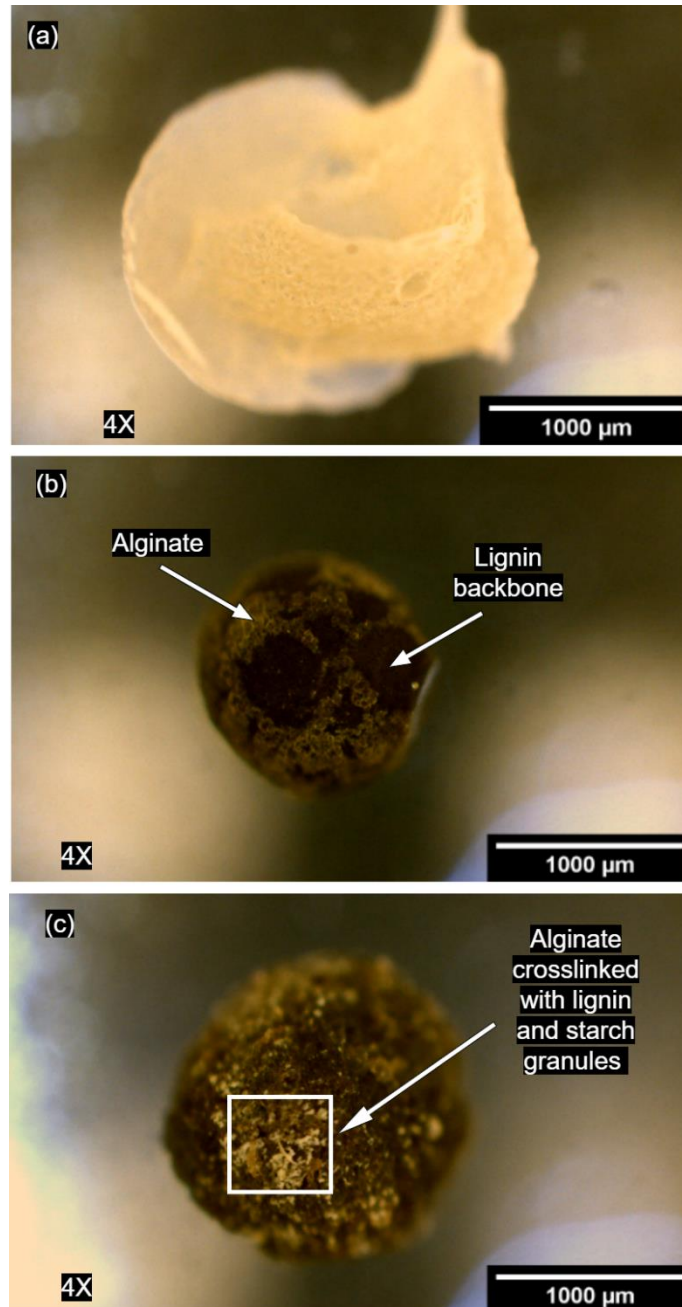


Figure 6.4. Microscopic images of the surface structure of the different bead formulations (a) alginate; (b) lignin-alginate; (c) lignin-alginate with starch additive.

Scanning electron microscopy (SEM) analysis was done to examine the surface morphology of the unfixed alginate, lignin-alginate, and lignin-alginate starch beads after oven-drying and after freeze-drying. As shown in Figure 6.5 (c) and (e), freeze-drying of the lignin-alginate and lignin-alginate starch beads produced beads with several large pores. Figure 6.5 (d) and (f) show the oven-dried lignin-alginate and lignin-alginate starch beads respectively with undulating spongy structures packed together without the presence of pores. Figure 6.5 (a) shows the freeze-dried alginate bead surface with no visible pores while Figure 6.5 (b) shows the oven-dried alginate bead surface with closely packed undulating spongy structures like Figure 6.5 (d) and (f). Using the SEM images of the dried beads, the average diameter of the pores was determined using Image J (version 1.53k) (Schneider et al., 2012). The average diameter of the pores in freeze-dried lignin-alginate beads (Figure 6.5c) was $19.87 \pm 6.01 \mu\text{m}$. The average diameter of the pores in freeze-dried lignin-alginate starch beads (Figure 6.5e) was $234.93 \pm 77.06 \mu\text{m}$. Thus, the pores in the lignin-alginate starch beads were on average 11 times larger than the pores in the lignin-alginate beads. While Vassilev (2020) remarks that the porosity of starch-based beads decrease with an increase in the starch content, the authors also emphasize that porosity can increase with time in storage which could be caused by the immobilized cells utilizing the starch. In addition, the rapid sublimation of frozen water during freeze-drying could result in the formation of pores at areas originally occupied by ice crystals (Amine et al., 2014; Smrdel et al., 2008).

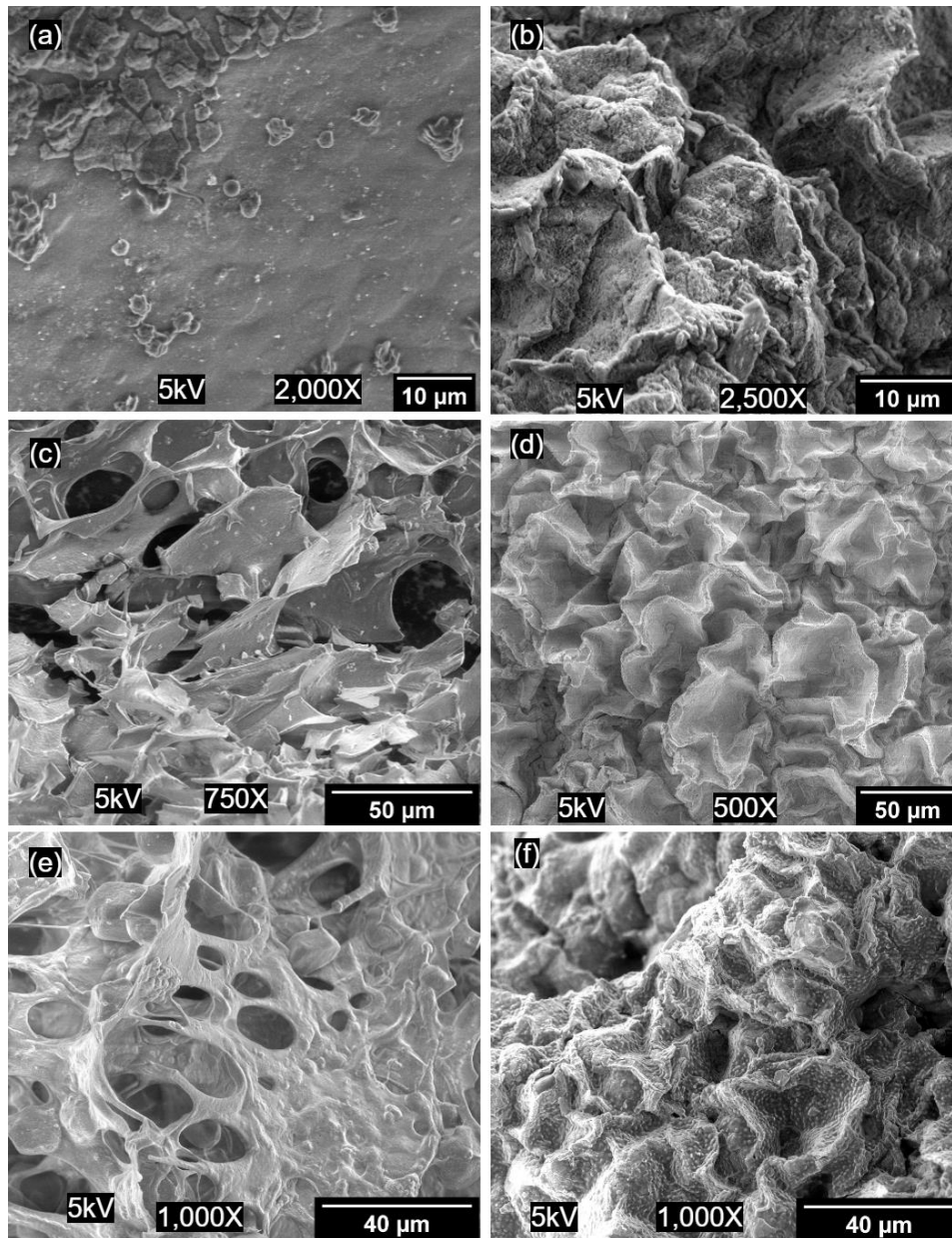


Figure 6.5. Scanning electron micrographs of the surface of the dried beads (a) freeze-dried alginate bead, (b) oven-dried alginate bead, (c) freeze-dried lignin-alginate bead, (d) oven-dried lignin-alginate bead, (e) freeze-dried lignin-alginate beads with starch additive, and (d) oven-dried lignin-alginate bead with starch additive.

After 2 weeks of storage, the survival of *Rhizobium* cells in lignin-alginate and lignin-alginate with starch was evaluated. This was done by immersion of the beads in 3% glutaraldehyde in Sorenson phosphate buffer (pH 7.2) for 24 hours and subsequently dehydrated using ethanol prior to observation using the scanning electron microscope. All alginate beads dissolved during the storage period when they were stored at 4°C in a 0.1M citrate buffer. The SEM micrographs of the lignin-alginate and lignin-alginate starch beads are shown in Figure 6.6. Attempts to locate *Rhizobium* cells on the surface of the lignin-alginate beads after fixation were not successful. Since the SEM images were taken on the surface of the beads, it is possible there could be *Rhizobium* cells immobilized inside the beads such that the SEM could not capture the cells. In contrast, clusters of *Rhizobium* cells were found at different magnifications on the surface of the lignin-alginate starch beads seen in Figure 6.6 (a). These *Rhizobium* cells were observed to be immobilized and adhered to the starch granules in the lignin-alginate starch beads. These results agree with Schoebitz et al. (2012) who reported that *R. terrigena*, a rhizobacteria immobilized on and adhered to the surface of starch granules under scanning electron microscope. The starch granules served as a platform on which the *Rhizobium* cells attached to during storage which protects them from desiccating (Vassilev et al., 2020). The *Rhizobium* cells were rod-shaped with an average length of $2.52 \pm 0.35 \mu\text{m}$ and an average width of $0.49 \pm 0.05 \mu\text{m}$. These results

agree with the typical length (1.2-3.0 μm) and width (0.5-0.9 μm) of *Rhizobium* cells (Somasegaran & Hoben, 2012).

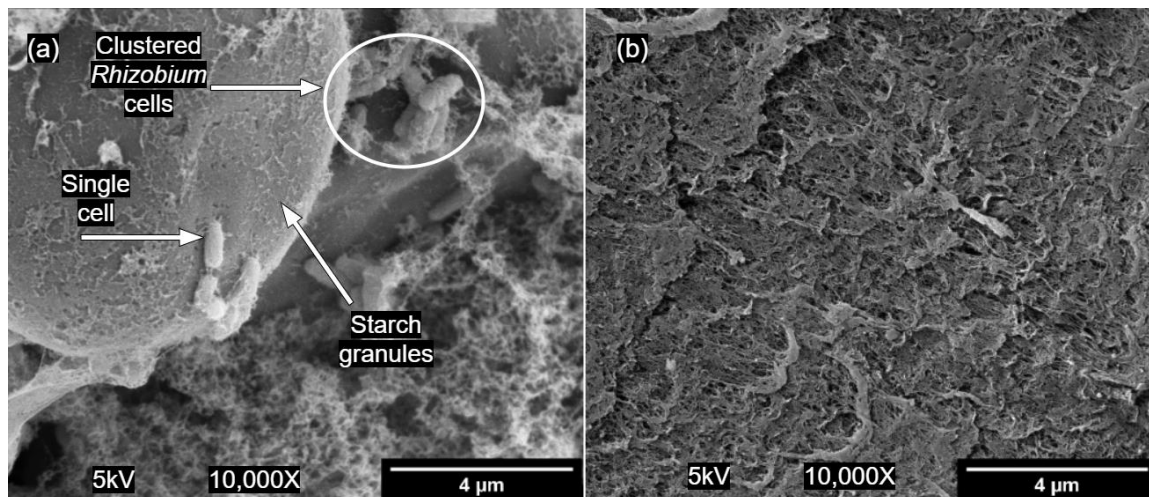


Figure 6.6. Scanning electron micrographs of (a) immobilized *Rhizobium* cells adhering to surface of starch granules in the lignin-alginate beads with starch additive; (b) lignin-alginate bead with no visible *Rhizobium* cells.

6.5.5 Release kinetics

The release kinetics of the *Rhizobial* cells from the encapsulated beads were investigated after immersing the wet beads in 0.85% saline water and then enumerating the number of cells released into the 0.85% saline water after 24 and 48 hours. Figure 6.7 illustrates the release kinetics in the three encapsulation treatments. After 24 hours, alginate beads released 7.10 ± 0.05 log CFU/mL *Rhizobial* cells, lignin-alginate beads released 7.32 ± 0.03 log CFU/mL, and lignin-alginate starch beads released 7.14 ± 0.01 log CFU/mL. After 24 hours, the number of cells released from the lignin-alginate beads were significantly higher than the number of cells released from the alginate beads ($p < 0.008$) and the lignin-alginate-starch beads ($p < 0.021$). Cell numbers in alginate beads were not

significantly different than cells numbers in the lignin-alginate-starch beads ($p > 0.621$). After 48 hours of shaking the beads in the 0.85% saline water, all alginate beads completely dissolved. For the lignin-alginate beads, 18 out of 20 beads disintegrated. However, the lignin-alginate starch beads were not dissolved after 48 hours and released 7.13 ± 0.19 log CFU/mL *Rhizobium* cells, which was not significantly different from the number of cells released after 24 hours ($p > 0.05$). The presence of the starch in the beads increases the mechanical strength of the beads (Chan et al., 2011; Ramdhan et al., 2020) which may explain why the lignin-alginate-starch beads did not dissolve after 48 hours. We hypothesize that the presence of the lignin may have improved the mechanical strength of the lignin-alginate beads (Kalinowski et al., 2020) which explains why the lignin-alginate beads only disintegrated but not completely dissolved. While alginate encapsulated beads were able to encapsulate and release *Rhizobium* as shown in this study, the addition of biopolymers like lignin and starch helped to strengthen the beads against dissolution in aqueous solutions.

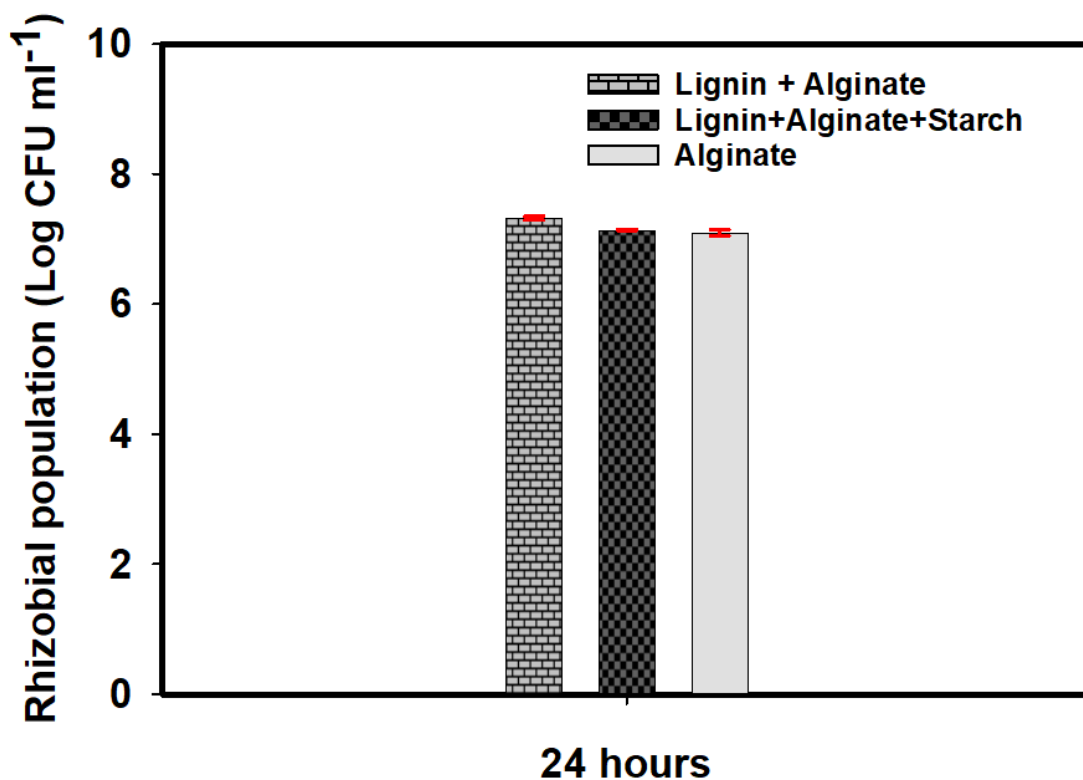


Figure 6.7. Release of *Rhizobial* cells from encapsulated beads after 24 hours. (per 20 beads) (n=3).

6.6 Conclusions

This study sought to evaluate the feasibility of synthesizing beads using alginate, lignin, and starch to encapsulate and release *Rhizobium* species. Lignin, a less utilized part of lignocellulosic material was used to synthesize a lignin alginate hydrogel and the compatibility of the hydrogel with *Rhizobium* bacterial cells tested. While our hypothesis of lignin-alginate hydrogel providing a better condition for the grow of *Rhizobium meliloti* and *Rhizobium leguminosarum* cells was not directly confirmed, our results suggest that the growth and survival of the *Rhizobial* cells were not affected by increasing the

concentration of the lignin-alginate hydrogel. Our second hypothesis that encapsulation efficiency of the different variations of bioencapsulation will differ was not directly confirmed. While all variations of the biopolymers (alginate, lignin-alginate, and lignin-alginate starch) used for the bioencapsulation of the *Rhizobial* cells attained a high (97%) encapsulation efficiency with wet beads, the presence of starch in the lignin-alginate beads increased the survival of *Rhizobial* cells after drying from 61 to 84% compared to only alginate encapsulation. Oven-drying of the beads caused the surface to shrink into tightly packed structures with no visible pores in all three variations of the beads. Freeze-drying of the lignin-alginate and lignin-alginate starch beads produced beads with several large pores. SEM images of fixed beads highlight the importance of starch for the storage of *Rhizobial* cells since they were found attached in clusters to beads with the starch additive which were not visible in lignin-alginate beads with no starch. While the lignin-alginate and lignin-alginate starch beads did not increase the slow release of *Rhizobial* cells after 24 hours compared to sodium alginate beads, the presence of lignin and starch enhanced the structure of the beads and prevented them from dissolving in aqueous solutions during storage. Unfortunately, we were unable to determine the C and N mineralization of the different lignin-alginate concentrations that were incubated with *Rhizobial* cells from this data. Thus, we only hypothesize that the presence of lignin-alginate hydrogel could provide a better nutritional condition for the survival of *Rhizobium* cells. The findings for this study are restricted to the short term (one week) effect of the lignin-alginate beads encapsulation on the efficiency and release kinetics of the *Rhizobial* cells. Future studies will test the potential of using lignin with other biopolymers as carriers for microbial encapsulation and release. Future studies will also test the release of *Rhizobial* cells from bioencapsulated

lignin-alginate beads into a soil environment. Notwithstanding its limitations, this study does suggest that alkali-lignin should be considered as a viable biopolymer for the bioencapsulation of *Rhizobium* since it is readily available and helps repurpose lignin waste streams especially from pulp and paper making industries and biofuel processing industries. Lignin-alginate microbial encapsulated beads may lead to potential applications in nutrient and microbial delivery systems in agricultural soils.

CHAPTER 7. GENERAL CONCLUSIONS AND FUTURE WORK

7.1 General Conclusions

This dissertation explored lignin-based hydrogels to be used to manage soil water and as engineered carriers of beneficial soil microorganisms. In addition, machine learning methods were used to develop new pedotransfer functions (PTFs) for predicting saturated hydraulic conductivity which is an important soil hydraulic property that affects how water moves in the soil.

The first question addressed in this dissertation was how effective lignin-based hydrogels were at influencing soil water retention in two soils (silt loam and loamy fine sand) from soil water at near saturation to dryness.

- While plant available water capacity was not increased, in the capillary regions of the soil water retention curve where soil water is easily accessible to plant roots, volumetric water content was increased after lignin-based hydrogel amendment at 0.1 and 0.3% (w/w) concentration for silt loam and loamy fine sand soils.
- To demonstrate the feasibility of this study on the field, calculations were carried out based on results from the laboratory study. Our calculations indicate that at a 1% (w/w) concentration, the application of the lignin-based hydrogels to a 15 cm layer of silt loam and loamy fine soils will not significantly increase plant available soil water storage.

Secondly, the impacts of incorporated lignin-hydrogel on saturated and unsaturated hydraulic conductivity of a silt loam soil were evaluated. Until now, there was no study that tested the effect of lignin-based hydrogel on unsaturated soil hydraulic conductivity. Key conclusions from this objective were:

- Amending a lignin-based hydrogel at concentrations of 0.1 and 0.3% (w/w) to a silt loam soil decreased saturated hydraulic conductivity by up to 88% but increased unsaturated hydraulic conductivity from a soil water pressure head range from -10 to -750 cm. Our results implied that lignin-based

hydrogel could reduce deep percolating water in saturated soils and release bound water in unsaturated soils which could be useful for improving the flow of soil water for easier plant root access.

In the third study, our objective was to use data from a large public database of soils to test the ability of several machine learning algorithms to develop new pedotransfer functions (PTFs) for predicting saturated hydraulic conductivity (K_s) in soil.

- Out of the six machine learning algorithms tested, random forest regression and gradient boosted regression both gave the best model performances with $R^2 = 0.71$ and $RMSE = 0.47 \text{ cm h}^{-1}$ on the test data (validation data set).
- Using the permutation feature importance technique, we showed that clay content described the most variation in the data, followed by bulk density.

Finally, we investigated the feasibility of using lignin-alginate beads with a starch additive to bioencapsulate and release *Rhizobium meliloti* and *Rhizobium leguminosarum* cells. This study introduced lignin, an abundant natural biopolymer that is often a waste stream in most pulp and paper making industry and biorefineries, along with alginate, a naturally occurring edible polysaccharide found in brown algae as base materials for encapsulating and releasing *Rhizobium sp.*

- Increasing the concentration of lignin-alginate hydrogel did not affect the survival of *Rhizobial* cells after 7 days which made it possible to bioencapsulate the *Rhizobial* cells using different biopolymer combinations (alginate, lignin-alginate, and lignin-alginate with starch additive) leading to a bioencapsulation efficiency of 97%.
- We found that alginate beads released significantly more *Rhizobial* cells than lignin-alginate and lignin-alginate-starch beads but the starch in the lignin-alginate-starch beads possibly enhanced the structure of the beads and prevented them from dissolving in aqueous solutions during storage. Our results indicate the potential applicability of lignin as a component for the manufacture of carrier materials for encapsulating *Rhizobial* cells.

7.2 Future Work

While copious amounts of data were gathered to answer the main research questions posed in this dissertation, further research work will be needed to fill the gaps that this dissertation did not address. The lignin-based hydrogels and bioencapsulated beads developed in this dissertation exhibited qualities that made them suitable for agricultural applications, however, their biodegradability in the plant/soil environment needs to be tested to ascertain their residence time in soil, as residence time could affect performance of the hydrogels in soil. To achieve this goal, data on all parameters that impact biodegradation such as soil temperature, pH, moisture, soil type, and duration should be investigated. There may also be benefits resulting from the application of lignin-based hydrogels such as long-term carbon sequestration which were not quantified in this study. Therefore, the amount of carbon added by the lignin-based hydrogel into the soil should be quantified by measuring the change in soil carbon at a given depth. Future work on objectives one and two should focus on testing other ranges of soil types at a wide range of hydrogel application rates i.e., 0 to 2% (w/w) to fully understand the extent to which lignin-based hydrogels affect soil water retention and soil hydraulic conductivity for practical field applications.

Furthermore, an extended study where the unsaturated hydraulic conductivity data from different textures of soil amended with lignin-based hydrogels are used to develop pedotransfer functions for predicting unsaturated hydraulic conductivity is needed. Past studies which estimated the unsaturated hydraulic conductivity of soil under hydrogel amendments seldom used measured data but estimated unsaturated hydraulic conductivity from the water retention curve and matched it to saturated hydraulic conductivity (K_s) of a single measured conductivity value. Estimated unsaturated hydraulic conductivity data are rarely validated using directly measured data. Thus, independent hydraulic conductivity data from a wide range of soil water pressure values will allow us to validate the models obtained using the machine learning algorithms.

Future work based on objective four should determine the carbon and nitrogen mineralization of the different lignin-alginate concentrations that were incubated with the *Rhizobial* cells in the *Rhizobial* compatibility with different lignin-alginate study. Data

from such a study could validate if *Rhizobial* cells consumed and metabolized carbon and nitrogen from the lignin-alginate hydrogel which improved their survivability. The findings for the encapsulation study were also restricted to the short term (one week) effect of the lignin-alginate beads encapsulation on the efficiency and release kinetics of the *Rhizobial* cells, thus the results should be investigated over a longer period (1 month to 1 year) to ascertain how storage time affects efficiency and release kinetics after encapsulation. Future studies should test the potential of using lignin with other biopolymers as carriers for microbial encapsulation and release. Future studies should also test the release of *Rhizobial* cells from bioencapsulated lignin-alginate beads into a soil environment. Finally, economic analysis of synthesizing lignin-based hydrogels and their subsequent application to field soils compared to direct irrigation should be investigated.

APPENDICES

APPENDIX A. 1. Lignin-based Hydrogel Synthesis

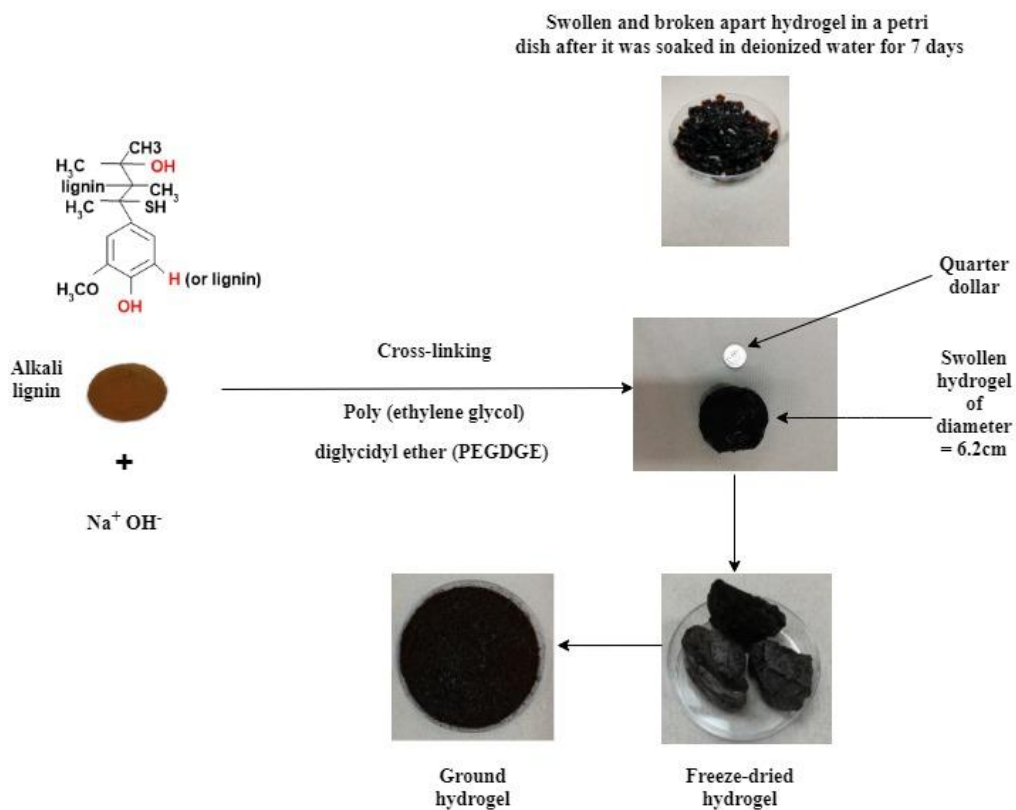


Figure A. 1. Synthesized hydrogel showing its swollen, freeze-dried and ground form.

APPENDIX A. 2. Observation of swelling in hydrogel-soil mixture.

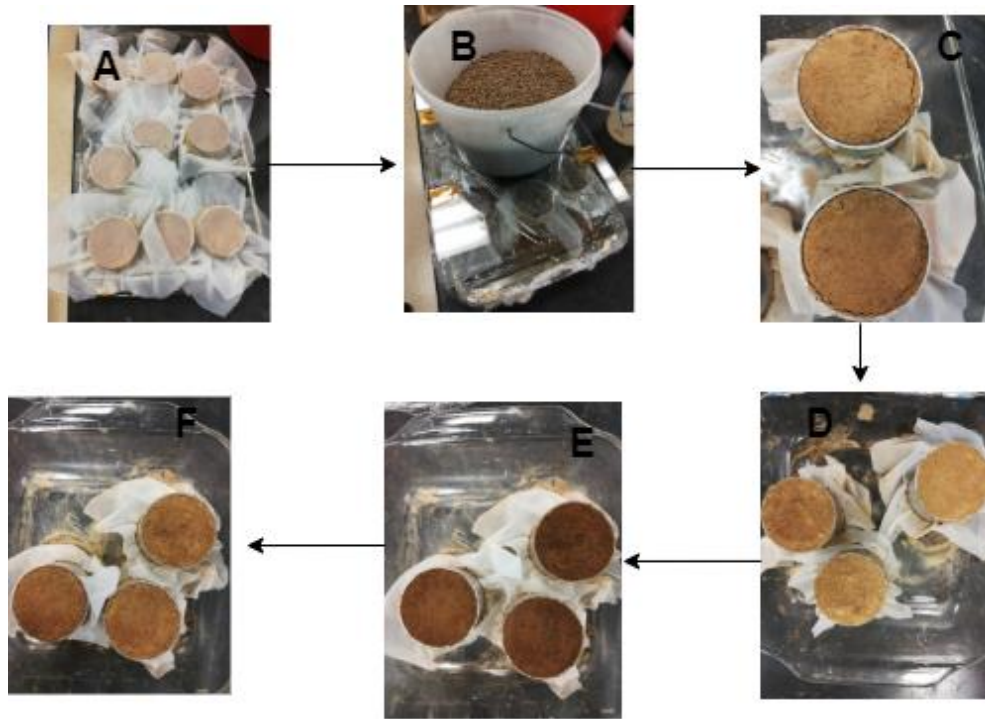


Figure A. 2. A visual representation of the various stages of multiple wetting and drying cycles of the hydrogel-soil mixtures: (A) shows the initial wetting of the samples with a nylon screen on top of the samples, (B) shows a load of (2.5 kg) placed on a glass slab and onto the samples to restrict swelling, (C) shows the cracks developed due to shrinkage in the samples after the first drying cycle, (D) shows when 1g of soil was used to fill in cracks in the samples after the 3rd wetting and drying cycle (E) shows the 4th wetting cycle and (F) shows the samples after the 4th drying cycle.

APPENDIX B. 1. Determination of the impact of lignin-based hydrogel on soil hydraulic conductivity.



Figure B. 1. The Eijkelkamp laboratory permeameter used to measure saturated hydraulic conductivity.

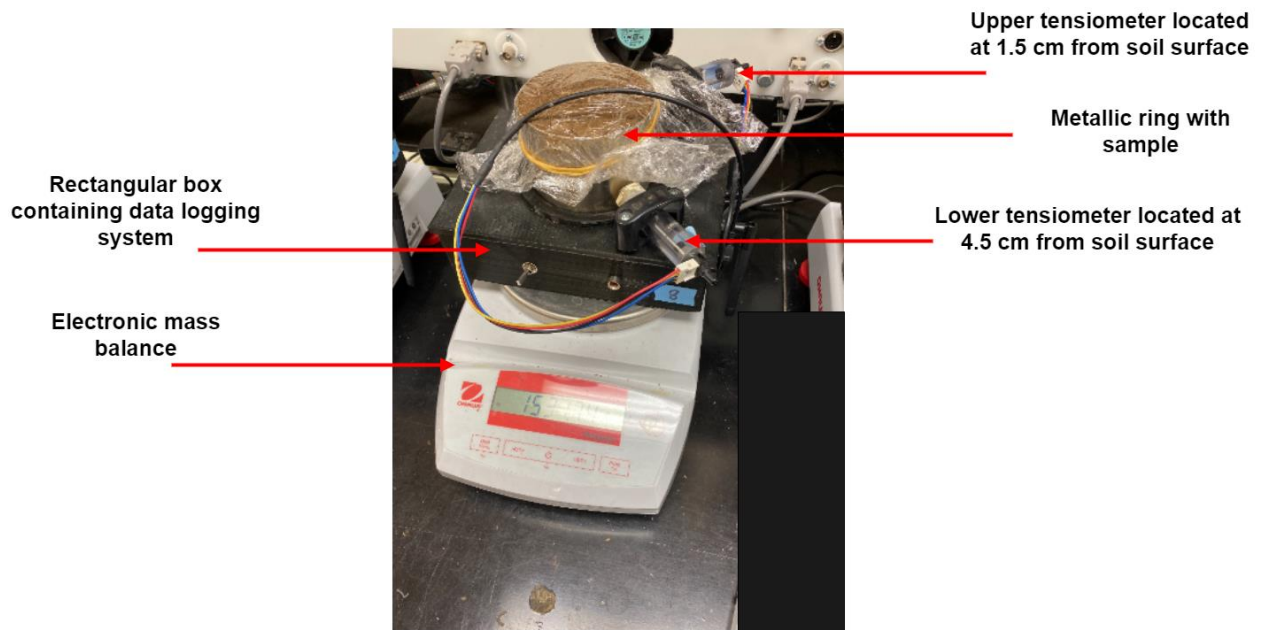


Figure B.2. Experimental set-up of evaporation method

APPENDIX C. 1 Machine Learning Implementation

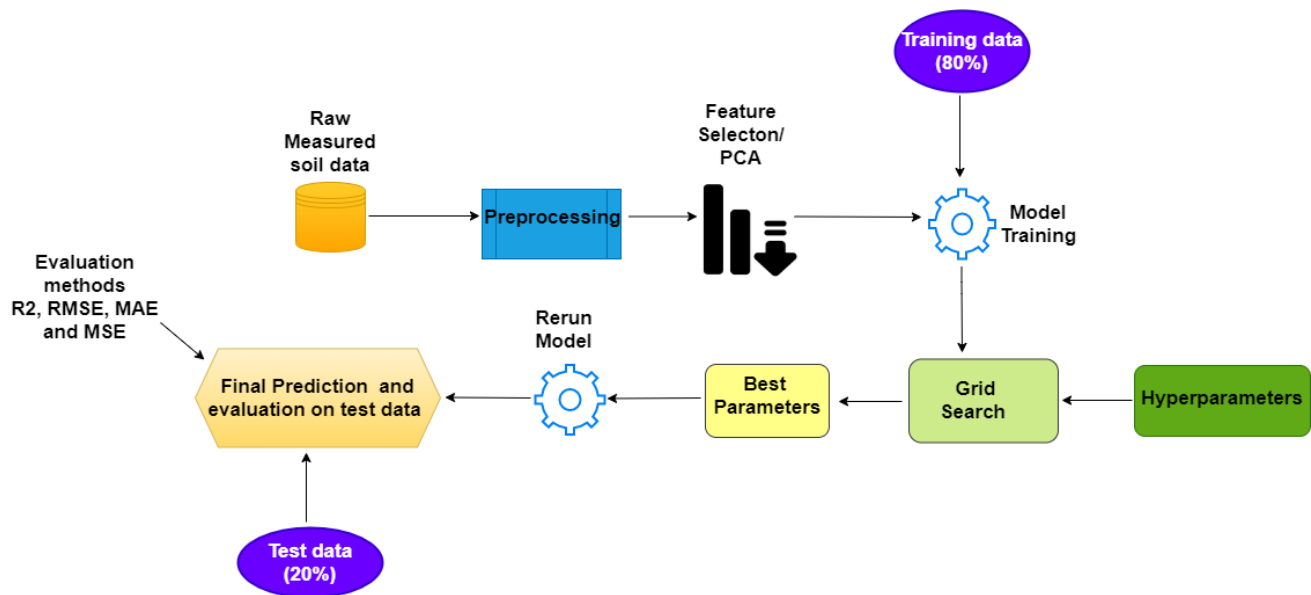


Figure C. 1. Steps used in developing machine learning models (RF, GB, KNN, and SVM).

APPENDIX C. 2. Machine learning algorithm hyperparameters

Table C.1. Hyperparameters for machine learning algorithms used for predicting saturated hydraulic conductivity.

Learning Algorithm	Hyperparameter
Multiple Linear Regression	None
K Nearest Neighbor Regression (KNN)	n_neighbors = 10, distance function = “Manhattan”
Support Vector Regression (SVR)	kernel = ‘rbf’, C= 40, ϵ = 0.1, and γ = 0.001
Gradient Boosted Regression (GB)	n_estimators = 36, learning rate = 0.1, max_depth = 7, loss = ‘huber’, alpha = 0.95, min_samples_split = 2
Random Forest Regression (RF)	n_estimators = 41, max_depth = 20, max_features = ‘sqrt’
Deep Neural Network Regression (DNN)	Epochs = 10, activation = ‘relu’, loss = ‘mean square error’, optimizer = ‘RMSprop’, neurons = 64, patience = 10

APPENDIX C. 3. Early Stopping for DNNR

Figure C.3 (a) and (b) illustrate the average error of the training and test set prior to implementation of early stopping and after implementation of early stopping respectively. Early stopping simply tells the algorithm to monitor the metric (i.e., mean square error) and to stop training the model once the error stops improving. Figure C.1 implies that increasing the number of epochs used for training will not necessarily improve performance of the model but would certainly increase computation time. Thus, the optimal number of epochs chosen was 10.

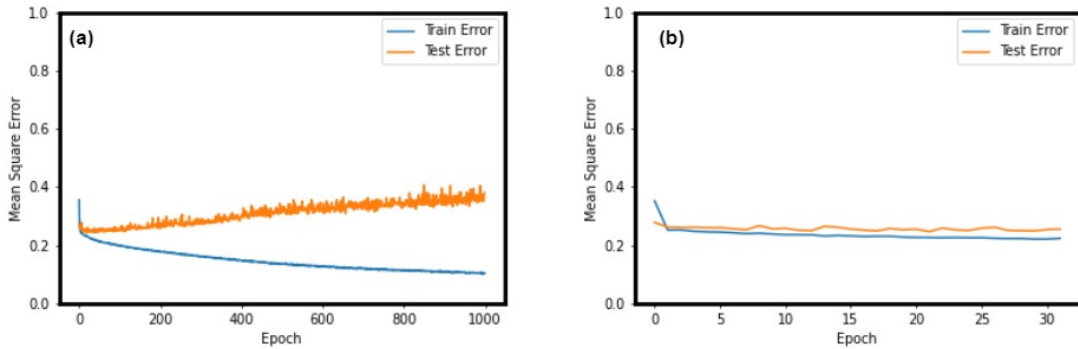


Figure C. 3. (a) Training and test error for the DNNR model; (b) Training and validation error for the DNNR model after implementation of early stopping.

APPENDIX C. 4. Predictor Importance

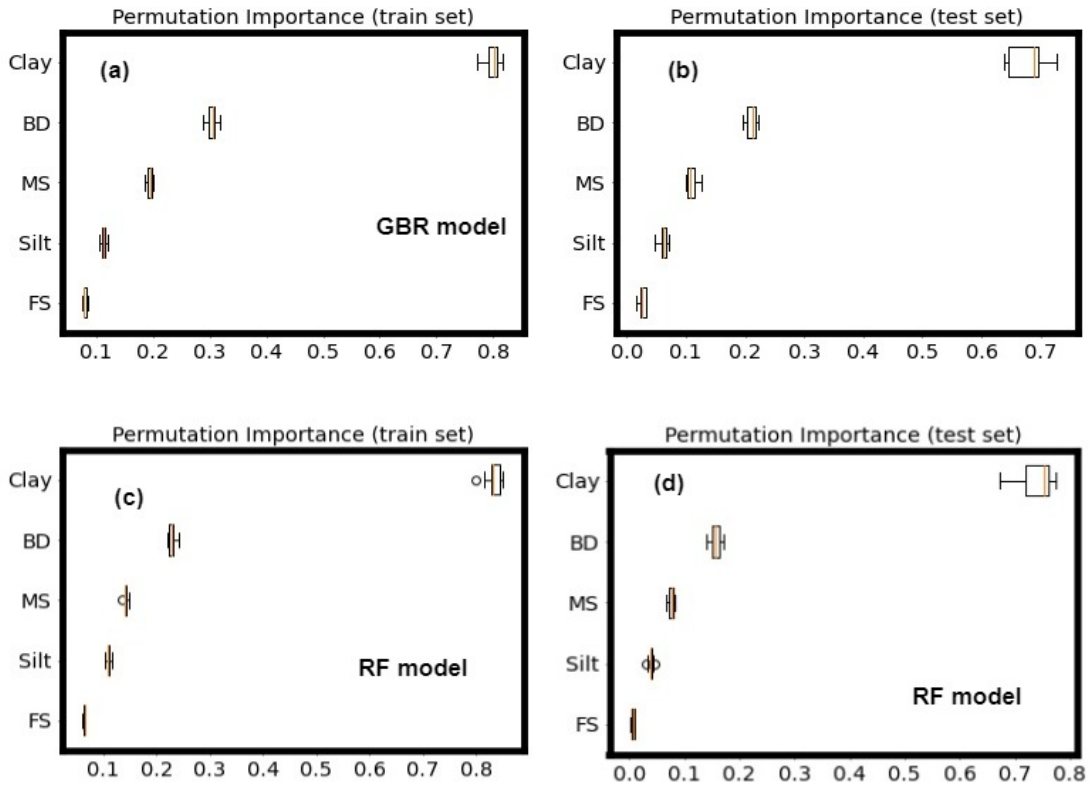


Figure C. 4. Permutation importance of the five predictors; (a) shows the permutation importance on the training dataset of the GB regression model (b) shows the permutation importance on the test dataset of the GB regression model; (c) shows the permutation importance on the train dataset of the RF model and (d) shows the permutation importance on the test set of the RF model. MS, medium sand; FS, fine sand; T_clay, total clay; T_silt, total silt; BD, bulk density

APPENDIX C. 5. Nomenclature

PTFs	Pedotransfer Functions
K_s	Saturated hydraulic conductivity
ML	Machine learning
MLR	Multiple linear regression
KNN	k-Nearest Neighbor
k	Parameter specified by a user in the KNN algorithm
SVR	Support Vector Regression
DNNR	Deep Neural Networks Regression
ML	Machine learning
MAE	Mean absolute error
RMSE	Root mean square error
R^2	Coefficient of determination
y	Observed (measured) saturated hydraulic conductivity (K_s) in cm h^{-1}
\hat{y}	Model predicted saturated hydraulic conductivity (K_s) in cm h^{-1}
\bar{y}	Mean of the measured saturated hydraulic conductivity (K_s)
n	The number of observations in the dataset
VCS	Very coarse sand

CS	Coarse sand
MS	Medium sand
FS	Fine sand
T_sand	Total sand
Clay	Clay content (% by mass)
Silt	Silt content (% by mass)
BD	Bulk density
R	Correlation coefficient

APPENDIX C. 6. Python code for developing machine learning models to predict saturated hydraulic conductivity.

Machine Learning Ksat Prediction Using FSCD

This code details the steps followed in developing machine learning regression models to predict saturated hydraulic conductivity using the Florida Characterization Database.

Email: adjuiktoby@gmail.com

Department of Biosystems and Agricultural Engineering

University of Kentucky

April 11, 2022

Download general packages needed for the simulation

```
import pandas as pd
import numpy as np
from sklearn.neighbors import KNeighborsClassifier
from sklearn.neighbors import KNeighborsRegressor
from sklearn.metrics import confusion_matrix
from sklearn.model_selection import cross_val_score
from scipy.stats import spearmanr, pearsonr
from sklearn.ensemble import RandomForestRegressor
from sklearn.tree import DecisionTreeRegressor
from sklearn.neighbors import KNeighborsRegressor
from sklearn.metrics import mean_squared_error
from sklearn.metrics import r2_score
from sklearn.model_selection import cross_validate
from sklearn.model_selection import validation_curve
from sklearn import preprocessing
from sklearn.preprocessing import StandardScaler
from sklearn.preprocessing import MinMaxScaler
import numpy as np
import pandas as pd
import seaborn as sns
import matplotlib.pyplot as plt
from sklearn.model_selection import train_test_split, cross_val_score
from sklearn.ensemble import RandomForestClassifier, RandomForestRegressor
from sklearn.metrics import classification_report, confusion_matrix, accuracy_score
from sklearn.neighbors import KNeighborsClassifier, KNeighborsRegressor
from sklearn.svm import SVC, SVR
from sklearn import datasets
import scipy.stats as stats
```

```
%matplotlib inline # allows plots to appear in the notebook
```

Data Cleaning and Preprocessing

```
#Creating a dataframe from the uploaded CSV file containing the original data
Florida_Soil_Data=pd.read_csv(r"D:\Data\Florida Soil Characterization Data.csv")

#Make new dataframe with empty cells dropped
Clean_Florida_Data= Florida_Soil_Data.dropna(axis=0, how="any")

#Comparing sizes of dataframe
print("Old data frame length:", len(Florida_Soil_Data), "\nNew data frame length:
", len(Clean_Florida_Data), "\nNumber of rows with at least 1 NA value:
",len(Florida_Soil_Data)-len(Clean_Florida_Data))

#Finding the average of the three replicates of bulk density and storing it as a
new column (Bulk_density_mean)
Bulk_density_mean = Clean_Florida_Data.loc[:, "Bulk_density_1":"Bulk_density_3"]
Bulk_density_mean= Bulk_density_mean.mean(axis=1)
Bulk_density_mean.head

#Finding the average of the three replicates of saturated hydraulic conductivity and storing it as
a new column (Sat_Conductivity_mean)
Sat_Conductivity_mean = Clean_Florida_Data.loc[:, "Sat_Hydrualic_Cond_1":
"Sat_Hydrualic_Cond_3"]
Sat_Conductivity_mean= Sat_Conductivity_mean.mean(axis=1)
Sat_Conductivity_mean

#Saving the new dataframe as a CSV file
Clean_Florida_Data.to_csv("clean_Florida_data.csv")

#Uploading a cleaned version of the dataset and creating a dataframe
New_soil_data=pd.read_csv(r"D:\Data\new_clean_Florida_data.csv")

# Import packages
import matplotlib.pyplot as plt
import matplotlib.cm as cm
import seaborn as sns
import scipy.sparse as sparse

# Create new dataframe containing predictors and target
New_soil_data = pd.DataFrame(np.c_[New_soil_data['VCS'],New_soil_data['CS'],
New_soil_data['MS'],New_soil_data['FS'],New_soil_data['VFS'],New_soil_data['T_sand'],
New_soil_data['Clay'], New_soil_data['Silt'], New_soil_data['SBD'], New_soil_data['Ks'],
columns = ['VCS','CS','MS','FS','VFS','T_sand','Clay','Silt','BD','Ks'])

#Descriptive statistics of data
New_soil_data.describe().transpose()
```

Creating a histogram to illustrate saturated hydraulic conductivity (ks)

```
[52]: import numpy as np
from matplotlib import colors
from matplotlib.ticker import PercentFormatter
import pandas as pd
import matplotlib
import matplotlib.pyplot as plt
from pylab import *
from sklearn.preprocessing import PowerTransformer
import seaborn as sns

from sklearn.pipeline import Pipeline

# Assigning predictors and target variables
X = pd.DataFrame(np.c_[New_soil_data['VCS'],New_soil_data['CS'],
New_soil_data['MS'],New_soil_data['FS'],New_soil_data['Clay'],New_soil_data['VFS'],New_soil_
data[:,columns = ['VCS','CS','MS','FS','VFS','T_sand','Silt','Clay','BD']])

y = New_soil_data['Ks']

# Creating a frequency distribution of the measured Ks
fig, ax = plt.subplots(figsize=(12, 9))
plt.hist(New_soil_data['Ks'], bins=33, align='right', color='green', _
,edgecolor='black')
plt.xscale("log")
plt.xlabel('Saturated hydraulic conductivity (cm/h)',fontsize=25)
plt.ylabel('# of observations',fontsize=25)
matplotlib.rc('xtick', labels=25)
matplotlib.rc('ytick', labels=25)
matplotlib.rc('axes', linewidth=5)
plt.xlim(0, 1000)
plt.ylim(0, 4686)
```

Principal Component Analysis

```
# Create dataframe for Predictors
X = pd.DataFrame(np.c_[New_soil_data['VCS'],New_soil_data['CS'],
New_soil_data['MS'],New_soil_data['FS'],New_soil_data['Clay'],New_soil_data['VFS'],New_soil_
data[:,columns = ['VCS','CS','MS','FS','VFS','T_sand','Silt','Clay','BD']])

#Download packages needed to run PCA
from sklearn.decomposition import PCA
from sklearn.preprocessing import StandardScaler
from sklearn import decomposition
```

```
from sklearn.preprocessing import scale
import numpy as np
import matplotlib.pyplot as plt
import pandas as pd
from sklearn import decomposition
from sklearn import datasets
from sklearn.preprocessing import scale
import matplotlib.pyplot as plt
import seaborn as sb
```

```
#Get variable/feature names
feature_names=list(X.columns.values)
feature_names
```

```
#Standardize data
X_scaled = scale(X)
```

```
# apply PCA
pca = decomposition.PCA(n_components=9)
X_pca = pca.fit_transform(X_scaled)
```

Calculation of the factor loadings

```
#To get the loadings, we just need to access the attribute components_ of the
sklearn.decomposition.pca.PCA object.
loadings = pd.DataFrame(pca.components_.T, columns=['PC1',
, 'PC2', 'PC3', 'PC4', 'PC5', 'PC6', 'PC7', 'PC8', 'PC9'], index= feature_names)
Loadings
```

Explained variance

```
# Percentage of variance explained for each components
variance=(pca.explained_variance_ratio_.round(3))
variance
```

```
# Cumulative sum of variances
cumsum=np.cumsum(np.round(variance, decimals=3)*100)
cumsum #cumulative sum of variance explained with [n] features
```

Check normality of data

```
#Uploading a cleaned dataset and creating a dataframe
```

```

New_soil_data=pd.read_csv(r"D:\Data\new_clean_Florida_data.csv")
# Create Datasets for Target and Predictors
New_soil_data = pd.DataFrame(np.c_[New_soil_data['VCS'],New_soil_data['CS'],
New_soil_data['MS'],New_soil_data['FS'],New_soil_data['VFS'],New_soil_data['T_sand'],New_s
oil],New_soil['Clay'],New_soil['Silt'],New_soil['BD'],New_soil["Log_Ks"]),
columns = ['VCS','CS','MS','FS','VFS','T_sand','Clay','Silt','BD','Log_Ks'])
Log_Ks = New_soil_data['Log_Ks'] # Create dataset with Ks
#Normality test for Ks values
#Shapiro wilks test of normality
from scipy.stats import shapiro
stat, p = shapiro(Log_Ks)
print('Statistics=%.3f, p=%.3f' % (stat, p))
# interpret
alpha = 0.05
if p > alpha:
print('Sample looks Gaussian (fail to reject H0)')
else:
print('Sample does not look Gaussian (reject H0)')

# histogram plot
from matplotlib import pyplot
pyplot.hist(Log_Ks)
pyplot.show()

# Box-cox Transformation of Log Ks values for normality
from scipy import stats
Log_Ks_trans, lmbda = stats.boxcox(Log_Ks)
# histogram plot after transformation
from matplotlib import pyplot
pyplot.hist(Log_Ks_trans)
pyplot.show()

```

Pearson Correlation Heat Map

```

#Uploading a cleaned dataset and creating a dataframe
New_soil_data=pd.read_csv(r"D:\Data\new_clean_Florida_data.csv")
# Importing packages
import numpy as np
import pandas as pd
from matplotlib import pyplot as plt

```

```

import seaborn as sns

# Create Datasets for Target and Predictors
df = pd.DataFrame(np.c_[New_soil_data['VCS'],New_soil_data['CS'],
New_soil_data['MS'],New_soil_data['FS'],New_soil_data['VFS'],New_soil_data['T_sand'],New_s
oil],New_soil[Clay'],New_soil['Silt'],New_soil['BD'],New_soil["Log_Ks"], columns =
['VCS','CS','MS','FS','VFS','T_sand','Clay','Silt','BD','Log_Ks'])

# Create the correlation matrix
corr = df.corr()

# Generate a mask for the upper triangle; True = do NOT show
mask = np.zeros_like(corr)
mask[np.triu_indices_from(mask)] = True

# Draw the pearson heatmap
fig = plt.figure(figsize=(10,7.5))
ax = sns.heatmap(corr, mask=mask, cmap='coolwarm', annot=True, vmax=1,vmin=-1,
square=True, linewidths=.5, cbar = True,
)

# Set x and y axis tick label font sizes
ax.set_xticklabels(ax.get_xmajorticklabels(), fontsize = 14)
ax.set_yticklabels(ax.get_ymajorticklabels(), fontsize = 14)

# Set tick label font size of color bar
cax = plt.gcf().axes[-1]
cax.tick_params(labelsize=14)

```

Normalize predictors

```

from sklearn.preprocessing import StandardScaler
scaler = StandardScaler()
X = scaler.fit_transform(X)

```

Random Forest Algorithm

```

# Create Datasets for Target and Predictors
X = pd.DataFrame(np.c_[New_soil_data['VCS'],New_soil_data['CS'],
New_soil_data['MS'],New_soil_data['FS'],New_soil_data['VFS'],New_soil_data['T_sand'],New_s
oil],New_soil[Clay'],New_soil['Silt'],New_soil['BD'], columns =
['VCS','CS','MS','FS','VFS','T_sand','Clay','Silt','BD'])
y = New_soil_data['Log_Ks']

```

```

# Splitting the data into training and testing sets
from sklearn.model_selection import train_test_split
X_train, X_test, y_train, y_test = train_test_split(X, y, test_size=0.30, random_state=10)
print("The shape of the X_trainset is",X_train.shape) # The shape of the X_trainset
print("The shape of the X_testset is", X_test.shape) # The shape of the X_testset
print("The shape of the Y_trainset is",y_train.shape) # The shape of the X_trainset
print("The shape of the y_testset is", y_test.shape) # The shape of the y_testset

#Download packages

from sklearn.model_selection import train_test_split
from sklearn.ensemble import RandomForestRegressor
from sklearn.metrics import r2_score,mean_squared_error

```

0.0.13 Parameter search

```

#Hyperparameter Search
from sklearn.model_selection import cross_val_score
from sklearn.model_selection import GridSearchCV
# Define the hyperparameter configuration space
rf_params = { 'n_estimators': [40,41,42,43,44,45,46,47,48,49,50], 'max_features': ["sqrt"],
'max_depth': [10,15,20,25,30],
}

clf = RandomForestRegressor(random_state=0)
grid = GridSearchCV(clf, rf_params, cv=5, scoring='r2')
grid.fit(X_train, y_train.ravel())
print(grid.best_params_)

print("R2:" + str(grid.best_score_))

clf = RandomForestRegressor(n_estimators=41, criterion='mae', max_depth=20,
min_samples_split=10, min_samples_leaf=6,
min_weight_fraction_leaf=0.0, max_features='sqrt', max_leaf_nodes=None,
min_impurity_decrease=0.0, min_impurity_split=None,
bootstrap=False, oob_score=False, n_jobs=-1, random_state=5, verbose=0,
warm_start=False)

#Fit model to training dataset
clf.fit(X_train, y_train.ravel())

#Predict using train dataset
y_train_RF = clf.predict(X_train)

```

```

# Predicting the test set results
y_pred_RF = clf.predict(X_test)

#Evaluation metrics for random forest
from sklearn.metrics import mean_absolute_error
import sklearn.metrics as metrics

#R2 metric
score = r2_score(y_train, y_train_RF)
print("Train accuracy (R2) for random forest regression: {}".format(score))
score_R2_RF = r2_score(y_test, y_pred_RF)
print("Test accuracy (R2) for random forest regression: {}".format(score_R2_RF))

#Mean absolute value metric
score = mean_absolute_error(y_train, y_train_RF)
print("Train accuracy(MAE) for random forest regression: {}".format(score))
score_MAE_RF = mean_absolute_error(y_test, y_pred_RF)
print("Test accuracy(MAE) for random forest regression: {}".format(score_MAE_RF))

#RMSE metric
score = np.sqrt(metrics.mean_squared_error(y_train, y_train_RF))
print("Train accuracy (RMSE) for RF: {}".format(score))
score_RMSE_RF = np.sqrt(metrics.mean_squared_error(y_test, y_pred_RF))
print("Test accuracy (RMSE) for RF: {}".format(score_RMSE_RF))

#Displaying evaluation metrics
Metric = " MAE = " + str(round(score_MAE_RF, 2)) + " (cm h$^{-1}$)" + "\n" + "
R$^2$ = " + str(round(score_R2_RF, 2)) + ", " + " RMSE = " +
str(round(score_RMSE_RF, 2)) + " (cm h$^{-1}$)"
print("Random Forest Model Performance: ", Metric)

#Scatter plot of predicted Ks vs measured Ks
import matplotlib.pyplot as plt
from pylab import *
import matplotlib as mpl
#Plot for multi linear regression
from scipy.optimize import curve_fit
from sklearn.model_selection import cross_val_predict
from sklearn import linear_model
lr = linear_model.LinearRegression()

```



```

predicted = cross_val_predict(lr, y_pred_RF, y_test, cv=10)

fig, ax = plt.subplots(figsize=(12, 9))
ax.set_title('Random Forest Regression', fontsize=30)
ax.scatter(y_test,predicted)
ax.plot([y.min(), y.max()], [y.min(), y.max()], 'k--', lw=5)
ax.set_xlabel('Observed Ks log (cm h$^{-1}$)',fontsize=30)
ax.set_ylabel('Predicted Ks log (cm h$^{-1}$)',fontsize=30)
ax.tick_params(axis="x", direction="out",length=8, width=2)
ax.tick_params(axis="y", direction="out",length=8, width=2)
plt.xlim(-2, 3)
plt.ylim(-2, 3)
plt.tick_params(axis='both', which='major', labelsize=30)
plt.text(-1.5, 2.2,Metric,fontsize=25, bbox=dict(facecolor='none', alpha=0.5))
rc('axes', linewidth=5)

plt.show()

```

Feature Importance for RF model created

```
#Import packages
```

```

import numpy as np
import matplotlib.pyplot as plt
from sklearn.inspection import permutation_importance
from sklearn.pipeline import make_pipeline
from sklearn.inspection import permutation_importance
from sklearn.metrics import mean_squared_error

```

```
#Feature importance on training dataset
```

```

result = permutation_importance(clf, X_train, y_train, n_repeats=10, random_state=42,
n_jobs=2)
sorted_idx = result.importances_mean.argsort()
plt.boxplot(result.importances[sorted_idx].T,
vert=False, labels=np.array(X.columns)[sorted_idx])
plt.xticks(size = 15)
plt.yticks(size = 15)
plt.title("Permutation Importance (train set)",fontsize=15)
fig.tight_layout()
plt.show()

```

```
#Feature importance on testing dataset
```

```

result = permutation_importance(clf, X_test, y_test, n_repeats=10,
random_state=42, n_jobs=2)
sorted_idx = result.importances_mean.argsort()
plt.boxplot(result.importances[sorted_idx].T,
vert=False, labels=np.array(X.columns)[sorted_idx])
plt.xticks(size = 15)

```

```
plt.yticks(size = 15)
plt.title("Permutation Importance (test set)",fontsize=15)
fig.tight_layout()
plt.show()
```

Multi linear regression

```
# Download packages
import matplotlib.pyplot as plt
import pandas as pd
import pylab as pl
import numpy as np
from sklearn import linear_model
from sklearn.linear_model import LinearRegression
from sklearn import metrics

#Fit model to training set
regressor = LinearRegression()
regressor.fit(X_train, y_train)

#Predict trainset
y_train_MLR = regressor.predict(X_train)

y_train_MLR

# Predicting the test set results
y_pred_MLR = regressor.predict(X_test)

#Evaluation metrics
from sklearn.metrics import mean_absolute_error

#R2 metrics
score =r2_score(y_train, y_train_MLR)
print("Train accuracy (R2) for multi linear regression: {}".format(score))
score_R2_MLR =r2_score(y_test, y_pred_MLR)
print("Test accuracy (R2) for multi linear regression: {}".format(score_R2_MLR))

#Mean absolute error metrics
score = mean_absolute_error(y_train, y_train_MLR)
print("Train accuracy(MAE) for multi linear regression: {}".format(score))
score_MAE_MLR = mean_absolute_error(y_test, y_pred_MLR)
print("Test accuracy(MAE) for multi linear regression: {}".format(score_MAE_MLR))
score = np.sqrt(metrics.mean_squared_error(y_train, y_train_MLR))
```

```

#RMSE metrics
print("Train accuracy (RMSE) for MLR: {}".format(score))
score_RMSE_MLR = np.sqrt(metrics.mean_squared_error(y_test, y_pred_MLR))
print("Test accuracy (RMSE) for MLR: {}".format(score_RMSE_MLR))

#Formatting evaluation metrics to be displayed on the scatter plot
Metric = " MAE = " + str(round(score_MAE_MLR, 2)) + " (cm h$^{-1}$)" + "\n" + "R$^2$ = " +
str(round(score_R2_MLR, 2)) + ", " + " RMSE = " + str(round(score_RMSE_MLR, 2)) + " (cm h$^{-1}$)"

print("Random Forest Model Performance: ", Metric)

#Scatter plot for multi linear regression
import matplotlib.pyplot as plt
from pylab import *
import matplotlib as mpl
from scipy.optimize import curve_fit
from sklearn.model_selection import cross_val_predict
from sklearn import linear_model
lr = linear_model.LinearRegression()
predicted = cross_val_predict(lr, y_pred_MLR, y_test, cv=10)
fig, ax = plt.subplots(figsize=(12, 9))
ax.set_title('Multiple Linear Regression', fontsize=30)
ax.scatter(y_test, predicted, c="orange")
ax.plot([y.min(), y.max()], [y.min(), y.max()], 'k--', lw=5)
ax.set_xlabel('Observed Ks log (cm h$^{-1}$)', fontsize=30)
ax.set_ylabel('Predicted Ks log (cm h$^{-1}$)', fontsize=30)
ax.tick_params(axis="x", direction="out", length=8, width=2)
ax.tick_params(axis="y", direction="out", length=8, width=2)
plt.xlim(-2, 3)
plt.ylim(-2, 3)
plt.tick_params(axis='both', which='major', labelsize=30)
plt.text(-1.5, 2.2, Metric, fontsize=25, bbox=dict(facecolor='none', alpha=0.5))
rc('axes', linewidth=2)
plt.show()

```

Coefficients of Multiple Linear Regression

```

from sklearn.preprocessing import StandardScaler
import pandas as pd
import numpy as np
import matplotlib.pyplot as plt
from sklearn.linear_model import LinearRegression
from sklearn.metrics import r2_score
import statsmodels.api as sm

```

```

X=New_soil_data[['MS','FS','BD','Silt','Clay']]
y = New_soil_data[['Log_Ks']]

# Multiple Regression Model

from sklearn.linear_model import LinearRegression
regression_model = LinearRegression()
regression_model.fit(X_train, y_train)

# Coefficients of MLR
for idx, col_name in enumerate(X_train.columns):
    print("The coefficient for {} is {}".format(col_name, regression_model.
    coef_[0][idx]))

# The intercepts of the MLR model
intercept = regression_model.intercept_[0]
print("The intercept for our model is {}".format(intercept))

#Determining statistical significance of model coefficients
X = np.column_stack((New_soil_data['MS'], New_soil_data['FS'],
New_soil_data['BD'],New_soil_data['Silt'],New_soil_data['Clay']))
y = New_soil_data['Log_Ks']
X2 = sm.add_constant(X)
est = sm.OLS(y, X2)
est2 = est.fit()

print(est2.summary())

```

KNN Regression Algorithm

```

#Cross-validation to find the best n_estimators

from sklearn.model_selection import cross_val_score
neighbors = list(range(10, 20))
cv_scores = []
cv_r2 = []

# perform 10-fold cross validation
for k in neighbors:
    knn = KNeighborsRegressor(n_neighbors=k, weights='uniform', algorithm='auto', leaf_size=1,
    p=2, metric='manhattan', metric_params=None, n_jobs=-1)

```

```

scores_cv = cross_validate(knn, X_train, y_train.ravel(), groups=None,
scoring=('r2', 'neg_mean_squared_error'), cv=10, n_jobs=None, verbose=0,
fit_params=None, pre_dispatch='2*n_jobs', return_train_score=True,
return_estimator=False)
print(scores_cv['test_neg_mean_squared_error'])
print(scores_cv['train_r2'])
cv_r2.append(scores_cv['train_r2'].mean())
cv_scores.append(np.mean(list(scores_cv.values())))

# Calculating misclassification error of the cross-validation
mse = [1 - x for x in cv_scores]

# determining best optimal k
optimal_k = neighbors[mse.index(min(mse))]
opt_r2 = cv_r2[mse.index(min(mse))]
print("The optimal number of neighbors is {}".format(optimal_k))
print("The R_Squared for optimal number of neighbors is {}".format(opt_r2))

# plot misclassification error vs k
plt.plot(neighbors, mse)
plt.xlabel("Number of K neighbors")
plt.ylabel("Misclassification Error")
plt.show()

# Fitting the KNN algorithm to the training data
from sklearn.neighbors import KNeighborsRegressor
knn = KNeighborsRegressor(n_neighbors=10, weights='uniform', algorithm='auto', leaf_size=1,
p=2, metric='manhattan', metric_params=None, n_jobs=-1)

knn.fit(X_train, y_train)

#Predict training dataset
y_train_KNN = knn.predict(X_train)

# Predicting the test set results
y_pred_KNN = knn.predict(X_test)

# Evaluation Metrics
from sklearn.metrics import mean_squared_error

#R2 metric
score = r2_score(y_train, y_train_KNN)
print("Train accuracy (R2) for KNN regression: {}".format(score))
score_R2_KNN = r2_score(y_test, y_pred_KNN)
print("Test accuracy (R2) for KNN regression: {}".format(score_R2_KNN))

```

```

# Mean absolute error metric
score = mean_absolute_error(y_train, y_train_KNN)
print("Train accuracy (MAE) for KNN regression: {}".format(score))
score_MAE_KNN = mean_absolute_error(y_test, y_pred_KNN)
print("Test accuracy (MAE) for KNN regression: {}".format(score_MAE_KNN))

#RMSE metric
score = np.sqrt(metrics.mean_squared_error(y_train, y_train_KNN))
print("Train accuracy (RMSE) for KNN: {}".format(score))
#Test set
score_RMSE_KNN = np.sqrt(metrics.mean_squared_error(y_test, y_pred_KNN))
print("Test accuracy (RMSE) for KNN: {}".format(score_RMSE_KNN))

#Formatting evaluation metrics to be displayed on the scatter plot
Metric= " MAE = " + str(round(score_MAE_KNN, 2)) + " (cm h$^{-1}$)" + "\n" + "
R$^2$ = " + str(round(score_R2_KNN, 2)) + ", " + " RMSE = " +
str(round(score_RMSE_KNN, 2)) + " (cm h$^{-1}$)"
print("Random Forest Model Performance: ", Metric)

# Create scatter plot for test and prediction values
import matplotlib.pyplot as plt

from pylab import *
from scipy.optimize import curve_fit
from sklearn.model_selection import cross_val_predict
from sklearn import linear_model
import matplotlib as mpl

lr = linear_model.LinearRegression()
predicted = cross_val_predict(lr, y_pred_KNN, y_test, cv=10)
fig, ax = plt.subplots(figsize=(12, 9))
ax.set_title('KNN Regression', fontsize=30)
ax.scatter(y_test, predicted, c="red")
ax.plot([y.min(), y.max()], [y.min(), y.max()], 'k--', lw=5)
ax.set_xlabel('Observed Ks log (cm h$^{-1}$)', fontsize=30)
ax.set_ylabel('Predicted Ks log (cm h$^{-1}$)', fontsize=30)
ax.tick_params(axis="x", direction="out", length=8, width=2)
ax.tick_params(axis="y", direction="out", length=8, width=2)
plt.xlim(-2, 3)
plt.ylim(-2, 3)
plt.tick_params(axis='both', which='major', labelsize=30)
plt.text(-1.6, 2.2, Metric, fontsize=25, bbox=dict(facecolor='none', alpha=0.5))
rc('axes', linewidth=5)

plt.show()

```

Support Vector Regression

```
#Hyperparameter search
from sklearn.model_selection import GridSearchCV
rf_params = {
'C': [10,50,100],
"kernel":['rbf', 'linear', 'sigmoid'],
"epsilon":[0.01,0.1,1],
"gamma":[0.001,0.01,0.1,1]
}
clf = SVR(gamma='scale')
grid = GridSearchCV(clf, rf_params, cv=10, scoring='neg_mean_squared_error')
grid.fit(X_train, y_train.ravel())
print(grid.best_params_)

print("MSE:"+ str(-grid.best_score_))

# Fitting the KNN algorithm to the training data
from sklearn.svm import SVR
sv_reg = SVR(kernel='rbf', degree=3, gamma=0.001, coef0=0.0, tol=0.001, C=40,
epsilon=0.1, shrinking=True, cache_size=200, verbose=False, max_iter=-1)
sv_reg.fit(X_train, y_train.ravel()) # fit the model for training data

#Predict trainset
y_train_SVR = sv_reg.predict(X_train)

# Predicting the test set results
y_pred_SVR = sv_reg.predict(X_test)

#Evaluation metrics
from sklearn.metrics import mean_squared_error
from sklearn.metrics import mean_absolute_error
import sklearn.metrics as metrics

#R2 metric
score = r2_score(y_train, y_train_SVR)
print("Train accuracy (R2) for SVR: {}".format(score))
score_R2_SVR = r2_score(y_test, y_pred_SVR)
print("Test accuracy (R2) for SVR: {}".format(score_R2_SVR))

#Mean absolute error metric
score = mean_absolute_error(y_train, y_train_SVR)
print("Train accuracy (MAE) for SVR: {}".format(score))
```

```

score_MAE_SVR = mean_absolute_error(y_test, y_pred_SVR)
print("Test accuracy (MAE) for SVR: {}".format(score_MAE_SVR))

#RMSE Metric
score = np.sqrt(metrics.mean_squared_error(y_train, y_train_SVR))
print("Train accuracy (RMSE) for SVR: {}".format(score))
score_RMSE_SVR = np.sqrt(metrics.mean_squared_error(y_test, y_pred_SVR))
print("Test accuracy (RMSE) for SVR: {}".format(score_RMSE_SVR))

#Formatting evaluation metrics to be displayed on the scatter plot
Metric= " MAE = " + str(round(score_MAE_SVR, 2)) + " (cm h$^{-1}$)" + "\n" + "
R$^2$ = " + str(round(score_R2_SVR, 2)) + ", " + " RMSE = " + str(round(score_RMSE_SVR, 2)) + "
(cm h$^{-1}$)"

print("Random Forest Model Performance: ", Metric)

#Create Scatter Plot for Test and Prediction values
import matplotlib.pyplot as plt
from pylab import *
from scipy.optimize import curve_fit
from sklearn.model_selection import cross_val_predict
from sklearn import linear_model
import matplotlib as mpl

lr = linear_model.LinearRegression()
predicted = cross_val_predict(lr, y_pred_SVR, y_test, cv=10)
fig, ax = plt.subplots(figsize=(12, 9))
ax.set_title('Support Vector Regression', fontsize=30)
ax.scatter(y_test, predicted, c="green")
ax.plot([y.min(), y.max()], [y.min(), y.max()], 'k--', lw=5)
ax.set_xlabel('Observed Ks log (cm h$^{-1}$)', fontsize=30)
ax.set_ylabel('Predicted Ks log (cm h$^{-1}$)', fontsize=30)
ax.tick_params(axis="x", direction="out", length=8, width=2)
ax.tick_params(axis="y", direction="out", length=8, width=2)
plt.xlim(-2, 3)
plt.ylim(-2, 3)
plt.tick_params(axis='both', which='major', labelsize=30)
plt.text(-1.6, 2.2, Metric, fontsize=25, bbox=dict(facecolor='none', alpha=0.5))
rc('axes', linewidth=4)

plt.show()

```

Gradient Boosting Regression

```

# Download packages
from sklearn.metrics import mean_squared_error, r2_score, mean_absolute_error

```



```

from sklearn.ensemble import GradientBoostingRegressor
from sklearn.model_selection import GridSearchCV

#Hyperparameter search
GBR_params = {
'n_estimators': [35],
'learning_rate':[0.1,0.2,0.3,0.4,0.5],
'max_depth': [7],
'loss': ['huber'],
'min_samples_split':[2],
}

GBR = GradientBoostingRegressor(**GBR_params)
grid = GridSearchCV(GBR, GBR_params, cv=5, scoring='neg_mean_squared_error')
grid.fit(X_train, y_train.ravel())
print(grid.best_params_)

print("MSE:" + str(-grid.best_score_))

#Fit GBR model
GBR_params = {'n_estimators': 36, 'max_depth': 7,
'learning_rate': 0.1, 'loss': 'huber', 'alpha':0.95, 'min_samples_split':2}

GBR = GradientBoostingRegressor(**GBR_params)

GBR.fit(X_train, y_train.ravel())

#Predict trainset
y_train_GBR = GBR.predict(X_train)

# Predicting the test set results
y_pred_GBR = GBR.predict(X_test)

from sklearn.datasets import make_regression
from sklearn.ensemble import GradientBoostingRegressor
from matplotlib import pyplot

#Evaluation Metrics
import sklearn.metrics as metrics

#R2
score = r2_score(y_train, y_train_GBR)
print("Train accuracy (R2) for GBR: {}".format(score))
score_R2_GBR = r2_score(y_test, y_pred_GBR)
print("Test accuracy (R2) for GBR: {}".format(score_R2_GBR))

```

```

#Mean absolute error metric
score = mean_absolute_error(y_train, y_train_GBR)
print("Train accuracy (MAE) for GBR: {}".format(score))
score_MAE_GBR = mean_absolute_error(y_test, y_pred_GBR)
print("Test accuracy (MAE) for GBR: {}".format(score_MAE_GBR))

#RMSE metric
score = np.sqrt(metrics.mean_squared_error(y_train, y_train_GBR))
print("Train accuracy (RMSE) for GBR: {}".format(score))
score_RMSE_GBR = np.sqrt(metrics.mean_squared_error(y_test, y_pred_GBR))

print("Test accuracy (RMSE) for GBR: {}".format(score_RMSE_GBR))

#Formatting evaluation metrics to be displayed on the scatter plot
Metric= " MAE = " + str(round(score_MAE_GBR, 2)) + " (cm h$^{-1}$)" + "\n" + "
R$^2$ = " + str(round(score_R2_GBR, 2)) + " , " + " RMSE = " +
str(round(score_RMSE_GBR, 2)) + " (cm h$^{-1}$)"
print("GBR Model Performance: ", Metric)

#Create Scatter Plot for Test and Prediction values

import matplotlib.pyplot as plt
from pylab import *
from scipy.optimize import curve_fit
from sklearn.model_selection import cross_val_predict
from sklearn import linear_model
import matplotlib as mpl

lr = linear_model.LinearRegression()
predicted = cross_val_predict(lr, y_pred_GBR, y_test, cv=10)
fig, ax = plt.subplots(figsize=(12, 9))
ax.set_title('Gradient Boosted Regression', fontsize=30)
ax.scatter(y_test, predicted, c="yellow")
ax.plot([y.min(), y.max()], [y.min(), y.max()], 'k--', lw=5)
ax.set_xlabel('Observed Ks log (cm h$^{-1}$)', fontsize=30)
ax.set_ylabel('Predicted Ks log (cm h$^{-1}$)', fontsize=30)
ax.tick_params(axis="x", direction="out", length=8, width=2)
ax.tick_params(axis="y", direction="out", length=8, width=2)
plt.xlim(-2, 3)
plt.ylim(-2, 3)
plt.tick_params(axis='both', which='major', labelsize=30)
plt.text(-1.5, 2.2, Metric, fontsize=25, bbox=dict(facecolor='none', alpha=0.5))
rc('axes', linewidth=5)

plt.show()

```

Determine the Features Importance for GBR Model

```
import numpy as np
import matplotlib.pyplot as plt
from sklearn.inspection import permutation_importance
from sklearn.pipeline import make_pipeline
from sklearn.inspection import permutation_importance
from sklearn.metrics import mean_squared_error

#Feature importance on train set
result = permutation_importance(GBR, X_train, y_train, n_repeats=10,
random_state=42, n_jobs=2)
sorted_idx = result.importances_mean.argsort()
plt.boxplot(result.importances[sorted_idx].T,
vert=False, labels=np.array(X.columns)[sorted_idx])
plt.xticks(size = 15)
plt.yticks(size = 15)
plt.title("Permutation Importance (train set)", fontsize=15)
fig.tight_layout()
plt.show()

#Feature importance on test set
result = permutation_importance(GBR, X_test, y_test, n_repeats=10,
random_state=42, n_jobs=2)
sorted_idx = result.importances_mean.argsort()
plt.boxplot(result.importances[sorted_idx].T,
vert=False, labels=np.array(X.columns)[sorted_idx])
plt.xticks(size = 15)
plt.yticks(size = 15)
plt.title("Permutation Importance (test set)", fontsize=15)
fig.tight_layout()
plt.show()
```

Deep Neural Networks

```
#Import packages needed

from keras.models import Sequential
from keras.layers import Dense
from keras.wrappers.scikit_learn import KerasRegressor
from sklearn.model_selection import train_test_split
from sklearn.model_selection import cross_val_score
from sklearn.model_selection import cross_validate
from sklearn.preprocessing import StandardScaler
from sklearn.pipeline import Pipeline
import tensorflow as tf
```

```
from tensorflow import keras
from tensorflow.keras import layers
from tensorflow.keras.layers.experimental import preprocessing
```

```
# Create Datasets for Target and Predictors
```

```
New_soil_data = New_soil_data.loc[:, ['MS', 'BD', 'Silt', 'FS', 'T_sand', 'Log_Ks']]
```

```
X = pd.DataFrame(np.c_[New_soil_data['VCS'], New_soil_data['CS'],
New_soil_data['MS'], New_soil_data['FS'], New_soil_data['VFS'], New_soil_data['T_sand'], New_s
oil], New_soil['Clay'], New_soil['Silt'], New_soil['BD'], columns =
['VCS', 'CS', 'MS', 'FS', 'VFS', 'T_sand', 'Clay', 'Silt', 'BD'])
```

```
y = New_soil_data['Log_Ks']
```

Split the data into train and test

```
train_dataset = New_soil_data.sample(frac=0.8, random_state=0)
```

```
test_dataset = New_soil_data.drop(train_dataset.index)
```

Split features from labels

```
from sklearn.model_selection import train_test_split
X_train, X_test, y_train, y_test = train_test_split(X, y, test_size=0.25,
random_state=10)
print("The shape of the X_trainset is", X_train.shape) # The shape of the X_trainset
print("The shape of the y_trainset is", y_train.shape) # The shape of the y_trainset
print("The shape of the X_testset is", X_test.shape) # The shape of the X_testset
print("The shape of the y_testset is", y_test.shape) # The shape of the y_testset
```

Normalization

```
def norm(x):
return (x - train_stats['mean']) / train_stats['std'] # Function to normalize input variables
normed_train_data = norm(train_dataset)
normed_test_data = norm(test_dataset)
```

Model building

```
# Function to build model
```

```
def build_model():
model = keras.Sequential([
layers.Dense(64, activation=tf.nn.relu, input_shape=[len(train_dataset.keys())]),
layers.Dense(64, activation=tf.nn.relu),
```

```

layers.Dense(1]))
optimizer = tf.keras.optimizers.RMSprop(0.001)
model.compile(loss='mean_squared_error', optimizer=optimizer,
metrics=['mean_absolute_error', 'mean_squared_error'])

return model

model = build_model()

```

Train model

Training the model for 1000 epochs, and recording the training and validation accuracy in the history object.

```

# Display training progress by printing a single dot for each completed epoch
class PrintDot(keras.callbacks.Callback):
def on_epoch_end(self, epoch, logs):
if epoch % 100 == 0: print("")
print('.', end='')

EPOCHS = 1000

history = model.fit(
normed_train_data, y_train,
epochs=EPOCHS, validation_split = 0.2, verbose=0,
callbacks=[PrintDot()])

```

Evaluation metrics for training data

```

from sklearn.metrics import mean_squared_error, r2_score, mean_absolute_error
from sklearn.metrics import mean_squared_error
from sklearn.metrics import mean_absolute_error
import sklearn.metrics as metrics

#Predict training dataset MAE
y_train_DNN = model.predict(normed_train_data)
score = mean_absolute_error(y_train, y_train_DNN)
print("Train accuracy (MAE) for DNN: {}".format(score))

# R2 metric for training dataset
score = r2_score(y_train, y_train_DNN)
print("Train accuracy (R2) for DNN: {}".format(score))

#RMSE metric for training dataset
score = np.sqrt(metrics.mean_squared_error(y_train, y_train_DNN))

```

```
print("Train accuracy (RMSE) for DNN: {}".format(score))
```

```
# Displaying graph for early stopping
def plot_history(history):
    hist = pd.DataFrame(history.history)
    hist['epoch'] = history.epoch
    plt.figure()
    plt.xlabel('Epoch')
    plt.ylabel('Mean Abs Error')
    plt.plot(hist['epoch'], hist['mean_absolute_error'],
             label='Train Error')
    plt.plot(hist['epoch'], hist['val_mean_absolute_error'],
             label = 'Test Error')
    plt.ylim([0,1])
    plt.legend()
    rc('axes', linewidth=3)
    plt.figure()
    plt.xlabel('Epoch')
    plt.ylabel('Mean Square Error')
    plt.plot(hist['epoch'], hist['mean_squared_error'],
             label='Train Error')
    plt.plot(hist['epoch'], hist['val_mean_squared_error'],
             label = 'Test Error')
    plt.ylim([0,1])
    plt.legend()
    plot_history(history)
plt.show()
```

Making predictions on test dataset for Ks

```
from sklearn.metrics import accuracy_score
from sklearn.metrics import mean_squared_error
from math import sqrt

loss, mae, mse = model.evaluate(normed_test_data, y_test, verbose=0)
RMSE_DNN= sqrt(mse)
print("Testing set Mean Abs Error: {:.2f}".format(mae))
print("Testing set MSE: {:.2f}".format(mse))

print("Testing set RMSE: {:.2f} cm/day".format(RMSE_DNN))
test_predictions = model.predict(normed_test_data).flatten()

#Formatting evaluation metrics to be displayed on the scatter plot
Metric= " MAE = " + str(round(mae, 2)) + " (cm h$^{-1}$)" + "\n" + " R$^2$ = " +
```

```
str(round(score_R2_DNN, 2))+ ", " + " RMSE = " + str(round(RMSE_DNN, 2))+ " (cm h$^{-1}$)"
print("DNN Model Performance: ", Metric)
```

Scatter plot for model

```
# Create Regression Plot for Test and Prediction values
import matplotlib.pyplot as plt
from pylab import *
from scipy.optimize import curve_fit
from sklearn.model_selection import cross_val_predict
from sklearn import linear_model
lr = linear_model.LinearRegression()
predicted = cross_val_predict(lr, test_predictions, y_test, cv=10)
fig, ax = plt.subplots(figsize=(12, 9))
ax.set_title('Deep Neural Network Regression', fontsize=30)
ax.scatter(y_test,predicted,c="gray")
ax.plot([y.min(), y.max()], [y.min(), y.max()], 'k--', lw=5)
ax.set_xlabel('Observed Ks log (cm h$^{-1}$)',fontsize=30)
ax.set_ylabel('Predicted Ks log (cm h$^{-1}$)',fontsize=30)
ax.tick_params(axis="x", direction="out",length=8, width=2)
ax.tick_params(axis="y", direction="out",length=8, width=2)
plt.xlim(-2, 3)
plt.ylim(-2, 3)
plt.tick_params(axis='both', which='major', labelsize=30)
plt.text(-1.5, 2.2,Metric,fontsize=25, bbox=dict(facecolor='none', alpha=0.5))
rc('axes', linewidth=4)

plt.show()
```

GENERAL REFERENCES

- Abadi, M., Barham, P., Chen, J., et al. (2016). *Tensorflow: A system for large-scale machine learning*. Paper presented at the 12th {USENIX} symposium on operating systems design and implementation ({OSDI} 16).
- Abdallah, A. (2019a). Influence of Hydrogel Type and Concentration, and Water Application Rate on some Hydraulic Properties of a Sandy Soil. *Alexandria Science Exchange Journal*, 40(APRIL- JUNE), 349-362. doi:10.21608/asejaiqjsae.2019.36940
- Abdallah, A. M. (2019b). The effect of hydrogel particle size on water retention properties and availability under water stress. *Int. Soil Water Conserv. Res.*, 7(3), 275-285. doi:10.1016/j.iswcr.2019.05.001
- Abedi-Koupai, J., Sohrab, F., & Swarbrick, G. (2008). Evaluation of Hydrogel Application on Soil Water Retention Characteristics. *Journal of Plant Nutrition*, 31(2), 317-331. doi:10.1080/01904160701853928
- Abrisham, E. S., Jafari, M., Tavili, A., et al. (2018). Effects of a super absorbent polymer on soil properties and plant growth for use in land reclamation. *Arid Land Research and Management*, 32(4), 407-420. doi:10.1080/15324982.2018.1506526
- Achieng, K. O. (2019). Modelling of soil moisture retention curve using machine learning techniques: Artificial and deep neural networks vs support vector regression models. *Computers & Geosciences*, 133, 104320. doi:<https://doi.org/10.1016/j.cageo.2019.104320>
- Adedeji, A. A., & Ngadi, M. (2011). Porosity determination of deep-fat-fried coatings using pycnometer (Fried batter porosity determination by pycnometer). *International Journal of Food Science & Technology*, 46(6), 1266-1275. doi:10.1111/j.1365-2621.2011.02631.x
- Agaba, H., Baguma Orikiriza, L. J., Osoto Esegu, J. F., et al. (2010). Effects of hydrogel amendment to different soils on plant available water and survival of trees under drought conditions. *Clean-Soil, Air, Water*, 38(4), 328-335.
- Agaba, H., Orikiriza, L., Obua, J., et al. (2011). Hydrogel amendment to sandy soil reduces irrigation frequency and improves the biomass of *Agrostis stolonifera*. *Agricultural Sciences*, 2(4), 544-550.
- Agyare, W. A., Park, S. J., & Vlek, P. L. G. (2007). Artificial Neural Network Estimation of Saturated Hydraulic Conductivity. *Vadose Zone Journal*, 6(2), 423-431. doi:10.2136/vzj2006.0131
- Ahmed, E. M. (2015). Hydrogel: Preparation, characterization, and applications: A review. *J. Adv. Res.*, 6(2), 105-121. doi:10.1016/j.jare.2013.07.006
- Akhtar, M. F., Hanif, M., & Ranjha, N. M. (2016). Methods of synthesis of hydrogels . A review. *Saudi Pharmaceutical Journal*, 24(5), 554-559. doi:10.1016/j.jsps.2015.03.022
- Akhter, J., Mahmood, K., Malik, K. A., et al. (2004). Effects of hydrogel amendment on water storage of sandy loam and loam soils and seedling growth of barley, wheat and chickpea. *Plant Soil and Environment*, 50(10), 463-469.
- Al-Darby, A. M. (1996). The hydraulic properties of a sandy soil treated with gel-forming soil conditioner. *Soil Technology*, 9(1-2), 15-28. doi:10.1016/0933-3630(95)00030-5

- Al-Dosary, N. M. N., Al-Hamed, S. A., & Aboukarima, A. M. (2019). K-NEAREST NEIGHBORS METHOD FOR PREDICTION OF FUEL CONSUMPTION IN TRACTOR-CHISEL PLOW SYSTEMS. *Engenharia Agrícola*, 39(6), 729-736. doi:<http://dx.doi.org/10.1590/1809-4430-Eng.Agric.v39n6p729-736/2019>
- Al-Humaid, A. I., & Moftah, A. E. (2007). Effects of Hydrophilic Polymer on the Survival of Buttonwood Seedlings Grown Under Drought Stress. *Journal of Plant Nutrition*, 30(1), 53-66. doi:10.1080/01904160601054973
- Alkhasha, A., & Al-Omran, A. (2020). Evaluating the Effects of Biochar and SAP Polymer on Soil Physical Quality Indices. *Communications in Soil Science and Plant Analysis*, 1-13.
- Alkhasha, A., Al-Omran, A., & Aly, A. (2018). Effects of Biochar and Synthetic Polymer on the Hydro-Physical Properties of Sandy Soils. *Sustainability*, 10(12), 4642. doi:10.3390/su10124642
- Allen, M. P. (1997). *The problem of multicollinearity*. New York, N. Y: Plenum Press.
- Altman, N. S. (1992). An Introduction to Kernel and Nearest-Neighbor Nonparametric Regression. *The American Statistician*, 46(3), 175-185. doi:10.1080/00031305.1992.10475879
- Amine, K. M., Champagne, C. P., Salmieri, S., et al. (2014). Effect of palmitoylated alginate microencapsulation on viability of Bifidobacterium longum during freeze-drying. *LWT - Food Science and Technology*, 56(1), 111-117. doi:10.1016/j.lwt.2013.11.003
- Andry, H., Yamamoto, T., Irie, T., et al. (2009). Water retention, hydraulic conductivity of hydrophilic polymers in sandy soil as affected by temperature and water quality. *Journal of Hydrology*, 373(1-2), 177-183. doi:10.1016/j.jhydrol.2009.04.020
- Araya, S. N. (2019). *Soil Structure and Land Surface Controls on Soil Hydraulic Properties and Processes: Applications of Machine Learning, Unmanned Aircraft Systems, and Observations from Long-Term Conservation Agriculture Management*. (PhD), UC Merced,
- Araya, S. N., & Ghezzehei, T. A. (2019). Using machine learning for prediction of saturated hydraulic conductivity and its sensitivity to soil structural perturbations. *Water Resources Research*, 55(7), 5715-5737. doi:<https://doi.org/10.1029/2018WR024357>
- Arias, N., Virto, I., Enrique, A., et al. (2019). Effect of Stoniness on the Hydraulic Properties of a Soil from an Evaporation Experiment Using the Wind and Inverse Estimation Methods. *Water*, 11(3), 440. doi:10.3390/w11030440
- Arora, N., Khare, E., Narayan, R., et al. (2008). Sawdust as a superior carrier for production of multipurpose bioinoculant using plant growth promoting rhizobial and pseudomonad strains and their impact on productivity of Trifolium repense. *Current Science*, 90-94.
- Arriola, N. D. A., de Medeiros, P. M., Prudencio, E. S., et al. (2016). Encapsulation of aqueous leaf extract of Stevia rebaudiana Bertoni with sodium alginate and its impact on phenolic content. *Food Bioscience*, 13, 32-40.
- Arshad, R. R., Sayyad, G., Mosaddeghi, M., et al. (2013). Predicting saturated hydraulic conductivity by artificial intelligence and regression models. *ISRN Soil Science*, 2013.

- Awad, M., & Khanna, R. (2015). Support Vector Regression. In *Efficient learning machines* (pp. 67-80). Berkeley, CA: Apress.
- Bai, C., Zhang, S., Huang, L., et al. (2015a). Starch-based hydrogel loading with carbendazim for controlled-release and water absorption. *Carbohydrate polymers*, *125*, 376-383.
- Bai, M., Wilske, B., Buegger, F., et al. (2015b). Relevance of nonfunctional linear polyacrylic acid for the biodegradation of superabsorbent polymer in soils. *Environ Sci Pollut Res*, *22*(7), 5444-5452. doi:10.1007/s11356-014-3772-0
- Bai, W., Zhang, H., Liu, B., et al. (2010). Effects of super-absorbent polymers on the physical and chemical properties of soil following different wetting and drying cycles. *Soil Use and Management*, *26*(3), 253-260. doi:10.1111/j.1475-2743.2010.00271.x
- Baki, M., & Abedi-Koupai, J. (2018). Preparation and characterization of a superabsorbent slow-release fertilizer with sodium alginate and biochar. *Journal of Applied Polymer Science*, *135*(10), 45966. doi:10.1002/app.45966
- Banedjschafie, S., & Durner, W. (2015). Water retention properties of a sandy soil with superabsorbent polymers as affected by aging and water quality. *Journal of Plant Nutrition and Soil Science*, *178*(5), 798-806. doi:10.1002/jpln.201500128
- Bao, Y., Ma, J., & Li, N. (2011). Synthesis and swelling behaviors of sodium carboxymethyl cellulose-g-poly (AA-co-AM-co-AMPS)/MMT superabsorbent hydrogel. *Carbohydrate Polymers*, *84*(1), 76-82.
- Baran, A., Zaleski, T., Kulikowski, E., et al. (2015). Hydrophysical and Biological Properties of Sandy Substrata Enriched with Hydrogel. *Polish Journal of Environmental Studies*, *24*(6).
- Bashan, Y. (1986). Alginate beads as synthetic inoculant carriers for slow release of bacteria that affect plant growth. *Applied and environmental microbiology*, *51*(5), 1089-1098.
- Bashan, Y. (1998). Inoculants of plant growth-promoting bacteria for use in agriculture. *Biotechnology Advances*, *16*(4), 729-770. doi:10.1016/s0734-9750(98)00003-2
- Bashan, Y., De-Bashan, L. E., Prabhu, S. R., et al. (2014). Advances in plant growth-promoting bacterial inoculant technology: formulations and practical perspectives (1998–2013). *Plant and Soil*, *378*(1-2), 1-33. doi:10.1007/s11104-013-1956-x
- Behera, S., & Mahanwar, P. A. (2020). Superabsorbent polymers in agriculture and other applications: a review. *Polymer-Plastics Technology and Materials*, *59*(4), 341-356.
- Berliner, P., Barak, P., & Chen, Y. (1980). An improved procedure for measuring water retention curves at low suction by the hanging-water-column method. *Canadian Journal of Soil Science*, *60*(3), 591-594.
- Bhardwaj, A. K., Shainberg, I., Goldstein, D., et al. (2007). Water Retention and Hydraulic Conductivity of Cross-Linked Polyacrylamides in Sandy Soils. *Soil Science Society of America Journal*, *71*(2), 406-412. doi:10.2136/sssaj2006.0138
- Bisaria, V. S., & Ghose, T. K. (1981). Biodegradation of cellulosic materials: Substrates, microorganisms, enzymes and products. *Enzyme and Microbial Technology*, *3*(2), 90-104. doi:10.1016/0141-0229(81)90066-1
- Blanco-Canqui, H. (2017). Biochar and soil physical properties. *Soil Science Society of America Journal*, *81*(4), 687-711.

- Blanco, A., González, G., Casanova, E., et al. (2013). Mathematical Modeling of Hydrogels Swelling Based on the Finite Element Method. *04(08)*, 161-170. doi:10.4236/am.2013.48a022
- Borboudakis, G., & Tsamardinos, I. (2019). Forward-backward selection with early dropping. *Journal of Machine Learning Research*, *20(1)*, 1-39. doi:<http://jmlr.org/papers/v20/17-334.html>
- Box, G. E., & Cox, D. R. (1964). An analysis of transformations. *Journal of the Royal Statistical Society: Series B*, *26(2)*, 211-243.
- Brauns, F. E. (1939). Native Lignin I. Its Isolation and Methylation. *Journal of the American Chemical Society*, *61(8)*, 2120-2127. doi:10.1021/ja01877a043
- Breiman, L. (2001). Random forests. *Machine learning*, *45(1)*, 5-32.
- Buck, J. D., & Cleverdon, R. C. (1960). The spread plate as a method for the enumeration of marine bacteria 1, 2. *Limnology and Oceanography*, *5(1)*, 78-80.
- Cai, Y., Zheng, W., Zhang, X., et al. (2019). Research on soil moisture prediction model based on deep learning. *PLOS ONE*, *14(4)*, e0214508. doi:10.1371/journal.pone.0214508
- Cameron, M. D., Post, Z. D., Stahl, J. D., et al. (2000). Cellobiose dehydrogenase-dependent biodegradation of polyacrylate polymers by *Phanerochaete chrysosporium*. *Environ Sci Pollut Res*, *7(3)*, 130.
- Cannazza, G., Cataldo, A., De Benedetto, E., et al. (2014). Experimental Assessment of the Use of a Novel Superabsorbent polymer (SAP) for the Optimization of Water Consumption in Agricultural Irrigation Process. *6(7)*, 2056-2069. doi:10.3390/w6072056
- Carrier, O., Shahidzadeh-Bonn, N., Zargar, R., et al. (2016). Evaporation of water: evaporation rate and collective effects. *Journal of Fluid Mechanics*, *798*, 774-786.
- Caulfield, M. J., Qiao, G. G., & Solomon, D. H. (2002). Some aspects of the properties and degradation of polyacrylamides. *Chemical reviews*, *102(9)*, 3067-3084.
- Chan, E.-S., Wong, S.-L., Lee, P.-P., et al. (2011). Effects of starch filler on the physical properties of lyophilized calcium–alginate beads and the viability of encapsulated cells. *Carbohydrate Polymers*, *83(1)*, 225-232.
- Chao, W.-L., & Alexander, M. (1984). Mineral soils as carriers for *Rhizobium* inoculants. *Applied and Environmental Microbiology*, *47(1)*, 94-97.
- Chen, J., Fan, X., Zhang, L., et al. (2020). Research Progress in Lignin-Based Slow/Controlled Release Fertilizer. *ChemSusChem*. doi:10.1002/cssc.202000455
- Chen, Y. W., Binti Hassan, S. H., Yahya, M., et al. (2019). Novel superabsorbent cellulose-based hydrogels: present status, synthesis, characterization, and application prospects. *Cellulose-Based Superabsorbent Hydrogels*, 155-195.
- Cheng, B., Pei, B., Wang, Z., et al. (2017). Advances in chitosan-based superabsorbent hydrogels. *RSC Advances*, *7(67)*, 42036-42046. doi:10.1039/c7ra07104c
- Chio, C., Sain, M., Qin, W. J. R., et al. (2019). Lignin utilization: a review of lignin depolymerization from various aspects. *107*, 232-249.
- Chirani, N., Gritsch, L., Motta, F. L., et al. (2015). History and applications of hydrogels. *Journal of biomedical sciences*, *4(2)*.
- Ciolacu, D., Oprea, A. M., Anghel, N., et al. (2012). New cellulose–lignin hydrogels and their application in controlled release of polyphenols. *Materials Science and Engineering: C*, *32(3)*, 452-463.

- Cornelis, W. M., Ronsyn, J., Van Meirvenne, M., et al. (2001). Evaluation of pedotransfer functions for predicting the soil moisture retention curve. *Soil Science Society of America Journal*, 65(3), 638-648. doi:<https://doi.org/10.2136/sssaj2001.653638x>
- Dane, J. H., Topp, G. C., Campbell, G. S., et al. (2002). *Methods of soil analysis. Part 4, Physical methods*: Madison, Wisconsin : Soil Science Society of America.
- Deaker, R., Roughley, R. J., & Kennedy, I. R. (2007). Desiccation tolerance of rhizobia when protected by synthetic polymers. *Soil Biology and Biochemistry*, 39(2), 573-580. doi:10.1016/j.soilbio.2006.09.005
- Decagon Devices, I. (1998-2007). WP4 Dewpoint Potential Meter Operator's Manual Version 5.
- Dehkordi, K. D. (2018). Effect of superabsorbent polymer on soil and plants on steep surfaces. *Water and Environment Journal*, 32(2), 158-163. doi:10.1111/wej.12309
- Demitri, C., Scalera, F., Madaghiele, M., et al. (2013). Potential of cellulose-based superabsorbent hydrogels as water reservoir in agriculture. *International Journal of Polymer Science*, 2013.
- Denardin, N., & Freire, J. (2000). Assessment of polymers for the formulation of legume inoculants. *World Journal of Microbiology and Biotechnology*, 16(3), 215-217.
- Dinu, M. V., & Dragan, E. S. (2018). Macroporous Hydrogels: Preparation, Properties, and Applications. In *Hydrogels* (pp. 51-85): Springer.
- Dommergues, Y., Diem, H. G., & Divies, C. (1979). Polyacrylamide-entrapped Rhizobium as an inoculant for legumes. *Appl. Environ. Microbiol.*, 37(4), 779-781.
- Drucker, H., Burges, C. J., Kaufman, L., et al. (1997). *Support vector regression machines*. Paper presented at the Advances in neural information processing systems, Cambridge, MA, USA.
- Durner, W., & Flüher, H. (2006). Soil hydraulic properties. *Encyclopedia of hydrological sciences*.
- Durpekova, S., Filatova, K., Cisar, J., et al. (2020). A Novel Hydrogel Based on Renewable Materials for Agricultural Application. *International Journal of Polymer Science*, 2020, 1-13. doi:10.1155/2020/8363418
- Eijkelkamp. (2017). Laboratory Permeameters User Manual. In.
- Ekielski, A., & Mishra, P. K. (2020). Lignin for Bioeconomy: The Present and Future Role of Technical Lignin. *International Journal of Molecular Sciences*, 22(1), 63. doi:10.3390/ijms22010063
- El-Tohamy, W. A., El-Abagy, H. M., Ahmed, E. M., et al. (2014). Application of super absorbent hydrogel poly (acrylate/acrylic acid) for water conservation in sandy soil. *Transaction of the Egyptian society of chemical engineering*, 40(2), 1-8.
- Elbisy, M. S. (2015). Support vector machine and regression analysis to predict the field hydraulic conductivity of sandy soil. *KSCE Journal of Civil Engineering*, 19(7), 2307-2316. doi:<https://doi.org/10.1007/s12205-015-0210-x>
- Elith, J., Leathwick, J. R., & Hastie, T. (2008). A working guide to boosted regression trees. *Journal of Animal Ecology*, 77(4), 802-813. doi:10.1111/j.1365-2656.2008.01390.x
- Estabragh, A. R., Parsaei, B., & Javadi, A. A. (2015). Laboratory investigation of the effect of cyclic wetting and drying on the behaviour of an expansive soil. *Soils and Foundations*, 55(2), 304-314. doi:10.1016/j.sandf.2015.02.007

- Estrada-Villegas, G., Morselli, G., Oliveira, M., et al. (2019). PVGA/Alginate-AgNPs hydrogel as absorbent biomaterial and its soil biodegradation behavior. *Polymer Bulletin*, 1-20.
- Feng, Q., Li, J., Cheng, H., et al. (2014). Synthesis and Characterization of Porous Hydrogel Based on Lignin and Polyacrylamide. *BioResources*, 9(3). doi:10.15376/biores.9.3.4369-4381
- Florida Soil Characterization Database, D. (2009). Florida Soil Characterization Data Retrieval System.
- Franzmeier, D., Hosteter, W., Roeske, R., et al. (2001). Drainage and wet soil management. *University of Purdue, Indiana*.
- Freund, Y., & Schapire, R. E. (1996). *Experiments with a new boosting algorithm*. Paper presented at the icml.
- Friedman, J. H. (2002). Stochastic gradient boosting. *Computational Statistics & Data Analysis*, 38(4), 367-378. doi:10.1016/s0167-9473(01)00065-2
- Galanakis, C. M. (2020). *The interaction of food industry and environment*: Academic Press.
- Gallage, C., Kodikara, J., & Uchimura, T. (2013). Laboratory measurement of hydraulic conductivity functions of two unsaturated sandy soils during drying and wetting processes. *Soils and Foundations*, 53(3), 417-430. doi:10.1016/j.sandf.2013.04.004
- Gargiulo, O., & Morgan, K. T. (2015). Procedures to Simulate Missing Soil Parameters in the Florida Soils Characteristics Database. *Soil Science Society of America Journal*, 79(1), 165-174. doi:10.2136/sssaj2014.05.0194
- Gee, G. W., Ward, A. L., Zhang, Z. F., et al. (2002). The Influence of Hydraulic Nonequilibrium on Pressure Plate Data. *Vadose Zone Journal*, 1(1), 172-178. doi:10.2136/vzj2002.1720
- Geesing, D., & Schmidhalter, U. (2006). Influence of sodium polyacrylate on the water-holding capacity of three different soils and effects on growth of wheat. *Soil Use and Management*, 20(2), 207-209. doi:10.1111/j.1475-2743.2004.tb00359.x
- Géron, A. (2017). *Hands-On Machine Learning with Scikit-Learn and TensorFlow: Concepts, Tools, and Techniques to build intelligent systems* (N. Tache Ed. 1st ed.). Sebastopol, CA , USA: O'Reilly Media, Inc.
- Ghobashy, M. M. (2018). Superabsorbent. In: InTech.
- Ghobashy, M. M. (2020). The application of natural polymer-based hydrogels for agriculture. In *Hydrogels Based on Natural Polymers* (pp. 329-356): Elsevier.
- Goheen, S., & Wool, R. J. J. o. a. p. s. (1991). Degradation of polyethylene–starch blends in soil. 42(10), 2691-2701.
- Goss, M., & Ehlers, W. (2003). *Water Dynamics in Plant Production*: CABI.
- Grima, S., Bellon-Maurel, V., Feuilloley, P., et al. (2000). Aerobic Biodegradation of Polymers in Solid-State Conditions: A Review of Environmental and Physicochemical Parameter Settings in Laboratory Simulations. *Journal of Polymers and the Environment*, 8(4), 183-195. doi:10.1023/a:1015297727244
- Guilherme, M. R., Aouada, F. A., Fajardo, A. R., et al. (2015). Superabsorbent hydrogels based on polysaccharides for application in agriculture as soil conditioner and nutrient carrier: A review. *European Polymer Journal*, 72, 365-385.
- Gulli, A., & Pal, S. (2017). *Deep learning with Keras* (D. Pawar Ed.). Birmingham, UK: Packt Publishing Ltd.

- Guo, J., Shi, W., Wen, L., et al. (2019). Effects of a super-absorbent polymer derived from poly- γ -glutamic acid on water infiltration, field water capacity, soil evaporation, and soil water-stable aggregates. *Archives of Agronomy and Soil Science*, 1-12.
- Gupta, S. C., & Larson, W. E. (1979). Estimating soil water retention characteristics from particle size distribution, organic matter percent, and bulk density. *Water Resources Research*, 15(6), 1633-1635. doi:10.1029/wr015i006p01633
- Haghverdi, A., Leib, B. G., & Cornelis, W. M. (2015). A simple nearest-neighbor technique to predict the soil water retention curve. *Transactions of the ASABE*, 58(3), 697-705. doi:<https://doi.org/10.13031/trans.58.10990>
- Haines, W. B. (1923). The volume-changes associated with variations of water content in soil. *The Journal of agricultural science*, 13(3), 296-310.
- Hamid, S. H. (2000). *Handbook of polymer degradation*: CRC Press.
- Han, Y., Yu, X., Yang, P., et al. (2013). Dynamic study on water diffusivity of soil with super-absorbent polymer application. *Environmental earth sciences*, 69(1), 289-296.
- Hasan, A. M., & Abdel-Raouf, M. E.-S. (2019). Cellulose-based superabsorbent hydrogels. *Cellulose-Based Superabsorbent Hydrogels*. Springer International Publishing, Cham, Switzerland, 245-267.
- Hayat, R., & Ali, S. (2004). Water absorption by synthetic polymer (Aquasorb) and its effect on soil properties and tomato yield. *Int. J. Agri. Biol*, 6(6), 998-1002.
- Ho, T. K. (1995). *Random decision forests*. Paper presented at the Proceedings of 3rd international conference on document analysis and recognition, Montreal , QC, Canada.
- Horwath, W. (2007). Carbon cycling and formation of soil organic matter. In *Soil microbiology, ecology and biochemistry* (pp. 303-339): Elsevier.
- Hu, M., Zheng, G., Zhao, D., et al. (2020). Characterization of the structure and diffusion behavior of calcium alginate gel beads. *Journal of Applied Polymer Science*, 137(31), 48923. doi:10.1002/app.48923
- Hu, Y., Guo, N., Hill, R. L., et al. (2019). Effects of the combined application of biomaterial amendments and polyacrylamide on soil water and maize growth under deficit irrigation. *Canadian Journal of Soil Science*, 99(2), 182-194. doi:10.1139/cjss-2018-0091
- Hussien, R. A., Donia, A. M., Atia, A. A., et al. (2012). Studying some hydro-physical properties of two soils amended with kaolinite-modified cross-linked polyacrylamides. *Catena*, 92, 172-178.
- Hüttermann, A., Orikiriza, L. J. B., & Agaba, H. (2009). Application of Superabsorbent Polymers for Improving the Ecological Chemistry of Degraded or Polluted Lands. *CLEAN - Soil, Air, Water*, 37(7), 517-526. doi:10.1002/clen.200900048
- Idso, S. B., Reginato, R. J., Jackson, R. D., et al. (1974). The Three Stages of Drying of a Field Soil. *Soil Science Society of America Journal*, 38(5), 831-837. doi:10.2136/sssaj1974.03615995003800050037x
- Isik, B., & Kıs, M. (2004). Preparation and determination of swelling behavior of poly(acrylamide-co-acrylic acid) hydrogels in water. *Journal of Applied Polymer Science*, 94(4), 1526-1531. doi:10.1002/app.21074
- Islam, M. R., Mao, S., Alam, A. M. S., et al. (2011). A Lysimeter Study for Leaching Losses, Sustainable Fertilization, and Growth Responses of Corn (*Zea mays* L.)

- Following Soil Amendment with a Water-Saving Superabsorbent Polymer. *Applied Engineering in Agriculture*, 27(5), 757-764. doi:10.13031/2013.39575
- Ismail, H., Irani, M., & Ahmad, Z. (2013). Starch-based hydrogels: present status and applications. *International Journal of Polymeric Materials and Polymeric Biomaterials*, 62(7), 411-420.
- Jankowski, T., Zielinska, M., & Wysakowska, A. (1997). Encapsulation of lactic acid bacteria with alginate/starch capsules. *Biotechnology Techniques*, 11(1), 31-34. doi:10.1007/bf02764447
- Jarvis, N. J., & Messing, I. (1995). Near-Saturated Hydraulic Conductivity in Soils of Contrasting Texture Measured by Tension Infiltrimeters. *Soil Science Society of America Journal*, 59(1), 27-34. doi:10.2136/sssaj1995.03615995005900010004x
- Jarvis, N. J., Zavattaro, L., Rajkai, K., et al. (2002). Indirect estimation of near-saturated hydraulic conductivity from readily available soil information. *Geoderma*, 108(1-2), 1-17. doi:10.1016/s0016-7061(01)00154-9
- Jiang, P., Sheng, X., Yu, S., et al. (2018). Preparation and characterization of thermo-sensitive gel with phenolated alkali lignin. *Scientific Reports*, 8(1). doi:10.1038/s41598-018-32672-z
- John, R. P., Tyagi, R., Brar, S., et al. (2011). Bio-encapsulation of microbial cells for targeted agricultural delivery. *Critical reviews in biotechnology*, 31(3), 211-226.
- Jolliffe, I. T. (2002). *Principal components in regression analysis* (2nd ed.). New York, NY: Springer-Verlag.
- Jones Jr, J. B. (1999). *Soil analysis handbook of reference methods*: CRC Press.
- Jorda, H., Bechtold, M., Jarvis, N., et al. (2015). Using boosted regression trees to explore key factors controlling saturated and near-saturated hydraulic conductivity. *European Journal of Soil Science*, 66(4), 744-756. doi:10.1111/ejss.12249
- Jung, G., Mugnier, J., Diem, H. G., et al. (1982). Polymer-entrapped rhizobium as an inoculant for legumes. *Plant and Soil*, 65(2), 219-231. doi:10.1007/bf02374652
- Kai, D., Tan, M. J., Chee, P. L., et al. (2016). Towards lignin-based functional materials in a sustainable world. *Green Chemistry*, 18(5), 1175-1200.
- Kaingo, J., Tumbo, S. D., Kihupi, N. I., et al. (2018). Prediction of Soil Moisture-Holding Capacity with Support Vector Machines in Dry Subhumid Tropics. *Applied and Environmental Soil Science*, 2018, 9263296. doi:10.1155/2018/9263296
- Kalinoski, R. M., Li, W., Mobley, J. K., et al. (2020). Antimicrobial Properties of Corn Stover Lignin Fractions Derived from Catalytic Transfer Hydrogenolysis in Supercritical Ethanol with a Ru/C Catalyst. *ACS Sustainable Chemistry & Engineering*. doi:10.1021/acssuschemeng.0c05812
- Kalinoski, R. M., & Shi, J. (2019). Hydrogels derived from lignocellulosic compounds: Evaluation of the compositional, structural, mechanical and antimicrobial properties. *Industrial crops and products*, 128, 323-330.
- Kashani, M. H., Ghorbani, M. A., Shahabi, M., et al. (2020). Multiple AI model integration strategy—application to saturated hydraulic conductivity prediction from easily available soil properties. *Soil & Tillage Research* 196, 104449. doi:<https://doi.org/10.1016/j.still.2019.104449>
- Kashkuli, H. A., & Zohrabi, N. (2013). The Effect of superabsorbent polymers on the water holding capacity and water potential of Karkhe Noor sandy soils. *International Journal of Scientific Research in Knowledge*, 1(9), 317.

- Kirk, T. K., & Farrell, R. L. (1987). Enzymatic "combustion": the microbial degradation of lignin. *Annual Reviews in Microbiology*, 41(1), 465-501.
- Kirkham, M. B. (2014). *Principles of soil and plant water relations*: Academic Press.
- Klute, A., & Dirksen, C. (1986). Hydraulic conductivity and diffusivity: Laboratory methods. *Methods of Soil Analysis: Part 1 Physical and Mineralogical Methods*, 5, 687-734. doi:<https://doi.org/10.2136/sssabookser5.1.2ed.c28>
- Kluyver, T., Ragan-Kelley, B., Fernando Perez, G., et al. (2016). Jupyter Notebooks – a publishing format for reproducible computational workflows. In (pp. pp. 87–90): Positioning and Power in Academic Publishing: Players, Agents and Agendas.
- Kotlar, A. M., Iversen, B. V., & Jong Van Lier, Q. (2019). Evaluation of Parametric and Nonparametric Machine-Learning Techniques for Prediction of Saturated and Near-Saturated Hydraulic Conductivity. *Vadose Zone Journal*, 18(1), 1-13. doi:10.2136/vzj2018.07.0141
- Koupai, J. A., Eslamian, S. S., & Kazemi, J. A. (2008). Enhancing the available water content in unsaturated soil zone using hydrogel, to improve plant growth indices. *Ecohydrology & Hydrobiology*, 8(1), 67-75.
- Kuhn, M., & Johnson, K. (2013). *Applied predictive modeling* (Vol. 26). New York Springer.
- Lal, R., & Shukla, M. K. (2004). *Principles of soil physics*: CRC Press.
- Lamorski, K., Pachepsky, Y., Sławiński, C., et al. (2008). Using support vector machines to develop pedotransfer functions for water retention of soils in Poland. *Soil Science Society of America Journal*, 72(5), 1243-1247. doi:<https://doi.org/10.2136/sssaj2007.0280N>
- Lamorski, K., Sławiński, C., Moreno, F., et al. (2014). Modelling soil water retention using support vector machines with genetic algorithm optimisation. *The Scientific World Journal*, 2014. doi:<https://doi.org/10.1155/2014/740521>
- Leciejewski, P. (2009). The effect of hydrogel additives on the water retention curve of sandy soil from forest nursery in Julinek. *Journal of water and land development*, 13, 239-247.
- Leij, F. J. (1996). *The UNSODA unsaturated soil hydraulic database: user's manual* (Vol. 96). Cincinnati, Ohio: National Risk Management Research Laboratory Office of Research and Development, U. S. Environmental Protection Agency.
- Lejcuś, K., Śpitalniak, M., & Dąbrowska, J. (2018). Swelling Behaviour of Superabsorbent Polymers for Soil Amendment under Different Loads. *Polymers (Basel)*, 10(3). doi:10.3390/polym10030271
- Lentz, R. D. (2007). Inhibiting Water Infiltration into Soils with Cross-linked Polyacrylamide: Seepage Reduction for Irrigated Agriculture. *Soil Science Society of America Journal*, 71(4), 1352-1362. doi:10.2136/sssaj2005.0380
- Lentz, R. D. (2020). Long-term water retention increases in degraded soils amended with cross-linked polyacrylamide. *Agronomy Journal*.
- Lentz, R. D., & Kincaid, D. C. (2008). Polyacrylamide Treatments for Reducing Seepage in Soil-Lined Reservoirs: A Field Evaluation. *Transactions of the ASABE*, 51(2), 535-544. doi:10.13031/2013.24395
- Levy, G., Smith, HJC*, Agassi, M. J. S. A. J. o. P., & Soil. (1988). Water temperature effect on hydraulic conductivity and infiltration rate of soils. 6(4), 240-244.

- Li, A., Wang, A., & Chen, J. (2004). Studies on poly(acrylic acid)/attapulgit superabsorbent composites. II. Swelling behaviors of superabsorbent composites in saline solutions and hydrophilic solvent-water mixtures. *Journal of Applied Polymer Science*, 94(5), 1869-1876. doi:10.1002/app.20850
- Li, X., & Pan, X. (2010). Hydrogels based on hemicellulose and lignin from lignocellulose biorefinery: a mini-review. *Journal of Biobased Materials and Bioenergy*, 4(4), 289-297.
- Liakos, K. G., Busato, P., Moshou, D., et al. (2018). Machine learning in agriculture: A review. *Sensors*, 18(8), 2674. doi:<https://doi.org/10.3390/s18082674>
- Liang, X., Qu, B., Li, J., et al. (2015). Preparation of cellulose-based conductive hydrogels with ionic liquid. *Reactive and Functional Polymers*, 86, 1-6. doi:10.1016/j.reactfunctpolym.2014.11.002
- Liao, R., Wu, W., Ren, S., et al. (2016). Effects of Superabsorbent Polymers on the Hydraulic Parameters and Water Retention Properties of Soil. *Journal of Nanomaterials*, 2016, 1-11. doi:10.1155/2016/5403976
- Liao, R., Yang, P., Wang, Z., et al. (2018). Development of a Soil Water Movement Model for the Superabsorbent Polymer Application. *Soil Science Society of America Journal*, 82(2), 436. doi:10.2136/sssaj2017.05.0164
- Liaw, A., & Wiener, M. (2002). Classification and regression by randomForest. *R news*, 2(3), 18-22.
- Lotfipour, F., Mirzaeei, S., & Maghsoodi, M. (2012). Evaluation of the effect of CaCl₂ and alginate concentrations and hardening time on the characteristics of Lactobacillus acidophilus loaded alginate beads using response surface analysis. *Advanced pharmaceutical bulletin*, 2(1), 71.
- Louf, J.-F., Lu, N. B., O'Connell, M. G., et al. (2021). Under pressure: Hydrogel swelling in a granular medium. *Science Advances*, 7(7), eabd2711. doi:10.1126/sciadv.abd2711
- Lu, N. (2016). Generalized Soil Water Retention Equation for Adsorption and Capillarity. *Journal of Geotechnical and Geoenvironmental Engineering*, 142(10), 04016051. doi:10.1061/(asce)gt.1943-5606.0001524
- Lu, N., & Likos, W. J. (2004). *Unsaturated soil mechanics*: Wiley.
- Lucas, N., Bienaime, C., Belloy, C., et al. (2008). Polymer biodegradation: Mechanisms and estimation techniques – A review. *Chemosphere*, 73(4), 429-442. doi:10.1016/j.chemosphere.2008.06.064
- Ma, J., Li, X., & Bao, Y. (2015). Advances in cellulose-based superabsorbent hydrogels. *RSC Advances*, 5(73), 59745-59757. doi:10.1039/c5ra08522e
- Majeed, Z., Mansor, N., Ajab, Z., et al. (2017). Lignin macromolecule's implication in slowing the biodegradability of urea-crosslinked starch films applied as slow-release fertilizer. *69(11-12)*, 1600362.
- Majeed, Z., Mansor, N., Man, Z., et al. (2016). Lignin reinforcement of urea-crosslinked starch films for reduction of starch biodegradability to improve slow nitrogen release properties under natural aerobic soil condition. *e-Polymers*, 16(2), 159-170. doi:10.1515/epoly-2015-0231
- Majeed, Z., Ramli, N. K., Mansor, N., et al. (2015). A comprehensive review on biodegradable polymers and their blends used in controlled-release fertilizer processes. *Reviews in Chemical Engineering*, 31(1), 69-95.

- Malusá, E., Sas-Paszt, L., & Ciesielska, J. (2012). Technologies for Beneficial Microorganisms Inocula Used as Biofertilizers. *The Scientific World Journal*, 2012, 1-12. doi:10.1100/2012/491206
- Mandal, U. K., Sharma, K. L., Venkanna, K., et al. (2015). Evaluating Hydrogel Application on Soil Water Availability and Crop Productivity in Semiarid Tropical Red Soil. *Indian Journal of Dryland Agricultural Research and Development*, 30(2), 1. doi:10.5958/2231-6701.2015.00018.4
- Martin, J. P., Haider, K., & Kassim, G. (1980). Biodegradation and Stabilization after 2 Years of Specific Crop, Lignin, and Polysaccharide Carbons in Soils. *Soil Science Society of America Journal*, 44(6), 1250-1255. doi:10.2136/sssaj1980.03615995004400060024x
- Martins, S. C. S., Martins, C. M., Fiúza, L. M. C. G., et al. (2013). Immobilization of microbial cells: A promising tool for treatment of toxic pollutants in industrial wastewater. *12(28)*.
- Masaro, L., & Zhu, X. J. P. i. p. s. (1999). Physical models of diffusion for polymer solutions, gels and solids. *24(5)*, 731-775.
- Mašková, H., & Kunc, F. J. F. m. (1988). Microbial decomposition of carboxymethyl cellulose continuously added to the soil. *33(6)*, 474.
- Mazloom, N., Khorassani, R., Zohuri, G. H., et al. (2019). Development and Characterization of Lignin-Based Hydrogel for Use in Agricultural Soils: Preliminary Evidence. *CLEAN – Soil, Air, Water*, 1900101. doi:10.1002/clen.201900101
- Meng, Y., Liu, X., Li, C., et al. (2019a). Super-swelling lignin-based biopolymer hydrogels for soil water retention from paper industry waste. *International Journal of Biological Macromolecules*, 135, 815-820. doi:10.1016/j.ijbiomac.2019.05.195
- Meng, Y., Lu, J., Cheng, Y., et al. (2019b). Lignin-based hydrogels: A review of preparation, properties, and application. *International journal of biological macromolecules*.
- Mikkelsen, R. L. (1994). Using hydrophilic polymers to control nutrient release. *Fertilizer research*, 38(1), 53-59.
- Miller, V. S., & Naeth, M. A. (2019). Hydrogel and Organic Amendments to Increase Water Retention in Anthroposols for Land Reclamation. *Applied and Environmental Soil Science*, 2019, 1-11. doi:10.1155/2019/4768091
- Miller, W., & Miller, D. (1987). A micro-pipette method for soil mechanical analysis. *Communications in soil science and plant analysis*, 18(1), 1-15.
- Min, S., Lee, B., & Yoon, S. (2016). Deep learning in bioinformatics. *Briefings in Bioinformatics*, bbw068. doi:10.1093/bib/bbw068
- Misiewicz, J., Głogowski, A., Lejcuś, K., et al. (2020). The Characteristics of Swelling Pressure for Superabsorbent Polymer and Soil Mixtures. *Materials*, 13(22), 5071. doi:10.3390/ma13225071
- Misiewicz, J., Lejcuś, K., Dąbrowska, J., et al. (2019). The Characteristics of Absorbency Under Load (AUL) for Superabsorbent and Soil Mixtures. *Scientific Reports*, 9(1). doi:10.1038/s41598-019-54744-4
- Mohawesh, O., & Durner, W. (2019). Effects of Bentonite, Hydrogel and Biochar Amendments on Soil Hydraulic Properties from Saturation to Oven Dryness. *Pedosphere*, 29(5), 598-607.

- Molnar, C., König, G., Herbinger, J., et al. (2020). Pitfalls to avoid when interpreting machine learning models. *arXiv preprint arXiv:04131*.
- Monteith, J. L. (1965). *Evaporation and environment*. Paper presented at the Symposia of the society for experimental biology.
- Montesano, F. F., Parente, A., Santamaria, P., et al. (2015). Biodegradable Superabsorbent Hydrogel Increases Water Retention Properties of Growing Media and Plant Growth. *Agriculture and Agricultural Science Procedia*, 4, 451-458. doi:10.1016/j.aaspro.2015.03.052
- Morales, A., Labidi, J., & Gullón, P. (2020). Assessment of green approaches for the synthesis of physically crosslinked lignin hydrogels. *Journal of Industrial and Engineering Chemistry*, 81, 475-487.
- Morgan, C. A., Herman, N., White, P. A., et al. (2006). Preservation of micro-organisms by drying; A review. *Journal of Microbiological Methods*, 66(2), 183-193. doi:10.1016/j.mimet.2006.02.017
- Müller, A. C., & Guido, S. (2016). *Introduction to machine learning with Python: a guide for data scientists*. Gravenstein Highway North, Sebastopol, CA, USA: O'Reilly Media, Inc.
- Narjary, B., & Aggarwal, P. (2014). Evaluation of soil physical quality under amendments and hydrogel applications in a soybean–wheat cropping system. *Communications in soil science and plant analysis*, 45(9), 1167-1180.
- Narjary, B., Aggarwal, P., Singh, A., et al. (2012). Water availability in different soils in relation to hydrogel application. *Geoderma*, 187-188, 94-101. doi:10.1016/j.geoderma.2012.03.002
- Nemes, A., Rawls, W. J., & Pachepsky, Y. A. (2006). Use of the nonparametric nearest neighbor approach to estimate soil hydraulic properties. *Soil Science Society of America Journal*, 70(2), 327-336. doi:<https://doi.org/10.2136/sssaj2005.0128>
- Ng, A. (2019). Machine learning yearning: Technical strategy for ai engineers in the era of deep learning. Retrieved online at <https://www.mlyearning.org>.
- Nie, H., Liu, M., Zhan, F., et al. (2004). Factors on the preparation of carboxymethylcellulose hydrogel and its degradation behavior in soil. *Carbohydrate Polymers*, 58(2), 185-189. doi:10.1016/j.carbpol.2004.06.035
- Nishida, M., Uraki, Y., & Sano, Y. (2003). Lignin gel with unique swelling property. *Bioresource Technology*, 88(1), 81-83. doi:10.1016/s0960-8524(02)00264-x
- Nivetha, A., Rangunath, K., Kumaraperumal, R., et al. (2019). Prediction of hydraulic conductivity and correlating it with soil properties for Coimbatore district. *IJCS*, 7(3), 3419-3422.
- Nyyssölä, A., & Ahlgren, J. (2019). Microbial degradation of polyacrylamide and the deamination product polyacrylate. *International Biodeterioration & Biodegradation*, 139, 24-33. doi:10.1016/j.ibiod.2019.02.005
- Oksińska, M. P., Magnucka, E. G., Lejcuś, K., et al. (2018). Colonization and biodegradation of the cross-linked potassium polyacrylate component of water absorbing geocomposite by soil microorganisms. *Applied Soil Ecology*, 133, 114-123.
- Oksińska, M. P., Magnucka, E. G., Lejcuś, K., et al. (2016). Biodegradation of the cross-linked copolymer of acrylamide and potassium acrylate by soil bacteria. *Environ Sci Pollut Res*, 23(6), 5969-5977. doi:10.1007/s11356-016-6130-6

- Ostrand, M. S., Desutter, T. M., Daigh, A. L. M., et al. (2020). Superabsorbent polymer characteristics, properties, and applications. *Agrosystems, Geosciences & Environment*, 3(1). doi:10.1002/agg2.20074
- Pachepsky, Y., & Park, Y. (2015). Saturated hydraulic conductivity of US soils grouped according to textural class and bulk density. *Soil Science Society of America Journal*, 79(4), 1094-1100.
- Pachepsky, Y., & Van Genuchten, M. (2011). Pedotransfer functions. *Encyclopedia of agrophysics*. Springer, Berlin.
- Padarian, J., Morris, J., Minasny, B., et al. (2018). Pedotransfer functions and soil inference systems. In *Pedometrics* (pp. 195-220): Springer.
- Pal, R. (2016). Validation methodologies. In *Predictive modeling of drug sensitivity*: Academic Press.
- Pasolli, L., Notarnicola, C., & Bruzzone, L. (2011). Estimating Soil Moisture With the Support Vector Regression Technique. *IEEE Geoscience and Remote Sensing Letters*, 8(6), 1080-1084. doi:10.1109/lgrs.2011.2156759
- Passauer, L. (2012). Highly swellable lignin hydrogels: Novel materials with interesting properties. In *Functional Materials from Renewable Sources* (pp. 211-228): ACS Publications.
- Passauer, L., Fischer, K., & Liebner, F. (2011). Preparation and physical characterization of strongly swellable oligo (oxyethylene) lignin hydrogels. *Holzforschung*, 65(3), 309-317.
- Passauer, L., Hallas, T., Bäucker, E., et al. (2015). Biodegradation of Hydrogels from Oxyethylated Lignins in Model Soils. *ACS Sustainable Chemistry & Engineering*, 3(9), 1955-1964. doi:10.1021/acssuschemeng.5b00139
- Paul, E., Fages, J., Blanc, P., et al. (1993). Survival of alginate-entrapped cells of *Azospirillum lipoferum* during dehydration and storage in relation to water properties. *40*(1), 34-39.
- Pedregosa, F., Varoquaux, G., Gramfort, A., et al. (2011). Scikit-learn: Machine learning in Python. *the Journal of machine Learning research*, 12, 2825-2830.
- Peppas, N. (2000). Hydrogels in pharmaceutical formulations. *European Journal of Pharmaceutics and Biopharmaceutics*, 50(1), 27-46. doi:10.1016/s0939-6411(00)00090-4
- Perkins, K. S. (2011). Measurement and modeling of unsaturated hydraulic conductivity. *Hydraulic Conductivity—Issues, Determination and Applications*, Intech, China, 419-434.
- Peters, A., & Durner, W. (2008). Simplified evaporation method for determining soil hydraulic properties. *Journal of Hydrology*, 356(1-2), 147-162. doi:10.1016/j.jhydrol.2008.04.016
- Phang, Y.-N., Chee, S.-Y., Lee, C.-O., et al. (2011). Thermal and microbial degradation of alginate-based superabsorbent polymer. *Polymer degradation and stability*, 96(9), 1653-1661.
- Pickering, C., & Byrne, J. (2014). The benefits of publishing systematic quantitative literature reviews for PhD candidates and other early-career researchers. *Higher Education Research & Development*, 33(3), 534-548. doi:10.1080/07294360.2013.841651

- Prakash, S., Vasudevan, S., Banerjee, A., et al. (2021). Sustainable Irrigation through Application of Hydrogel: A Review. *Alinteri Journal of Agriculture Sciences*, 36(2), 38-52. doi:10.47059/alinteri/v36i2/ajas21113
- Przyklenk, M., Vemmer, M., Hanitzsch, M., et al. (2017). A bioencapsulation and drying method increases shelf life and efficacy of *Metarhizium brunneum* conidia. *Journal of microencapsulation*, 34(5), 498-512.
- Ramdhan, T., Ching, S. H., Prakash, S., et al. (2020). Physical and mechanical properties of alginate based composite gels. *Trends in Food Science*.
- Ramli, R. A. (2019). Slow release fertilizer hydrogels: a review. *Polymer Chemistry*, 10(45), 6073-6090. doi:10.1039/c9py01036j
- Ranganathan, N., Joseph Bensingh, R., Abdul Kader, M., et al. (2019). Cellulose-Based Hydrogels for Agricultures. In M. I. H. Mondal (Ed.), *Cellulose-Based Superabsorbent Hydrogels* (pp. 1039-1059). Cham: Springer International Publishing.
- Rashid, T., Kait, C. F., & Murugesan, T. (2016). A “Fourier Transformed infrared” compound study of lignin recovered from a formic acid process. *Procedia engineering*, 148, 1312-1319.
- Rasoulzadeh, A. (2011). Estimating hydraulic conductivity using pedotransfer functions. *Hydraulic Conductivity—Issues, Determination and Applications, Intech, China*, 145-164. doi:<https://doi.org/10.5772/22753>
- Rathore, S., Desai, P. M., Liew, C. V., et al. (2013). Microencapsulation of microbial cells. *Journal of Food Engineering*, 116(2), 369-381. doi:10.1016/j.jfoodeng.2012.12.022
- Rawls, W. J., Brakensiek, D. L., & Saxton, K. (1982). Estimation of soil water properties. *Transactions of the ASAE*, 25(5), 1316-1320.
- Rawls, W. J., Nemes, A., Pachepsky, Y. A., et al. (2007). Using the NRCS National Soils Information System (NASIS) to provide soil hydraulic properties for engineering applications. *Transactions of the ASABE*, 50(5), 1715-1718. doi:<https://doi.org/10.13031/2013.23960>
- Reddy, K. S., Vijayalakshmi, Maruthi, V., et al. (2015). Influence of Super Absorbent Polymers on Infiltration Characteristics of Alfisols in Semi-Arid Region. *Indian Journal of Dryland Agricultural Research and Development*, 30(2), 11. doi:10.5958/2231-6701.2015.00019.6
- Reed, J. F., & Cummings, R. W. (1945). Soil reaction—glass electrode and colorimetric methods for determining pH values of soils. 59(1), 97-105.
- Reynolds, W. (2008). Saturated hydraulic properties: laboratory methods. *Soil sampling and methods of analysis. 2nd ed. CRC Press, Boca Raton, FL*, 1013-1024. doi:<https://doi.org/10.1201/9781420005271.ch75>
- Rico-García, D., Ruiz-Rubio, L., Pérez-Alvarez, L., et al. (2020). Lignin-Based Hydrogels: Synthesis and Applications. *Polymers (Basel)*, 12(1), 81. doi:10.3390/polym12010081
- Ringné, M. (2008). What is principal component analysis? *Nature Biotechnology*, 26(3), 303-304. doi:10.1038/nbt0308-303
- Rivera, D., Obando, M., Barbosa, H., et al. (2014). Evaluation of polymers for the liquid rhizobial formulation and their influence in the *Rhizobium-Cowpea* interaction. *Universitas Scientiarum*, 19(3), 265-275.

- Riyajan, S.-a., Sukhlaaied, W., & Keawmang, W. (2015). Preparation and properties of a hydrogel of maleated poly (vinyl alcohol)(PVAM) grafted with cassava starch. *Carbohydrate polymers*, 122, 301-307.
- Rose, D. (1968). Water movement in porous materials III. Evaporation of water from soil. *Journal of Physics D: Applied Physics*, 1(12), 1779.
- Rosevear, A. (1984). Immobilised biocatalysts-a critical review. *Journal of Chemical Technology and Biotechnology. Biotechnology*, 34(3), 127-150. doi:10.1002/jctb.280340302
- Roy, R. V., Das, M., Banerjee, R., et al. (2006). Comparative studies on crosslinked and uncrosslinked natural rubber biodegradation by *Pseudomonas* sp. 97(18), 2485-2488.
- Ruiz, G. R., & Bandera, C. F. (2017). Validation of calibrated energy models: Common errors. *Energies*, 10(10), 1587.
- Saberi-Riseh, R., Moradi-Pour, M., Mohammadinejad, R., et al. (2021). Biopolymers for Biological Control of Plant Pathogens: Advances in Microencapsulation of Beneficial Microorganisms. *Polymers (Basel)*, 13(12), 1938. doi:10.3390/polym13121938
- Saha, A., Rattan, B., Sekharan, S., et al. (2020a). Quantifying the interactive effect of water absorbing polymer (WAP)-soil texture on plant available water content and irrigation frequency. *Geoderma*, 368, 114310. doi:10.1016/j.geoderma.2020.114310
- Saha, A., Sekharan, S., & Manna, U. (2020b). Superabsorbent hydrogel (SAH) as a soil amendment for drought management: A review. *Soil and Tillage Research*, 204, 104736. doi:10.1016/j.still.2020.104736
- Sahoo, P. K., & Rana, P. K. (2006). Synthesis and biodegradability of starch-g-ethyl methacrylate/sodium acrylate/sodium silicate superabsorbing composite. *Journal of Materials Science*, 41(19), 6470-6475. doi:10.1007/s10853-006-0504-y
- Salim, S. A. (2015). EFFECT OF WATER-RETAINING AGENT (SKY GEL) ON SOIL PHYSICAL PROPERTIES, GROWTH, YIELD AND WATER USE EFFICIENCY OF WHEAT (*Triticum aestivum* L.) PLANT. *J. Biol. Chem*, 6, 1.
- Sannino, A., Demitri, C., & Madaghiele, M. (2009). Biodegradable Cellulose-based Hydrogels: Design and Applications. *Materials*, 2(2), 353-373. doi:10.3390/ma2020353
- Sarker, I. H. (2021). Machine Learning: Algorithms, Real-World Applications and Research Directions. *SN Computer Science*, 2(3). doi:10.1007/s42979-021-00592-x
- Sarker, I. H., Kayes, A. S. M., & Watters, P. (2019). Effectiveness analysis of machine learning classification models for predicting personalized context-aware smartphone usage. *Journal of Big Data*, 6(1). doi:10.1186/s40537-019-0219-y
- Sarmah, D., & Karak, N. (2019). Biodegradable superabsorbent hydrogel for water holding in soil and controlled-release fertilizer. *Journal of Applied Polymer Science*, 48495.
- Sarmah, D., & Karak, N. (2020). Biodegradable superabsorbent hydrogel for water holding in soil and controlled-release fertilizer. *Journal of Applied Polymer Science*, 137(13), 48495. doi:10.1002/app.48495

- Schaap, M. G., & Leij, F. J. (1998a). Using neural networks to predict soil water retention and soil hydraulic conductivity. *Soil and Tillage Research*, 47(1-2), 37-42. doi:[https://doi.org/10.1016/S0167-1987\(98\)00070-1](https://doi.org/10.1016/S0167-1987(98)00070-1)
- Schaap, M. G., & Leij, F. J. J. S. S. (1998b). Database-related accuracy and uncertainty of pedotransfer functions. *163*(10), 765-779. doi:<https://doi.org/10.1097/00010694-199810000-00001>
- Schelle, H., Heise, L., Jänicke, K., et al. (2013). Water retention characteristics of soils over the whole moisture range: a comparison of laboratory methods. *European Journal of Soil Science*, 64(6), 814-821.
- Schindler, U., & Müller, L. (2006). Simplifying the evaporation method for quantifying soil hydraulic properties. *Journal of Plant Nutrition and Soil Science*, 169(5), 623-629. doi:10.1002/jpln.200521895
- Schneider, C. A., Rasband, W. S., & Eliceiri, K. W. (2012). NIH Image to ImageJ: 25 years of image analysis. *Nature Methods*, 9(7), 671-675. doi:10.1038/nmeth.2089
- Schoebitz, M., Simonin, H., & Poncelet, D. (2012). Starch filler and osmoprotectants improve the survival of rhizobacteria in dried alginate beads. *Journal of microencapsulation*, 29(6), 532-538.
- Schwartz, R. C., & Evett, S. R. (2002). Estimating Hydraulic Properties of a Fine-textured Soil Using a Disc Infiltrometer. *Soil Science Society of America Journal*, 66(5), 1409-1423. doi:10.2136/sssaj2002.1409
- Shahid, S. A., Qidwai, A. A., Anwar, F., et al. (2012). Improvement in the Water Retention Characteristics of Sandy Loam Soil Using a Newly Synthesized Poly(acrylamide-co-acrylic Acid)/AlZnFe₂O₄ Superabsorbent Hydrogel Nanocomposite Material. *Molecules*, 17(8), 9397-9412. doi:10.3390/molecules17089397
- Sharma, K., Kumar, V., Kaith, B. S., et al. (2014). A study of the biodegradation behaviour of poly(methacrylic acid/aniline)-grafted gum ghatti by a soil burial method. *RSC Advances*, 4(49), 25637. doi:10.1039/c4ra03765k
- Shi, J., Xing, D., & Lia, J. (2012). FTIR studies of the changes in wood chemistry from wood forming tissue under inclined treatment. *Energy Procedia*, 16, 758-762.
- Shuttleworth, W. J. (1979). Evaporation.
- Sihag, P. (2017). Modeling of Unsaturated Hydraulic Conductivity of Soil. *J. Indian Water Resour. Soc*, 37(4).
- Sihag, P., Tiwari, N., & Ranjan, S. (2018). Prediction of cumulative infiltration of sandy soil using random forest approach. *Journal of Applied Water Engineering and Research*, 7(2), 118-142.
- Silva, B. M., Silva, É. A. D., Oliveira, G. C. D., et al. (2014). Plant-available soil water capacity: estimation methods and implications. *Revista Brasileira de Ciência do Solo*, 38(2), 464-475. doi:10.1590/s0100-06832014000200011
- Singh, A., Sarkar, D. J., Singh, A. K., et al. (2011). Studies on novel nanosuperabsorbent composites: Swelling behavior in different environments and effect on water absorption and retention properties of sandy loam soil and soil-less medium. *Journal of Applied Polymer Science*, 120(3), 1448-1458. doi:10.1002/app.33263
- Sipponen, M. H., Lange, H., Crestini, C., et al. (2019). Lignin for Nano- and Microscaled Carrier Systems: Applications, Trends, and Challenges. *ChemSusChem*, 12(10), 2039-2054. doi:10.1002/cssc.201900480

- Sivapalan, S. (2001). *Effect of polymer on soil water holding capacity and plant water use efficiency*. Paper presented at the 10th Australian Agronomy Conference.
- Slaughter, B. V., Khurshid, S. S., Fisher, O. Z., et al. (2009). Hydrogels in regenerative medicine. *Advanced materials*, 21(32-33), 3307-3329.
- Smagin, A. V., Sadovnikova, N. B., Shnyrev, N. A., et al. (2019). Saturated and unsaturated hydraulic conductivity of synthetic gel structures in coarse textured soil substrates. *IOP Conference Series: Earth and Environmental Science*, 368, 012048. doi:10.1088/1755-1315/368/1/012048
- Smagin, A. V., Sadovnikova, N. B., & Smagina, M. V. (2014). Biodestruction of strongly swelling polymer hydrogels and its effect on the water retention capacity of soils. *Eurasian Soil Science*, 47(6), 591-597. doi:10.1134/s1064229314060088
- Smola, A. J., & Schölkopf, B. (2004). A tutorial on support vector regression. *Statistics and computing*, 14(3), 199-222. doi:<https://doi.org/10.1023/B:STCO.0000035301.49549.88>
- Smrdel, P., Bogataj, M., Zega, A., et al. (2008). Shape optimization and characterization of polysaccharide beads prepared by ionotropic gelation. *Journal of microencapsulation*, 25(2), 90-105.
- Sojka, R. E., Bjorneberg, D. L., Entry, J. A., et al. (2007). Polyacrylamide in Agriculture and Environmental Land Management. In (pp. 75-162): Elsevier.
- Somasegaran, P., & Hoben, H. J. (2012). *Handbook for rhizobia: methods in legume-Rhizobium technology*: Springer Science & Business Media.
- Song, B., Liang, H., Sun, R., et al. (2020). Hydrogel synthesis based on lignin/sodium alginate and application in agriculture. *International Journal of Biological Macromolecules*, 144, 219-230.
- Śpitalniak, M., Lejcuś, K., Dąbrowska, J., et al. (2019). The Influence of a Water Absorbing Geocomposite on Soil Water Retention and Soil Matric Potential. *Water*, 11(8), 1731. doi:10.3390/w11081731
- Stahl, J. D., Cameron, M. D., Haselbach, J., et al. (2000). Biodegradation of superabsorbent polymers in soil. *Environ Sci Pollut Res*, 7(2), 83-88. doi:10.1065/espr199912.014
- Sultana, K., Godward, G., Reynolds, N., et al. (2000). Encapsulation of probiotic bacteria with alginate–starch and evaluation of survival in simulated gastrointestinal conditions and in yoghurt. *International journal of food microbiology*, 62(1-2), 47-55.
- Suman, A., Verma, P., Yadav, A. N., et al. (2016). Development of hydrogel based bio-inoculant formulations and their impact on plant biometric parameters of wheat (*Triticum aestivum* L.). *Int J Curr Microbiol Appl Sci*, 5(3), 890-901.
- Suresh, R., Prasher, S. O., Patel, R. M., et al. (2018). Super Absorbent Polymer and Irrigation Regime Effects on Growth and Water Use Efficiency of Container-Grown Cherry Tomatoes. *Transactions of the ASABE*, 61(2), 523-531. doi:10.13031/trans.12285
- Sutherland, G. R. J., Haselbach, J., & Aust, S. D. (1997). Biodegradation of crosslinked acrylic polymers by a white-rot fungus. *Environ Sci Pollut Res*, 4(1), 16-20. doi:10.1007/bf02986258
- Taban, M., & Movahedi Naeini, S. (2006). Effect of aquasorb and organic compost amendments on soil water retention and evaporation with different evaporation

- potentials and soil textures. *Communications in soil science and plant analysis*, 37(13-14), 2031-2055.
- Taboada, M. A. (2004). *Soil shrinkage characteristics in swelling soils*. Retrieved from
- Tahri, N., Bahafid, W., Sayel, H., et al. (2013). Biodegradation: Involved Microorganisms and Genetically Engineered Microorganisms. In: InTech.
- Tamari, S., Bruckler, L., Halbertsma, J., et al. (1993). A Simple Method for Determining Soil Hydraulic Properties in the Laboratory. *Soil Science Society of America Journal*, 57(3), 642-651. doi:10.2136/sssaj1993.03615995005700030003x
- Tanan, W., Panichpakdee, J., & Saengsuwan, S. (2019). Novel biodegradable hydrogel based on natural polymers: Synthesis, characterization, swelling/reswelling and biodegradability. *European Polymer Journal*, 112, 678-687.
- Thakur, V. K., & Thakur, M. K. (2015). Recent advances in green hydrogels from lignin: a review. *International Journal of Biological Macromolecules*, 72, 834-847. doi:10.1016/j.ijbiomac.2014.09.044
- Thakur, V. K., & Thakur, M. K. (2018). *Hydrogels: Recent Advances*: Springer.
- Tittabutr, P., Payakapong, W., Teaumroong, N., et al. (2007). Growth, survival and field performance of bradyrhizobial liquid inoculant formulations with polymeric additives. *Science Asia*, 33(1), 69-77.
- Tomadoni, B., Casalongué, C., & Alvarez, V. A. (2019). Biopolymer-Based Hydrogels for Agriculture Applications: Swelling Behavior and Slow Release of Agrochemicals. In *Polymers for Agri-Food Applications* (pp. 99-125): Springer.
- Tomadoni, B., Salcedo, M., Mansilla, A., et al. (2020). Macroporous alginate-based hydrogels to control soil substrate moisture: effect on lettuce plants under drought stress. *European Polymer Journal*, 109953.
- Tripathy, S., Rao, K. S., & Fredlund, D. (2002). Water content-void ratio swell-shrink paths of compacted expansive soils. *Canadian geotechnical journal*, 39(4), 938-959.
- Tsamardinos, I., & Aliferis, C. F. (2003). *Towards principled feature selection: Relevancy, filters and wrappers*. Paper presented at the International Workshop on Artificial Intelligence and Statistics.
- Tukey, J. W. (1949). Comparing Individual Means in the Analysis of Variance. *Biometrics*, 5(2), 99. doi:10.2307/3001913
- Turioni, C., Guerrini, G., Squartini, A., et al. (2021). Biodegradable Hydrogels: Evaluation of Degradation as a Function of Synthesis Parameters and Environmental Conditions. 5(3), 47.
- Twarakavi, N. K. C., Šimůnek, J., & Schaap, M. G. (2009). Development of Pedotransfer Functions for Estimation of Soil Hydraulic Parameters using Support Vector Machines. *Soil Science Society of America Journal*, 73(5), 1443-1452. doi:10.2136/sssaj2008.0021
- Ullah, F., Othman, M. B. H., Javed, F., et al. (2015). Classification, processing and application of hydrogels: A review. *Materials Science and Engineering: C*, 57, 414-433.
- Vabalas, A., Gowen, E., Poliakoff, E., et al. (2019). Machine learning algorithm validation with a limited sample size. *PLOS ONE*, 14(11), e0224365. doi:10.1371/journal.pone.0224365
- van der Zee, M. (2005). *Handbook of biodegradable polymers* (C. Bastioli Ed.). Shawbury, Shropshire, Shropshire, SY4 4NR, United Kingdom: Rapra Technology Limited.

- Van Der Zee, M. (2011). Analytical methods for monitoring biodegradation processes of environmentally degradable polymers. *Handbook of Biodegradable Polymers: Synthesis, Characterization and Applications*.
- Van Genuchten, M. T. (1980). A closed-form equation for predicting the hydraulic conductivity of unsaturated soils 1. *Soil science society of America journal*, 44(5), 892-898.
- Van Genuchten, M. T., Leij, F., & Yates, S. (1991). The RETC code for quantifying the hydraulic functions of unsaturated soils. *U.S. Environmental Protection Agency*.
- Van Genuchten, M. T., & Pachepsky, Y. A. (2011). Hydraulic properties of unsaturated soils. *Encyclopedia of agrophysics*, 368-376.
- Van Looy, K., Bouma, J., Herbst, M., et al. (2017). Pedotransfer Functions in Earth System Science: Challenges and Perspectives. *Reviews of Geophysics*, 55(4), 1199-1256. doi:10.1002/2017rg000581
- Vassilev, N., Vassileva, M., Martos, V., et al. (2020). Formulation of Microbial Inoculants by Encapsulation in Natural Polysaccharides: Focus on Beneficial Properties of Carrier Additives and Derivatives. *Frontiers in Plant Science*, 11.
- Veihmeyer, F., & Hendrickson, A. (1927). The relation of soil moisture to cultivation and plant growth. *Proc. 1st Intern. Congr. Soil Sci*, 3, 498-513.
- Vejan, P., Khadiran, T., Abdullah, R., et al. (2019). Encapsulation of plant growth promoting Rhizobacteria—prospects and potential in agricultural sector: a review. *Journal of Plant Nutrition*, 42(19), 2600-2623.
- Vudjung, C., & Saengsuwan, S. (2017). Synthesis and properties of biodegradable hydrogels based on cross-linked natural rubber and cassava starch. *Journal of Elastomers & Plastics*, 49(7), 574-594. doi:10.1177/0095244316676868
- Wang, D., Song, Z.-Q., & Shang, S.-B. (2008). Characterization and biodegradability of amphoteric superabsorbent polymers. *Journal of Applied Polymer Science*, 107(6), 4116-4120. doi:10.1002/app.27639
- Wang, G., Zhanga, Y., & Yu, N. (2012). Prediction of Soil Water Retention and Available Water of Sandy Soils using Pedotransfer Functions. *Procedia Engineering*, 37, 49-53. doi:10.1016/j.proeng.2012.04.200
- Wei, Y., & Durian, D. J. (2014). Rain water transport and storage in a model sandy soil with hydrogel particle additives. *The European Physical Journal E*, 37(10). doi:10.1140/epje/i2014-14097-x
- Wen, Q., Chen, Z., Zhao, Y., et al. (2010). Biodegradation of polyacrylamide by bacteria isolated from activated sludge and oil-contaminated soil. *Journal of Hazardous Materials*, 175(1-3), 955-959.
- Wendroth, O., Ehlers, W., Kage, H., et al. (1993). Reevaluation of the evaporation method for determining hydraulic functions in unsaturated soils. *Soil Science Society of America Journal*, 57(6), 1436-1443.
- Wendroth, O., Simunek, J., & van Genuchten, M. T. (1999). *Soil hydraulic properties determined from evaporation and tension infiltration experiments and their use for modeling field moisture status*. Paper presented at the Proceedings of the Workshop on Characterization and Measurement of the Hydraulic Properties of Unsaturated Porous Media. Riverside, CA, USA, submitted.
- Wendroth, O., Wypler, N., Carter, M., et al. (2008). Unsaturated hydraulic properties: Laboratory evaporation. *Soil sampling and methods of analysis*, 1089-1127.

- Wendroth, O., Zhang, X., Reyes, J., et al. (2018). *Irrigation: Basics and principles of an approach involving soil moisture measurements*.
- Wilske, B., Bai, M., Lindenstruth, B., et al. (2014). Biodegradability of a polyacrylate superabsorbent in agricultural soil. *Environ Sci Pollut Res*, 21(16), 9453-9460. doi:10.1007/s11356-013-2103-1
- Wind, G. (1966). *Capillary conductivity data estimated by a simple method*. Retrieved from
- Wösten, J. H. M., Finke, P. A., & Jansen, M. J. W. (1995). Comparison of class and continuous pedotransfer functions to generate soil hydraulic characteristics. *Geoderma*, 66(3-4), 227-237. doi:10.1016/0016-7061(94)00079-p
- Wösten, J. H. M., Lilly, A., Nemes, A., et al. (1999). Development and use of a database of hydraulic properties of European soils. *Geoderma*, 90(3-4), 169-185. doi:10.1016/s0016-7061(98)00132-3
- Xie, J., Liu, X., Liang, J., et al. (2009). Swelling properties of superabsorbent poly(acrylic acid-co-acrylamide) with different crosslinkers. *Journal of Applied Polymer Science*, 112(2), 602-608. doi:10.1002/app.29463
- Xiong, B., Loss, R. D., Shields, D., et al. (2018). Polyacrylamide degradation and its implications in environmental systems. *npj Clean Water*, 1(1). doi:10.1038/s41545-018-0016-8
- Yan, X., & Su, X. (2009). *Linear regression analysis: theory and computing*. Toh Tuck Link, Singapore: World Scientific Publishing Co. Pte. Ltd.
- Yang, L., Han, Y., Yang, P., et al. (2015). Effects of superabsorbent polymers on infiltration and evaporation of soil moisture under point source drip irrigation. *Irrigation and Drainage*, 64(2), 275-282.
- Yang, L., & Shami, A. (2020). On hyperparameter optimization of machine learning algorithms: Theory and practice. *Neurocomputing*, 415, 295-316. doi:10.1016/j.neucom.2020.07.061
- Yang, L., Yang, Y., Chen, Z., et al. (2014). Influence of super absorbent polymer on soil water retention, seed germination and plant survivals for rocky slopes eco-engineering. *Ecological Engineering*, 62, 27-32. doi:10.1016/j.ecoleng.2013.10.019
- Yao, R.-J., Yang, J.-S., Wu, D.-H., et al. (2015). Evaluation of pedotransfer functions for estimating saturated hydraulic conductivity in coastal salt-affected mud farmland. *Journal of Soils and Sediments*, 15(4), 902-916. doi:10.1007/s11368-014-1055-5
- Yeom, S., Giacomelli, I., Menaged, A., et al. (2020). Overfitting, robustness, and malicious algorithms: A study of potential causes of privacy risk in machine learning. 28(1), 35-70.
- Yeomans, J., Bremner, J. J. C. i. S. S., & Analysis, P. (1991). Carbon and nitrogen analysis of soils by automated combustion techniques. 22(9-10), 843-850.
- Young, C.-C., Rekha, P. D., Lai, W.-A., et al. (2006). Encapsulation of plant growth-promoting bacteria in alginate beads enriched with humic acid. *Biotechnology and Bioengineering*, 95(1), 76-83. doi:10.1002/bit.20957
- Yu, J., Shi, J., Dang, P., et al. (2012). Soil and polymer properties affecting water retention by superabsorbent polymers under drying conditions. *Soil Science Society of America Journal*, 76(5), 1758-1767.

- Yu, J., Shi, J., Ma, X., et al. (2017). Superabsorbent polymer properties and concentration effects on water retention under drying conditions. *Soil Science Society of America Journal*, 81(4), 889-901.
- Zerpa, A., Pakzad, L., & Fatehi, P. (2018). Hardwood Kraft Lignin-Based Hydrogels: Production and Performance. *ACS Omega*, 3(7), 8233-8242. doi:10.1021/acsomega.8b01176
- Zhang, J., Liu, R., Li, A., et al. (2006). Preparation, swelling behaviors and application of polyacrylamide/attapulgit superabsorbent composites. *Polymers for Advanced Technologies*, 17(1), 12-19. doi:10.1002/pat.676
- Zhang, X., Zhu, J., Wendroth, O., et al. (2019). Effect of Macroporosity on Pedotransfer Function Estimates at the Field Scale. *Vadose Zone Journal*, 18(1), 1 –15. doi:10.2136/vzj2018.08.0151
- Zhang, Y., & Schaap, M. G. (2019). Estimation of saturated hydraulic conductivity with pedotransfer functions: A review. *Journal of Hydrology*, 575, 1011-1030. doi:10.1016/j.jhydrol.2019.05.058
- Zhang, Y. S., & Khademhosseini, A. (2017). Advances in engineering hydrogels. *Science*, 356(6337), eaaf3627.
- Zhao, W., Cao, T., Dou, P., et al. (2019a). Effect of various concentrations of superabsorbent polymers on soil particle-size distribution and evaporation with sand mulching. *Scientific Reports*, 9(1). doi:10.1038/s41598-019-39412-x
- Zhao, W., Hu, J., Cui, Z., et al. (2019b). Effects of superabsorbent polymers on the vertical infiltration of soil water with sand mulching. *Environmental Earth Sciences*, 78(23). doi:10.1007/s12665-019-8665-6
- Zhou, H., Chen, C., Wang, D., et al. (2020). Effect of long-term organic amendments on the full-range soil water retention characteristics of a Vertisol. *202*, 104663.
- Zhou, Y., & Jin, L. (2020). Hydrolysis-induced large swelling of polyacrylamide hydrogels. *Soft Matter*, 16(24), 5740-5749. doi:10.1039/d0sm00663g
- Zhuang, W., Li, L., & Liu, C. (2013). Effects of sodium polyacrylate on water retention and infiltration capacity of a sandy soil. *Springer Plus*, 2(Suppl 1), S11. doi:10.1186/2193-1801-2-s1-s11
- Zohuriaan-Mehr, M., Omidian, H., Doroudiani, S., et al. (2010). Advances in non-hygienic applications of superabsorbent hydrogel materials. *Journal of materials science*, 45(21), 5711-5735.
- Zuberer, D. A. (1994). Recovery and enumeration of viable bacteria. In *Methods of Soil Analysis, Part 2. Microbiological and Biochemical Properties* (Vol. 5, pp. 119-144). Madison, WI, USA: Soil Science Society of America.
- Zumstein, M. T., Schintlmeister, A., Nelson, T. F., et al. (2018). Biodegradation of synthetic polymers in soils: Tracking carbon into CO₂ and microbial biomass. *Science Advances*, 4(7), eaas9024. doi:10.1126/sciadv.aas9024
- Żur, J., Wojcieszewska, D., & Guzik, U. (2016). Metabolic responses of bacterial cells to immobilization. *Molecules* 21(7), 958.

VITA

EDUCATION

MS., Environmental Studies, Ohio University, 2019

BS., Food Process Engineering, University of Ghana, 2016

PROFESSIONAL EXPERIENCE

1. Graduate Research Assistant, University of Kentucky. Biosystems and Agricultural Engineering Department, Lexington, KY: August 2019 to present.
2. Graduate Research Assistant, Ohio University, Environmental Studies Program, Athens, OH: August 2017 to May 2019.
3. Teaching / Research Assistant, University of Ghana, Food Process Engineering Department, Legon, Accra: August 2016 to August 2017.

PUBLICATIONS

1. **Adjuik, T.A.**, Nokes, S.E., Montross, M.D., Sama, M.P, & O. Wendroth. Predictor Selection and Machine Learning Regression Methods to Predict Saturated Hydraulic Conductivity. *Journal of the ASABE* (Revision Submitted July 2022).
2. **Adjuik, T.A.**, Wendroth, O., Nokes, S.E., Montross, M.D., & Riley, W. Alkali Lignin-based hydrogel: Synthesis, characterization, and impact on soil water retention from near saturation to dryness. *Journal of the ASABE* (Under Review)
3. **Adjuik, T.A.**, Nokes, S.E., & Montross, M.D. Evaluating the feasibility of using a lignin/alginate hydrogel as a carrier for encapsulating *Rhizobium*. *Journal of Applied Polymer Science* (Under Review)
4. **Adjuik, T.A.**, Nokes, S.E., Montross, M.D., Riley, W. & O. Wendroth. Laboratory determination of the impact of incorporated alkali-lignin hydrogel on the hydraulic conductivity of soil. *Water* (Under Review)
5. **Adjuik, T. A.**, & Ananey-Obiri, D. (2022). Word2vec neural model-based technique to generate protein vectors for combating COVID-19: a machine learning approach. *International Journal of Information Technology*, 1-9.
6. **Adjuik, T.A.**; Davis, S.C. (2022). Machine Learning Approach to Simulate Soil CO₂ Fluxes under Cropping Systems. *Agronomy*, 12, 197, [doi:10.3390/agronomy12010197](https://doi.org/10.3390/agronomy12010197).

7. **Adjuik, T. A.**, Nokes, S. E., Montross, M. D & Wendroth, O. (2021). Lignin-based Hydrogel for Water Retention in Silt Loam Soil. Conference paper presented at the 2021 *ASABE Annual International Virtual Meeting*.
<https://doi.org/10.13031/aim.202100216>
8. **Adjuik, T.**, Rodjom, A. M., Miller, K. E., Reza, M. T. M., & Davis, S. C. (2020). Application of Hydrochar, Digestate, and Synthetic Fertilizer to a *Miscanthus x giganteus* Crop: Implications for Biomass and Greenhouse Gas Emissions. *Applied Sciences*, 10(24), 8953.
<https://doi.org/10.3390/app10248953>

AWARDS AND HONORS

1. Center for Graduate and Professional Diversity Initiatives Professional Development Grant, 2021.
2. Alpha Epsilon (Honor Society of American Society of Agricultural and Biological Engineers), 2020 - Present
3. Outstanding graduate assistant award, Environmental Studies Program, Ohio University, 2019
4. Ecological Society of America Annual Diversity and Inclusion Scholarship, 2019
5. Ecological Society of America Annual Meeting Travel Award, 2019